Density functional theory investigation into mechanisms of metal ion-promoted and base-promoted phosphorothioate cleavage reactions

and

Lanthanide ion catalysts for kinetic resolution of amino acid esters

by

Christopher Ian Maxwell

A thesis submitted to the Department of Chemistry

In conformity with the requirements for the

Degree of Doctor of Philosophy

Queen's University

Kingston, Ontario, Canada

January, 2012

Abstract

Described here are chiral Ln^{3+} complexes of Schiff-base ligands and their use as catalysts for the kinetic resolution of the 4-nitrophenyl esters of N-Boc glutamine and phenylalanine through an enantioselective methanolysis/ethanolysis reaction. Catalysts were screened in various solvents and temperatures to optimize the selectivity value k_2^L/k_2^D or k_2^D/k_2^L. The greatest selectivity at 25°C determined was 7.1, however, reducing reaction temperature increases selectivity and after kinetic resolution at -40°C a product mixture with >99% e.e. with ~80% of the desired product remaining.

A computational method is presented for the prediction of the Brønsted parameter β^{eq}, for a phosphorothioyl group transfer in methanol by comparing relative free energy values of starting materials and phenolate products for a series of related substrates. Direct comparison of starting material and anionic leaving group free energies results in a poor approximation of β^{eq}, however given that the β^{eq} value for the equilibrium of phenol and phenoxide is -1, the comparison of computed free energies of neutral starting material with neutral phenol product provides β^{eq} approximations that are satisfactorily close to the experimentally derived values.

The detailed mechanism of base-promoted hydrolysis and methanolysis of O,O′-dimethyl O-aryl phosphorothioates and phosphates was examined computationally. Generally, with increased leaving group acidity, the reactions showed a tendency toward being concerted (a single transition state) and while substrates with leaving groups with lower acidity tend to involve 5-coordinate phosphorane intermediates. Brønsted β^{lg} values

are also computed, and found to be similar to experimentally determined values.

The mechanism of palladacycle-promoted phosphorothioate methanolysis is also modeled computationally, showing a change in rate determining step from substrate binding ($^{S}_{S}pK_a$ of leaving group phenol < 13) to leaving group departure ($^{S}_{S}pK_a$ of leaving group phenol > 13). The calculations also predict the existence of a stable metal-bound 5-coordinate thiophosphorane intermediate which has been tentatively verified experimentally by others.

The preliminary results of a computational investigation into the mechanism for the methanolytic cleavage of a series of N-methyl N-aryl thiobenzamides catalyzed by a similar palladacycle complex is also presented, showing metal-assisted nucleophilic attack and leaving group departure.

Acknowledgements

First and foremost, I'd like to thank my supervisors Dr. R. Stan Brown and Dr. Nick Mosey. Over the years Stan has guided and encouraged me through the ups and downs of this project, and never given up on me. His high standards of quality made me challenge myself and strive to constantly improve. He has not only taught me, but imparted to me a passion for understanding chemical reactions.

Although I've only been working with Nick for a couple years, he has taught me much, including how much fun computational chemistry can be. Whenever I came to his office to ask a question, he always knew the answer and would provide invaluable suggestions. He has an amazing gift for making the most complicated concepts seem simple and understandable.

I am just as indebted to Dr. Alex Neverov for his guidance and friendship. He has always been an inexhaustible source of knowledge and ideas not just about chemistry, but cars, carpentry and everything else.

I would also like to thank Dr. Tony Liu and Dr. Mark Mohamed. Since we all began graduate school five years ago, they have been great friends and have made my time in the lab fun. I will always fondly remember our spirited discussions.

Outside chemistry, I owe so much to my parents, Keith and Heather, for all they've done and the sacrifices they have made for me. I would also like to thank my brother, James, and my sister, Kate. Finally I'd like to thank my wife, Catherine, for her love, support and patience over the years – especially these last few months I've been hunched over the keyboard typing.

Statement of Originality

To the best of the author's knowledge, the original work in this thesis includes:

1. Development of lanthanide ion based complexes for catalyzing the kinetic resolution of racemic N-protected 4-nitrophenyl esters of glutamine and phenylalanine through a methanolysis reaction.

2. A method, using density functional theory, for predicting the Brønsted parameter β^{eq} for some phosphoryl, phosphorothioyl and carbonyl transfer reactions in water and methanol.

3. A detailed computational mechanistic study of phosphoryl and phosphorothioyl transfer reactions in water, methanol and the gas phase. A change in mechanism from concerted to step-wise is predicted as leaving group acidity decreases. Brønsted β^{lg} values are also predicted.

4. A computational study of the mechanism of O,O′-dimethyl O-aryl phosphorothioate methanolysis catalyzed by the palladacycle complex **5.1** which shows a change in rate-determining step from substrate binding to leaving group expulsion from a Pd-bound phosphorane intermediate depending on the acidity of the leaving group.

5. An initial computational exploration of the mechanism of thioamide methanolysis catalyzed by the palladacycle **6.1** indicating that the likely mechanism involves metal ion enhancing the rate of both nucleophilic attack and leaving group departure.

Table of Contents

List of Figures

List of Schemes

List of Tables

List of Abbreviations

°C	Degrees Celcius
Å	Angstrom
Abs	Absorbance
AP	Alkaline Phosphatase
B3LYP	Becke three parameter, Lee-Yang-Par
Boc	Di-*t*-butoxycarbonyl
C=O	Carbonyl
C=S	Thiocarbonyl
CHELP-G	Charges from Electrostatic Potentials – Grid method
C-N	Carbon-nitrogen bond
DFT	Density Functional Theory
DNA	Deoxyribonucleic Acid
e.e.	Enantiomeric Excess
Et	Ethyl
Gln	Glutamine
HF	Hartree-Fock
HPLC	High Performance Liquid Chromatography
HPNPP	2-hydroxypropyl-*p*-nitrophenyl phosphate
Hz	Hertz

IEFPCM	Integral Equation Formalism Variant Polarizable Continuum Model
Int	Intermediate
K	Equilibrium constant, Kelvin
k	Rate constant
KR	Kinetic Resolution
Me	Methyl
M^{x+}	Metal ion with x positive charge
NLLSQ	Nonlinear Least Square
NMR	Nuclear Magnetic Resonance
OAr	Aryloxy leaving group
OCC	Optimal Catalytic Conversion
Olg or lg	Leaving group
OMe	Methoxide
OPNP	*p*-nitrophenoxy
OTf	Triflate
P=O	Phosphonyl
P=S	Thiophosphonyl
PBE1PBE	Pure functional of Perdew, Burke, Ernzerhof; as made into a hybrid by Adamo
PES	Potential Energy Surface
Phe	Phenylalanine

P-Olg	Phosphorus - leaving group bond
P-OMe	Phosphorus – methoxide bond
Py or Pyr	Pyridine
QM/MM	Quantum Mechanics/Molecular Mechanics
RNA	Ribonucleic Acid
s	Second
SM	Starting material
T	Temperature
TS	Transition State
TS_{lg}	Leaving Group Departure Transition State
TS_{nuc}	Nucleophilic Attack Transition State
UV/Vis	Ultraviolet-Visible
β^{eq}	Relationship between log equilibrium constant and nucleophile/leaving group pK_a
β^{lg}	Gradient of a linear free energy relationship between log of rate constant and leaving group pK_a
β^{nuc}	Gradient of a linear free energy relationship between log of rate constant and nucleophile pK_a
ΔG	Change in free energy

Chapter 1. General Introduction

1.1. Overview of this dissertation

This thesis is divided into two major projects: The first is an experimental work toward the development of lanthanide-based catalysts for the kinetic resolution of chiral esters through stereoselective methanolysis processes.[1] The second project is theoretical and is further divided into two parts. The first of these is the detailed computational investigation of the base promoted hydrolysis/methanolysis of neutral phosphates and phosphorothioate triesters.[2] The second theoretical project involves a mechanistic study of the methanolysis of neutral phosphorothioate triesters catalyzed by a palladium complex using density functional theory.[3] Finally, the mechanism of palladacycle-catalyzed methanolysis of thioamide substrates is examined computationally.[4]

1.2. Background for the development of lanthanum-ion catalysts for the kinetic resolution of racemic ester mixtures

This section serves as an introduction to the work involving the kinetic resolution of chiral esters described in Chapter 2. Here, the mechanism of metal-ion catalyzed transesterification is examined in detail. This is followed by a brief theoretical outline of kinetic resolution and its terminology. Finally, some examples of enzymatic, organocatalytic and metal-ion catalyzed kinetic resolutions through transesterification reactions are described.

1.2.1. Mechanism of Lanthanum ion catalyzed transesterification

Metal ions have been shown to catalyze the transesterification of carboxylate esters, an important and ubiquitous reaction in organic chemistry.[5] Lanthanide ion catalyzed acylation of an alcohol was first reported by Barrett and Braddock[6], who observed the direct acylation of primary, secondary and tertiary alcohols by acetic acid promoted by lanthanum and scandium ions; however, a mechanism was not reported. The Brown group, having worked with the lanthanum ion catalyzed methanolysis of acetylimidazole[7], established the catalytic prowess of these catalysts for the methanolysis of activated and non-activated carboxylate esters.[8] This group has also shown that metal ions can be potentiometrically titrated in methanol[9] and ethanol[10], allowing detailed mechanistic studies to be conducted on these systems as a function of ${}^{s}_{s}\mathrm{pH}$.*

The metal ion performs multiple roles while catalyzing the hydrolysis or transesterification of esters, amides or phosphate esters.[11] First, the metal ion decreases the pK_a of the metal bound HOR, allowing the formation of nucleophilic hydroxide or alkoxide at near neutral pH and facilitates its delivery to the electrophilic site on the ester.

---

* For the designation of pH in non-aqueous solvents we use the nomenclature suggested by the IUPAC, *Compendium of Analytical Nomenclature. Definitive Rules, 1997,* 3rd ed.; Blackwell, Oxford, U.K., **1998**. The relationship of acidity in water and a non-aqueous solvent is ${}^{s}_{s}\mathrm{pH} = {}^{s}_{w}\mathrm{pH} - \delta$ (where ${}^{s}_{s}\mathrm{pH}$ is the pH of the non-aqueous solvent referenced to that solvent, ${}^{s}_{w}\mathrm{pH}$ is the pH of the non-aqueous solvent referenced to water and δ is a correction constant unique to that solvent (δ = -2.24 in methanol: deLigny, C. L.; Rehback, M. *Recl. Trav. Chim.* **1960**, *79,* 727.)).

Second, the metal ion, binding transiently to the C=O or P=O, acts as a Lewis acid to stabilize the developing negative charge on the carbonyl oxygen. It can also assist in the breakdown of any intermediates through binding the leaving group and assisting in its departure.

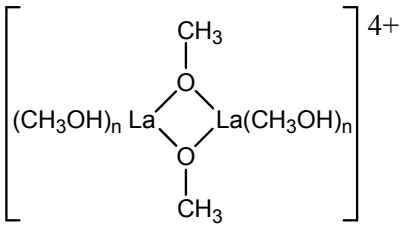

1.01

The lanthanum ion concentration dependence on the rate of methanolysis of acetylimidazole[7] show an upward curvature at low concentrations, followed by a linear region at higher concentrations, suggesting second- or higher order terms for $[La^{3+}]$. In conjunction with potentiometric titration data, and a pH rate profile for the catalyzed *p*-nitrophenyl acetate methanolysis, the catalytic form of lanthanum was proposed to be the bis-methoxy bridged dimer $(CH_3OH)_nLa^{3+}(CH_3O^-)_2La^{3+}(CH_3OH)_n$, (**1.01**) which forms through the ${}^{s}_{s}pH$ dependent equilibrium shown in Scheme 1-1. A proposed mechanism, shown in Scheme 1-2, for this transesterification involves C=O binding to the dimerized lanthanum ion. A methoxide bridge opens, increasing the nucleophilicity of the methoxide, which attacks the C=O unit.[12] The mechanism of the breakdown of the tetrahedral intermediate is dependent on the nature of the leaving group. With good leaving groups (the ${}^{s}_{s}pK_a$ of the leaving group's conjugate acid < ~14.7), the nucleophilic attack is proposed to be rate limiting and with poor leaving groups the breakdown of the tetrahedral intermediate is slower. It should be noted that such a break

should occur at a quasi-symmetrical point at the ${}^{s}_{s}pK_a$ of the attacking nucleophile, however it is unlikely that the ${}^{s}_{s}pK_a$ of the attacking metal-bound methoxide is so high.

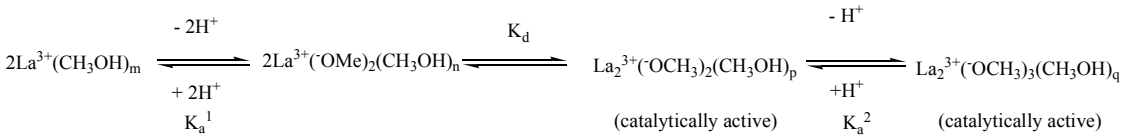

Scheme 1-1. ${}^{s}_{s}pH$ dependent formation of the catalytically active bis-methoxy lanthanum ion dimer.

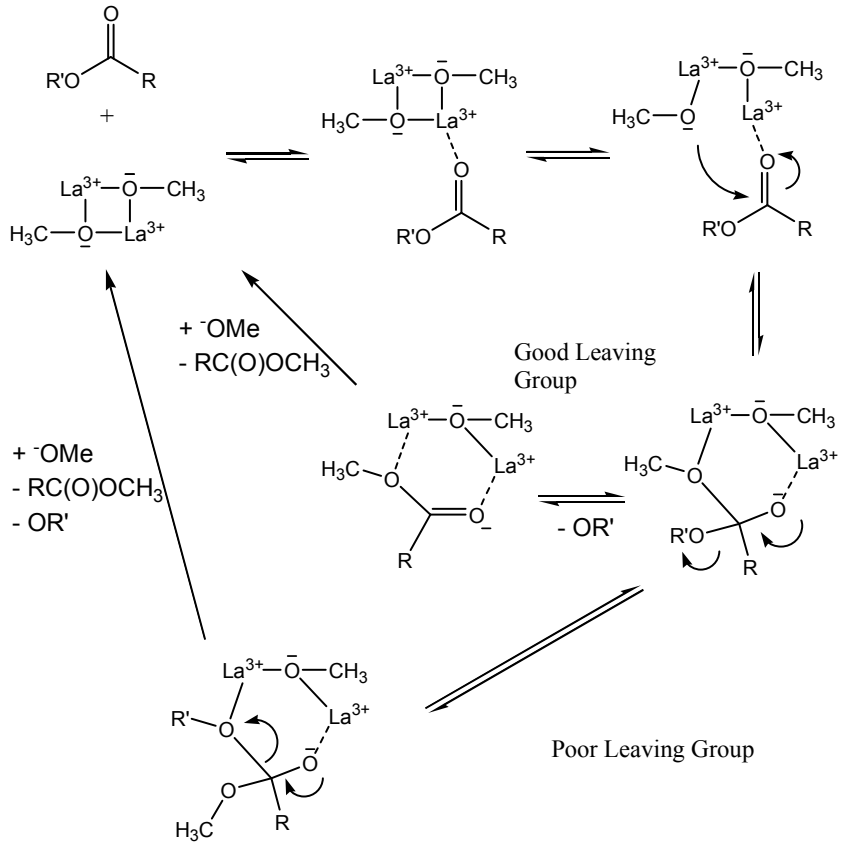

Scheme 1-2. Proposed mechanism for the $La^{3+}{}_2(^{-}OCH_3)_2$ catalyzed methanolysis of carboxylate esters with good (${}^{s}_{s}pK_a < 14.7$) and poor (${}^{s}_{s}pK_a > 14.7$) leaving groups. Solvating methanol molecules have been omitted for clarity.

1.2.2. Kinetic Resolution

Producing chiral substances with high enantiopurity is of great interest in modern chemical and pharmaceutical research.[13] There are several techniques for the purification of mixtures of enantiomers, such as chiral chromatography, crystallizations with enantiopure seed crystals[14] or reactions with chiral auxiliaries to form separable diastereomers.[15] Kinetic resolution (KR), involves resolution of enantiomers in a racemate due to unequal rates of their reaction with a chiral agent (eq. 1 and 2).[16] The free energy difference of the competing diastereomeric transition states dictates the relative rates of conversion of each enantiomer within the mixture (Figure 1-1). Provided that $\Delta G^{\ddagger}_{S}$ and $\Delta G^{\ddagger}_{R}$ (k_S and k_R) are not identical, the product mixture will be enantiomerically enriched, as well as the initial substrate mixture. Although traditionally kinetic resolution has focused on the recovery of unreacted product,[17] the enriched product can also be recovered if it is desired. Of the aforementioned methods for the separation of a racemate, kinetic resolution is capable of producing enantiomers of the greatest purity.[18]

$$S_R \xrightarrow{k_R} P_R \qquad (1)$$

$$S_S \xrightarrow{k_S} P_S \qquad (2)$$

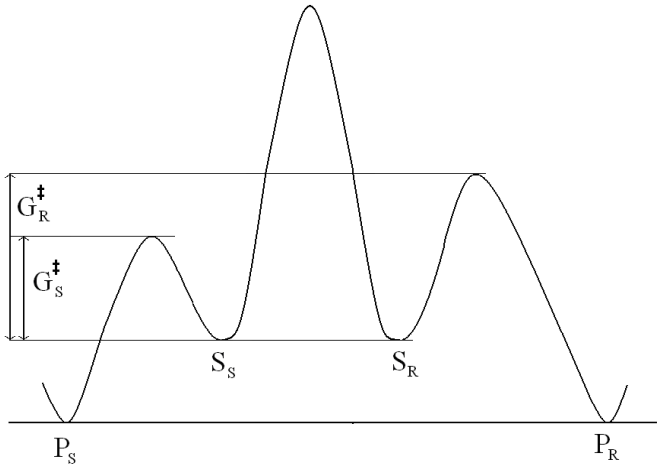

Figure 1-1. Free energy profile for a kinetic resolution process.

The KR of racemic mixtures has been observed for over 150 years. It was first seen by Pasteur in his work with the fermentation of ammonium tartrate by mold.[18] He found that the dextrorotary isomer of tartrate was selectively consumed by the organism, while the levorotary isomer remained. As chirality was not yet understood at this time, this first example of KR helped in the recognition of this important chemical concept. The first non-enzymatic KR was reported in 1899, with the resolution of racemic mandelic acid through its esterification reaction with (-)-menthol by Marckwald and McKenzie.[19] A small amount of the less-reactive enantiomer of mandelate ester found in the product suggested that this process was imperfect. The resolution of ethyl mandelate with a lipase was reported by Dakin[20] in 1904. In this case, hydrolysis products of the less reactive enantiomer were discovered, leading to a conclusion similar to that of Marckwald and McKenzie. Previously, it had been assumed that the enzyme would react with only one enantiomer within a mixture. Thus, Dakin showed that natural catalysts are also not perfectly enantioselective. Catalytic KR was developed later, in 1908 with

the decarboxylation of camphor-3-carboxylic acid in the presence of a chiral alkaloid catalyst.[18]

1.2.3. Issues with terminology in kinetic resolution

A large portion of kinetic resolution researchers report their results in the form of an enantiomeric excess (e.e.) value at a certain percent conversion of starting materials to products. Early work in the field of chirality depended on the use of circular dichroism for the measurement of optical purity, and the e.e. values are convenient to this type of measurement (Eq. 3). When optical purity is expressed as an e.e. value, it is implied that the impurity is not the minor enantiomer, but a racemic mixture of both enantiomers.

$$\text{e.e.} = \frac{[R]-[S]}{[R]+[S]} = \frac{[\alpha]_{obs}}{[\alpha]_{max}} \qquad (3)$$

Gawley[21] questions this method of describing the effectiveness of a kinetic resolution. This e.e. expression is dependent on the notion that there is a linear relationship between the composition of the mixture and the optical rotation. However, this relationship has been found to not hold true in some cases[22,23], where deviations from linearity are reported. With this in mind, one must question the use of a term like e.e., as it is based on a measurement that is not necessarily representative of the enantiomeric composition, especially with the development of better analytical methods for examining mixtures of enantiomers, such as chiral chromatography.

There are other issues with using e.e. at a certain percent conversion to benchmark the selectivity of a kinetic resolution. Over the course of a KR, e.e. values

vary dramatically as the enantiomers are consumed at rates depending on their concentration (Figure 1-2). It can be seen that the e.e. values approach 1.0 as remaining substrate concentrations approach 0. Even with a very modest difference in rate of conversion of each enantiomer, very high e.e. values can be attained, albeit with only trace amounts of starting material left.[24] The relationship between e.e. and conversion is complicated, and depends greatly on the relative rates of consumption of each enantiomer (Eq. 4), where C is the conversion. Examination of this phenomenon causes one to consider when is the best time to stop a kinetic resolution, as the observed increase of e.e. is accompanied by the loss of enantiomerically enriched starting material.

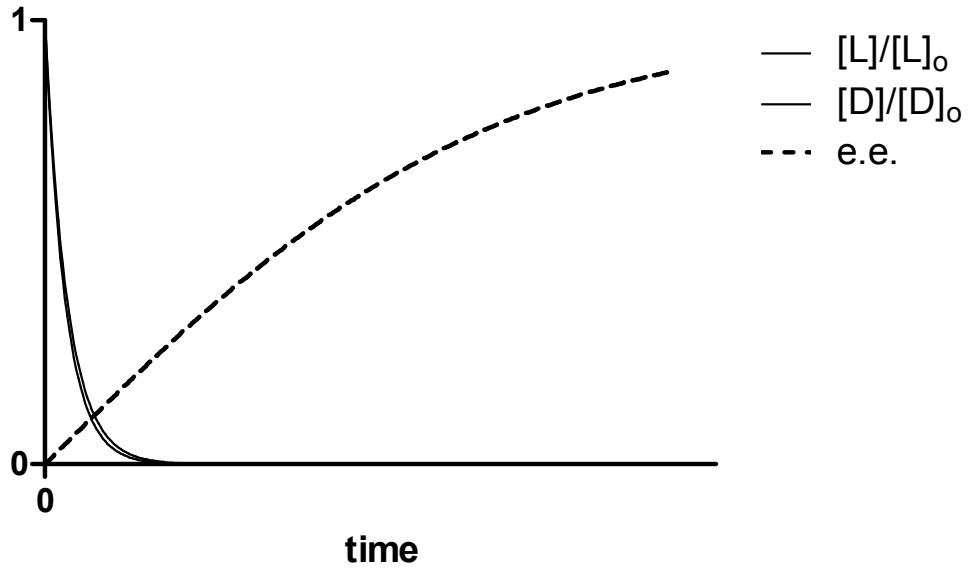

Figure 1-2. Hypothetical residual L and D enantiomers remaining during a kinetic resolution. Even a modest selectivity factor (shown here s=1.1) is capable of achieving very high e.e. values at the cost of infinitesimal yields.

$$s = \frac{k_R}{k_S} = \frac{\ln\left[(1-C)(1-e.e.)\right]}{\ln\left[(1-C)(1+e.e.)\right]}, \text{ where } k_R \geq k_S \qquad (4)$$

Gawley[21] suggests that it is more convenient to use the selectivity factor, s, for the comparison of enantioselective reactions. This value will remain constant over the course of the reaction, and the amount of conversion that is required for any given e.e. value can easily be calculated. Selectivity factors are usually reported such that $s \geq 1.0$, *ie;* k_{fast}/k_{slow}.

Kinetic resolution has found widespread use in the separation of epoxides,[25] amines,[26] alkenes,[27] and others.[28] This work is related to the catalytic kinetic resolution of chiral carboxylate esters, specifically amino acid esters, so it will focus on the resolution of these substrates.

1.2.4. Separation of racemic mixtures of chiral esters through kinetic resolution

1.2.4.1. Enzymatic catalysts

Enzymes have found widespread use kinetic resolution applications involving acyl transfers. These include lipases, esterases, peptidases, amidases and acylases[29]. In synthesis, the most commonly used biocatalysts are the lipases[30], due to their ability to discriminate between the enantiomers of a racemate and their stability at high temperatures and in organic solvents. The natural function of these enzymes is to catalyze

the hydrolysis of triacylglycerols[31], however they have been known to accept many other substrates for hydrolysis, including thioesters[32] and phosphonates[33]. These versatile enzymes are able to catalyze the formation of a variety of esters and amides[34], but lipases have been used most extensively for the kinetic resolution of ester substrates[35]. Some select examples of enzymatic kinetic resolution of substrates through acyl transfer reactions will now be discussed.

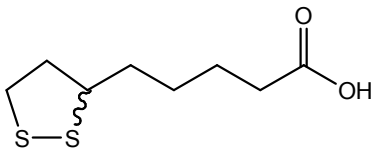

1.02

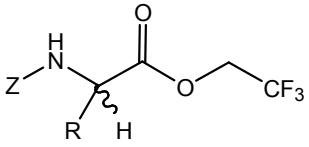

1.03

R = amino acid side chain
Z = carboxybenzyl

The high degree of enantioselectivity demonstrated by lipases is exemplified by a study by Fadnavis and Koteshwar[36], wherein α-lipoic acid (**1.02**) is resolved using *Candida rugosa* lipase, even though the chiral center of the substrate is 5 carbon atoms distant from the reactive carboxylate group. Modest e.e. values (58%) were reported from this acid's esterification reaction with long chain alcohols, however no e.e. was detected using smaller alcohols such as methanol or ethanol. The relatively impressive remote selectivity when using long chain alcohols is explained by the presence of a molecular recognition site, as well as two hydrophobic binding sites, within the active site of the enzyme.

The enantioselectivity lipase possesses toward substrates in which the chirality is close to the reactive carboxyl site is much more impressive, as is demonstrated by the *Carica papaya* lipase-catalyzed KR of amino acid esters[37]. In this example, some amino acid 2,2,2-trifluoroethyl esters (**1.03**) were converted to their methyl, ethyl, propyl and

hexyl esters through a transesterification reaction with high e.e. values at high conversion.

1.2.4.2. Organocatalysts for the kinetic resolution of chiral esters

Several chiral organocatalysts have been successfully applied to the resolution of racemic chiral carboxylic acids through their reaction with achiral alcohols.[38] An example of this is a benzotetramisol-type catalyst[39] **1.04** that reacts with α-propanoic acids **1.05** to form the diastereomeric zwitterionic intermediate of which only one diastereomer will react with a bulky alcohol (**1.06**) (Scheme 1-3). The reported enantioselectivities for these reactions are as high as 93% e.e. and they have been applied to the production of anti-inflammatory drugs such as ibuprofen and its derivatives.

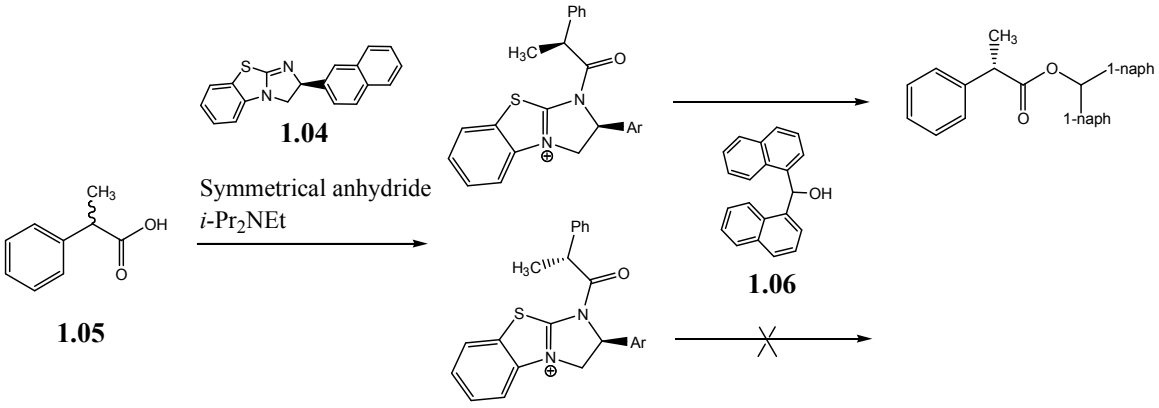

Scheme 1-3. KR of α-propanoic acids through esterification using an a benzotetramisol organocatalyst.

1.2.4.3. Metal ion catalysts in kinetic resolutions through transacylation reactions

The specifically tailored first and second coordination spheres of enzyme active sites generally make them unparalleled in substrate selectivity[40]. In comparison to

artificial catalysts, enzymes also have advantages in the area of turnover number and catalyst recovery. However, the disadvantage to high substrate selectivity is a reduced scope of useable substrates and catalyzed reactions. Artificial catalysts have an advantage in that they can catalyze a larger range of reactions on a more diverse field of substrates. They are also able to be utilized in organic solvents. Synthetic catalysts are not as common in the literature as natural catalysts for uses in KR[41], and generally, selectivity values are lower for transacylation reactions, due to the difficulty in mimicking the chiral environment of an enzyme's active site with an artificial catalyst[42]. Although there are many kinetic resolutions using organic reagents and catalysts in the literature, this section will focus on catalysts involving metal ions with chiral ligands designed to promote acyl transfer reactions. Due to the mechanistic intricacies of these catalyzed processes, it is difficult to design ligands specifically for the structural criteria of the reactants and products. For this reason, most chiral catalysts are developed empirically.[43]

Dro *et al.* have recently developed a dinuclear zinc catalyst in a biomimetic study of metalloenzymes[44]. They use a chiral trisoxazoline tripod ligand **1.07** which upon addition of zinc triflate forms a dinuclear zinc complex. X-ray crystallography reveals that the metal centers are bridged by three triflate ligands with C_3 symmetry. This complex shows fair enantioselectivity (s = ~2) in the hydrolytic kinetic resolution of the N-protected amino acid derivatives **1.08**, however selectivity increases with different anions (selectivity: triflate < acetate < trifluoracetate).

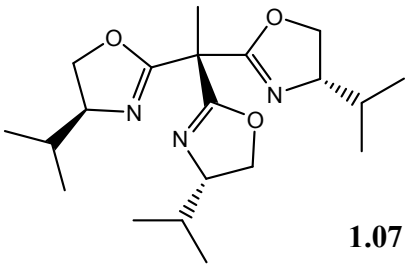

1.07

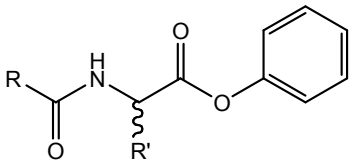

R = Ph, Me
R' = Me, Ph, Bz

1.08

The authors also note the importance of the tripodal ligand, as they report no selectivity with the corresponding bidentate bis-oxazoline ligand. The greatest selectivity determined with the $Zn^{2+}{}_2$:**1.07** system was s = 5.1, with the resolution of **1.08**. It is possible that the two metal ions act in a manner similar to catalysts developed by our group[45], *i.e.*; to act as a dual Lewis acid to position and activate the carbonyl group. The dimerization of the complex may only act to add steric bulk, enhancing the chiral environment, however it is unlikely that the tris-triflate complex is the catalytically active species. No mechanistic study was conducted, so it is difficult to clarify the specific roles of each part of the catalyst.

The enantioselective hydrolysis of N-protected *p*-nitrophenyl esters of amino acids published by Ryabov *et al.*[46] indicates a major drawback to some catalytic kinetic resolutions or asymmetric synthesis, namely the existence of a background reaction that occurs without enantiomeric discrimination. The observed rate of hydrolysis of the leucine and methionine derivatives catalyzed by palladacycle **1.09** involves a substantial background reaction and the observed rate constant is the sum of the palladacycle catalyzed reaction and the spontaneous hydrolysis ($k_{obs} = k_{background} + k_{cat}$). Because the background reaction is not influenced by the chiral catalyst, it causes the reaction of the slow substrate, damaging the overall selectivity of the system. Catalytic selectivities can

be determined by subtracting the background reaction from each observed rate constant. In water, the chloride ligand is hydrolyzed to form the hydroxide substituted palladacycle which participates in an intermolecular nucleophilic attack on the carbonyl group of the leucine substrate (**1.10**) with a selectivity of 4.7. The authors propose that the selectivity arises from the interactions of the chiral α-methyl fragment of the ligand and the alkyl side chain. In the hydrolysis of the methionine derivative, the sulfur of the side chain coordinates to palladium to provide a 'pseudo-catalytic center' which promotes leaving group departure. The hydrolysis of the methionine substrate has a selectivity value of 1.68, lower than that of the leucine derivative (**1.11**).

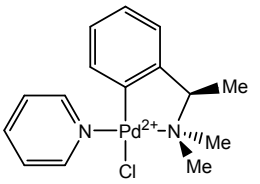

1.09

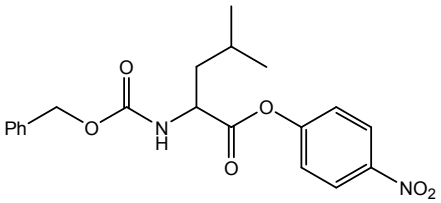

1.10

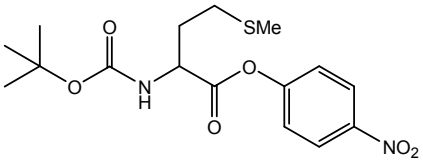

1.11

Although this catalyst has fair selectivity values, the substantial background reaction causes poor results for enantioselective hydrolysis. To date there are still few successful artificial catalysts for the KR of this type of mixture, and their potential value merits research toward further development.

1.3. Phosphate ester cleavage

1.3.1. Background

Phosphoryl transfer reactions from phosphate esters and anhydrides are ubiquitous in living systems, playing vital roles in the storage of genetic material, energy regulation, metabolism, signal transduction, and other important biological processes.[47] Their importance in Nature has warranted their extensive study, and a rich chemistry has been revealed. Phosphate mono- and diesters are crucial for life; however neutral phosphate triesters (of the general structure **1.12**) do not exist naturally. These man-made compounds are employed agriculturally as pesticides[48] and militarily as chemical warfare (CW) agents[49].

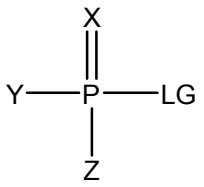

LG = OR, SR, CN, F
X = O, S
Y = OR, R
Z = OR

1.12

The acute toxicity of these poisons toward their target organisms arises from their strong inhibition of acetylcholinesterase, the enzyme responsible for the hydrolysis of the neurotransmitter acetylcholine.[50] Mechanistically, this inhibition occurs through a reaction with an essential serine hydroxyl in the enzyme active site, forming a stable phosphoserine bond and the expulsion of the leaving group.[51] The de-activation of this enzyme results in the accumulation of acetylcholine in the synaptic space, resulting in skeletal muscle hyper-stimulation and altered nervous system behavior, and can lead to

death.[52]

Nerve agents such as phosphonofluoridates Sarin (**1.13**) and Soman (**1.14**), the phosphoroamidocyanidate Tabun (**1.15**), and the methylphosphonothioate VX (**1.16**) are acutely toxic to human beings.[53] In fact, VX is considered the most lethal man-made substance known.[49a] While these chemical agents are banned through the International Chemical Weapons Convention Treaty, they are easily prepared and represent a continuing threat. Terrorist incidents such as the Tokyo Subway Attacks of 1994 demonstrate the necessity to develop methods for the destruction and decontamination of these materials.

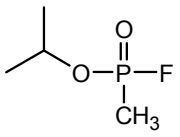

1.13

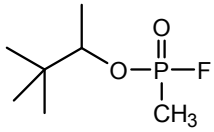

1.14

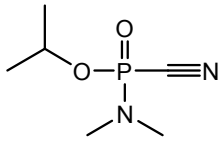

1.15

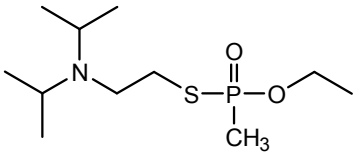

1.16

Organophosphorus pesticides such as malathion (**1.17**), fenitrothion (**1.18**), paraoxon (**1.19**, R = Et) and parathion (**1.20**, R = Et) are not acutely toxic to mammals[54]; however their accumulation in the environment is an ecological threat with potentially harmful effects on human beings through long-term exposure[55], especially in developing countries.[56] The toxicity of these compounds is highly dependent on the structure. To insects, P=S pesticides such as malathion and parathion are only weak acetylcholinesterase inhibitors; however, following activation by desulfuration to the oxygen analogues malaoxon (**1.21**) and paraoxon, their acetylcholinesterase inhibition increases.[57] However, in mammals metabolism tends to cleave lipophilic side groups from the phosphorus, resulting in inactive products.[58] While the effects of chronic

exposure to organophosphorus pesticides are difficult to identify, they have been linked to a diverse set of health problems.[59, 60]

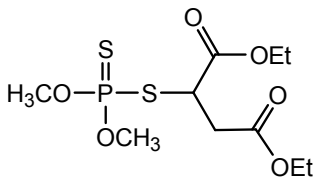

1.17

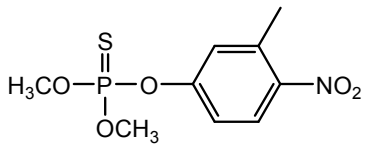

1.18

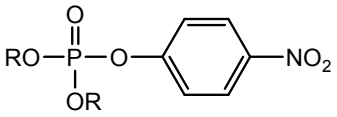

1.19

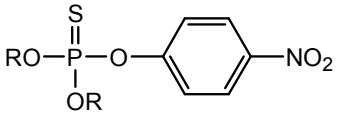

1.20

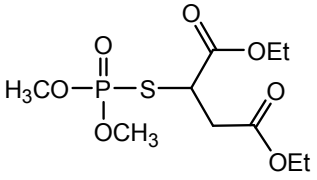

1.21

The decomposition of these materials is challenging due to the fact that they depend on oxidative or hydrolytic processes[61] that are inefficient and require harsh reaction conditions. The problems are compounded by the production of by-products that may be as toxic as the starting materials themselves. The development of catalysts for their decomposition requires detailed mechanistic knowledge of how their uncatalyzed reactions occur. The following sections deal with those specific mechanisms of phosphate and phosphorothioate hydrolysis, comparing the triester reactivity to that of the biologically relevant mono- and diesters.

1.3.2. The mechanism of phosphoryl transfer

How biologically relevant phosphoryl transfer reactions occur in solution is still a subject of debate, largely due to the large kinetic stability of mono- and diesters making them difficult to measure experimentally. In terms of reaction geometry, phosphoryl

transfer reactions are described as occurring within three mechanistic regimes in terms of nucleophilic bond forming and leaving group bond breaking.[62] This is described graphically with the More O'Ferrall – Jencks diagram shown in Figure 1-3. The mechanism of monoester cleavage is considered "loose" as leaving group bond fission occurs ahead of nucleophile bond formation. These mechanisms are progressively more associative with diesters and triesters.

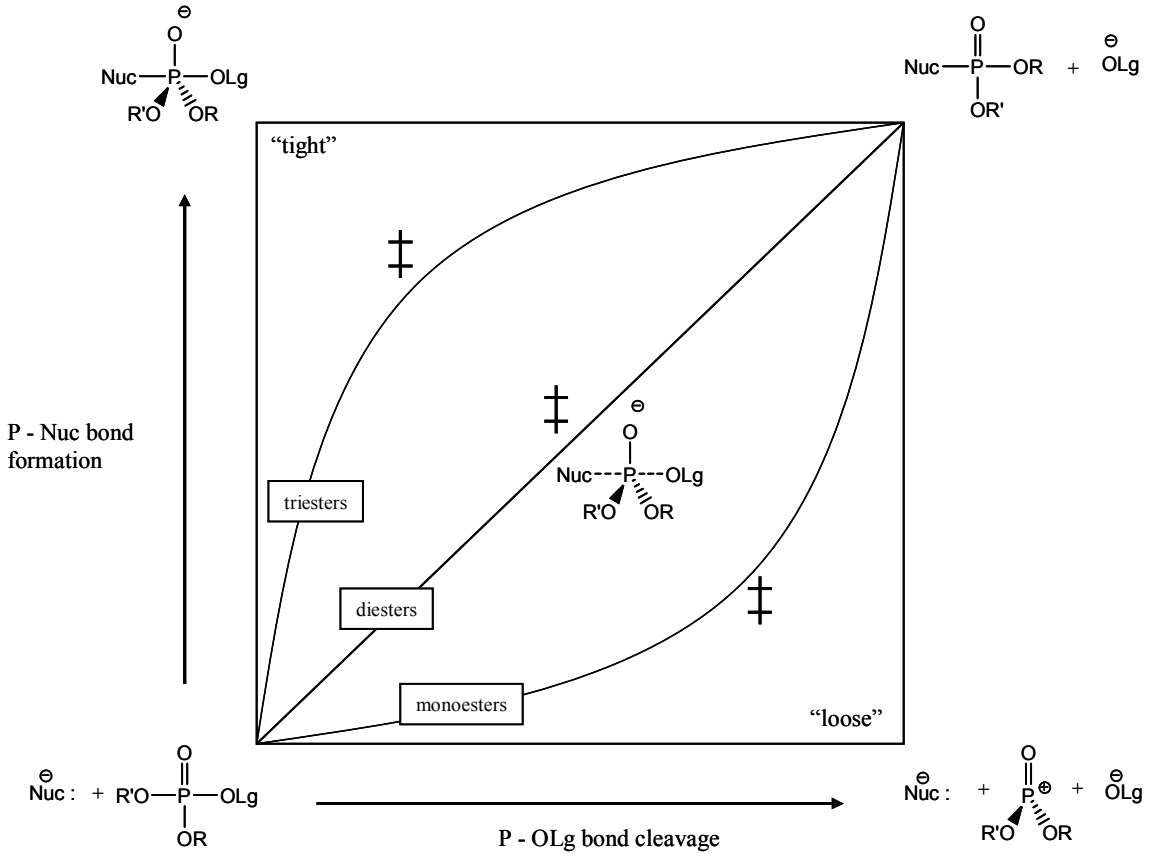

Figure 1-3. A simplified More O'Ferrall Jencks diagram illustrating the 2D free energy surface and reaction pathways for phosphate monoesters, diesters and triesters. Adapted from Purcell and Hengge.[75]

1.3.2.1. Reactions of phosphate/phosphorothioate monoesters

The hydrolysis of phosphate monoesters such as ATP and GTP are crucially important to biological systems for energy and signal transduction processes.[63] In neutral conditions at 25 °C the rate constant for the hydrolysis of methyl phosphate is measured at 2×10^{-20} s^{-1} with a corresponding half life of ~1.1×10^{12} years.[64] Though the hydrolysis is thermodynamically favoured, it is kinetically slow due to the electrostatic repulsion between the anionic phosphate and the anionic nucleophile. The accepted hydrolysis mechanism in water is a concerted A_ND_N[65] mechanism, wherein a single transition state exists along a "loose" reaction pathway in Figure 1-3. However, specifics of the mechanism are dictated by the leaving group identity and the solvent environment.

Brønsted plots describe the relationship of the log of rate constants and the pK_a of the conjugate acid of the leaving group or nucleophile and are a useful tool for measuring substituent effects on the rates of reactions and detecting potential intermediates.[66] The gradient of the correlation of the log of rate constants with leaving group pK_a (β^{lg}) is treated as a measure of the degree of leaving group bond fission in the rate-limiting transition state. Likewise, the relationship of rate constants with nucleophile pK_a (β^{nuc}) describes the measure of bond formation in that transition state. For the hydrolysis of monophosphate dianions, there exists a small β^{nuc} (~ 0.2 depending on the nature of the nucleophile[68]) and a large β^{lg} (-1.2).[67a] This suggests that the hydrolysis of phosphate monoester dianions is a dissociative process that involves little nucleophile association and a high degree of leaving group bond cleavage in the transition state. This conclusion is also supported by a very small entropy of activation.[68]

Kinetic isotope data involving cleavage of an ^{18}O-labeled monoester substrate indicates substantial P-Olg cleavage in the transition state.[69] Evidence for a concerted reaction in water is the complete inversion of stereochemistry of a phosphate monoester made chiral by ^{17}O, ^{18}O labels, indicating that there is no free metaphosphate intermediate.[70] The observation of linear Bronsted relationships for similar reactions supports this conclusion.[71] Interestingly, when the reaction of the isotopically labeled substrate is conducted in *tert*-butanol (which acts as the phosphoryl transfer acceptor), the product is racemized. [72] This result was interpreted as an indication of the formation of a free metaphosphate intermediate in the less-nucleophilic media and evidence of a D_N + A_N mechanism.

In most cases, the monoanionic phosphate is more receptive to hydrolysis than the dianion. The source of this rate acceleration is thought to be a protonation of the leaving group oxygen prior to cleavage or by a six-coordinate proton transfer process involving water.[67] This activates the leaving group by neutralizing its developing negative charge and facilitating its departure. Supporting this conclusion is the fact that rates become less sensitive to the leaving group pK_a than the corresponding dianion's reaction (a less negative $\beta^{lg} = -0.27$).[67a]

The Warshel Group at the University of Southern California has conducted an in-depth computational study of the hydrolysis of phosphate monoesters through the attack of water on dianionic substrates using *ab initio* with implicit solvent models as well as *ab initio* QM/MM free energy calculations. In that work, they examine the potential energy surface (PES) as it relates to the H_2O-P and P-Olg bond lengths, and make the claim that these reactions are more associative than previously thought; that is, the reaction of

substrates with highly basic leaving groups follow a reaction trajectory passing through the top left corner of Figure 1-3. The PES for the dissociative and associative paths is flat, and the relative barrier of each path is dependent on the leaving group. With increased leaving group acidities, the reaction mechanism changes from associative to dissociative. They argue the validity of their model by its ability to reproduce experimental Brønsted relationships. They dispute the conclusions of the previously mentioned[69] heavy-atom kinetic isotope effects with evidence that observed $^{16}O/^{18}O$ isotope effect cannot be uniquely linked with a loose transition state.[73] It should be noted that in their associative mechanisms for substrates with high leaving group pK_as, there has been a complete transfer of a proton from the attacking water to the phosphate oxygen, while this transfer has not occurred in the transition state for substrates with relatively good leaving groups. Therefore, they calculate an associative mechanism for the nucleophilic attack of hydroxide on the phosphate monoanion and a nucleophilic attack of water on the dianion, which occurs through a dissociative mechanism. It is unclear if these are directly comparable, and calls into question how this proton transfer affects the accuracy of their model.

Phosphorothioate monoanions are similar to their P=O counterparts in many ways; however, their hydrolytic reactivity differs both in rate and mechanism. Substitution of sulfur for oxygen in a non-bridging position increases the rate of dianion hydrolysis by a factor of 12.6 and increases the rate of monoanion hydrolysis by a factor of 1380.[74] Although the enthalpic barrier is higher for phosphorothioates, the increase in rate is due to favourable changes in entropy;[75] these reactions are found to follow a fully dissociative $D_N + A_N$ mechanism, which has been established with racemization[76] and

activation volume experiments.[76b]

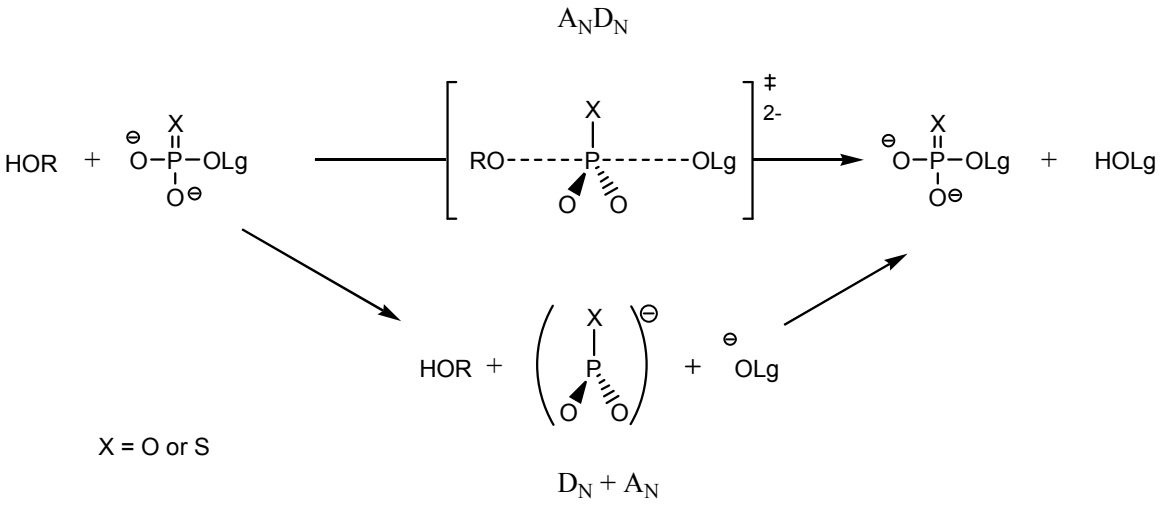

Figure 1-4. Pathways proposed for phosphoryl transfer from monoester dianions (A_ND_N) and thiophosphoryl transfer from monoester dianions ($D_N + A_N$).

1.3.2.2. Reactions of phosphate/phosphorothioate diesters

Phosphate diesters form the backbone of the nucleic acids, and their inertness helps preserve genetic fidelity. Studying the hydrolysis of these esters typically involves the use of model substrates instead of the DNA or RNA polymers themselves (Figure 1-5). Model substrates such as methyl *p*-nitrophenyl phosphate **1.22** and *bis*(*p*-nitrophenyl) phosphate **1.23** are attractive experimentally due to their simple synthesis and the easily monitored UV-Vis chromophore of the *p*-nitrophenol/phenoxide leaving group. The activated leaving group allows the study of exceedingly slow reactions by accelerating them to occur in a manageable timeframe. Structure-activity studies that access less activated leaving groups require higher temperatures and extrapolation to standard conditions. Though they are convenient experimentally, the reactivity of *p*-nitrophenyl and other activated substrate models should not be expected to be entirely

similar to the systems modeled. [2b, 77]

RNA and DNA differ in that the former features a hydroxyl group in the 2′-position of the pentose ring, rendering it more prone to hydrolysis. Thus, small molecule models of RNA, such as the widely used 2-hydroxypropyl-*p*-nitrophenyl phosphate[78] (**1.24**), include a corresponding β-hydroxyl group.

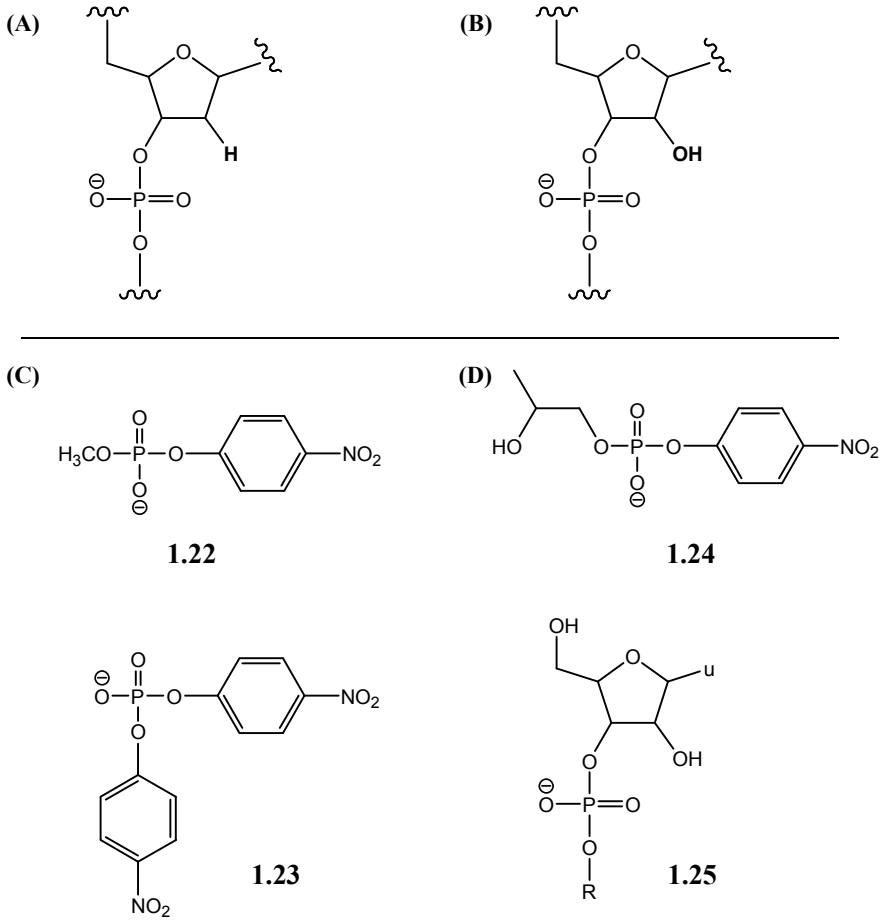

Figure 1-5. Representative structures of (A) DNA and (B) RNA. Small molecules models for (C) DNA and (D) RNA.

For the hydrolysis of DNA model diesters, the Brønsted β^{nuc} is larger and β^{lg} is less negative[79] when compared to the corresponding values for the monoesters. This

indicates a greater amount of bond formation in the transition state and less bond scission, and supports the conclusion shown in Figure 1-3. In terms of the detailed mechanism of thymidine-5′-*p*-nitrophenyl phosphate, a measured ^{18}O kinetic isotope effect of 1.027 in the nucleophilic oxygen[80] paired with a normal ^{18}O isotope effect of the leaving group oxygen indicates both bond formation and bond breaking occurring in the rate determining transition state. This and other experimental data support concerted reactions of phosphate diesters with external nucleophiles.[81]

It is suspected that the reaction of phosphate diesters with internal nucleophiles, and therefore RNAs, occur with a step-wise mechanism.[82] Investigations into the Brønsted relationship between the rate of alkaline cyclization of RNA models reveal a β^{lg} of -0.59[83] for 2-hydroxypropyl aryl phosphates similar to **1.24** and a similar β^{lg} value of -0.56 for **1.25** where R = Ar.[78] However, the cyclization of **1.25** with alkyl leaving groups (higher leaving group pK_as) results in a much a steeper β^{lg} of -1.28.[84] When a complete Brønsted plot is constructed using the alkyl and aryl data, a break occurs at the quasi-symmetrical point wherein the pK_a of the leaving group is equal to the pK_a of the nucleophile (in this case the 2′-hydroxyl). This is consistent with a step-wise mechanism, wherein the nucleophilic attack is rate limiting for substrates with $pK_a^{lg} < \sim 12.6$ and leaving group bond scission is limiting for substrates with $pK_a^{lg} > \sim 12.6$. This conclusion depends on the assumption that alkyl and aryl leaving groups are directly comparable; that is, there is no inherent difference in reactivity throughout the range of pK_a values, which has been shown to be not true for alkyl and aryl substrates.[2b,85]

Isomerisation studies further elucidate the nature of possible intermediates that may occur during these cyclizations. In acidic conditions where the phosphate is

protonated (as established through KIE studies[86]), dinucleotide-3′-phosphate diesters react to form cyclized products as well as the isomerized 2′-phosphate.[87] These processes are thought to proceed *via* a common set of pseudorotation intermediates (Scheme 1-4).

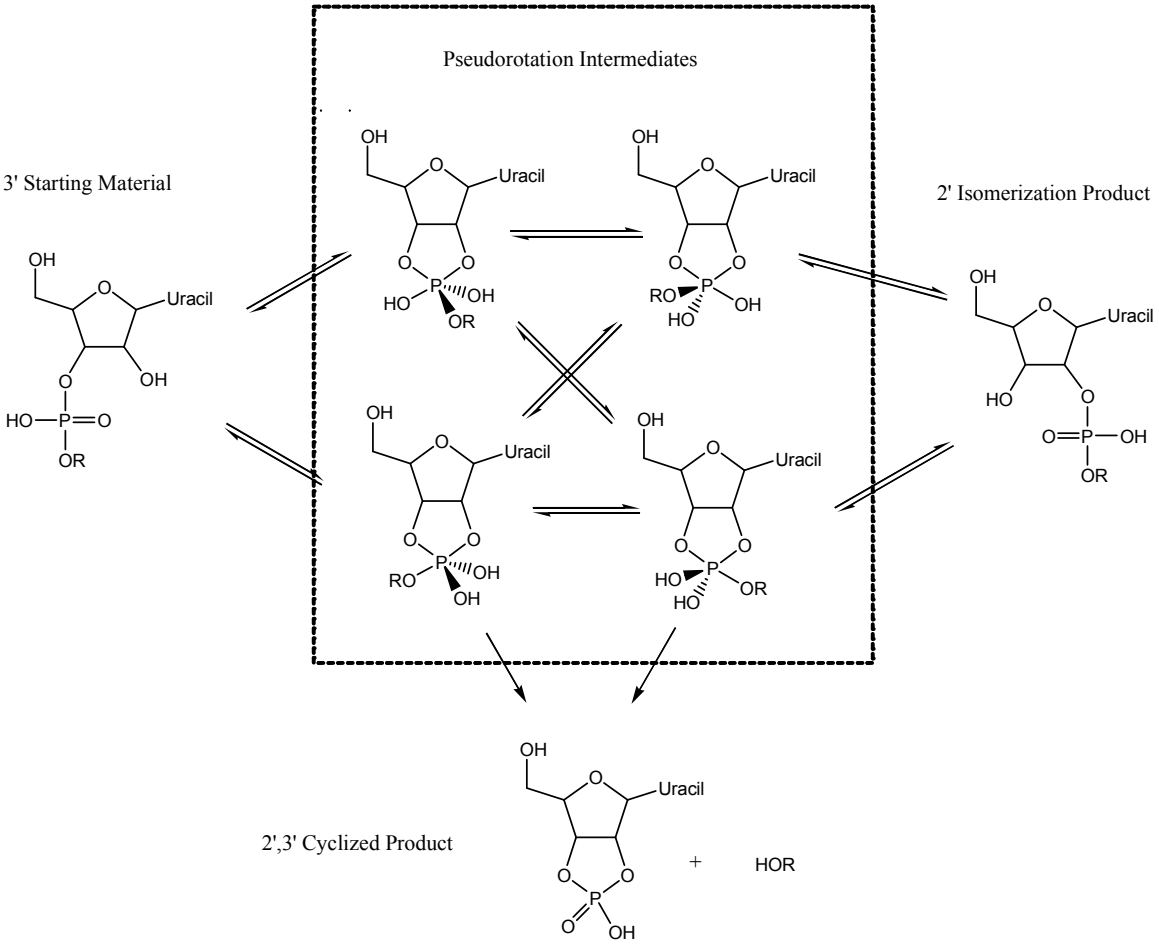

Scheme 1-4. Isomerization and cyclization of uridine-3′-alkyl phosphates under acidic conditions.

In alkaline conditions, no isomerization product is observed.[88] This may suggest the absence of five-coordinate phosphorane intermediates and suggests a concerted process. These findings are reconciled by the explanation that the reaction is indeed step-wise with an intermediate is too short-lived to allow isomerization.[84]

The importance of the cleavage of phosphate diesters has made them a popular subject of computational studies, which over time have become more sophisticated as new methods are developed.[89] Recently, the Warshel Group has followed up their monoester work with a similar computational study of the hydrolysis of simple methyl aryl phosphate diesters using *ab initio* methods.[90] Their results support the conclusion that the reaction proceeds through a concerted A_ND_N mechanism which is tight (in terms of transition state bond distances) at high pK_a^{lg} values and becomes progressively looser as the leaving group acidity increases. This observation can be illustrated by Figure 1-6, wherein the Hammond effect of the better leaving groups moves the transition state toward the reactants. This is coupled with a movement of reaction coordinate toward a more expansive mechanism through an anti-Hammond effect.

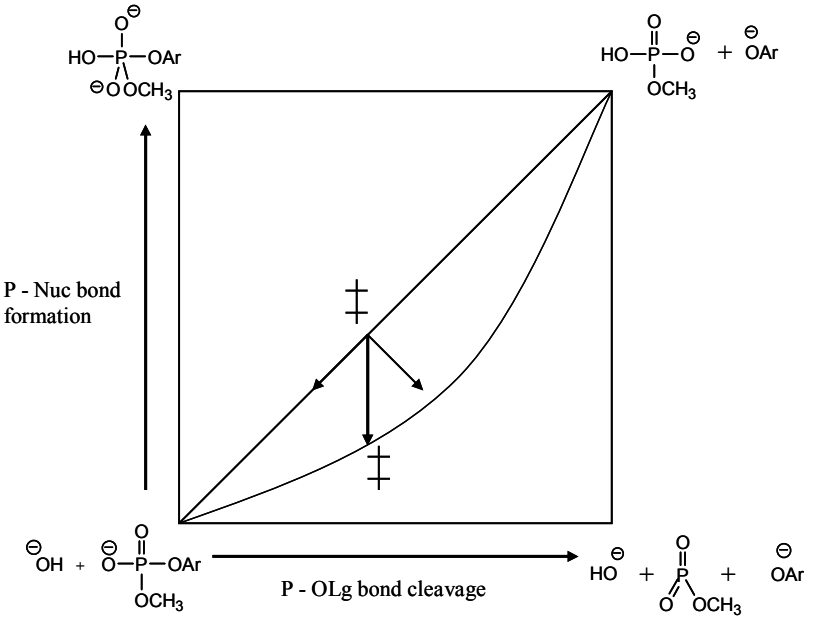

Figure 1-6. A More O'Ferrall – Jencks diagram showing the effect on the hydroxide promoted hydrolysis of methyl aryl phosphate diesters' reaction pathway caused by increasing the acidity of the leaving group.

Phosphorothioate analogues of phosphate diesters have been used as mechanistic probes for enzymatic phosphoryl transfer reactions,[91] and have been shown to be more resistant to enzymatic cleavage[92] and alkali hydrolysis.[75] As seen with the monoesters, the enthalpy of activation for the phosphorothioate hydrolysis is greater. However, in the diester case, a less positive $\Delta S^{\ddagger}$ for the phosphorothioate ester is not able to overcome the larger $\Delta H^{\ddagger}$ term, resulting in greater free energies of activation for the P=S species. The smaller $\Delta S^{\ddagger}$ for the P=S diesters could also be interpreted as evidence of a more dissociative mechanism. However, the Brønsted β^{lg} for the hydrolysis of uridine-3′-aryl phophorothioates is similar to the P=O variant,[93,83] indicating similar reactivities for these species although it is not known whether the reactivities of the cyclic and non-cyclic phosphorothioates can be directly compared.

1.3.2.3. Reactivities of neutral phosphate/phosphorothioate triesters

The triesters are the most reactive of the three classes of phosphate esters, and as shown above in Figure 1-3, their reaction pathway is the most associative. In terms of the looseness or tightness of the displacement, their reactivity is highly dependent on the nature of the spectator groups.

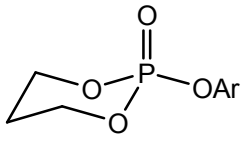

1.26

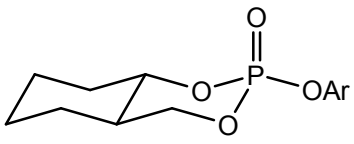

1.27

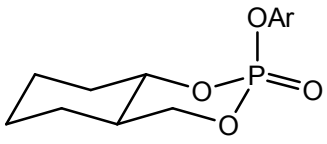

1.28

Khan and Kirby[94] studied the reactions of the cyclic triester **1.26**. They show that β^{lg} is dependent on the basicity of the nucleophile. With weakly basic nucleophiles such

as water, they measured a β^{lg} of -0.99. With increasing basicity, the β^{lg} increased (became less negative) toward a constant value of ~ -0.35 for nucleophiles of $pK_a > 11.6$. This observation was interpreted as evidence for a step-wise reaction in which $k_2 >> k_{-1}$ for good nucleophiles and the phosphorane intermediate preferentially breaks down to form products (Scheme 1-5). With poor nuclophiles ($pK_a < 11.6$), k_{-1} is fast and k_2 is rate limiting. Thus, there is strong evidence that the cleavage of these phosphates proceeds *via* a step-wise mechanism. They note, however, that the data are also consistent with a concerted mechanism wherein the transition state occurs at varying points along the reaction coordinate depending on the leaving group and nucleophile.

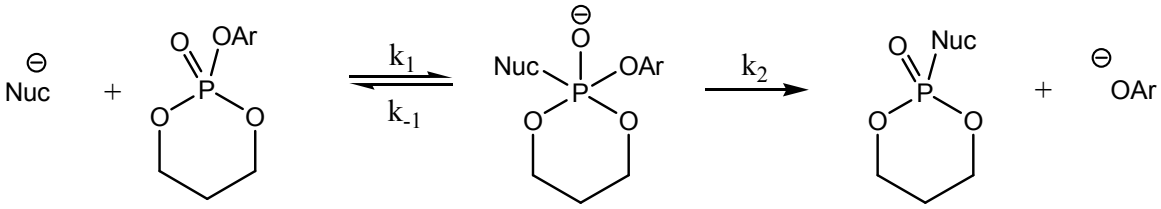

Scheme 1-5. Step-wise reaction of nucleophiles with cyclic phosphate triesters.

A similar study was conducted on the epimeric cyclic phosphate triesters **1.27** and **1.28** by Rowell and Gorenstein.[95] Again, β^{lg} becomes less negative with the increasing pK_a of the nucleophile and β^{nuc} increases with leaving group pK_a. They also observe curvature in a plot of β^{lg} values vs. pK_a^{nuc}, which is interpreted as a change in mechanism from concerted to step-wise with increasing pK_a of the nucleophile or the leaving group. This mechanistic change can be rationalized by the hypothetical 3D More O'Ferrall – Jencks diagram shown in Figure 1-7. If the basicity of the nucleophile is increased, the energies of the bottom two corners of the diagram increase, moving the trajectory toward the step-wise mechanism. If the basicity of the leaving group is increased, the energy of

the right portion of the diagram increases, also pushing the reaction trajectory toward the top right corner. Thus, the combined effect of both the nucleophile and leaving group dictates the concerted or step-wise nature of these reactions. Also shown in Figure 1-7 (c) is the asymmetrical reaction of a good nucleophile with a substrate with a good leaving group. This can be described as an "enforced concerted" mechanism, wherein the lifetime of the intermediate is shorter than a bond vibration.

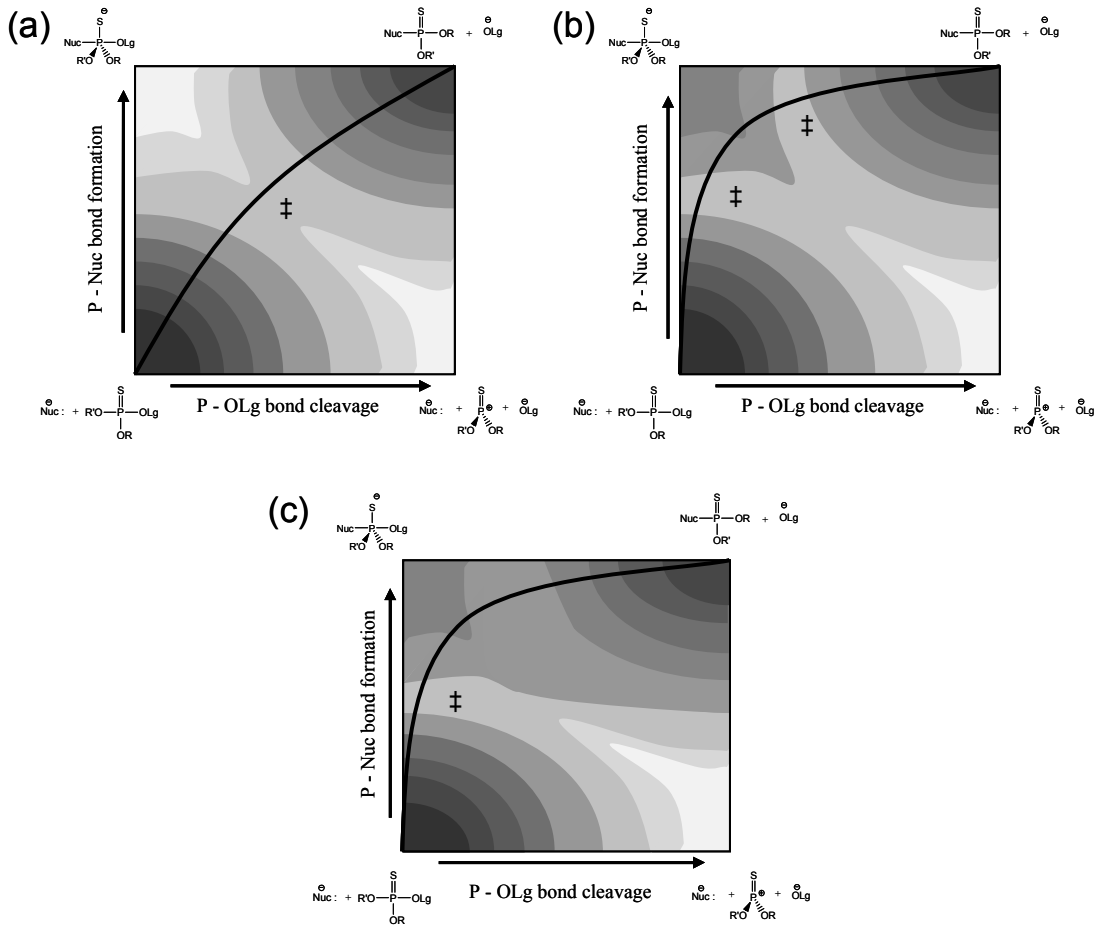

Figure 1-7. 3D More O'Ferrall – Jencks diagrams for the reaction of nucleophiles with **1.27**, **1.28** with (a) concerted mechanisms and (b) step-wise mechanisms. In (c) is shown the case of asymmetrical reactions of good nucleophiles substrates with good leaving groups. Darker areas represent lower free energies.

Stereochemical data also support this conclusion as products with more basic nucleophiles/leaving groups comprise mixtures as the intermediate structures pseudorotate prior to leaving group departure. Concerted reactions are made evident by inversion of stereochemistry.

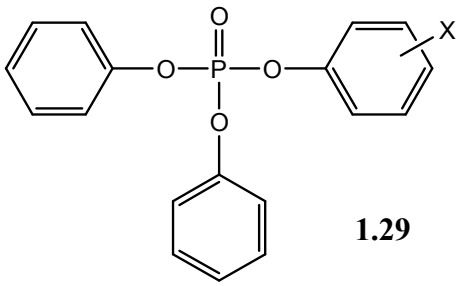

1.29

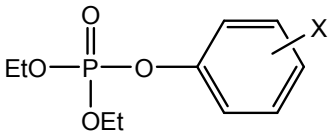

1.30

While β^{nuc} and β^{lg} are considered measures of charge change of the nucleophile and leaving group between starting material and transition state, β^{eq} is considered a measurement of charge change for leaving group/starting material for a symmetrical reaction from starting materials to products. These values are standardized against the charge change of deprotonation of the free leaving group (-1)[96], and are interrelated according to Equation 5. β^{nuc} and β^{lg}, when used in conjuction with β^{eq}, allow one to consider the charge change in the transition state within the frame of the total charge change of the reaction. Thus, the transition state can be mapped in relation to starting materials and products. Leffler's parameter, α (eq. 6, 7), is a measure of this charge progression.

$$\beta^{eq} = \beta^{nuc} - \beta^{lg} \qquad (5)$$

$$\alpha^{nuc} = \beta^{nuc} / \beta^{eq} \qquad (6)$$

$$\alpha^{lg} = \beta^{lg} / \beta^{eq} \qquad (7)$$

Ba-Saif and Williams conducted an in depth study of the phosphoryl transfer

between aryl oxides and imidazole with the aim of determining β^{eq} values using β^{nuc} and β^{lg} in accordance with Eq. 5.[97] This involves the measurement of Brønsted β^{nuc} for the attack of phenoxides on N-(diethoxyphosphoryl)imidazolium (0.85) and β^{lg} for the attack of imidazole on diethyl aryl phosphates (-1.02). The resulting β^{eq} of -1.87 can be used to calculate Leffler indices; α^{lg} in this case, is -1.02/-1.87 = 0.55, indicating that in the transition state, the leaving group has completed 55% of its progression from starting materials to products. This is consistent with a concerted reaction, or a step-wise one in which the leaving group release is rate limiting.

The measured β^{lg} for the hydroxide reaction (-0.44) with **1.29** is lower than that for the imidazole attack. Because the hydroxide is a more powerful nucleophile, the leaving group scission has progressed to a lesser degree than it would with a poorer nucleophile in the transition state. Again, this result can support either a step-wise or concerted mechanism; however, the authors[97] note that because the hydroxide lacks the electrostatic stabilizing ability of the imidazole that could potentially stabilize a phosphorane intermediate, it is likely that the hydroxide reaction is of a more concerted nature.

Linear free energy relationship data support concerted mechanisms for the transfer of the O,O′-diphenylphosphoryl group between phenoxides in water. The Brønsted plot for a series of *p*-nitrophenyl substituted **1.30** could be considered linear throughout the pK_a range tested, including the quasisymmetrical point; however, a plot of residuals shows the possibility of a shallow break.[98] This is consistent with a concerted mechanism, but it does not completely exclude a step-wise mechanism in which a high energy intermediate is located between two energetically similar transition states for bond

formation and bond cleavage.

Analysis of the Brønsted β values for this reaction, with respect to charge development, also supports a concerted reaction (Scheme 1-6) as it indicates that a step-wise pathway is unfeasible. For nucleophiles with $pK_a < pK_a^{lg}$ (pK_a values below the quasisymmetrical point), $\beta^{nuc} = 0.5$. This value refers to the effective charge change (relative to the identity reaction of phenol deprotonation) between the ground state and the rate-determining transition structure, which is the breakdown of the intermediate (k_2) within this pK_a range. Using the $\beta^{eq} = 1.3$,[98b] one can calculate Leffler's α^{nuc}, a quantity that refers to the fractional amount of change in effective charge of the nucleophile from the ground state to the transition state (Eq. 6).[99] For these reactions, α^{nuc} was found to be 0.38, indicating that at the rate determining transition state, 38% of the total charge change 'felt' by the nucleophile throughout the course of the reaction has occurred. Thus, $\beta^{eq,\ int}$ must be less than 0.5 (< 38% of effective charge developed) and $\beta'^{\ eq,\ int}$ must be greater than 0.8 (< 62% of effective charge development). This is highly unlikely, as it is expected that the change in effective charge in the nucleophile should be larger for its association than for the departure of the leaving group. Thus, the step-wise model is inconsistent with this charge-mapping data, and the concerted mechanism is favored.

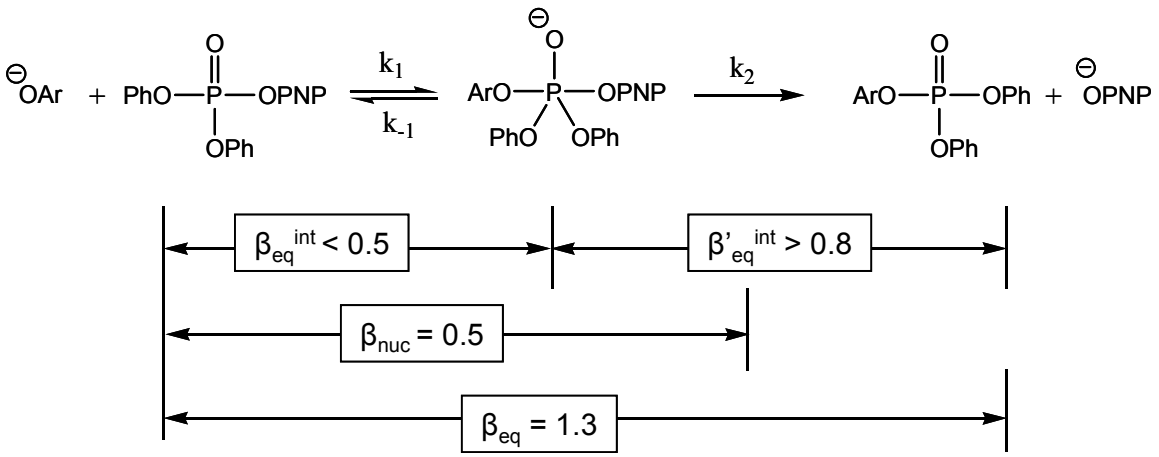

Scheme 1-6. Brønsted β values for the hypothetical step-wise reaction of p-nitrophenyl **1.29** with aryl oxides ($pK_a < 7.14$).

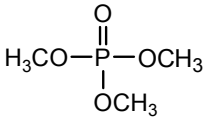

1.31

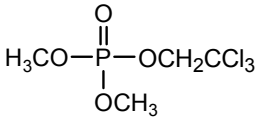

1.32

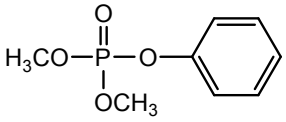

1.33

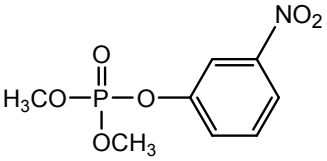

1.34

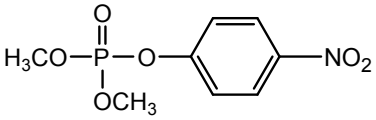

1.35

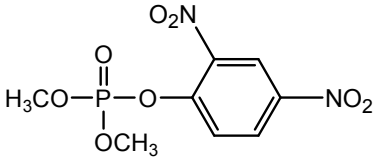

1.36

Computational studies have revealed further mechanistic complexity. Tarrat[100] and coworkers have conducted extensive theoretical work into elucidating the concertedness of these reactions. They modeled the nucleophilic attack of hydroxide on a series of O,O′-dimethyl phosphate triesters with alkyl (**1.31**, **1.32**) and aryl (**1.33** – **1.36**) leaving groups (Scheme 1-7). For leaving groups with $pK_a > 8$ (**1.31**, **1.32**, **1.33**, **1.34**), the intermediate structure ***INT*** occupies a minimum on the potential energy surface and is

bordered by two transition states (nucleophilic attack, $\mathbf{TS_{nuc}}$; leaving group departure, $\mathbf{TS_{lg}}$). For leaving groups with pKa < 8, ***INT*** does not occupy a minimum on the potential energy surface; the attempted optimization of this structure leads to a product structure wherein the leaving group O-P bond had cleaved. The absence of an energetic local minimum corresponding to ***INT*** on the potential energy surface was treated as evidence for a concerted reaction. For these reactions, this seems to indicate the 'concertedness' of the reaction depends on the leaving group's pK_a. Their results also predict that the lifetime of the intermediate is also dependent on the leaving group; that is, the free energy of the intermediate is lower than the free energies of $\mathbf{TS_{nuc}}$ or $\mathbf{TS_{lg}}$ with increased leaving group pK_a. It should be noted that with substrates **1.33** and **1.34**, the ***INT*** structure is lower in free energy than $\boldsymbol{TS_{lg}}$ by only ~2 kcal/mol. This makes their mechanism characteristic of Jenck's "enforced concerted mechanism", wherein only one transition state is considered ($\boldsymbol{TS_{nuc}}$) because the lifetime of the intermediate is shorter than the duration of a bond vibration.[101]

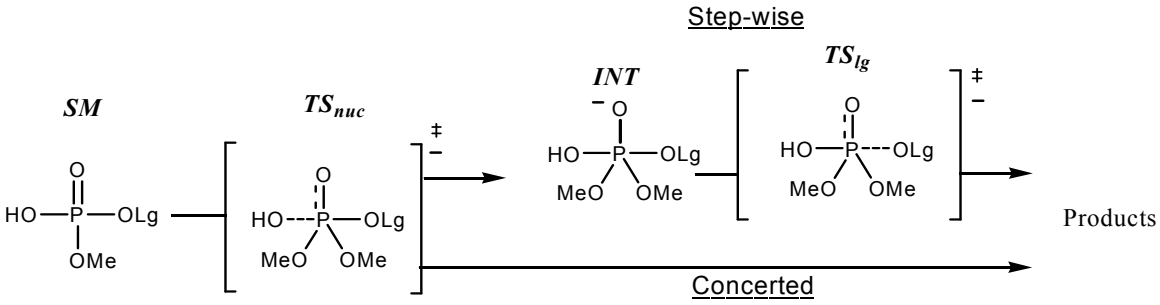

Scheme 1-7. Criteria for computationally determining the concertedness of the hydrolysis reaction of phosphate triesters.

Tarrat points out that the calculated β^{lg} (-0.435) for the most acidic aryl substrates

1.35, **1.36** is similar to the experimentally determined value of 0.4 (uncited, presumably from Hong and Raushel, ref. 102). When the rest of the aryl groups are taken into account, the β^{lg} (-0.7 ± 0.2) becomes less similar to the experimental value. They defend the exclusion of **1.33** and **1.34** in their β^{lg} determination due to the fact that they react with a different mechanism (step-wise rather than concerted). However, when data from all phosphate triesters studied are taken into account, the total β^{lg} is similar to the experimentally derived value, although this could be considered coincidental as alkyl and aryl substrates appear to fall on different lines and may not be comparable. To clarify their conclusions, more work is required in this area (see Section 1.5, Proposed Research).

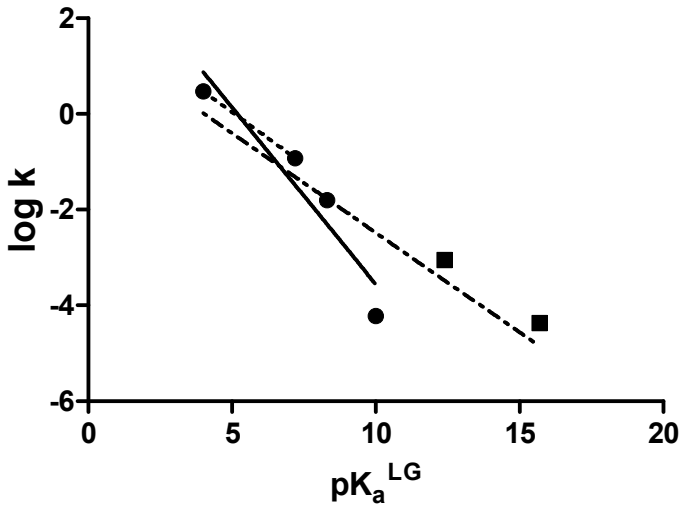

Figure 1-8. Computed Brønsted plot of the log of rate constants (calculated from data in ref. 100b, supplementary information) vs. the pK_a of the leaving group conjugate acid (alkyl substrates, (■); aryl substrates, (●)). For substrates **1.35**, **1.36** β^{lg} = -0.435 (·····); aryl substrates β^{lg} = -0.7 ± 0.2 (——); total β^{lg} = -0.4 ± 0.1 (· — · —).

Mechanistically, the reactions of P=S phosphorothioate triesters are considered to

be related to those of the corresponding P=O phosphates, although slower. It is found that the thio-effect (k^o/k^s) for this class of phosphate/phosphorothioates is 10-50.[75] Although the hydrolysis of P=S esters is entropically favoured, P=O phosphates cleave at a greater rate due to their much smaller enthalpy of activation.

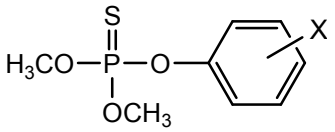

1.37

Omakor and co-workers[103] conducted a series of structure-reactivity studies using **1.18** and related O,O-dimethyl O-aryl phosphorothioates (**1.37**). A Brønsted correlation for the attack of different nucleophiles on **1.18** was constructed, and the plot of log k vs. the pK_a of the nucleophile features a linear portion surrounding the pK_a of the leaving group (quasi-symmetrical point), indicative of a concerted reaction. The plot exhibited some downward curvature with the stronger nucleophiles trifluoroethoxide and hydroxide. This reduction in rate was attributed to an abnormally high degree of solvation around these strongly basic nucleophiles relative to the weakly basic phenoxides.

The log k vs. pK_a of the leaving group for the attack of phenoxide on the series of substituted phosphorothioates (**1.37**) was linear with a β^{lg} of -0.39. With this and a β^{nuc} of -0.49, a charge map can be constructed for the symmetrical reaction of **1.18** (eq. 5, 6, 7) and Leffler's α^{nuc} (0.56) and α^{lg} (0.44) can be assigned. In the transition state, charge on the nucleophile has progressed 56% toward its charge within the product, and the leaving group's charge has progressed 44% toward its charge as the free aryloxide (Figure 1-9). It is reasoned that, because the bond formation is only slightly ahead of bond cleavage, any thiophosphorane intermediate that might exist for this reaction would not have any

significant lifetime and this is likely a concerted reaction.

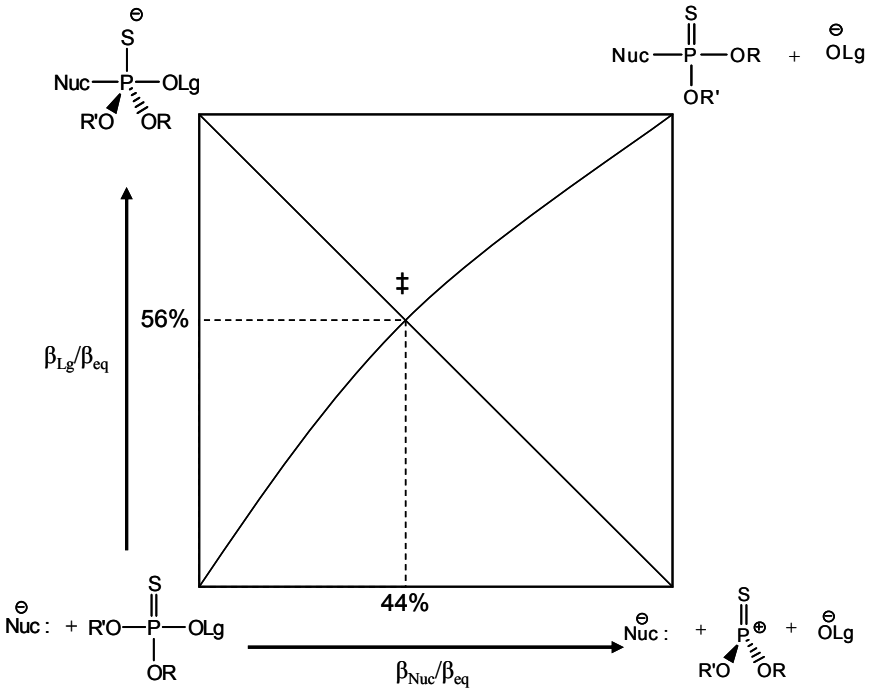

Figure 1-9. Reaction map for the symmetrical reaction of **1.18** with 3-methyl-4-nitrophenoxide.

As part of the study of metal-catalyzed phosphate cleavages in methanol, our laboratory has studied the methoxide-promoted methanolysis reactions of a series of O,O-diethyl O-aryl phosphates.[104] The β^{lg} value determined, -0.70, is more negative than that of the corresponding $^{-}$OH-promoted hydrolysis process,[102] indicating that the reaction is more sensitive to the leaving group in this solvent and with the methoxide nucleophile. Using the β^{eq} value published for the transfer of the O,O-diethyl phosphoryl group in water (1.87)[97], Leffler's α can be estimated as 0.37, indicating that the P-Olg bond is 37% cleaved at the transition state. This assumes that β^{eq} in water is the same as β^{eq} in methanol. This is consistent with a step-wise reaction with largely rate-limiting

nucleophilic attack or a concerted process, the latter of which is considered more likely. Inverse solvent kinetic isotope effects $k_D/k_H > 1$ indicate that this is likely a direct nucleophilic attack of methoxide on phosphorus involving desolvation of the nucleophile and resolvation of the transition state.[105]

1.4. Catalyzed phosphate triester cleavage

1.4.1. Comparing catalyzed and background reactions

A continuing problem in the study of enzymes and artificial catalysts is whether rate accelerations arise from stabilizing the inherent transition state of the background reactions, or by introduction of new lower energy reaction pathways. A good enzymatic example of this is alkaline phosphatase (AP), a promiscuous enzyme whose main function is hydrolyzing phosphate monoesters although it is capable of hydrolyzing diesters as well.[106] As discussed earlier, the non-catalyzed phosphate monoester hydrolysis proceeds via a loose, metaphosphate-like transition state. The AP catalyzed hydrolysis of phosphate monoesters is very similar to the reaction that occurs in solution in terms of it being loose.[107]

In the AP catalyzed hydrolysis of phosphate diesters, one of two things was expected. 1) the enzyme would 'force' the diesters to adopt a looser transition state similar to that of the monoester, or 2) the enzyme would recognize and stabilize the tighter transition state similar to that in solution. Experiments have shown that the latter seems to be the case, as the AP catalyzed phosphate diester hydrolysis proceeds through a

more synchronous transition state involving more bond formation.[108]

Conversely, several man-made catalysts have shown evidence of a changed mechanism from that of the solution reaction.[109] For instance, in the hydrolysis of monoesters and diesters, a dinuclear cobalt catalyst causes both substrate classes to have tighter transition states.[110]

1.4.2. Mechanisms of enzymatic phosphate triester cleavages

Because phosphate triesters are not naturally occurring, any enzymatic means for their hydrolysis have evolved in insects[111] and bacteria[112] very recently in the 20th century as an adaptation to the pesticides and acaricides used agriculturally. Perhaps the best understood is the phosphotriesterase from the soil bacteria *Pseudomonas diminuta*, which is capable of accelerating the hydrolysis of paraoxon (**1.19**) 10^{12}-fold over the uncatalyzed rate to approach the diffusion limit.[113] This is impressive considering that this enzyme has evolved in only the last few decades. This enzyme is fairly specific to triesters, as its catalytic activity is reduced for diesters and non-existent for monoesters.[114] The active site has two Zn^{2+} ions bridged by a carbamate-modified lysine moiety and hydroxide (Figure 1-10),[115] although substituting Co, Ni, Cd or Mn can result in similar or even greater activities.[116] The rate of the reaction is pH dependent, with the greatest activities above the pK_a of the metal bound water.[117]

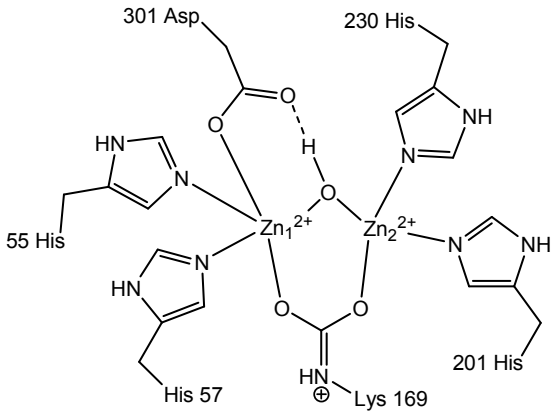

Figure 1-10. Representation of the active site of *Pseudomonas diminuta* phosphotriesterase.

The mechanism of phosphotriesterase catalyzed hydrolysis of **1.19** is proposed to occur as shown in Scheme 1-8. The reaction proceeds with full inversion of configuration at phosphorus indicating a concerted transfer of the phosphoryl group to the metal bound hydroxide.[118] It is suspected that an Asp-40 is involved in deprotonating the attacking hydroxide, as indicated by site-directed mutagenesis studies.[119] There is a prominent break in the Brønsted plot of log k vs. leaving group pK_a for the phosphotriesterase catalyzed hydrolyses of O,O-diethyl, O-aryl phosphates with a linear portion with β^{lg} of ~ 0 with leaving group pK_as < 7.[120] With leaving group pK_a > 7, a large negative β^{lg} = -1.8 is found, indicating a large amount of leaving group cleavage in the rate limiting step and likely no assistance by coordination with the metal ions. This break is explained by a change in rate limiting step from substrate binding with substrates having good leaving groups to the chemical cleavage process for substrates with poor leaving groups.

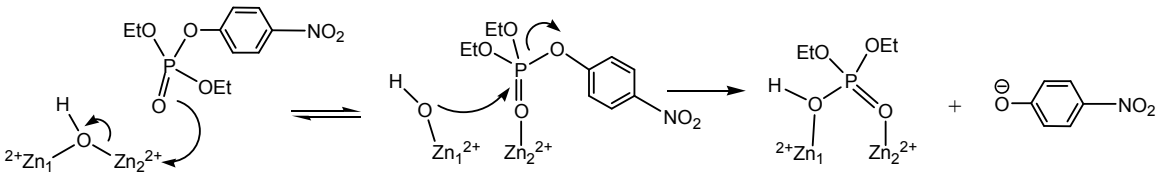

Scheme 1-8. Mechanism for the phosphotriesterase catalyzed hydrolysis of ethyl paraoxon (**1.19**, R = Et).

1.4.3. Metal ion catalysts for the phosphate triester hydrolysis

In order to discover the root of the immense catalytic power of phosphate cleaving enzymes, small molecule mimics of their active sites, containing one or more metal ions, have been synthesized. Zinc, which is often found in these enzymes, forms the catalytic core of these catalysts; however, other metal ions are often present.[121] It is thought that the lessons learned from the optimization of enzyme mimics will lead to the better understanding of how natural enzymes function. Experimenting with smaller, manageable systems is a simpler task, allowing the isolation of the effects of adjusting structural elements not accessible in enzymes. Designing these small molecule mimics is a challenge, as they must incorporate structural elements of the enzyme active site as well as accommodating metal binding.

Metal ions, forming the catalytic core of these enzymes and their mimics, are known to catalyze the hydrolysis of esters,[5] amides,[122] and phosphorus esters.[123] Typically, these hydrolyses involve the catalytically active $M^{x+}(^{-}OH)$ with the metal ion serving three possible purposes.[12,124] These are: (1) by coordinating a solvent molecule, the electropositive metal ion reduces its pK_a so that the nucleophilic hydroxide can be formed at near-neutral pH; (2) activating the P=O or C=O group through metal

coordination, thereby increasing its electrophilicity; and (3) accelerating the breakdown of any intermediates that might form through coordinating the leaving group and assisting in its departure.

There is a massive amount of research into the mechanisms of models of mononuclear and dinuclear zinc phosphoesterases involving the cleavage of naturally occuring monoesters and diesters including DNA and RNA substrates and their models,[125] however they will not be discussed here. Instead, this work will focus on catalysts for triester hydrolysis. These catalysts are designed with practical applications in mind, where gains in catalytic efficiency will translate into shorter reaction times for hazardous material decomposition.

Although there was some early success in the use of metal ions for the hydrolysis of P=O phosphate triesters,[126] it is apparent that water is not the ideal solvent for these reactions. While it is required as a reagent in hydrolysis, in the bulk it heavily solvates the metal ion, impeding substrate-catalyst interaction. Neutral phosphate triesters also have poor solubility in water. Ultimately, the $M^{x+}(^{-}OH)$ is a poor catalyst in water, with rate enhancements typically not extraordinary.

The metal ion-catalyzed hydrolysis reactions of P=S phosphorothioates are less studied than their P=O counterparts, and only a few examples are known. Cu^{2+} was found to hydrolyze parathion (**1.20**), accelerating the reaction by a modest factor of 20.[127] Improved catalysis was found with the softer metal ions Hg^{2+} and Pb^{2+} which were found to catalyze the hydrolysis of a wider range of pesticides (malathion **1.17**, fenitrothion **1.18**, methyl parathion **1.20** and others), accelerating by a factor of $10^{2\text{-}3}$.[128] The

drawback to using these metals is obvious, as they are themselves toxic.

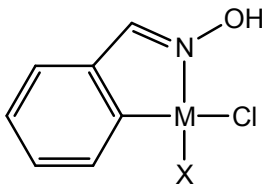

$M = Pt^{2+}, Pd^{2+}$
X = Py, DMSO

1.38

The most successful catalysts yet developed for phosphorothioate hydrolysis are the orthometalated complexes of Pt^{2+} and Pd^{2+} (**1.38**) developed by Ryabov and co-workers, similar to their enantioselective catalysts for acyl derivative hydrolysis discussed earlier.[129] The catalysis is pH dependent, showing higher accelerations at higher pHs, and plateaus at pHs > 7.9, the pK_a for ionization of the ketoxime group of the metal ligand. This is required for the proposed mechanism (Scheme 1-9) featuring the ketoxime group, which when deprotonated acts as a supernucleophile. The proposed mechanism is preliminary, and does not reveal any details about whether the nucleophilic attack and leaving group departure are concerted or stepwise, or any details about how the sulfur dissociates from the metal centre. While mechanistic details are not complete, the catalysis is quite impressive, with the platinum complex accelerating the reaction 10^9-fold over the background reaction at pH 8.5.

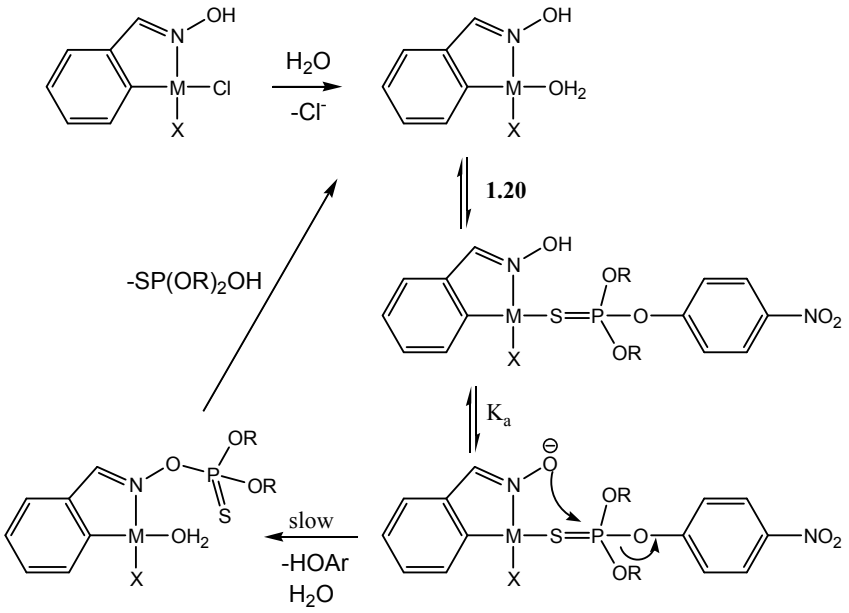

Scheme 1-9. Proposed reaction mechanism for the hydrolysis of parathion catalyzed by a cyclometalated complex. M = Pt(II) or Pd(II), X = Py, DMSO.

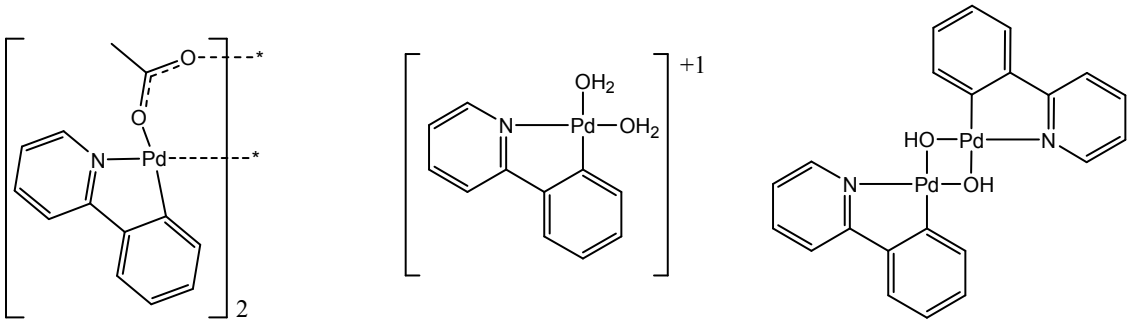

1.39 **1.40** **1.41**

This work was expanded upon by Gabbaï and coworkers[130] with the dimeric palladacycle acetate complex **1.39** that shows high reactivity toward the hydrolysis of methyl parathion **1.20** (R = Me). These catalysts do not feature the internal ketoxime supernucleophile, indicating that this internal nucleophile is not required for impressive catalysis of the hydrolysis of this type of substrate. In neutral pH conditions, the reaction is first order in catalyst and substrate, consistent with the catalytically active species

being the diaqua monomer **1.40** (Scheme 1-10). The reaction has large, negative entropy of activation which is attributed to a rate determining substrate binding step, as ligand exchange mechanisms of square planar Pd(II) complexes occur via an associative mechanism with large entropic costs.[131] This is followed by a fast nucleophilic attack and leaving group expulsion.

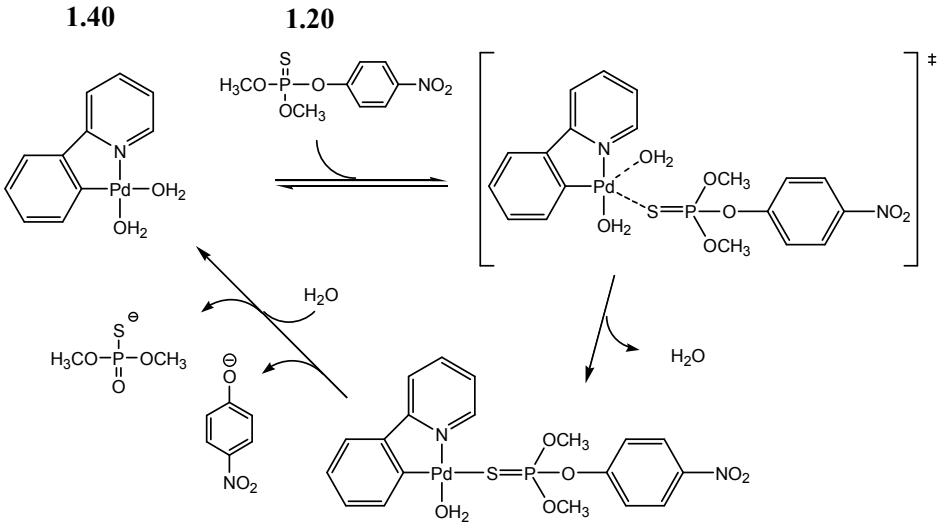

Scheme 1-10. Hydrolysis of **1.20** (R = Me) catalyzed by dissociated palladacycle monomer **1.40** in neutral pH conditions.

In alkaline conditions the reactions proceed with a greater rate, however the kinetics display a half-order dependence on the catalyst concentration, consistent with the active catalyst monomer being in equilibrium with an inactive dimer (**1.41**). It is proposed that the reaction proceeds with the nucleophilic attack of a metal bound hydroxide (Scheme 1-11). To explain the large, negative entropy of activation, the authors propose a substrate binding event concurrent with the nucleophilic attack. Throughout the range of pHs tested, the authors report no evidence of any phosphorane

intermediate present along the reaction pathway.

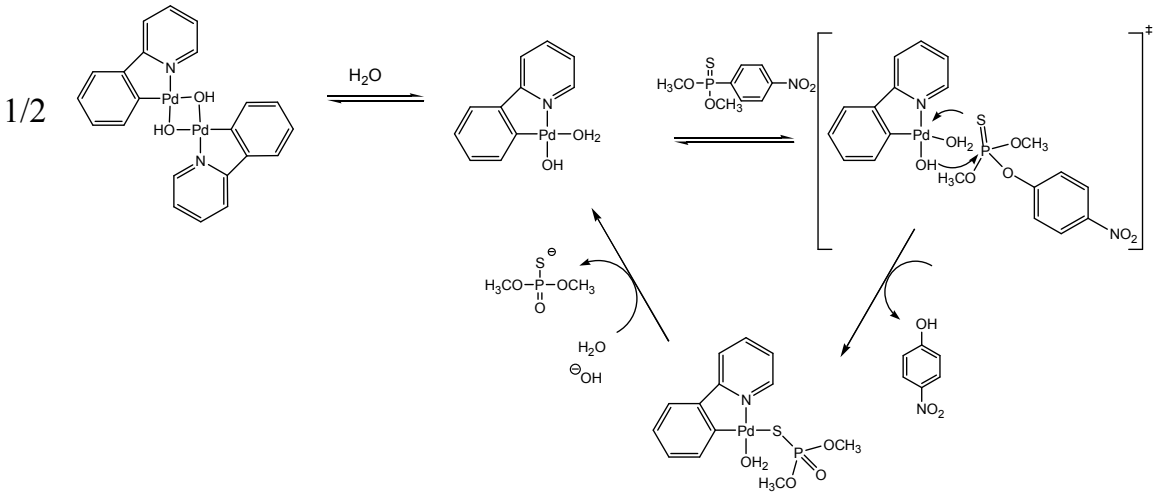

Scheme 1-11. Catalytic cycle for the hydrolysis of methyl parathion catalyzed by the dissociated palladacycle monomer of **1.41**.

1.4.4. Metal ion catalysts for phosphate triester alcoholysis

Our laboratory has extensively studied the metal-ion catalyzed methanolysis reactions of phosphate monoesters, diesters and triesters.[45,85,104,105,124,132] Methanol is advantageous over water as a reaction medium as the metal ions are not as heavily solvated, and the binding of anionic and neutral substrates is enhanced. It also avoids the formation of metal hydroxide oligomers and precipitates that are common in water. For the metal-catalyzed hydrolysis reactions of phosphate triesters in particular, the product is a hydroxy-diester, which when deprotonated can bind to, and inhibit, the catalyst. The product of phosphate triester methanolysis is another neutral triester, and thus substantially less inhibitory. It has been argued that a low-dielectric medium better mimics enzyme active sites,[133] which makes methanol attractive for biomimetic studies.

As we have seen in previous sections, La^{3+} is a potent catalyst for the methanolysis of carboxylate esters. La^{3+} is also a catalyst for phosphate triester methanolysis, with the $La^{3+}{}_2(^{-}OMe)_{2,3,4}$ dimers being the active forms of the catalyst. The rate acceleration is impressive, being 10^9-fold over the base reaction at neutral pH.[134] The La^{3+}-catalyzed methanolysis of O-aryl O,O′-dialkyl phosphate triesters has a linear log k_2 *vs.* $pK_a{}^{lg}$ plot with a β^{lg} of -1.43,[104] much steeper than the β^{lg} of the methoxide-promoted reaction (-0.70). This indicates a much greater degree of bond cleavage in the rate determining transition state, and is characteristic of a free aryloxide leaving group departure, with no metal ion involvement. The β^{eq} (-1.87)[97] for the equilibrium of O,O-diethyl O-aryl phosphates **1.30** (see Section 1.3.2.3) and its hydrolysis products can then be used to calculate a Leffler's α of $\beta^{lg}/\beta^{eq} = 0.76$, indicating that the leaving group bond scission has progressed 76% of the way from starting material to products. This is consistent with a concerted process with a large degree of leaving group departure in the transition state (Scheme 1-12-A), or a step-wise process in which leaving group departure is rate limiting (Scheme 1-12-B, $k_1 > k_2$).

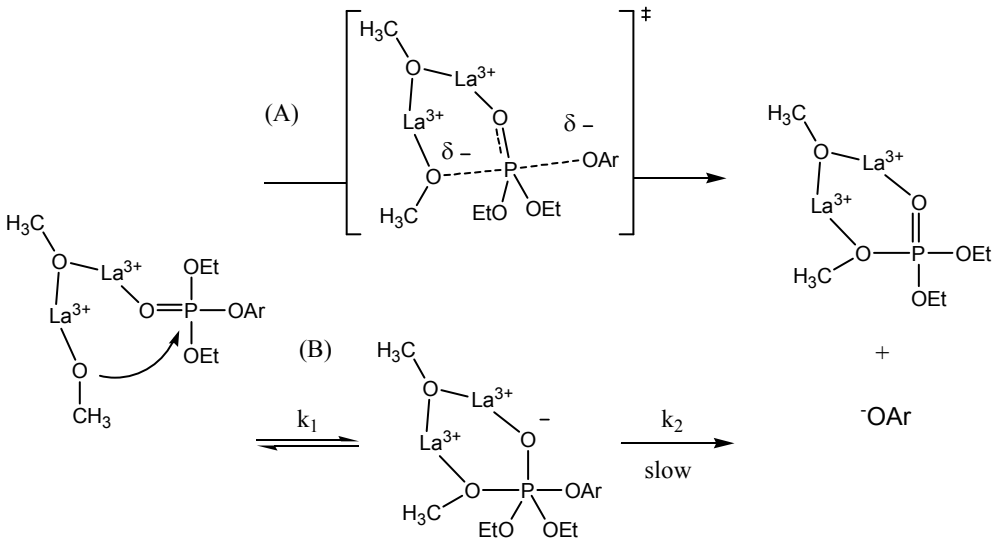

Scheme 1-12. Concerted and step-wise mechanism for **1.30** methanolysis catalyzed by La^{3+} in methanol.

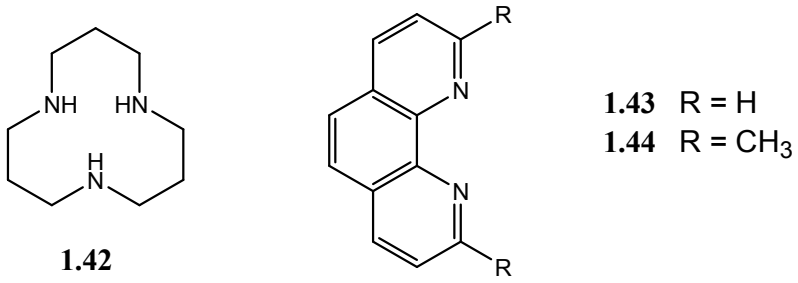

1.42

1.43 R = H
1.44 R = CH_3

The Zn^{2+} complexes of ligands **1.42**, **1.43** and **1.44** have also been shown to catalyze the methanolysis of phosphate triesters.[135] The active catalyst (MeO^-):Zn^{2+}:**1.43** has a propensity to dimerize to the catalytically inactive **1.43**:Zn^{2+}:($^-OMe)_2$:Zn^{2+}:**1.43** form, however the introduction of methyl groups at the 2 and 9 positions of the ligand (**1.44**) breaks up the dimers increasing the overall observed catalytic ability.

A linear Brønsted plot of log k_2 vs pK_a^{lg} plot for the methanolysis of **1.30** catalyzed by (MeO^-):Zn^{2+}:**1.42** has a similar large, negative β^{lg} of -1.12 and a calculated Leffler's α of 0.60.[104] This again signifies extensive P-O bond fission in the transition

state, but less so than in the case of the La^{3+} catalysis, a trend consistent with either a concerted reaction or rate determining leaving group cleavage. This reaction proceeds through a mechanism wherein the metal centre simultaneously binds the P=O group and delivers a nucleophilic methoxide.

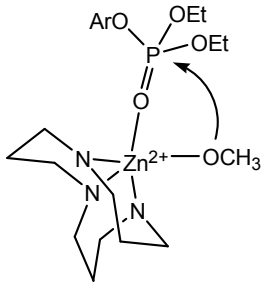

Scheme 1-13. Nucleophilic attack of methoxide on **1.30** catalyzed by Zn^{2+}:**1.42**.

La^{3+} is a hard cation in the Pearson 'hard soft' sense,[136] and interacts poorly with soft substrates such as P=S phosphorothioates and does not catalyze their methanolysis.[135a,137] Softer metals are more successful, with Zn^{2+}:**1.44** providing rate acceleration for the methanolysis of fenitrothion (**1.18**) of 1.3×10^6-fold. With an even softer metal complex, Cu^{2+}:**1.42**, the rate of methanolysis is accelerated by an impressive factor of 1.7×10^9.

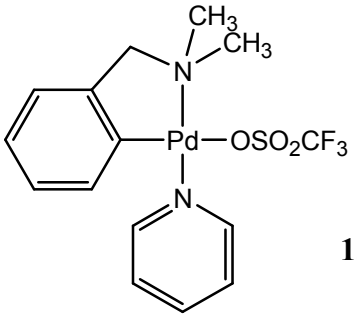

1.45:(Py):($^-$OTf)

Following the trend in increased methanolysis reactivity with softer metal ion catalysts, the next target for investigation was the *ortho*-palladated complex **1.45**,[138] similar to the complexes that had proven successful for the hydrolysis process by Ryabov and co-workers.[129] Upon dissolution it is suspected that the triflate readily dissociates from **1.45**:(¯OTf):(Py) and is replaced by methanol (Scheme 1-14). In acidic conditions, some pyridine dissociates and is protonated, and is replaced by methanol forming **1.45**: $(MeOH)_2$. Above the kinetic pK_a of 10.4, a bound methanol deprotonates, forming the active catalysts **1.45**:(¯OMe):(Py) or **1.45**:(¯OMe):(MeOH). The latter exists in an equilibrium with the catalytically inactive dimer $(\mathbf{1.45})_2(OMe)_2$.

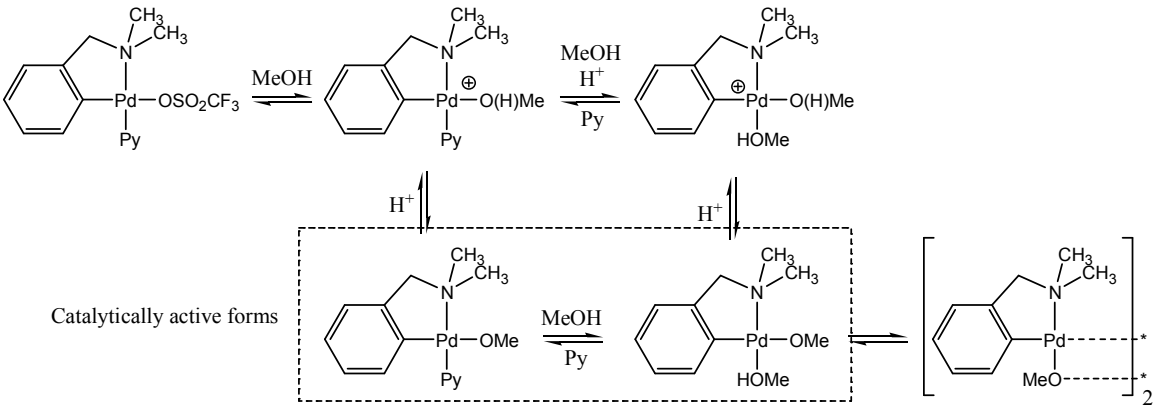

Scheme 1-14. Solution behavior of **1.45** in methanol.

The mechanism proposed for the catalyzed methanolysis of phosphorothioate triesters, which is consistent with a subsequently observed common species rate depression in [pyridine], involves substrate coordination to **1.45**:(¯OMe)[(Py) or (MeOH)] without methanol or pyridine departure, forming a 4-coordinate palladium intermediate (Scheme 1-15). Substrate binding is evident as this catalyst is inert toward the corresponding P=O triesters. There is a catalytic ${}^{s}_{s}pK_a$ of 10.8 associated with this

reaction corresponding to the deprotonation of a metal bound methanol, forming a nucleophilic internal methoxide that attacks the metal bound phosphorothioate. The full mechanism was not completely elucidated, and further work was needed.

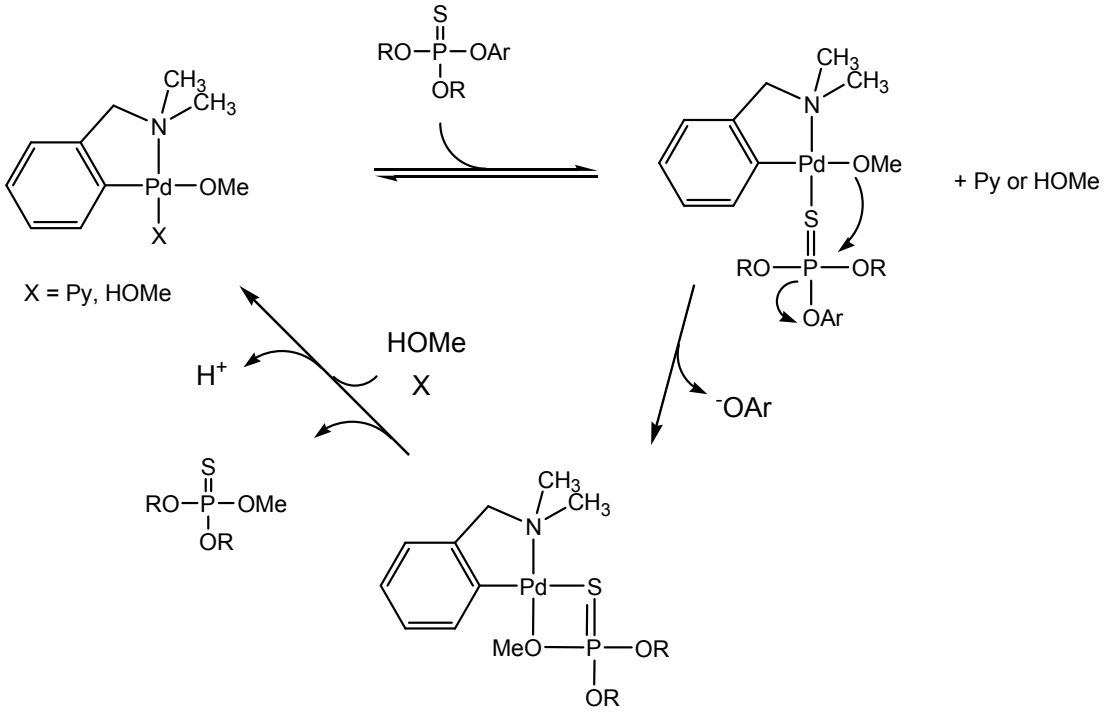

Scheme 1-15. Proposed mechanism for the methanolysis of a phosphorothioate triester catalyzed by **1.45**:($^{-}$OMe):[(HOMe) or (Py)]. This is slightly different than the published[138] to account for a subsequently observed common species rate depression in added [pyridine].

1.5. Proposed Research

1.5.1. Kinetic resolution of racemic mixtures N-protected amino acid esters

Chirality is an important property, exemplified by the fact that nearly all natural products are chiral. The production of chiral drugs or natural products from achiral or

racemic source materials requires a method of isolating the desired enantiomer, preferably early in the synthetic procedure. Kinetic resolution, a method of isolating enantiomers through their different rates of reaction with a chiral catalyst, is one such method. As such, a great deal of effort has been spent on the development of asymmetric catalysts for the kinetic resolution of racemic mixtures.

Our group has experimented extensively with lanthanide ions in methanol directed to find efficient catalytic systems for the cleavage of carboxylate esters. Our aim, in this project, is to develop ligands to complex with the catalytic core of lanthanum ions to produce enantioselectivity in the catalytic cleavage of chiral esters and be of use in the kinetic resolution of these mixtures. For model substrates, we use Boc-protected *p*-nitrophenyl esters of glutamine and phenylalanine. In Chapter 2, we report our efforts in developing and improving catalysts and tuning reaction conditions for the kinetic resolution of these esters.

1.5.2. Computational investigation of the mechanism of solvolytic cleavage of phosphorothioate and phosphate esters

The solvolytic cleavage of phosphorus esters represents a rich and varied chemistry with the various mechanisms being highly dependent on their structure and substitution. We have seen that phosphates can react with concerted or step-wise mechanisms. Mechanistic details can be discovered using a variety of techniques, including linear free energy studies, kinetic isotope effects and the stereochemical analysis of products. These results are subject to interpretation, and do not conclusively

prove potential mechanisms, but they can eliminate mechanisms inconsistent with the results.

Linear free energy relationships, such as Brønsted β^{nuc}, β^{lg} and β^{eq}, are important concepts in uncovering a reaction mechanism. In Chapter 3 we present a computational method for predicting β^{eq} and in Chapter 4 we present a computational method for predicting β^{lg}. Also presented in Chapter 4 is a computational mechanistic work conducted on the base-promoted methanolysis and hydrolysis of phosphates and phosphorothioates with specific attention paid to the concerted or step-wise nature of the reaction.

1.5.3. Computational insights into the mechanism of phosphorothioate and thioamide methanolysis catalyzed by a palladacycle

The catalytic activity of a palladacycle **1.45** toward the hydrolysis of phosphorothioates has recently been documented, however in water the complex has poor solubility and suffers from product inhibition. The process in methanol has many advantages, and work from our laboratory has shown that the catalyst can accelerate the rate of P=S phosphorothioate methanolysis by an impressive factor of 10^9. In Chapter 5, a computational investigation into the mechanism of this catalysis is presented. The reaction mechanism is mapped for two substrates, and the results are used to explain the experimental observations. A preliminary mechanistic investigation into the palladacycle catalyzed methanolysis of thioamide substrates is presented in Chapter 6.

1.6. References

1) Maxwell, C. I.; Shaw, K.; Samuleev, P. V.; Neverov, A. A.; Brown, R. S. *Org. Biomol. Chem.* **2008**, *6*, 2796.

2) a) Edwards, D. R.; Maxwell, C. I.; Harkness, R. W.; Neverov, A. A.; Mosey, N. J.; Brown, R. S. *J. Phys. Org. Chem,* Published online, July 31, 2011; DOI:10.1002/poc.1903. b) Maxwell, C. I.; Liu, C. T.; Neverov, A. A.; Mosey, N. J.; Brown, R. S. *J. Phys. Org. Chem*. Published online, October 21, 2011; DOI:10.1002/poc.1938.

3) Liu, C. T.; Maxwell, C. I.; Edwards, D. R.; Neverov, A. A.; Mosey, N. J.; Brown, R. S. *J. Am. Chem. Soc.* **2010**, *132,* 16599.

4) Liu, C. T.; Maxwell, C. I.; Pipe, S. G.; Neverov, A. A.; Mosey, N. J.; Brown, R. S. *Submitted to J. Am. Chem. Soc.*

5 a) Ranu, B. C.; Dutta, P.; Sarkar, A. *J. Org. Chem.* **1998**, *63,* 6027. b) Cacciapaglia, R.; DiStefano, S.; Kelderman, E.; Mandolini, L. *Angew. Chem. Int. Ed.* **1999**, *38,* 348.

6) Barrett, A.G.M.; Braddock, D.C. *J. Chem. Soc. Chem. Commun.* **1997**, 351.

7) Neverov, A. A.; Brown R. S. *Can. J. Chem.* **2000**, *78,* 1247.

8) a) Brown, R. S.; Neverov, A. A. *J. Chem. Soc. Perkin Trans. 2,* **2002**, 1039. b) Neverov, A.A.; MacDonald, T.; Gibson, G.; Brown, R.S. *Can. J. Chem.* **2001**, *79,* 1704.

9) Gibson, G. T. T.; Neverov, A. A.; Brown, R. S. *Can. J. Chem.* **2003**, *81,* 495.

10) Gibson, G. T. T.; Mohamed, M. F.; Neverov, A. A.; Brown, R. S. *Inorg. Chem.* **2006**, *45,* 7891.

11) Brown, R. S.; Neverov, A. A.; Tsang, J. S. W.; Gibson, G. T. T.; Montoya-Pelaez, P. J. *Can. J. Chem.* **2004**, *82,* 12.

12) Brown, R. S.; Neverov, A. A. *Adv. Phys. Org. Chem.* **2007**, *42,* 271.

13) a) Blaser, H. U.; Spindler, F.; Studer, M. *Appl. Catal. A.* **2001**, *221,* 119. b) Wu, G.; Huang, M. *Chem. Rev.* **2006**, *10,* 2596.

14) Zaugg, H. E. *J. Am. Chem. Soc.* **1955**, *77,* 2910.

15) Gnas, Y.; Glorius, F. *Synthesis.* **2006**, 1899.

16) a) Moss, G. P. *Pure Appl. Chem.* **1996**, *68,* 2193. b) Fogassy, E.; Nogradi, M.; Kozma, D.; Egri, G.; Palovics, E.; Kiss, V. *Org. Biomol. Chem.* **2006**, *4,* 3011. c) Vedejs, E.; Jure, M. *Angew. Chem. Int. Ed.* ***2005****, 117,* 4040. d) Breuer, M.; Ditrich, K.; Habicher, T.; Hauer, B.; Keβeler, M.; Stürmer, R.; Zelinski, T. *Angew. Chem. Int. Ed.* **2004**, *43,* 788. d) Robinson, D. E. J. E.; Bull, S. D. *Tetrahedron: Asymmetry.* **2003**, *14,* 1407.

17) Kagan, H. B.; Fiaud, J. C. *Top. Stereochem.* **1988**, *18,* 249.

18) Vedejs, E.; Jure, M. *Angew. Chem. Int. Ed.* **2005**, *44,* 3974.

19) Marckwald, W.; McKenzie, A. *Ber. Dtsch. Chem. Ges.* **1899**, *32,* 2130.

20) Dakin, H. D. *J. Physiol.* **1904**, *30,* 253.

21) Gawley, R. E. *J. Org. Chem.* **2006**, *71,* 2411.

22) Krow, G.; Hill, R. K. *Chem. Commun.* **1968**, 430.

23) Horeau, A. *Tetrahedron Lett.* **1969**, 3124.

24) Martin, V. S.; Woodard, S. S.; Katsuki, T.; Yamada, Y.; Ikeda, M.; Sharpless, K. B. *J. Am. Chem. Soc.* **1981**, *103,* 6237.

25) Jacobsen, E. N. *Acc. Chem. Res.* **2000**, *33,* 421.

26) a) Miyano, L. S.; Lu, L. D. L.; Viti, S. M.; Sharpless, K. B. *J. Org. Chem.* **1983**, *48,* 3611. b) Hang, J.; Deng, L. *Bioorg. Med. Chem. Lett.* **2009**, *19,* 3856.

27) a) Rosas-Hernandez, A.; Vargas-Malvaez, E.; Martin, E.; Crespi, L.; Bayon, J. C. *J. Mol. Catal. A.* **2010**, *328,* 68. b) Jansat, S.; Gomez, M.; Philippot, K.; Muller, G.; Guiu, E.; Claver, C.; Castillon, S.; Chaudret, B. *J. Am. Chem. Soc.* **2004**, *126,* 1592.

28) Pellissier, H. *Adv. Synth. Catal.* **2011**, *353,* 1613.

29) Davis, B. G.; Boyer, V. *Nat. Prod. Rep.* **2001**, *18,* 618.

30) Theil, F. *Chem. Rev.* **1995**, *95,* 2203.

31) Theil, F. *Catal. Today.* **1994**, *22,* 517.

32) Izawa, T.; Terao, Y.; Suzuki, K. *Tetrahedron: Asymmetry*. **1997**, *8,* 2645.

33) Kielbasinski, P.; Goraleczyk, P.; Mikolajczyk, M.; Wieczorek, W.; Majznere, W. R. *Tetrahedron: Asymmetry*. **1998**, *9,* 2641.

34) Garcia-Urdiales, E.; Rebolledo, F.; Gotor, V. *Tetrahedron Asymmetry*. **1999**, *10,* 721.

35) Chen, C. S.; Sih, C. J. *Angew. Chem.* **1989**, *101,* 711.

36) Fadnavis, N. W.; Koteshwar, K. *Tetrahedron: Asymmetry*. **1997**, *8,* 337.

37) Miyazawa, T.; Onishi, K.; Murashima, T.; Yamada, T.; Tsai, S-W. *Tetrahedron: Asymmetry*. **2005**, *16,* 2569.

38) a) Sakakura, A.; Umemura, S.; Ishihara, K. *Synlett.* **2009**, *10,* 1647. b) Narasaka, K.; Kanai, F.; Okudo, M.; Miyoshi, N. *Chem. Lett.* **1989**, 1187. c) Tian, S.-K.; Chen, Y.; Hang, J.; Pang, L.; McDaid, P.; Deng, L. *Acc. Chem. Res.* **2004**, *37,* 621. d) Ishihara, K.; Kosugi, Y.; Umemura, S.; Sakakura, A. *Org. Lett.* **2008**, *10,* 3191.

39) a) Shiina, I.; Nakata, K.; Onda, Y.-s. *Eur. J. Org. Chem.* **2008**, 5887. b) Shiina, I.; Nakata, K.; Ono, K.; Onda, Y.-s.; Itagaki, M. *J. Am. Chem. Soc.* **2010**, *132,* 11629.

40) Ward, T. *Chem. Eur. J.* **2005**, *11,* 3798.

41) Tokunaga, M.; Aoyama, H.; Kiyosu, J.; Shirogane, Y.; Iwasawa, T.; Obora, Y.; Tsuji, Y. *J. Organometal. Chem.* **2007**, *692,* 472.

42) Carey, F. A.; Sundberg. R. J. *Advanced Organic Chemistry, Fourth Edition. Part A: Structure and Function.* **2000**, Kluwer Academic/ Plenum Publishers, New York

43) Pfaltz, A.; Drury, W. J. *Proc. Natl. Acad. Sci*. **2004**, *101,* 5723.

44) Dro, C.; Bellemin-Laponnaz, S.; Welter, R.; Gade, L.H. *Angew. Chem. Int. Ed.* **2004**. *43,* 4479.

45) Neverov A. A.; Lu, Z-L.; Maxwell, C. I.; Mohamed, M. F.; White, C. J.; Tsang, J. S. W.; Brown, R. S. *J. Am. Chem. Soc.* **2006**, *128,* 16398.

46) Ryabov, A. D.; Kazankov, G. M.; Kurzeev, S. A.; Samuleev, P. V.; Polyakov, V. A. *Inorg. Chim. Acta.* **1998**. *280,* 57.

47) a) Westheimer, F. H. *Science*. **1987**, *235,* 1173. b) Westheimer, F. H. *Chem. Rev.* **1981**, *81,* 313. c) Hengge, A. C. *Adv. Phys. Org. Chem.* **2005**, *40,* 49. d) Hengge, A. C.; Onyido, I. *Curr. Org. Chem.* **2005**, *9,* 61.

48) a) Toy, A. D. F.; Walsh, E. N. In *Phosphorus Chemistry in Everyday Living,* 2nd Edition. American Chemical Society, Washington D.C. **1987.** b) Gallo, M. A.; Lawryk, N. J. In *Organic Phosphorus Pesticides. The Handbook of Pesticide Toxicology,* Academic Press, San Diego CA. **1991.**

49) a) Quin, L. D. *A Guide to Organophosphorus Chemistry.* Wiley-Interscience, New York, 2000. b) Yang, Y.-C.; Baker, J. A.; Ward, J. R. *Chem. Rev.* **1992**, *92,* 1729. c) Yang, Y.-C. *Acc. Chem. Res.* **1999**, *32,* 109.

50) a) Koelle, G. B.; Gilman, A. *Pharmacol. Rev.* **1949**, *1,* 166.

51) George, K. M.; Schule, T.; Sandoval, L. E.; Jennings, L. L.; Taylor, P.; Thompson, C. M. *J. Biol. Chem.* **2008**, *278,* 45512.

52) Reigart, J. R.; Roberts, J. R. *Recognition and Management of Pesticide Poisonings,* Publication No. 735-R-98-003, United States Environmental Protection Agency, Washington D. C.

53) Smith, B. M. *Chem. Soc. Rev.* **2008**, *37,* 470.

54) Morales-Rojas, H.; Moss, R. A. *Chem. Rev.* **2002**, *102,* 2497.

55) Sultatos, L. G. *J. Toxicol. Environ. Health.* **1994**, *43,* 271.

56) Buckley, N. A.; Roberts, D.; Eddleston, M. *Br. Med. J.* **2004**, *329,* 1231.

57) Mutch, E.; Blain, P. G.; Williams, F. M. *Toxicol. Lett.* **1999**, *107,* 177.

58) Agrawal, A.; Sharma, B. *Int. J. Biol. Med. Res.* **2010**, *1,* 90.

59) Bonner, M. R.; Coble, J.; Blair, A.; Freeman, L. E. B.; Hoppin, J. A.; Sandler, D. P. Alavanja, C. R. *Am. J. Epidemiol.* **2007**, *166,* 1023.

60) Rauh, V. A.; Garfinkel, R.; Perera, F. P.; Andrews, H. F.; Hoepner, L.; Barr, D. B.; Whitehead, R.; Tang, D.; Whyatt, R. W. *Pediatrics.* **2006**, *118,* 1845.

61) Menger, F. M.; Tsuno, T. *J. Am. Chem. Soc.* **1989**, *111,* 4903.

62) Cleland, W. W.; Hengge, A. C. *Chem. Rev.* **2006**, *106,* 3252.

63) Vetter, I. R.; Wittighopher, A. *Q. Rev. Biophys.* **1999**, *32,* 1.

64) a) Wolfenden, R. *Chem. Rev.* **2006**, *106,* 3379. b) Wolfenden, R.; Snider, M. J.; *Acc. Chem. Res.* **2001**, *34*, 938. c) Wolfenden, R.; Ridgeway, C.; Young, G. *J. Am. Chem. Soc.* **1998**, *120,* 833.

65) IUPAC nomenclature: Guthrie, R. D. *Acc. Chem. Res.* **1989**, *22,* 343.

66) Leffler, J. E.; Grunwald, E. *Rates and Equilibria of Organic Reactions as treated by Statistical, Thermodynamic and Extrathermodynamic Methods.* **1989**, Wiley, N. Y.

67) a) Kirby, A. J.; Varvolglis, G. *J. Am. Chem. Soc,* **1967**, *89,* 415. b) Butcher, W. W.; Westheimer, F. H. *J. Am. Chem. Soc.* **1955**, *77,* 2420.

68) Kirby, A. J.; Jencks, W. P. *J. Am. Chem. Soc.* **1965**, *87,* 3209.

69) Hengge, A. C.; Edens, W. A.; Elsing, H. *J. Am. Chem. Soc.* **1994**, *116,* 5045.

70) a) Buchwald, S. L.; Friedman, J. M.; Knowles, J. R. *J. Am. Chem. Soc.* **1984**, *106,* 4911. b) Buchwald, S. L.; Knowles, J. R. *J. Am. Chem. Soc.* **1982**, *104,* 1438.

71) Bourne, N.; Williams, A. *J. Am. Chem. Soc.* **1984**, *106,* 7591.

72) Friedman, J. M.; Freeman, S.; Knowles, J. R. *J. Am. Chem. Soc.* **1988**, *110,* 1268.

73) Åqvist, J.; Kolmodin, K.; Florian, J.; Warshel, A. *Chem. Biol.* **1999**, *6,* R71.

74) Catrina, I. E.; Hengge, A. C. *J. Am. Chem. Soc.* **1999**, *121*, 2156.

75) Purcell, J.; Hengge, A. C. *J. Org. Chem.* **2005**, *70,* 8437.

76) a) Cullis, P. M.; Iagrossi, A. *J. Am. Chem. Soc.* **1989**, *108,* 7870. b) Burgess, J.; Blundell, N; Cullis, P. M.; Hubbard, C. D.; Misra, R. *J. Am. Chem. Soc.* **1988**, *110,* 7900.

77) Menger, F. M.; Ladika, M. J. *J. Am. Chem. Soc.* **1987**, *109,* 3145.

78) Brown, D. M.; Usher, D. A. *J. Chem. Soc.* **1965**, 6558.

79) a) Kirby, A. J.; Younas, M. *J. Chem. Soc. (B)*. **1970**, 1165. b) Khan, S. A.; Kirby, A. J. *J. Chem. Soc. (B)*. **1970**, 1172.

80) Cassano, A. G.; Anderson, V. E.; Harris, M. E. *J. Am. Chem. Soc.* **2002**, *124,* 10965.

81) Ba-Saif, S. A.; Davis, A. M.; Williams, A. *J. Org. Chem.* **1989**, *54,* 5483.

82) a) Haake, P. C.; Westheimer, F. H. *J. Am. Chem. Soc.* **1961**, *83,* 1102. b) Segal, Y.; Granoth, I. *J. Am. Chem. Soc.* **1978**, *100,* 5130.

83) Davis, A. M.; Hall, A. D.; Williams, A. *J. Am. Chem. Soc.* **1988**, *110,* 5105.

84) Lönnberg, H.; Strömberg, R.; Williams, A.; *Org. Biomol. Chem.* **2004**, *2,* 2165.

85) Neverov, A. A.; Sunderland, N. E.; Brown, R. S. *Org. Biomol. Chem.* **2005**, *3,* 65.

86) Gerratana, B.; Sowa, G. A.; Cleland, W. W. *J. Am. Chem. Soc.* **2000**, *122,* 12615.

87) a) Oivanen, M.; Schnell, R.; Pfleidere, W.; Lönnberg, H. *J. Org. Chem.* **1991**, *56,* 3623. b) Perreault, D. M.; Anslyn, E. V. *Angew. Chem. Int. Ed. Engl.* **1997**, *36,* 432.

88) Järvinen, P.; Oivanen, M.; Lönnberg, H. *J. Org. Chem.* **1991**, *56,* 5396.

89) a) Zhou, D.-M.; Taira, K. *Chem. Rev.* **1998**, *98,* 991. b) Wilkie, J.; Gani, D. *J. Chem. Soc., Perkin Trans. 2.* **1996**, 783.

90) a) Rosta, E.; Kamerlin, S. C. L.; Warshel, A. *Biochemistry.* **2008**, *47,* 3725. b) Alkherraz, A.; Kamerlin, S. C. L.; Feng, G.; Sheikh, Q. I.; Warshel, A.; Williams, N. H. *Faraday Discuss.* **2010**, *145,* 281.

91) a) Loverix, S.; Winqvist, A.; Strömberg, R.; Steyaert, J. *Chem. Biol.* **2000**, *7,* 651. b) Holtz, K. M.; Catrina, I. E.; Hengge, A. C.; Kantrowitz, E. R. *Biochemistry.* **2000**, *39,* 9451. c) Lassila, J. K.; Herschlag, D. *Biochemistry.* **2008**, *47,* 12853.

92) a) Nakamaye, K.; Eckstein, F. *Nucleic Acids Res.* **1986**, *14,* 9679. b) Hollfelder, F.; Herschlag, D. *Biochemistry*. **1995**, *34,* 12255.

93) Almer, H.; Stromberg, R. *J. Am. Chem. Soc.* **1996**, *118,* 7921.

94) Khan, S. A.; Kirby, A. J. *J. Chem. Soc. B.* **1970**, 1172.

95) Rowell, R. and Gorenstein, D. G.; *J. Am. Chem. Soc.* **1981**, *103,* 5894.

96) Williams, A. *Acc. Chem. Res.* **1984**, *17,* 425.

97) Ba Saif, S. A.; Williams, A. *J. Org. Chem.* **1988**, *53,* 2204.

98) a) Ba-Saif, S. A.; Waring, M. A.; Williams, A. *J. Am. Chem. Soc.* **1990**, *112,* 8115. b) Ba-Saif, S. A.; Waring, M. A.; Williams, A. *J. Chem. Soc. Perkins Trans 2.* **1991**, 1653.

99) a) Thea, S.; Williams, A. *Chem. Soc. Rev.* **1986**, *15,* 125. b) Leffler, J. E. *Science.* **1953**, *117,* 340.

100) a) Iché-Tarrat, N.; Barthelat, J.-C.; Rinaldi, D.; Vigroux, A. *J. Phys. Chem. B.* **2005**, *109,* 22570. b) Tarrat, N. *THEOCHEM.* **2010**, *941,* 56.

101) Jencks, W. P. *Acc. Chem. Res.* **1980**, *13,* 161.

102) Hong, S.-B.; Raushel, F. M. *Biochemistry*. **1996**, *35,* 10904.

103) Omakor, J. E.; Onyido, I.; vanLoon, G. W.; Buncel, E. *J. Chem. Soc., Perkin Trans. 2.* **2001**, 324.

104) Liu, T.; Neverov, A. A.; Tsang, J. S. W.; Brown, R. S. *Org. Biomol. Chem.* **2005**, *3,* 1525.

105) Maxwell, C.; Neverov, A. A.; Brown, R. S. *Org. Biomol. Chem.* **2005**, *3,* 4329.

106) Coleman, J. E. *Annu. Rev. Biophys. Biomol. Struct.* **1992**, *21,* 441.

107) a) Hollfelder, F.; Herschlag, D. *Biochemistry*. **1995**, *34,* 12255. b) Weiss, P. M.; Cleland, W. W. *J. Am. Chem. Soc.* **1989**, *111,* 1928. c) O'Brien, P. J.; Herschlag, D. *J. Am. Chem. Soc.* **1999**, *121,* 11022.

108) Zalatan, J. G.; Herschlag, D. *J. Am. Chem. Soc.* **2006**, *128,* 1293.

109) a) Williams, N. H.; Cheung, W.; Chin, J. *J. Am. Chem. Soc.* **1998**, *120,* 8079. b) Humphry, T.; Iyer, S.; Iranzo, O.; Morrow, J. R.; Richard, J. P.; Paneth, P.; Hengge, A. C. *J. Am. Chem. Soc.* **2008**, *130,* 17858. c) Padovani, M.; Williams, N. H.; Wyman, P. *J. Phys. Org. Chem.* **2004**, *17,* 472.

110) Humphry, T.; Forconi, M.; Williams, N. H.; Hengge, A. C. *J. Am. Chem. Soc.* **2004**, *126,* 11864.

111) Dumas, D. P.; Caldwell, S. R.; Wild, J. R.; Raushel, F. M. *J. Biol. Chem.* **1989**, *264,* 19659.

112) Scanlan, T. S.; Reid, R. C. *Chem. Biol.* **1995**, *2,* 71.

113) Danarski, W. J.; Dumas, D. P.; Heitmeyer, D. P.; Lewis, V. E.; Raushel, F. M. *Biochemistry.* **1989**, *28,* 4650.

114) Shim, H.; Hong, S.-B.; Raushel, F. M. *J. Biol. Chem.* **1998**, *273,* 17445.

115) Vanhooke, J. L.; Benning, M. M.; Raushel, F. M.; Holden, H. M. *Biochemistry***.** **1996**, *35,* 6020.

116) a) Omburo, G. A.; Mullins, L. S.; Raushel, F. M. *Biochemistry.* **1993**, *32,* 9148. b) Hong, S.-B.; Raushel, F. M. *Biochemistry.* **1996**, *35,* 10904.

117) Dumas, D. P.; Raushel, F. M. *J. Biol. Chem.* **1990**, *35,* 21498.

118) Lewis, V. E.; Donarski, W. J.; Wild, J. R.; Raushel, F. M. *Biochemistry,* **1988**, *27,* 1591.

119) Aubert, S. D.; Li, Y.; Raushel, F. M. *Biochemistry.* **2004**, *43,* 5707.

120) Caldwell, S. R.; Newcomb, J. R.; Schlecht, K. A.; Raushel, F. M. *Biochemistry.* **1991**, *30,* 7438.

121) Parkin, G. *Chem. Rev.* **2004**, *104,* 699.

122) a) Fife, T. H.; Bembi, R. *J. Am. Chem. Soc.* **1993**, *115,* 11358. b) Parac, T. N.; Kostic, N. M. *J. Am. Chem. Soc.* **1996**, *118,* 51.

123) a) Blasko, A.; Bruice, T. C. *Acc. Chem. Res.* **1999**, *32,* 475. b) Williams, N. H.; Takasaki, B.; Wall, M.; Chin, J. *Acc. Chem. Res.* **1999**, *32,* 485. c) Morrow, J. R.; Burttrey, L. A. ; Shelton, V. M.; Berback, K. M. *J. Am. Chem. Soc.* **1992**, *114,* 1903. d) Morrow, J. R.; Buttrey, L. A. Berback, K. A. *Inorg. Chem.* **1992**, *31,* 16. e) Liu, C. T.; Neverov, A. A.; Brown, R. S. *J. Am. Chem. Soc.* **2008**, *130,* 13870.

124) Weston, J. *Chem. Rev.* **2005**, *105,* 2151.

125) a) Krämer, R. *Coord. Chem. Rev.* **1999**, *182,* 243. b) Hegg, E. L.; Burstyn, J. N. *Coord. Chem. Rev.* **1998**, *173,* 133. c) Morrow, J. R.; Iranzo, O. *Curr. Op. Chem. Biol.* **2004**, *8,* 192. d) Brown, R. S.; Lu, Z.- L.; Liu, C. T.; Tsang, W. Y.; Edwards, D. R.; Neverov, A. A. *J. Phys. Org. Chem.* **2010**, *23,* 1. e) Breslow, R.; Singh, S. *Bioorg. Chem.* **1988**, *16,* 408. f) Prince, R. H.; Stotter, D. A.; Wooley, P. R. *Inorg. Chim. Acta.* **1974**, *9,*

51. g) Chapman, W. H. (Jr.); Breslow, R. *J. Am. Chem. Soc.* **1995**, *117,* 5462. h) Iranzo, O.; Kovalevsky, A. Y.; Morrow, J. R.; Richard, J. P. *J. Am. Chem. Soc.* **2003**, *125,* 1988. i) Iranzo, O.; Elmer, T.; Richard, J. P.; Morrow, J. R. *Inorg. Chem.* **2003**, *42,* 7737.

126) a) Brown, R. S.; Zamkanei, M. *Inorg. Chim. Acta.* **1985**, *108,* 201. b) Gellman, S. H.; Petter, R.; Breslow, R. *J. Am. Chem. Soc.* **1986**, *108,* 2388. c) Bunton, C. A.; Scrimin, P.; Tecilla, P. *J. Chem. Soc. Perkin Trans. 2.* **1995**, 419. d) Hay, R. W.; Govan, N. *J. Chem. Soc. Chem. Commun.* **1990**, 714. e) Kenley, R. A.; Fleming, R. H.; Laine, R. M.; Tse, D. S.; Winterle, J. S. *Inorg. Chem.* **1984**, *23,* 1870. f) Menger, F. M.; Gan, L. H.; Johnson, E.; Durst, D. H. *J. Am. Chem. Soc.* **1987**, *107,* 2800. g) Klinkel, K. L.; Kiemele, L. A.; Gin, D. L.; Hagadorn, J. R. *Chem. Commun.* **2006**, 2919. h) Morrow, J. R.; Trogler, W. C. *Inorg. Chem.* **1989**, *28,* 2330. i) Scrimin, P.; Ghirlanda, G.; Tecilla, P.; Moss, R. A. *Langmuir* **1996**, *12,* 6235.

127) Ketallaar, J. A. A.; Gersmann, H. R.; Beck, M. *Nature*. **1956**, *177,* 392.

128) a) Wan, H. B.; Wong, M. K.; Mok, C. Y. *Pest. Sci.* **1994**, *42,* 93. b) Smolen, J. M.; Stone, A. T. *Environ. Sci. Technol.* **1997**, *31,* 1664.

129) a) Kazankov, G. M.; Sergeeva, V. S.; Efremenko, E. N.; Alexandrova, L.; Varfolomeev, S. D.; Ryabov, A. D. *Angew. Chem.* **2000**, *112,* 3247. b) Kazankov, G. M.; Sergeeva, V. S.; Borisenko, A. A.; Zatsman, A. I.; Ryabov, A. D. *Russ. Chem. Bull. Int. Ed.* **2001**, *50,* 1844.

130) a) Kim, M.; Gabbaï, F. P. *Dalton Trans.* **2004**, 3403. b) Kim, M.; Picot, A.; Gabbaï, F. P. *Inorg. Chem.* **2006**, *45,* 5600. c) Kim, M.; Liu, Q.; Gabbaï, F. P. *Organometallics,* **2004**, *23,* 5560.

131) Frankcmobe, K. E.; Cavell, K. J.; Yates, B. F.; Knott, R. B. *J. Phys. Chem.* **1996**, *100*, 18363.

132) a) Mohamed, M. F.; Brown, R. S. *Inorg. Chem.* **2011**, *50,* 1786. b) Neverov, A. A.; Brown, R. S.; *Inorg. Chem.* **2001**, *40,* 3588. c) Tsang, J. S. W.; Neverov, A. A.; Brown, R. S. *J. Am. Chem. Soc.* **2003**, *125,* 1559. d) Gibson, G. T. T.; Neverov, A. A.; Teng, A. C.-T.; Brown, R. S. *Can. J. Chem.* **2005**, *83,* 1268. e) Liu, C. T.; Neverov, A. A.; Brown, R. S. *Inorg. Chem.* **2007**, *46,* 1778. f) Lu, Z.-L.; Liu, C. T.; Neverov, A. A.; Brown, R. S. *J. Am. Chem. Soc.* **2007**, *129,* 11642. g) Bunn, S. E.; Liu, C. T.; Lu, Z.-L.; Neverov, A. A.; Brown, R. S. *J. Am. Chem. Soc.* **2007**, *129,* 16238. h) Neverov, A. A.; Liu, C. T.; Bunn, S. E.; Edwards, D. R.; White, C. J.; Melnychuk, S. A.; Brown, R. S. *J. Am. Chem. Soc.* **2008**, *130,* 6639. i) Liu, C. T.; Melnychuk, S. A.; Liu, C.; Brown, R. S. *Can. J. Chem.* **2009**, *87,* 640. j) Tsang, W. Y.; Edwards, D. R.; Melnychuk, S. A.; Liu, C. T.; Liu, C.; Neverov, A. A.; Brown, R. S. *J. Am. Chem. Soc.* **2009**, *131,* 4158. k) Brown, R. S.; Lu, Z.-L.; Liu, C. T.; Tsang, W. Y.; Edwards, D. R.; Neverov, A. A.; Brown, R. S. *J. Phys. Org. Chem.* **2009**, *23,* 1. l) Edwards, D. R.; Tsany, W.-T. Neverov, A. A.; Brown, R. S. m) Mohammed, M. F.; Neverov, A. A.; Brown, R. S. *Inorg. Chem.* **2009**, *48,* 11425.

133) a) Cleland, W. W.; Frey, P. A.; Gerlt, J. A. *J. Biol. Chem.* **1998**, *273,* 25529. b) Simonson, T.; Carlsson, F.; Case, D. A. *J. Am. Chem. Soc.* **2004**, *126,* 4167.

134) Tsang, J. S.; Neverov, A. A.; Brown R. S. *J. Am. Chem. Soc.* **2003**, *125,* 7602.

135) a) Desloges, W.; Neverov, A. A.; Brown, R. S. *Inorg. Chem.* **2004**, *43,* 6752. b) Lewis, R. E.; Neverov, A. A.; Brown, R. S. *Org. Biomol. Chem.* **2005**, *3,* 4082. c) Melnychuk, S. A.; Neverov, A. A.; Brown, R. S. *Angew. Chem. Int. Ed.* **2006**, *45,* 1767.

136) Pearson, R. G. *J. Am. Chem. Soc.* **1963**, *83,* 3533.

137) Neverov, A. A.; Brown. R. S. *Org. Biomol. Chem.* **2004**, *2,* 2245.

138) Lu, Z.-L.; Neverov, A. A.; Brown, R. S. *Org. Biomol. Chem.* **2005**, *3,* 3379.

Chapter 2. Kinetic Resolution of Esters using Lanthanide Catalyzed Methanolysis Reactions

2.1. Preface

With minor formatting changes and unit conversions (kJ mol^{-1} to kcal mol^{-1}), this chapter is largely as it was published in *Organic & Biomolecular Chemistry* (Maxwell, C. I.; Shah, K.; Samuleev, P.V.; Neverov, A. A.; Brown, R. S. *Org. Biomol. Chem.*, **2008**, *6,* 2796). Additional information has been added to Note 18 concerning isokinetic temperatures. Kinetics with **2.3**, **2.4** were conducted by Kalpa Shaw and Pavel Samuleev. All other work (kinetics with ligand **2.5**, low temperature experiments) were conducted by Chris Maxwell.

2.2. Introduction

Kinetic resolution of racemates is an emerging tool for the separation of enantiomers[1] although it has an inherent problem in that the yield of a given enantiomeric product necessarily decreases with time due to the relative increase in concentration of the less reactive enantiomer of the starting material. This is particularly so when the chiral kinetic discrimination between the L and D substrates (defined as the kinetic selectivity, k_L/k_D) is not large. Several successful kinetic resolutions are known using man-made catalysts[2] and the use of enzymes for the purpose of selective hydrolysis has been investigated for many years.[3] Although transesterification reactions are well-known,[4] and recent work has provided the mechanistic intricacies of metal ion catalyzed transesterifications,[5] the use of this technique for kinetic resolution of esters is still very

under-developed.[6,7,8,9,10,11]

Our extensive mechanistic investigations of the rapid methanolysis reactions of both activated and non-activated esters in the presence of $[La^{3+}(^{-}OCH_3)]_2$, $Eu^{3+}(^{-}OCH_3)$ and the $Zn^{2+}(^{-}OCH_3)$-complex of 1,5,9-triazacyclododecane[5] suggested that these metal ion/alkoxides, when complexed to chiral ligands, might provide useful catalysts for the kinetic resolution of esters and related compounds. Herein, we describe our proof-of-principle attempts at the kinetic resolution of the *p*-nitrophenyl esters of the D and L N-*tert*-butoxycarbonyl derivatives of glutamine (Boc-Gln-OPNP, **2.1**) and phenylalanine (Boc-Phe-OPNP, **2.2**) promoted by various metal complexes of the bis(2-pyridyl carboxaldehyde) Schiff base of (1R),(2R)-trans 1,2-diaminocyclohexane[12] (Pyr-R,R-chxn:M, **2.3:M**).

In addition, we have screened some metal ion complexes of two other Schiff base variants, namely those of 6-methyl-2-pyridyl carboxaldehyde and (1R),(2R)-*trans* 1,2-diaminocyclohexane[13] (MePyr-chxn:M, **2.4:M**) and the macrocyclic tetra-Schiff base formed from 2,6-pyridyl dicarboxaldehyde and (1R),(2R)-trans 1,2-diaminocyclohexane ((Pyr-R,R´-chxn)$_2$:M, **2.5:M**). Herein, we report the results of these studies along with the rate constants, k_L and k_D, for the catalyzed reactions of the enantiomers at room temperature. We also present a useful method for a single kinetic experiment to determine the k_L and k_D rate constants for a given ester from which one can readily calculate the e.e. vs. percent conversion curves. Finally, in two cases we have determined the activation parameters for the transesterification, and from these have predicted, and subsequently experimentally verified, enantiomeric excesses (e.e.'s) of greater than 99%

at selected reduced temperatures.

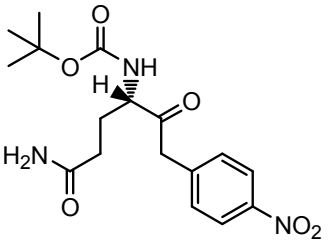

2.1

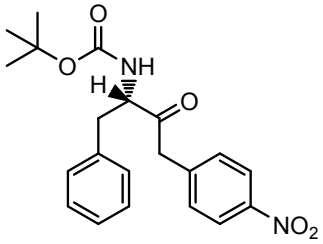

2.2

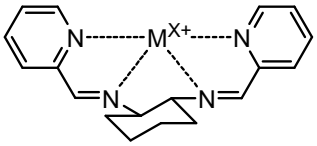

2.3:M^{X+}

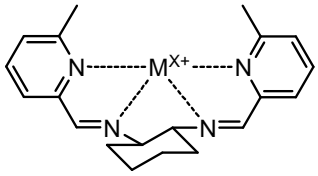

2.4:M^{X+}

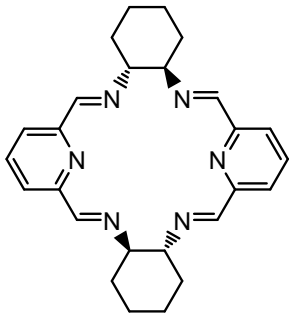

2.5

2.3. Experimental

2.3.1. Materials

Methanol (99.8% anhydrous), sodium methoxide (0.5 M solution in methanol), Boc-L-glutamine 4-nitrophenyl ester (98%+), Boc-D-glutamine 4-nitrophenyl ester (98%+), Boc-L-phenylalanine 4-nitrophenyl ester (98%+), Boc-D-phenylalanine 4-nitrophenyl ester (98%+), 6-methyl-2-pyridine carboxaldehyde, 2-pyridine carboxaldehyde and (+)-and (-)-*trans*-1,2-cyclohexanediamine (99%) were obtained from Aldrich and used as received. $M^{x+}(^{-}OTf)_n$ salts, where M = Zn, Yb, Tm, Nd, La, Eu, Ho were all obtained from Aldrich and anhydrous ethanol was obtained from Commercial Alcohols, Brampton, Ontario. **2.3** and **2.4** were synthesized as reported,[12,13] as was the

cyclic ligand **2.5** [14].

2.3.2. General methodology for determination of enantiomeric excess by kinetic studies

Stock solutions (50 mM) of the catalyst $M^{x+}(^{-}OTf)_x$ where M = Zn, Yb, Tm, Nd, La, Eu, Ho (50 mM), ligand (50 mM), and NaOMe (25 mM) were prepared in anhydrous methanol. Stock solutions (4 mM) of the two enantiomers of the substrate (BOC-Gln-OPNP and BOC-Phe-OPNP) were prepared in anhydrous acetonitrile.

For each kinetic run the catalyst was formulated *in situ* by the addition of 25 μL of each of $M(OTf)_x$, ligand and NaOMe stock solution and subsequently 50 μL of the stock solution of substrate to methanol such that the final volume was 2.5 mL. The **2.5**:La^{3+}-complex formation was relatively slow as judged by the increase in catalytic rate constant as a function of time, so the freshly made complex solutions were allowed to stand at room temperature overnight prior to use. The reaction rates were followed at 324 nm (for the formation of *p*-nitrophenol) using a Cary Bio-100 spectrophotometer with the cell compartment thermostated at 25.0±0.1°C. First order rate constants (k_{obs}) were evaluated from fits of the absorbance vs. time profiles to a standard exponential model. Specifically, two identical sample solutions in 1 cm cuvettes were prepared. To one sample the L-enantiomer was added and the reaction was allowed to go to completion to determine the first order rate constant for its disappearance (k_L). Subsequently an aliquot of the stock solution of the D-enantiomer was added to the same cuvette and a first order rate constant for its disappearance (k_D) was similarly obtained. For the other sample

solution, the D-enantiomer was added followed by the L-enantiomer and two first order rate constants corresponding to k_D and k_L were obtained. The rate constants for each enantiomer were then averaged to give the reported rate constant. This methodology controls for variations between prepared samples and effects due to the order of addition of the enantiomers but has an estimated 2% error attributed to dilution of the catalysts in the subsequent experiments which is incorporated into the standard deviations reported.

The single kinetic run method to obtain both the k_D and k_L was conducted as per the following example. Two UV/vis cuvettes, each containing 0.1 mM **2.3**:Yb^{3+}($^-OCH_3$) catalyst, were prepared as described above. To one cuvette was added 25 μL of the enantiomerically pure D-Boc-Gln-OPNP substrate (4.0 mM in acetonitrile), and the cuvette was placed into the sample chamber of a dual beam UV/vis spectrophotometer. To the second cuvette was added 25 μL of a stock solution of racemic substrate (4.0 mM in acetonitrile) after which it was placed in the reference cell position. The resulting biphasic kinetic traces were analyzed to determine k_L and k_D by NLLSQ fitting the absorbance vs. time data to eq. (1);

$$Abs_t = Abs_0 + 0.5(\Delta Abs)e^{-k_L t} - 0.5(\Delta Abs)e^{-k_D t} \qquad (1)$$

where $\Delta Abs = Abs_\infty - Abs_0$. The Abs_0 term is used to account for optical imperfections that can lead to differences in absorbencies between the two cells.

2.3.3. Determination of activation parameters

Following the general methodology outlined above, the k_{obs} constants for transesterification of each enantiomer of Boc-Gln-OPNP were obtained in MeOH and

EtOH solvent at four to five temperatures between 25°C and 5°C with the R,R'-**2.3**:Yb^{3+}($^-$OR) catalyst, and four to seven temperatures between 40°C to 10°C for the **2.5**:La($^-$OR) catalyst. Three reactions of each substrate were followed at each temperature and the corresponding k_{obs} values were averaged to give the values reported in Table 2-5 and Table 2-6. The k_2 rate constants were then fit to a standard Eyring equation $k=ATe^{(-\Delta H/RT+\Delta S/R)}$ based on a 1/k weighting: the activation parameters, $\Delta H^{\ddagger}$ and $\Delta S^{\ddagger}$ are given in Table 2-7.

2.3.4. General methodology for determination of enantiomeric excess by HPLC

A Hewlett Packard Series 1050 HPLC using a Chiralcel OD-H column (Daicel Chemical Industries) chromatographic system was used for the determination of the enantiomeric excess produced by **2.5**:La^{3+}($^-$OEt), R,R′-**2.3**:Yb^{3+}($^-$OEt) and S,S′-**2.3**:Yb^{3+}($^-$OEt) catalyzed reactions of a racemic mixture of L- and D-Boc-Gln-OPNP (formulated by adding equal amounts of the authentic enantiomers). All chromatograms were run with a mobile phase of 10% isopropanol/90% hexanes at 2.00 mL/min and monitored at a wavelength of 270 nm. The retention times for the starting materials and catalysts were determined from authentic samples. A 25 μL aliquot of a 4 mM solution of the commercial D-Boc-Gln-OPNP substrate was found to contain about 6-7% of the corresponding L-enantiomer as an impurity.

To monitor the enantiomeric excess of the reaction as a function of time, a typical experiment comprised a reaction vial equipped with a rubber septum charged with

$Yb(OTf)_3$ (5 μL, 50 mM), ligand R,R′-**2.3** (5 μL, 50 mM), NaOEt (5 μL, 25 mM) and an internal standard of toluene (50 μL, 1.63 M) in 0.5 mL of ethanol. A second reference vial was prepared with substrate but no catalyst. The vials were placed in the freezer in $CaCl_2$/acetone bath held at a temperature of –15 ^oC or -40 ^oC with dry ice. After 15 minutes of cooling, the reaction was initiated by adding the racemic Boc-Gln-OPNP substrate (50 μL, 10 mM) to each vial. After the addition of substrate the final volume in each vial was 0.635 mL, with final concentrations of 0.39 mM $Ln(OTf)_3$, 0.39 mM R,R′-**2.3**; or **2.5**, 0.20 mM NaOEt, 0.8 mM of the racemic Boc-Gln-OPNP substrate and 0.13 mM toluene. For experiments run at -17 ^oC, after the addition of substrate, a 10 μL aliquot of the reference mixture without catalyst was injected to provide a time zero point. Subsequent injections of 10-25 μL aliquots from the reaction vial containing catalyst were made at 25 minute intervals. For experiments run at -40 ^oC, into multiple vials were placed catalyst mixtures in the concentrations described above, and placed in a freezer at -40 ^oC. At appropriate times, the reaction was stopped with the addition of $HClO_4$ (0.78 mM) and LiCl (3.9 mM) for future HPLC analysis. The relative concentrations of each residual starting enantiomers calculated based on the peak areas of the L and D enantiomers corrected by dividing the peak area of interest by that of the internal standard. The e.e. was calculated using eq. (2), where A_L and A_D are the corrected peak areas of the L and D enantiomers.

$$e.e.(\%) = 100\left(\frac{A_L - A_D}{A_L + A_D}\right) \qquad (2)$$

2.4. Results and discussion

2.4.1. Kinetics

Shown in Figure 2-1 and Figure 2-2 are plots of the k_{obs} values vs. [R,R′-**2.3**:Yb^{3+}:0.5($^{-}OCH_3$)] for the catalyzed methanolysis reaction of L and D Boc-Gln-OPNP L and D Boc-Phe-OPNP. Similar plots are obtained (but not shown) for the reaction of L- and D-Boc-Gln-OPNP promoted by La^{3+}:**2.5** in the presence of 0.5 eq. of $NaOCH_3$. Previous work[5] established that the active forms of these and related complexes contain one methoxide per metal ion, but the 0.5 eq. $NaOCH_3$ buffers the medium at the $^{s}_{s}pH$ [15] corresponding to the pK_a of the catalyst system when the [**2.3**:M^{3+}:($HOCH_3$)]/[**2.3**:M^{3+}:($^{-}OCH_3$)] ratio is unity. The fact that the plots in Figure 2-1 and Figure 2-2 are linear with intercepts of zero rules out the involvement of free methoxide in the production of the *p*-nitrophenol product, and also rules out involvement of higher order species such as dimers.

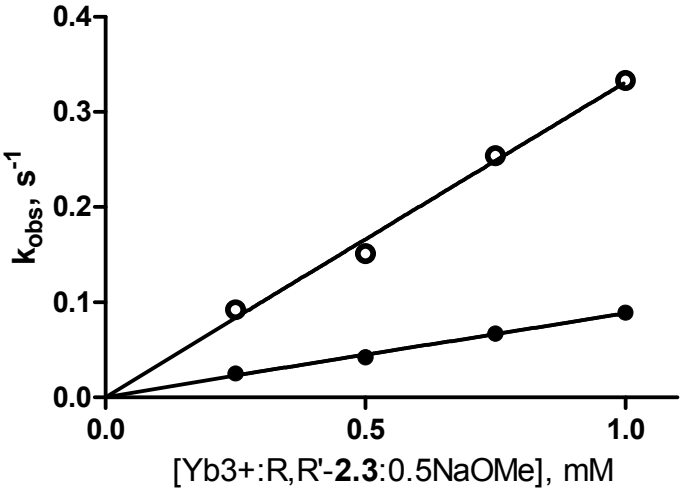

Figure 2-1. Plots of k_{obs} vs. [R,R′-**2.3**:Yb^{3+}: 0.5(NaOMe)] for methanolysis of D- Boc-Gln-ONp (●) and L- Boc-Gln-ONp (○) (0.05 mM) in methanol at 25 °C.

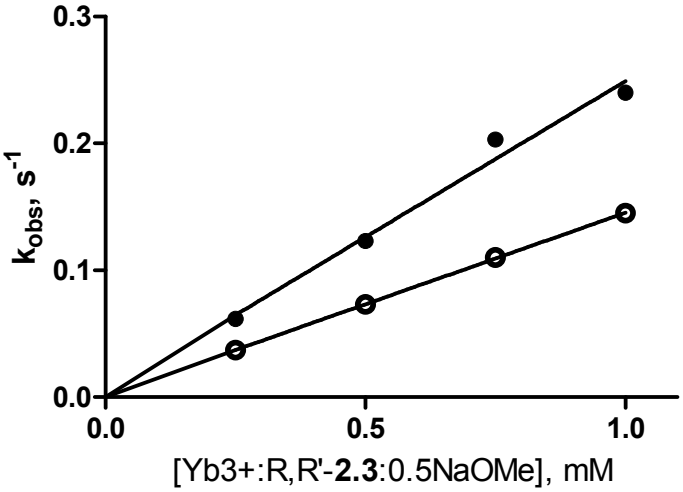

Figure 2-2. Plots of k_{obs} vs. [R,R′-**2.3**:Yb^{3+}: 0.5NaOMe] for methanolysis of D- Boc-Phe-ONp (●) and L- Boc-Phe-ONp (○) (0.05 mM) in methanol at 25 °C.

Given in Table 2-1 are the catalytic second order rate constants for methanolysis of the L and D substrates promoted by $La^{3+}(^{-}OCH_3)$, $Eu^{3+}(^{-}OCH_3)$, and $Yb^{3+}(^{-}OCH_3)$

complexes of R,R′-**2.3** as well as the La^{3+}-complex of **2.5** in pure methanol at 25 ^{o}C. The k_2 constants are computed as the gradients of the lines in Figure 2-1 and Figure 2-2, although we know that only half of the complex is present as the active CH_3O^--containing form. None of the three complexes is particularly active with the Boc-Phe-OPNP substrate, and all the selectivity values, defined as k_2^L/k_2^D, are less than unity. On the other hand, the k_2^L/k_2^D ratios are all greater than unity with the R,R′-**2.3**:Ln^{3+} complexes for the Boc-Gln-OPNP substrate, while the **2.5**:La^{3+}catalyst has the opposite preference where k_2^L/k_2^D is <1 for reasons that are not clear.

Table 2-1. Second order rate constants (k_2) for the methanolysis of L- and D-Boc-Phe-OPNP and Boc-Gln-OPNP catalyzed by R,R′-**2.3**:Ln^{3+}:($^-OCH_3$) and **2.5**:La^{3+} complexes at 25 °C.[a]

Substrate → / Catalyst ↓	Boc-Phe-OPNP			Boc-Gln-OPNP		
	k_2^L	k_2^D	k_2^L / k_2^D [b]	k_2^L	k_2^D	k_2^L / k_2^D [b]
R,R′-**2.3**:La^{3+}:($^-OCH_3$), ^s_spH =8.3	7.5	10.8	0.70 (18% e.e., 43% L)	31.5	27.0	1.17 (8% e.e., 37% D)
R,R′-**2.3**:Eu^{3+}:($^-OCH_3$), ^s_spH =6.5	4.9	6.4	0.77 (13% e.e., 42% L)	63.8	25.0	2.6 (44% e.e., 55% D)
R,R′-**2.3**:Yb^{3+}:($^-OCH_3$), ^s_spH =6.5	14.5	24.6	0.50 (25% e.e., 47% L)	340	89	3.8 (58% e.e., 62% D)
2.5:La^{3+}:($^-OCH_3$), ^s_spH = 8.8	2.5	7.0	0.35 (47% e.e., 56% L)	2.8	7.8	0.36 (47% e.e., 56% L)

[a] k_2 defined from the gradient of the plot of k_{obs} vs. [ligand:M^{3+}:($^-OCH_3$)].

[b] e.e. values and residual yield of predominant stereoisomer calculated at optimal catalytic conversion (OCC) using eq. (3)-(5).

We introduce here a faster way to do the screening where one can determine both the k_D and k_L constants and selectivity factors for a given catalyst in a single reaction. This is similar to the 'quasi-racemate' method for determining small kinetic isotope effects,[16] which we have modified slightly to adapt to dual-beam UV/vis spectrophotometry. In the typical example, illustrated here with the methanolysis of Boc-Gln-OPNP promoted by the Yb^{3+}:($^{-}OCH_3$) complex of **2.3**, the reference and sample cells of the spectrometer are respectively charged with equal amounts of the racemic and enantiomerically pure substrates, along with identical amounts of catalyst, and the absorbance difference *vs*. time curve (Figure 2-3) is monitored until the completion of the reaction. Characteristically these have an 'up/down' or 'down/up' behavior depending on which enantiomer reacts more rapidly, and if both react at the same rate, then there is no rise/fall behavior. The k_L and k_D rate constants can be easily obtained from fits of the Abs *vs.* time curve to the expression in eq. (1). For the example chosen here, $k_L = 0.028\ s^{-1}$ and $k_D = 0.0068\ s^{-1}$, ($k_L/k_D = 4.1$), is experimentally the same as what was obtained from the single run experiment in Table 2-1, row 1. The ΔAbs vs. time curve in Figure 2-3 also visually provides the time (t_{occ}) at which the rates of catalytic conversion of the D and L isomers are the same (vertical dashed line) which we will define here as the 'optimal catalytic conversion (OCC)'. The exact equations for the determination of t_{OCC} and the [residual D] and [residual L] isomers at that time are given as:

$$t_{OCC} = \left(\frac{\ln\left(\frac{k_L}{k_D}\right)}{k_L - k_D} \right) \quad (3)$$

$$\frac{[L]}{[L_0]} = \exp\left(-k_L t_{OCC}\right) \quad (4)$$

$$\frac{[D]}{[D_0]} = \exp\left(-k_D t_{OCC}\right) \quad (5)$$

The e.e. at t_{OCC} is defined as: ([L]-[D])/ ([L]+[D])*100. These values are given in Tables 2-1 - 2-6 along with the percentage of the dominant enantiomer remaining at the OCC.

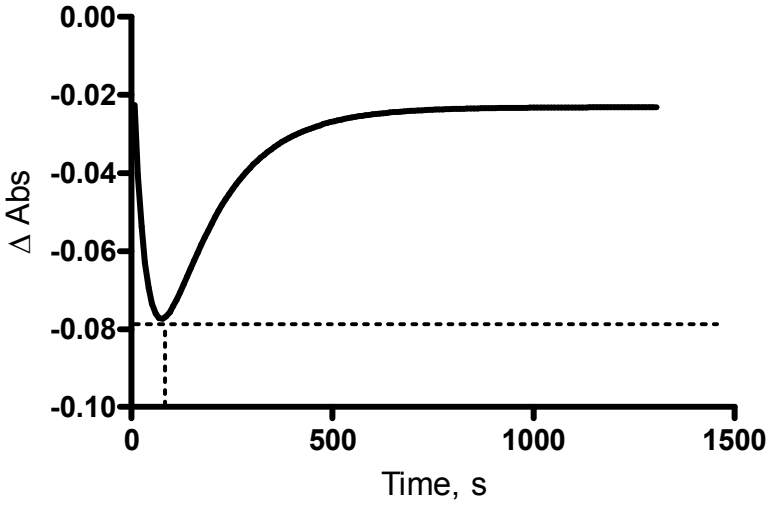

Figure 2-3. A ΔAbs vs. time plot for the methanolysis of D-Boc-Gln-OPNP and racemic Boc-Gln-OPNP (0.04 mM in sample and reference cell respectively) promoted by 0.1 mM R,R′-**2.3**:Yb^{3+} in the presence of 0.05 mM $NaOCH_3$. Dashed vertical line defines the time (~65 sec) where the catalyzed rates of conversion of the D- and L- isomers are equal (t_{OCC}).

The effect of changing the metal ion and ligand to metal ion ratio was investigated in a series of single run experiments in methanol with 0.5 mM of metal ion (added as the corresponding triflate), one or two equivalents of R,R′-**2.3** and 0.25 mM of added $NaOCH_3$. The same series of reactions was investigated in a solvent comprising 90% CH_3CN/10% methanol and the results are also presented in Table 2-2. Of the various metal ions Yb^{3+} and Tm^{3+} have the greatest selectivity factors, and although increasing the ligand/M^{x+} ratio from one to two may increase, decrease or have no effect on the reaction rate in selected cases, this does not seem to have any profound effect on the selectivity factors. Only in the case of Nd^{3+} does the change in the solvent to 9:1 acetonitrile:methanol increase the rate and the selectivity factor appreciably: in all other cases the k_L/k_D ratio drops or remains constant. The same thing is seen for La^{3+}:**2.5** where the 9:1 acetonitrile: methanol solvent system increases the selectivity factor to 3.5 from 2.8 in methanol. Some additional screening was done to investigate the effect of 9:1 solvent:methanol compositions on the selectivity factor for the Yb^{3+}:($^{-}OCH_3$) complex of R,R′-**2.3** with L- and D-Boc-Gln-OPNP using THF, ether, dichloromethane, 1,2-dichloroethane an toluene. Only THF and toluene with 2:1 ligand:Yb^{3+} ratio gave selectivity factors approaching those in methanol, the respective values being 3.9 and 3.4.

Table 2-2. Observed first order rate constants for the catalysis methanolysis of 4 x 10^{-5} mol dm^{-3} L and D Boc-Gln-OPNP in methanol and 90% acetonitrile:methanol promoted by 0.5 mM of metal ion, one or two equivalents of R,R´-**2.3** and 0.25 mM of added $NaOCH_3$.

M^{x+}	Lig: M^{x+}	$10^3 k_L$ (s^{-1})	$10^3 k_D$ (s^{-1})	k_L/k_D	e.e., with residual yield[b]
Yb^{3+}	1:1	155.1	40.8	3.8	58%, 62% D
CH_3OH	2:1	192.0	40.5	4.7	65%, 66% D
9:1(A:M)[a]	2:1	163	41.2	4.0	60%, 63% D
Tm^{3+}	1:1	102.0	27.2	3.8	58%, 62% D
CH_3OH	2:1	170.5	45.2	3.8	58%, 62% D
9:1(A:M)[a]	1:1	152.0	53.2	2.9	48%, 57% D
9:1(A:M)[a]	2:1	201.8	71.3	2.8	47%, 57% D
Nd^{3+}	1:1	24.7	12.3	2.0	33%, 50% D
CH_3OH	2:1	12.0	7.0	1.7	26%, 47% D
9:1(A:M)[a]	1:1	28.3	12.7	2.3	38%, 52% D
Zn^{2+}	1:1	21.2	11.0	1.9	31%, 49% D
CH_3OH	2:1	21.0	9.5	2.2	37%, 52% D
9:1(A:M)[a]	1:1	52.5	33.8	1.6	22%, 45% D
9:1(A:M)[a]	2:1	52.5	34.3	1.5	21%, 45% D

[a] 90% acetonitrile : 10% methanol solution.

[b] e.e. values and residual yield of predominant stereoisomer calculated at optimal catalytic conversion (OCC) using eq. (3)-(5)

2.4.2. Complex 2.4

As one expects a more sterically demanding complex might lead to greater chiral discrimination, we undertook single run kinetic studies of the rates of methanolysis of the $Yb^{3+}(^{-}OCH_3)$ and $La^{3+}(^{-}OCH_3)$ complexes of **2.4**. The results in Table 2-3 indicate that only in the cases of the Yb^{3+} complexes in the presence of two ligands is there an appreciable selectivity, and under these conditions the reactions are markedly slower in the presence of a single equivalent of ligand. This probably means that the complexes are not fully formed when the ligand/M^{3+} ratio is 1. Even so, the dramatic reduction in reaction rate coupled with a poorer selectivity than was realized with **2.3**:Yb^{3+} and La^{3+}:**2.5** made us discontinue study with ligand **2.4**.

Table 2-3. First order rate constants for methanolysis of substrates promoted by $Yb^{3+}(^{-}OCH_3)$ and $La^{3+}(^{-}OCH_3)$ complexes of ligand **2.4** in MeOH, T=25 ^{o}C, $[M^{3+}]$ = 0.5 mM, $[^{-}OCH_3]$ = 0.25 mM.

Subst.	M^{3+}	Lig:M^{3+}	$10^3\ k_L$ (s^{-1})	$10^3\ k_D$ (s^{-1})	e.e. with residual yield[a]	k_L/k_D
2.1	Yb	1:1	31.0	27.0	7%, 39% D	1.1
		2:1	19.3	8.5	38%, 52% D	2.3
	La	1:1	26.2	26.3	0.2%, 37% D	1
		2:1	35.8	34.0	2.6%, 38% D	1
2.2	Yb	1:1	0.30	0.28	3.4%, 38% D	1.1
		2:1	0.20	0.13	21%, 45% D	1.5
	La	1:1	7.8	7.5	1.9%, 38% D	1
		2:1	8.3	9.0	4.0%, 35% D	0.9

[a] e.e. values and residual yield of predominant stereoisomer calculated at optimal catalytic conversion (OCC) using eq. (3)-(5).

2.4.3. Comparison of selectivity factors in methanol, ethanol and n-propanol

As our earlier results indicated that the metal ion catalysts are generally active in other light alcohols such as ethanol and propanol, we compared the selectivity factors obtained in these three solvents. For this series of reactions, the k_L and k_D constants were obtained in a single cell containing 0.5 mM each of Yb^{3+} (introduced as its triflate) and of **2.3**, and 0.25 mM of added $NaOCH_3$ which immediately equilibrates to form the NaOR of the ROH solvent. Into this cell was added 0.05 mM of L Boc-Gln-OPNP, and its

transesterification reaction was followed to completion. To the same cell was then added 0.05 mM of the D isomer of Boc-Gln-OPNP, and this reaction was again followed to completion. The entire process was repeated with a fresh solution of the catalyst formulated in the same way, and the reaction of the D and then L isomer of the substrate was followed to completion. Given in Table 2-4 are the averages of the various first order rate constants determined in this way, and it can be seen that the selectivity factors are highest with ethanol as the solvent. For **2.5**:La^{3+} in the presence of 0.5 eq. of added methoxide, the second order rate constants in ethanol for transesterification of L- and D-Boc-Gln-OPNP are $k_2^L = 2.0\ M^{-1}\ s^{-1}$ and $k_2^D = 11.1\ M^{-1}\ s^{-1}$ for a stereoselectivity factor of 5.5.

Table 2-4. First order rate constants for the alcoholysis reaction of L and D Boc-Gln-OPNP promoted by 0.5 mM R,R´-**2.3**:Yb^{3+}:($^-$OR) in various alcohols at T = 25 ^oC.

Solvent	$10^3\ k_L\ (s^{-1})$	$10^3\ k_D\ (s^{-1})$	k_L/k_D	e.e., with residual yield[b]
MeOH	155 ± 10	40.8 ± 1.0	3.8	58%, 62% D
EtOH	51.5 ± 1.5	7.2 ± 0.4	6.9	75%, 73% D
PrOH	6.4 ± 1.9	2.0 ± 0.7	3.2	52%, 59% D

2.4.4. Activation parameters for the methanolysis and ethanolysis reactions of L- and D-Boc-Gln-OPNP promoted by R,R′-2.3:Yb^{3+}(^{-}OR) and 2.5:La^{3+}:($^{-}OCH_3$)

Although none of the complexes provided excellent selectivity at 25 ^{o}C, any difference in the activation enthalpies ($\Delta H^{\ddagger}$) for the catalytic transesterification of the D and L isomers must be manifested in a changing k_L/k_D ratio as a function of temperature, with the magnitude of the change being a reflection of the $\Delta\Delta H^{\ddagger}$ $^{(L\ vs\ D)}$. Knowledge of the activation parameters for the catalyzed reactions is essential for calculating the temperature where the best compromise between e.e. and maximal residual enantiomer is realized. The activation parameters were determined in methanol and ethanol following the procedures described in the previous sections. Given in Table 2-5 and Table 2-6 are the observed first order rate constants of the catalyzed reactions along with the selectivity factors at various temperatures. The error limits are computed as the maximum deviation from the mean of two or three determinations of the constant. When the first order rate constants are divided by the [active catalyst][17] ([R,R′-**2.3**:Yb^{3+}:(^{-}OR)] = 0.25 mM or [**2.5**:La^{3+}:(^{-}OR)] = 0.1 mM in ethanol and 0.05 mM in methanol), the so-produced second order rate constants (k_2) can be used to compute the activation parameters for the catalyzed transesterifications of L and D Boc-Gln-OPNP given in Table 2-7.

Table 2-5. First order rate constants for the alcoholysis of L and D Boc-Gln-OPNP (0.04 mM) promoted by 0.25 mM R,R′-**2.3**:Yb^{3+}:($^{-}$OR), in ethanol and methanol at various temperatures. [a]

		EtOH		
T (^{o}C)	10^3 k_L (s^{-1})	10^3 k_D (s^{-1})	k_L/k_D	e.e. with residual yield[b]
25	51.5 ± 1.5	7.2 ± 0.4	7.2	75%, 73% D
20	36.9 ± 2.4	4.6 ± 0.1	8.5	78%, 74% D
10	13.9 ± 1.0	1.9 ± 0.1	7.3	76%, 73% D
5	11.0 ± 0.8	1.0 ± 0.2	11.0	83%, 79% D
		MeOH		
25	155 ± 10	40.8 ± 1.0	3.8	58%, 62% D
20	115 ± 1	31.0 ± 0.7	3.7	58%, 62% D
10	70.7 ± 2.0	17.3 ± 0.3	4.1	60%, 63% D
5	52.6 ± 1.8	11.1 ± 1.0	4.7	65%, 66% D

[a] error limits are given as maximum deviation from the mean of 2 or 3 independent runs for each constant.

[b] e.e. values and residual yield of predominant stereoisomer calculated at optimal catalytic conversion (OCC) using eq. (3)-(5).

Table 2-6. First order rate constants for the alcoholysis of L and D Boc-Gln-OPNP (0.04 mM) promoted by 0.2 mM **2.5**:La^{3+}:($^{-}$OR) in methanol and ethanol at various temperatures.[a]

		EtOH		
T (^{o}C)	10^3 k_D (s^{-1})	10^3 k_L (s^{-1})	k_D/k_L	e.e. with residual yield[b]
40	3.8 ± 0.2	1.95 ± 0.1	2.0	32%, 50% L
35	2.7 ± 0.2	1.1 ± 0.1	2.4	42%, 54% L
30	2.5 ± 0.1	0.95 ± 0.07	2.6	55%, 44% L
25	1.9 ± 0.3	0.69 ± 0.02	3.0	56%, 47% L
		MeOH		
40	17.0 ± 0.2	9.3 ± 0.3	1.8	29%, 48% L
35	12.0 ± 0.9	5.7 ± 0.7	2.1	36%, 51% L
30	9.7 ± 1.1	4.4 ± 0.9	2.2	38%, 52% L
25	7.8 ± 0.7	2.8 ± 0.3	2.8	47%, 56% L
20	4.9 ± 0.6	1.4 ± 0.3	3.5	56%, 61% L
15	3.59 ± 0.02	0.82 ± 0.02	4.3	62%, 65% L
10	2.5 ± 0.1	0.54 ± 0.01	4.6	64%, 66% L

[a] error limits are given as maximum deviation from the mean of 2 or 3 independent runs for each constant.

[b] e.e. values and residual yield of predominant stereoisomer calculated at optimal catalytic conversion (OCC) using eq. (2)-(5).

Table 2-7. Activation parameters for the ethanolysis and methanolysis of L and D Boc-Gln-OPNP promoted by R,R′-**2.3**:Yb^{3+}:($^{-}$OR) and **2.5**:La^{3+}:($^{-}$OR).

	$\Delta H^{\ddagger}$ (kcal mol^{-1})		$\Delta S^{\ddagger}$ (cal $mol^{-1}\cdot K^{-1}$)	
2.3:Yb^{3+}:($^{-}$OR)	**L**	**D**	**L**	**D**
MeOH	8.1 ± 0.2	9.4 ± 0.3	-17.6 ± 0.9	-15.8 ± 1.1
EtOH	13.0 ± 0.6	16.2 ± 0.9	-3.9 ± 2.0	-1.1 ± 3.0
2.5:La^{3+}:($^{-}$OR)	**L**	**D**	**L**	**D**
MeOH	16.5 ± 0.6	11.4 ± 0.5	5.7 ± 1.9	-9.3 ± 1.9
EtOH	16.1 ± 0.9	10.9 ± 0.8	-2.2 ± 2.9	-17.4 ± 2.6

The activation parameters refer to the overall catalyzed process which we have shown previously[5] with $La^{3+}{}_2(^{-}OCH_3)_2$ and a 1,5,9-triazacyclononane:$Zn^{2+}(^{-}OCH_3)$ complex, involves the steps shown in eq. (6) and (7) with a pre-equilibrium binding of the catalyst and substrate followed by the formation of an anionic tetrahedral intermediate (T_O^-) that is stabilized by complexation. With good leaving groups such as *p*-nitrophenoxy, the breakdown of the tetrahedral intermediate is fast[5], so that the k_1 step for formation of the metal-stabilized intermediate is rate limiting. Thus, for the metal catalyzed alcoholyses operative here, the activation parameters refer to the overall second order rate constant given as $k_2^{obs} = K_b k_1$. At 25 ^{o}C the transesterification reactions in ethanol for D and L isomers with both catalysts are about three to five times slower than the corresponding reactions in methanol. In both alcohols, the selectivity factors with the

catalysts get larger as the temperatures drop as expected, indicating that one can choose an appropriate lower temperature to enhance the selectivity factors to a point that this would be a viable kinetic resolution technique for selected substrates.

$$M^{X+}(^{-}OCH_3) + RCO_2R' \overset{K_b}{\rightleftharpoons} RCO_2R':M^{X+}(^{-}OCH_3) \qquad (6)$$

$$RCO_2R':M^{X+}(^{-}OCH_3) \underset{k_{-1}}{\overset{k_1}{\rightleftharpoons}} (CH_3O^{-}T_o\text{-}):M^{X+} \xrightarrow{k_2} P \qquad (7)$$

In order to demonstrate experimentally that the enantiomeric excesses of the reaction do improve markedly at low temperature, we determined, using HPLC, the time course for disappearance of each of the enantiomers of a racemic Boc-Gln-OPNP mixture (0.8 mM) in the presence of each of the chiral R,R′-**2.3**:Yb^{3+}($^{-}$OR) and S,S′-**2.3**:Yb^{3+}:($^{-}$OR) complexes (0.39 mM) in EtOH at –15 ^{o}C over the course of three hours. Given in Figure 2-4 is the time course promoted by the R,R′-**2.3** complex showing the residual amounts of the D and L isomers and the enantiomeric excesses in the total product mixture as a function of time. After three hours, essentially all the starting L-isomer has reacted while about 60% of the enantiomerically pure D-isomer is left (experimental e.e. after 180 min is 97%). A similar plot (not shown) obtained with the S,S′-**2.3**:Yb^{3+}($^{-}$OCH$_3$) complex reveals a corresponding fast reduction of the D-isomer, with about 54% of the residual enantiomerically pure L-isomer remaining after about 195 minutes, e.e. ~100%).

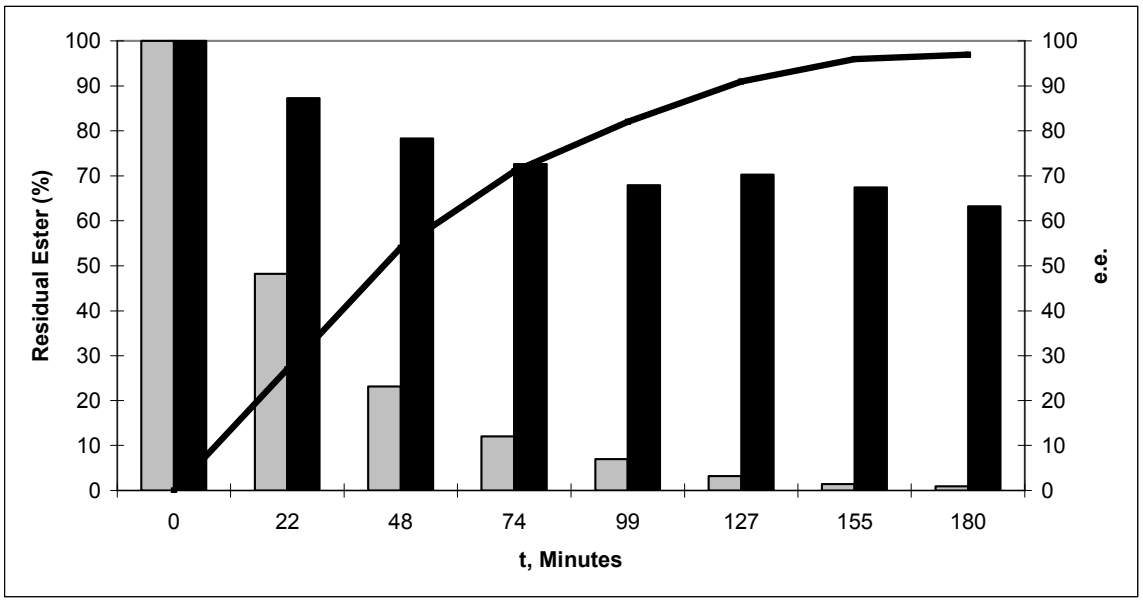

Figure 2-4. Time course for the ethanolysis of racemic Boc-Gln-OPNP promoted by R,R´-**2.3**:Yb^{3+}($^{-}OCH_3$) at -15 ^{0}C : black bar, residual D-isomer; grey bar, residual L-isomer; solid line, enantiomeric excess.

As a final demonstration of the utility of prediction of e.e. for the ethanolysis of a racemic Boc-Gln-OPNP mixture at reduced temperature, the activation parameters for the reaction of the D and L enantiomers with **2.5**:La^{3+}:($^{-}$OEt) given in Table 2-7 were used to compute the k_2^L and k_2^D rate constants at -40 ^{o}C and the plot of residual D and L isomers, e.e. and Δ Abs. vs. time given in Figure 2-5 was computed. In computing the time course, we used the first order rate constants predicted for 1 mM of catalyst and the second order rate constants for each enantiomer were extrapolated to -40 ^{o}C where $k_2^D/k_2^L = 40.4$. The computed data indicate that at 2200 minutes the predicted e.e. will be >99%, with 84% of residual L isomer remaining with no residual D isomer. We confirmed this prediction by running the reaction at -40 °C in multiple vials, stopping the reaction at three times (720, 1440 and 2160 minutes) with the addition of an excess of perchloric acid and LiCl, the

duplicate experimental points for residual L and D isomers being placed on Figure 2-5 as ○ and ● symbols respectively. These experimental data confirm the prediction that at 2160 minutes, 79% of the L isomer remains with an enantiomeric excess of >99%.

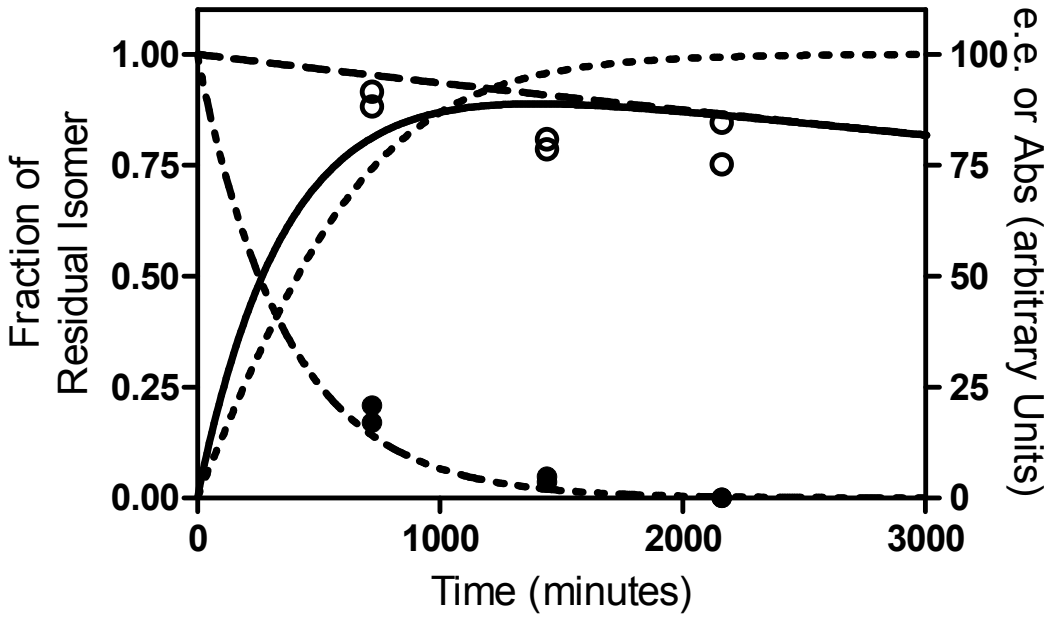

Figure 2-5. Time course for various parameters arising from the ethanolysis of D-Boc-Gln-OPNP and (1.0 mM) and *rac*- Boc-Gln-OPNP, each promoted by 1.0 mM **2.5**:La^{3+}:($^-$OEt) in ethanol at -40°C. Plots are constructed using first order rate constants calculated from activation parameter values ($k^D = 4.53 \times 10^{-5}$ s^{-1}, $k^L = 1.12 \times 10^{-6}$ s^{-1}). Shown are the e.e. (dotted line, right axis), and the residual fractions of D and L enantiomers vs. time (··–, -----, left axis). Solid line is the computed Δ Abs. vs. time plots where the right y-axis represents the maximum absorbance expected for cleavage of one isomer. ● and ○ symbols are duplicates of experimentally observed amounts of residual of D and L isomers at times 720, 1440 and 2160 minutes.

2.5. Conclusion

We have described a study of the use of some chiral lanthanide metal ion complexes to effect kinetic resolution of the nitrophenyl esters of N-Boc protected amino acids of glutamine and phenylalanine under mild conditions of essentially neutral 'pH' (in alcohol). The choice of the *p*-nitrophenyl esters was dictated by the ease with which the kinetics of the reactions can be determined by UV/Vise spectrophotometry. Only the La^{3+} complex of ligand **2.5** is moderately effective at room temperature for selective cleavage of the phenyl alanine derivative (k_L/k_D = 0.26). The best selectivity for the glutamine derivative comes from the R,R´-**2.3**:Yb^{3+} complex in ethanol where the k_L/k_D ratio is 11 at 5 °C, but activation parameter analysis indicates that a far better selectivity can be achieved with both catalyst at lower temperatures. The activation parameters allow one to predict an optimum reaction condition for a given concentration of catalyst where maximum values of the ee and residual unreacted enantiomer can be achieved in a conveniently accessible time. In a selected example we showed that a catalyst having an unimpressive k_2^D/k_2^L = 3 at 25 °C is predicted to have a k_2^D/k_2^L = 40.4 at -40 °C and we experimentally confirmed a predicted large e.e. of >99% with ~80% of the L isomer remaining.[18]

In order to more rapidly screen the catalytic sytems at various temperatures, we have presented a simplified kinetic method where the rate constants for both enantiomers can be determined in a single experiment. Application of this methodology can allow a rapid determination of the activation parameters of the reactions for a given catalyst with each of the two enantiomers. This is essential for calculation of a temperature where one can obtain high enantiomeric excesses in reasonable times with appreciable amounts of

the less reactive isomer remaining.

2.6. References and notes

1) Kagan, H. B.; Fiaud, J. C. *Top. Stereochem*. **1988**, *18*, 249.

2) a) Vedejs, E.; Jure, M. *Angew. Chem. Int. Ed.* **2005**, *44*, 3974. b) Ghanem, A.; Aboul-Eneim, H. Y. *Chirality*. **2005**, *17*, 1. c) Robinson, D. E. J. E.; Bull, S. D., *Tetrahedron: Asymmetry*. **2003**, *14*, 1407. d) Keith, M.; Larrow, J. F.; Jacobsen, E. N. *Adv. Synth. Catal*. **2001**, *5,* 343. e) Hoyveda, A. H.; Didiuk, M. T. *Curr. Org. Chem.* **1998**, *2,* 489.

3) a) Davis, B. G.; Borer, V. *Nat. Prod. Rep.* **2001**, *18*, 618. b) Groger, H. *Adv. Synth. Catal.* **2001**, *343,* 547. c) Roberts, S. M. *J. Chem. Soc. Perkin Trans. 1.* **2001**, 1475. d) Reetz, M. T. *Angew. Chem. Int. Ed.* **2001**, *113,* 292.

4) a) Otera, J. *Chem. Rev.* **1993**, *93,* 1449. b) Cleij, M. C.; Drenth, W.; Nolte, R. J. M., *J. Org. Chem.* **1991**, *56,* 3883.

5) a) Neverov, A. A.; McDonald, T.; Gibson, G.; Brown, R.S. *Can. J. Chem.* **2001**, *79,* 1704. b) Neverov, A. A.; Gibson, G.; Brown, R. S. *Inorg. Chem.* **2003**, ***42,*** 228. c) Neverov, A. A.; Sunderland, N. E.; Brown, R. S. *Org. Biomol. Chem*. **2005**, *3,* 65.

6) Tokunaga, M.; Kiyosu, J.; Obora, Y.; Tsuji, Y. *J. Am. Chem. Soc.* **2006**, *128,* 44817.

7) Tokunaga, M.; Aoyama, H.; Kiyosu, J.; Shirogane, Y.; Iwasawa, T.; Obora, Y.; Tsuji, Y. *J. Organometal. Chem.* **2007**, *692,* 472.

8) Dro, C.; Bellemin-Laponnaz, S.; Welter R.; Gade, L. H. *Angew. Chem. Int. Ed.* **2004**, *43,* 4479.

9) You, J. S.; Yi, X.-Q.; Su, X.-Y.; Wang, T.; Xiang, Q.-X.; Yang, M.; Xie, R.-G. *J. Mol. Catal. A: Chemistry.* **2003**, *202,* 17.

10) Ryabov, D.; Kazankov, G. M.; Kurzeev, S. A.; Samuleev P. V.; Polyakov, V. A.; *Inorg. Chim. Acta*. **1998**, *280,* 57.

11) a) Cleij, M. C.; Mancin, F.; Scrimin, P.; Tecilla, R.; Tonellato, U. *Tetrahedron*. **1997**, *53,* 357. b) Cleij, C.; Scrimin, P.; Tecilla, P.; Tonellato, U. *Langmuir*. **1996**, *12,* 2956. c) Scrimin, P.; Tecilla P.; Tonellato, U. *J. Org. Chem.* **1994**, *59,* 4194.

12) Larrow, J. F.; Jacobsen, E. N. *J. Org. Chem.* **1994**, *59,* 1939.

13) Jo, D.-H.; Chiou Y.-M.; Que, L. *Inorg. Chem.* **2001**, *40,* 3181.

14) Bligh, S. W.; Choi, N.; Cummins, W. J.; Evagorou, E. G.; Kelley, J. D.; McPartlin, M. *J. Chem. Soc. Dalton Trans.* **1994**, *23,* 3369.

15) For the designation of pH in non-aqueous solvents we use the forms described by Bosch and co-workers (Given that the autoprotolysis constant of methanol is $10^{-16.77}$(mol $dm^{-3})^2$, neutral ${}^{s}_{s}pH$ in methanol is 8.4; Bosch, E.; Rived, F.; Rosés M.; Sales, J. *J. Chem. Soc., Perkin Trans.* **1999**, *2,* 1953.) based on the recommendations of the IUPAC, *Compendium of Analytical Nomenclature. Definitive Rules 1997* 3rd ed., Blackwell, Oxford, U. K. 1998. If one calibrates the measuring electrode with aqueous buffers and then measures the pH of an aqueous buffer solution, the term ${}^{w}_{w}pH$ is used; if the electrode

is calibrated in water and the 'pH' of the neat buffered methanol solution then measured, the term ${}^{s}_{w}pH$ is used; and if a correction factor of -2.24 (in the case of methanol) is subtracted from the latter reading, then the term ${}^{s}_{s}pH$ is used.

16) a) Bergson, G.; Matsason, O.; Sjoberg, S. *Chem. Scripta,* **1977**, *11,* 25. b) Bennet, A. J.; Sinnott, M. L. *J. Am. Chem. Soc.* **1986**, *108,* 7287.

17) In order to compute the accurate activation parameters, the first order rate constants are divided by the concentration of the active catalyst which is ½ of the total amount of ligand:M^{3+} put in solution.

18) The fact that an enantioactive catalyst shows little selectivity at a given experimental temperature does not necessarily indicate that it is a poor catalyst at all temperatures. This can only be verified by activation parameter analysis using Eyring or Arrhenius plots. If the gradients for these plots, which define the $\Delta H^{\ddagger}$ for the catalyzed reaction of each isomer are very close to each other, then the selectivity will be the same at all accessible temperature. On the other hand, if the gradients are substantially different, the two plots will generally cross at the isokinetic temperature. At this temperature the $\Delta G^{\ddagger}$ for the reaction with each enantiomer will be equal and the selectivity k_D/k_L will therefore be unity. The selectivity value, and in fact the D(R) *vs*. L(S) selectivity itself, then depends on how close and on which side of the isokinetic temperature the experiment is run. A case exists wherein, relative to the reaction of its enantiomer, the entropy of activation for the reaction of one enantiomer is smaller and the enthalpy of activation is larger. This

results in a ln k *vs.* 1/T plot with divergent lines that only intercept at a value where $1/T < 0$. In this case, there is no isokinetic temperature.

Chapter 3. Computational β^{eq} determination

3.1. Introduction

As seen in the general introduction chapter, determinations of substituent effects on reaction rates and equilibria are an invaluable tool for investigating reaction mechanisms. For reactions involving O-aryl nucleophiles and leaving groups, the kinetically determined Brønsted β^{nuc} and β^{lg} describe the charge development in the nucleophile or leaving group in the transition state. For instance, the transfer of the O,O-dimethyl phosphorothioyl group between oxyanion nucleophiles in water has β^{nuc} and β^{lg} values of 0.57 and -0.88.[1] These show the relative sensitivity of nucleophile and leaving group substitution on the reaction rate. These values are indicative of the relative charge development on the nucleophile and leaving group in the transition state for the symmetrical reaction of 2,4,5-trichlorophenoxide on O,O-dimethyl O-(2,4,5-trichlorophenyl) phosphorothioate. This sensitivity can be thought of as being proportional to the degree of charge development in the transition state relative to the ionization reactions of the substituted phenols; however, it is difficult to use this information to assign a position to the transition state within a framework of the reaction coordinate. The sensitivity constant for the equilibrium process, β^{eq}, can be used to normalize β^{nuc} and β^{lg}, allowing the charge development in the transition state to be placed within the context of the complete reaction. Leffler's parameter,[2] α, is defined as β^{nuc}/β^{eq} or β^{lg}/β^{eq} is a normalized measure of bond formation or bond cleavage at the rate-determining transition state for a given reaction.

Provided that there is a single rate-determining transition state for a process, β^{eq} can be calculated by eq. (1). This can be rationalized by examination of the following similar hypothetical equilibrium,[3] wherein β_A represents the charge change in the equilibrium between a reporter group x-A and the transition state and likewise β_B with x-B and the transition state.

$$\beta^{eq} = \beta^{lg} - \beta^{nuc} \qquad (1)$$

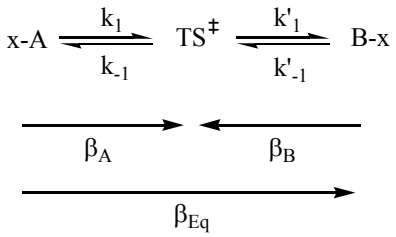

Scheme 3-1. Hypothetical equilibrium between two species separated by a single transition state.

For the phosphorothioyl group transfer in water described above, β^{eq} is calculated to be (-0.88) - 0.57 = -1.45. Using this β^{eq}, a charge map can be created for the symmetrical reaction: In the transition state, the charge progression in the nucleophile has progressed 39% ($\alpha = \beta^{nuc}/\beta^{eq}$ = 0.57 / |-1.45|) while charge progression in the leaving group has progressed 61% ($\alpha = \beta^{lg}/\beta^{eq}$ = -0.88 / -1.45). The charge imbalance of -0.14 results from the difference between 2(-0.43) on the aryl oxygens and the net -1 charge at the transition state, and is explained as being distributed over the extremities of the phosphorothioyl group.

Unfortunately, the experimental determination of β^{eq} is labour intensive, requiring many kinetic experiments to find the Brønsted coefficients β^{nuc} and β^{lg}. In this work, the

goal is to develop a straightforward computational method to estimate β^{eq} for a series of acyl and phosphoryl transfers between aryloxy anion nucleophiles in water and methanol. The primary virtue of this methodology is that it reduces the effort required for the experimental determination of β^{eq} values and should present an attractive way of determining initial estimates for these coefficients. The computational work is paired with an experimental determination of Brønsted coefficients for transfer of the O,O-dimethyl phosphorothioyl group between oxyanion nucleophiles, and was published in the Journal of Physical Organic Chemistry.[1] All calculations were conducted by Chris Maxwell.

3.2. Computational details

Structure optimizations, energy calculations and frequency calculations of starting material and products were performed at the B3LYP[4] level of theory using Gaussian 09[5] with the application of the IEFPCM[6] methanol or water solvation model. In all calculations, the 6-31G(d,p) basis set was used for carbon and hydrogen, while heteroatoms were represented by 6-31++G(d,p). Frequency calculations were conducted as a basis for determining free energy values at 298 K. Explicit solvation was included where indicated in the form of a methanol or water molecule that is oriented and fully optimized such that it can donate or accept hydrogen bonds.

3.3. Results and Discussion

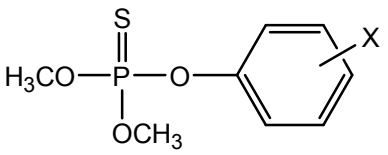

3.1

a) 4-nitro-2-chloro
b) 4-nitro
c) 4-nitro-3-methyl
d) 3-nitro
e) 4-chloro
f) parent
g) 4-methyl
h) 4-methoxyl

For the alkoxide or hydroxide promoted solvolyses of O,O′-dimethyl O-aryl phosphorothioates **3.1** presented in Scheme 3-2, β^{eq} relates to the equilibrium constant, K^*, and pK_a^{HOAr} of the leaving group as given in eq. (2). The equilibrium constant, K^*, is related to the absolute equilibrium thermodynamics, and is not directly used to calculate the computational β^{eq}.

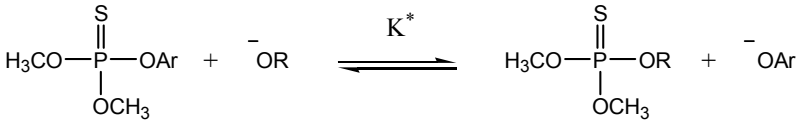

Scheme 3-2. Equilibrium relationship between O,O′-dimethyl O-aryl phosphorothioates and their alcoholysis products following the nucleophilic attack of the nucleophile $^-$OR.

$$\log K^* = \beta^{eq} \bullet pK_a^{HOAr} + \text{constant} \qquad (2)$$

eq. (2) can then be expressed in terms of the free energy of reaction, ΔG^*, as:

$$\frac{(-\Delta G^*)}{2.303RT} = \beta^{eq} \bullet pK_a^{HOAr} + \text{constant} \qquad (3)$$

Defining $\Delta G^* = (G_P + G_{-OAr} - G_{SM} - G_{Nu})$, leads to:

$$\frac{(G_{SM} - G_{-OAr})}{2.303RT} = \beta^{eq} \bullet pK_a^{HOAr} + \frac{(G_P - G_{Nu})}{2.303RT} + \text{constant} \qquad (4)$$

The substrates **3.1a-h** all lead to the same phosphorothioate product in their reaction with a common nucleophile, for example $(CH_3O)_3P{=}S$ if a methoxy ion is the nucleophile. The absolute free energy values of G_{Nu} and G_P are constant across a series of related substrates, which allows the last two terms in eq. 4 to be combined to form a different constant, A, to yield eq. (5):

$$\frac{\Delta G}{2.303RT} = \beta^{eq} \bullet pK_a^{HOAr} + A \qquad (5)$$

where $\Delta G = G_{SM} - G_{-OAr}$ is the difference in the free energies of the initial phosphorothioate **3.1** and the free aryloxide anion product. ΔG in eq. (5) does not correspond to an absolute free energy for this reaction because overall atom balance is not maintained. However, incorporating the two free energies needed to achieve atom balance (G_{Nu} and G_P) into the constant, A, reduces the number of calculations that must be performed and has a greater computational efficiency. The value of the β^{eq} parameter obtained as the slope of a plot of $\Delta G/2.303RT$ versus pK_a^{HOAr} (or ${}^{s}_{s}pK_a^{HOAr}$) and is unaffected by the isolation of free energy contributions, which only affects the intercept of such a plot.

A plot of $\Delta G/2.303RT$ versus pK_a^{HOAr} for the hydrolysis of **3.1** is shown in Figure 3-1. This series of free energy differences were obtained computationally to yield a large, negative β^{eq} value of -3.9 ± 0.4, significantly different from the experimentally determined value of -1.45. The poor agreement between the calculated and experimental

values is likely due to an increased exaggeration of destabilization effects of the negative charge in the absence of explicit solvation of poorer leaving groups.

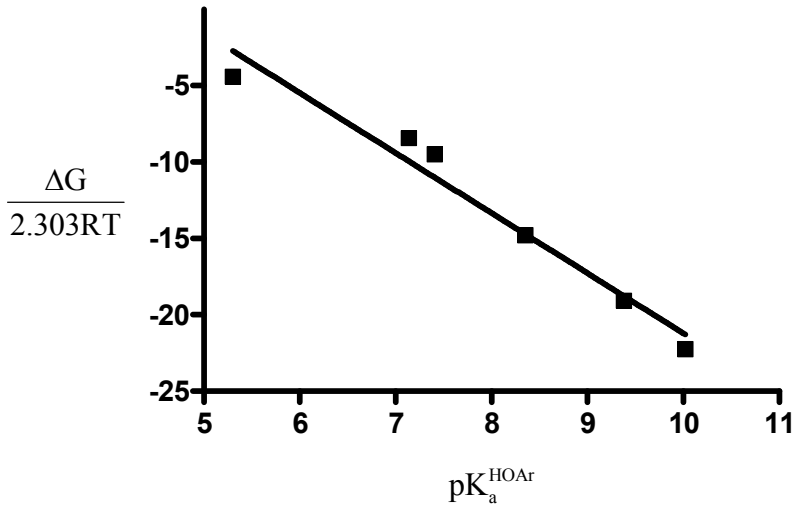

Figure 3-1. A computational pseudo-Brønsted plot for the determination of β^{eq} for the hydrolysis of **3.1** obtained via calculating absolute free energy differences between starting materials and aryl oxides as in eq. (5). Calculated $\beta^{eq} = -3.9 \pm 0.4$.

In an effort to correct the difficulty in modeling charged phenoxide leaving group species, an approach was developed that employed the free energies of the neutral substrates and their corresponding neutral phenols. The assumption is that the comparison of neutral structures with neutral structures will correlate better than that of neutral with anionic. The overall reaction is represented by the thermochemical steps outlined in Scheme 3-3. The first step involves the exchange of a methanol for a neutral phenol. The associated value of β' can be determined according to eq. 6 from a plot of $\Delta G/2.303RT$ versus ${}_s^s pK_a^{HOAr}$, where $\Delta G = G_{SM} - G_{HOAr}$. The second step involves the deprotonation of the phenol, which by definition has a value of $\beta = -1.0$. Based on this thermochemical

cycle, the value of β^{eq} is given by β' - 1.0.

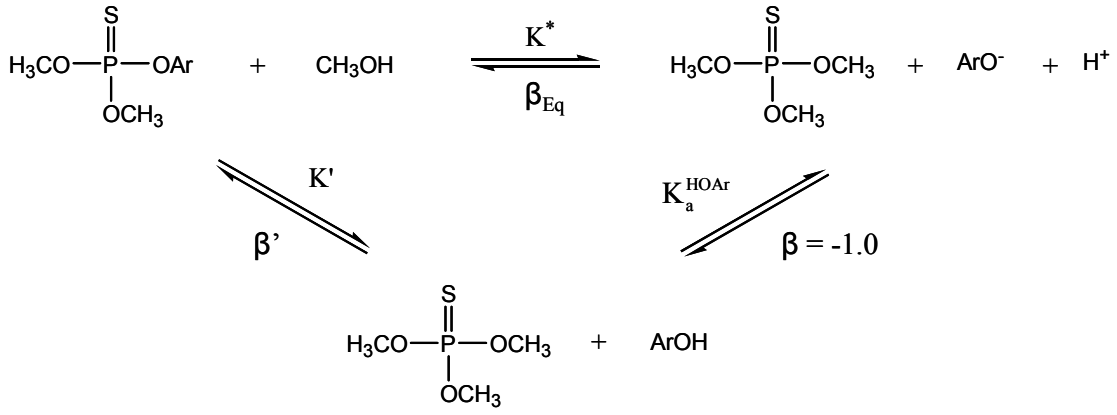

Scheme 3-3. Cycle linking starting material and corresponding leaving group phenol, where $\beta^{eq} = \beta'-1$.

Figure 3-1 and Figure 3-2 show the Brønsted plots using the experimental pK_a^{HOAr} values that give rise to the computed β^{eq} values for the hydrolysis and methanolysis of phosphorothioate esters using the methods described above. For these β^{eq} calculations, aryl leaving groups with pK_a^{HOAr} values greater than 10.02 in water (or ${}^{s}_{s}pK_a^{HOAr}$ greater than 14.3 in methanol) were excluded (4-methylphenol, **3.1g**; 4-methoxyphenol, **3.1h**), because they are outside the limits of the leaving groups used for the experimental β^{eq} values, and their use in the computations consistently showed a tendency to deviate downward from linearity. The resulting values of β^{eq} = -1.75 (hydrolysis) and -1.69 (methanolysis) are in better agreement with the experimentally determined values of -1.45 and -1.39, respectively, than the values reported above using the aryloxide anions. These calculated values are 0.3 units higher than the experimental

values; however when the errors associated with each value is considered, at the 95% confidence interval, they can be considered the same.

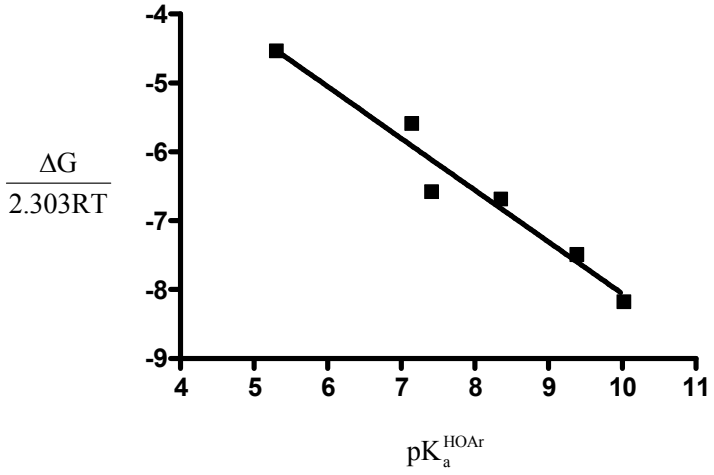

Figure 3-2. Computed Brønsted plot for determination of β^{eq} for the hydrolysis of dimethyl aryl phosphorothioates where the calculated $\beta^{eq} = \beta' -1.0 = -1.75 \pm 0.08$.

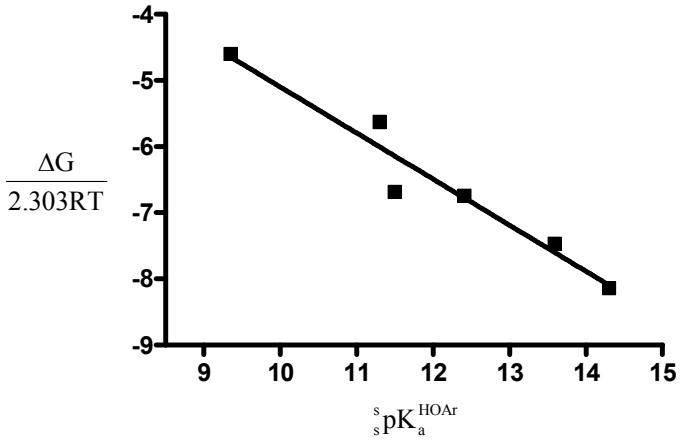

Figure 3-3. Computed Brønsted plot for determination of β^{eq} for the methanolysis of dimethyl aryl phosphorothioates in methanol where calculated $\beta^{eq} = \beta' - 1.0 = -1.69 \pm 0.05$.

3.4. Computational β^{eq} values for acyl and phosphoryl transfer reactions with other neutral substrates.

The versatility of the computational method was tested by determining whether it could satisfactorily replicate other experimentally determined β^{eq} values for transfer of phosphoryl or acyl groups from the substrates shown in Table 3-1. The results are in good agreement with experimental β^{eq} values. Plots are not shown. This is only a small sampling of the β^{eq} determination studies available, and includes only those with neutral starting materials and protonated leaving groups. Nevertheless, the calculated β^{eq} values shown in Table 3-1 show good agreement with the experimental values.

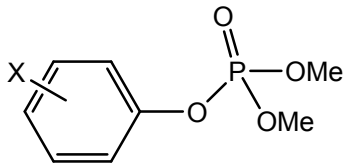

3.2

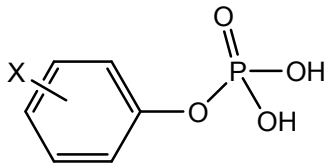

3.3

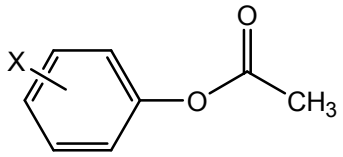

3.4

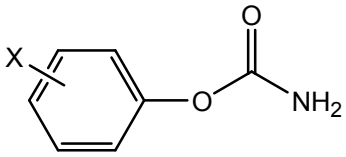

3.5

Table 3-1. Computed β^{eq} values and published experimental β^{eq} for the hydrolysis of O,O'-diethyl O-aryl phosphates[7] (**3.2**), PO_3H_2OAr esters[8] (**3.3**), acetate esters[9] (**3.4**), O-aryl carbamates[10] (**3.5**). Errors in calculated values are standard deviations of the computed Brønsted plots. Errors in experimental values calculated from the original data. *Calculated value of -1.68 was for dimethyl aryl phosphates **3.2** while experimental value is for the diethyl analogues.

Substrate	β^{eq} (Experimental)^{ref}	β^{eq} (Calculated)
3.2*	-1.87 ± 0.13 [7]	-1.68 ± 0.07
3.3	-1.83 ± 0.07 [8]	-1.70 ± 0.08
3.4	-1.70 ± 0.07 [9]	-1.8 ± 0.2
3.5	-1.80 ± 0.09 [10]	-1.84 ± 0.08

3.5. Inclusion of explicit solvation effects on the leaving group

The above described calculations represent a "barebones" solvent model without explicit solvent interactions. The next step in more accurately representing the protic solvent, logically, is to introduce these explicit substrate-solvent interactions. Modeling the H-bonding environment around the aryloxygen was attempted in three ways: 1) solvent donating a hydrogen-bond to leaving group aryloxygen; 2) solvent accepting a hydrogen bond from the HOAr hydroxyl group; and, 3) both (Table 3-2). The addition of one hydrogen bond from solvent proton to leaving group oxygen uniformly decreases the absolute value of the calculated β^{eq} making it closer to the experimental values for phosphorothioates and perhaps acetates. The inclusion of H-bonds involving the phenolic proton increases the absolute β^{eq} values. In view of the somewhat arbitrary decisions

about which H-bonds to include, we have opted for the simplest computational protocol where the solvent is treated by a continuum model without explicit H-bonding interactions to the phenol. These values are shown in Table 3-2. Examination of these results shows that in the case of acetates and phosphorothioates, explicit hydrogen bonding brings the calculated values closer to the experimental values. However, for all other cases, explicit hydrogen bonding does not improve the reproduction of the experimental values.

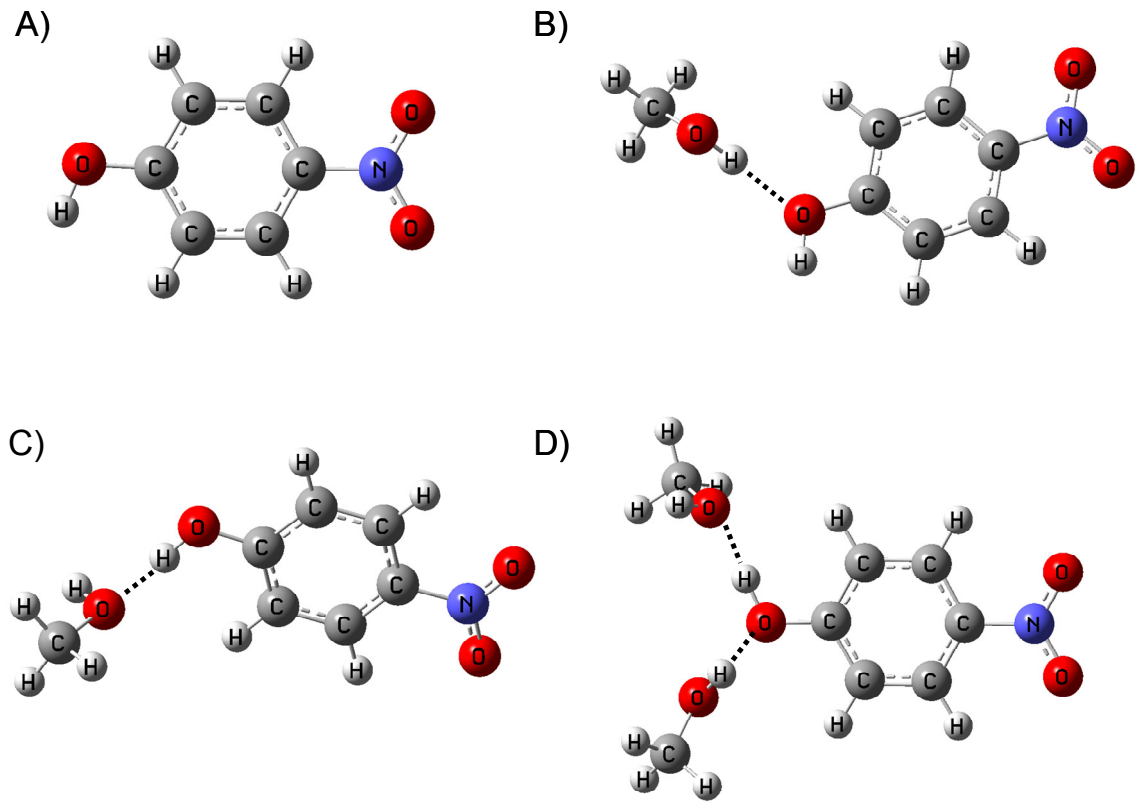

Figure 3-4. Hydrogen bonding motifs used in this work. A) No Hydrogen bonds, B) phenol oxygen accepting hydrogen bond from solvent, C) phenol acting as a hydrogen bond donor to solvent oxygen and D) phenol acting as both a hydrogen bond donor and acceptor.

Table 3-2. Calculated β^{eq} values for the hydrolysis and methanolysis of substrates with different phenol/solvent H-bonding environments.

Substrate	Solvent	LgOH	LgO(H) --- HOR	LgOH --- OR(H)	LgO(H) --- HOR, H --- OR
3.1	H_2O	-1.75 ± 0.08	-1.66 ± 0.09	-2.14 ± 0.05	-2.14 ± 0.03
3.1	MeOH	-1.69 ± 0.08	-1.54 ± 0.05	-2.00 ± 0.06	-1.71 ± 0.06
3.2	H_2O	-1.68 ± 0.07	-1.58 ± 0.07	-2.1 ± 0.1	-2.06 ± 0.08
3.2	MeOH	-1.54 ± 0.07	-1.39 ± 0.04	-1.88 ± 0.05	-1.6 ± 0.1
3.3	H_2O	-1.70 ± 0.11	-1.61 ± 0.09	-2.0 ± 0.1	-2.0 ± 0.1
3.4	H_2O	-1.8 ± 0.2	-1.7 ± 0.2	-2.2 ± 0.2	-2.3 ± 0.2
3.5	H_2O	-1.84 ± 0.08	-1.8 ± 0.1	-2.32 ± 0.05	-2.32 ± 0.05

3.6. Conclusion

Presented here is a straightforward density functional theory method for estimation of Brønsted β^{eq} values for phosphoryl and carbonyl transfer reactions. Different hydrogen bonding environments have been closely examined and it was found that the simplest solvent approximation of the naked phenol with continuum solvent model applied gives β^{eq} values that most closely reproduce the experimental values, and reproduce them well considering uncertainties in both numbers.

3.7. References

1) Edwards, D. R.; Maxwell, C. I.; Harkness, R. W.; Neverov, A. A.; Mosey, N. J.; Brown, R. S. *J. Phys. Org. Chem,* Published online, July 31, 2011; DOI:10.1002/poc.1903.

2) Leffler, J. E. *Science,* **1953**, *117,* 340.

3) Thea, S.; Williams, A. *Chem. Soc. Rev.* **1986**, *15,* 125.

4) a) Becke, A. D. *Phys. Rev. A.* **1988**, *38*, 3098; b) Lee, C.; Yang, W.; Parr, R. G. *Phys. Rev. B*. **1988**, *37*, 785.

5) Gaussian 09, Revision **A.1**, Frisch, M. J.; Trucks, G. W.; Schlegel, H. B.; Scuseria, G. E.; Robb, M. A.; Cheeseman, J. R.; Scalmani, G.; Barone, V.; Mennucci, B.; Petersson, G. A.; Nakatsuji, H.; Caricato, M.; Li, X.; Hratchian, H. P.; Izmaylov, A. F.; Bloino, J.; Zheng, G.; Sonnenberg, J. L.; Hada, M.; Ehara, M.; Toyota, K.; Fukuda, R.; Hasegawa, J.; Ishida, M.; Nakajima, T.; Honda, Y.; Kitao, O.; Nakai, H.; Vreven, T.; Montgomery, Jr., J. A.; Peralta, J. E.; Ogliaro, F.; Bearpark, M.; Heyd, J. J.; Brothers, E.; Kudin, K. N.; Staroverov, V. N.; Kobayashi, R.; Normand, J.; Raghavachari, K.; Rendell, A.; Burant, J. C.; Iyengar, S. S.; Tomasi, J.; Cossi, M.; Rega, N.; Millam, N. J.; Klene, M.; Knox, J. E.; Cross, J. B.; Bakken, V.; Adamo, C.; Jaramillo, J.; Gomperts, R.; Stratmann, R. E.; Yazyev, O.; Austin, A. J.; Cammi, R.; Pomelli, C.; Ochterski, J. W.; Martin, R. L.; Morokuma, K.; Zakrzewski, V. G.; Voth, G. A.; Salvador, P.; Dannenberg, J. J.; Dapprich, S.; Daniels, A. D.; Farkas, Ö.; Foresman, J. B.; Ortiz, J. V.; Cioslowski, J.; Fox, D. J. Gaussian, Inc., Wallingford CT, 2009.

6) a) Tomasi, J.; Mennuccia, B.; Cancés, E. *THEOCHEM*. **1999**, *464*, 211; b) Tomasi, J.; Mennuccia, B.; Cammi, R. *Chem. Rev.* **2005**, *105*, 2999.

7) S. A. Ba-Saif, A. Williams. *J. Org. Chem.* **1988**, *53*, 2204.

8) Bourne, N.; Williams, A. *J. Org. Chem.* **1984**, *49*, 1200.

9) Gerstein, J.; Jencks, W. P. *J. Am. Chem. Soc.* **1964**, *86*, 4655.

10) Al-Rawi, H.; Williams, A. *J. Am. Chem. Soc.* **1977**, *99*, 2671.

Chapter 4. Density Functional Theory and Experimental Study of Lyoxide-Promoted Cleavages of Phosphorothioate and Phosphate Triesters in Water and Methanol.

4.1. Preface

With minor formatting changes, and modification of some figures to remove colour, this chapter is as it was accepted for publication to the *Journal of Physical Organic Chemistry*. All theoretical calculations were completed by C. Maxwell, and all experiments were conducted by C. Tony Liu. Relevant information from the Supplementary information has been added in the Post Script (Section 4.7) to maintain the flow of the main concepts.

4.2. Introduction

Phosphoryl transfer reactions are among the most common chemical transformations in living systems,[1] and the mechanisms by which they proceed have been studied extensively via experimental[2,3] and computational means.[4] Reactions involving the transfer of phosphorothioyl groups ($(OR)_2P{=}S$ or $^{-}O(OR)P{=}S$) from phosphorothioate tri- and diesters (**4.1**) to oxyanion nucleophiles have been subject to recent attention due to their industrial and possible pharmaceutical applications. For example, phosphorothioate modification of oligonucleotides, where a non-bridging phosphate oxygen is replaced by a sulfur atom, has been studied as a means of protecting oligodeoxynucleotides from nuclease degradation,[5] which may make them novel therapeutic agents.[6] Additionally, phosphorothioate triesters have been widely employed

as insecticides and acaricides due to their neurotoxic properties.[7] The reactivities of neutral phosphorothioates are related to those of their P=O phosphate counterparts (**4.2**), but it is generally found that the thio-effect (defined as the ratio of rate constants for base-promoted reaction of a phosphate di- or tri-ester relative to that of the corresponding phosphorothioate ester (k^O/k^S)) is 5-20.[8] Members of the neutral phosphate/phosphonate classes of compounds have significant toxicity, as epitomized by the insecticides and nerve agents such as paraoxon (*O,O*-diethyl *O*-*p*-nitrophenyl phosphate), parathion (*O,O*-diethyl *O*-*p*-nitrophenyl phosphorothioate), sarin (*O*-isopropyl methylphosphonofluoridate), soman (*O*-pinacolyl methylphosphonofluoridate) and VX (*O*-ethyl *S*-(2-(diisopropylamino)ethyl) methylphosphonothioate).[7b] Because of their environmental accumulation, health threats and possible use as 'weapons of opportunity' by terrorist organizations, detailed studies of their decomposition mechanisms are warranted, as is the development of efficient catalytic means for their decontamination. Recent contributions to the latter area from our labs have disclosed the results of metal-catalyzed methanolytic cleavages of phosphorothioate (**4.1**)[9,10] and phosphate triesters (**4.2**)[11] where substantial rate accelerations over the background reactions at ambient temperature and essentially neutral pH (in alcohol) are observed. The present report is an extension of these studies, but deal with new aspects of the mechanism of the base-promoted solvolysis.

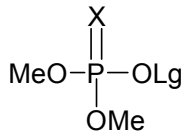

4.1 X=S
4.2 X=O

OLg =
a. 2,4-dinitrophenyl
b. 2-chloro-4-nitrophenyl
c. 3,5-dinitrophenyl
d. 2,4,5-trichlorophenyl
e. 4-nitrophenyl
f. 3-methyl-4-nitrophenyl
g. 3,5-dichlorophenyl
h. 3-nitrophenyl
i. 4-chlorophenyl
j. phenyl
k. 4-methoxyphenyl
l. 2,2,2-trifluoroethyl
m. 2,2-difluoroethyl
n. 2-monofluoroethyl
o. methyl
p. ethyl

For P=O containing *cyclic* phosphate triesters, extensive experimental evidence suggests that, depending on the leaving group and the nature of the attacking oxyanionic nucleophile, there is a continuum of mechanisms depending on both the leaving group and nucleophile from concerted displacement of the leaving group to a stepwise addition/elimination process involving a 5-coordinate anionic phosphorane intermediate.[3a,12,13] However, for *acyclic* triesters, the bulk of the extant linear free energy[14] and heavy atom kinetic isotope[15] data obtained from study of the solvolysis of phosphate triesters containing aryloxy leaving groups indicate that phosphoryl transfer to oxygen acceptors is concerted. Recent provocative computational data disclosed by Tarrat[16] indicate that the alkaline hydrolysis of acyclic *O,O*-dimethyl *O*-aryl phosphate triesters containing aryloxy leaving groups with $pK_a^{HOAr} > 8$ proceeds through a stepwise mechanism with a high energy, 5-coordinate, phosphorane intermediate. All these involve rate-limiting HO^- attack on the P=O center with fast departure of the leaving group, but when the leaving group becomes better, with $pK_a^{HOAr} < 8$, the reaction becomes an 'enforced concerted'[17] one, with no stable intermediate. Since the hydrolyses of P=S phosphorothioate triesters are believed to be mechanistically similar to those of their P=O analogues,[8] it is reasonable to speculate that the cleavage of neutral P=S

phosphorothioate triesters might also involve a continuum between concerted and stepwise processes depending on the goodness of the leaving group. Such a finding would provide an important supplement to the interpretation of experimental studies that reported linear Brønsted relationships (plotting log k_{nuc} vs. pK_a^{lg} (lg designates alkoxy or aryloxy) for the solvolysis of a series of phosphorothioate triesters in water[10,18] and light alcohols[9a,10,19]). There the reactions were described as either concerted, without the formation of an intermediate, or stepwise with rate limiting formation of an intermediate which rapidly broke down to product. It should be noted that the Brønsted plots were for triesters having leaving groups (Olg) that are less basic than the incoming oxanion nucleophiles. Thus, if a stepwise mechanism were operating, the departure of Olg will always be less energetically demanding than expulsion of the nucleophile. Accordingly, a linear Brønsted plot does not exclude a stepwise mechanism with rate-limiting nucleophilic attack to form a high energy intermediate with subsequent P-Olg bond fission.[20] In fact, we have recently demonstrated that a palladacycle-catalyzed methanolysis of a series of phosphorothioates triesters does involve a highly stable palladacycle bound 5- coordinate thiophosphorane along the reaction pathway.[9]

In the present study, we mapped the energy profiles for the solvolytic reactions involving hydroxide and methoxide attack on a series of *O*-aryloxy and *O*-alkoxy containing *O,O*-dimethyl phosphorothioate esters **4.1** through DFT calculations in order to show that the solvolytic mechanism undergoes a progressive change from concerted to stepwise. The methanolysis reactions of esters **4.1h-p**, containing poorer leaving groups with high pK_a^{lg}, proceed through a stepwise mechanism with rate-limiting nucleophilic attack to form an anionic 5-coordinate thiophosphorane intermediate. The computed

phosphorane fits with Jencks[21] and More O'Ferrall's[22] definition of a true reaction intermediate located in a well on the potential energy surface, and having a lifetime longer than that of a molecular vibration of ~ 10^{-13} s. The methanolysis reactions of more activated substrates having better leaving groups (**4.1a-g**), can be considered as 'enforced concerted' processes with barrierless P-Olg bond fission. Here, the single rate limiting transition state has extensive formation of the nucleophile---P bond with little lengthening of the P-Olg bond. For comparison, we have expanded the substrate scope presented in Tarrat's original study[16] and investigated the hydrolysis of phosphate triesters **4.2a-p**, finding a similar mechanistic change as determined with the phosphorothioate counterparts.

We also experimentally determined the Brønsted relationships (log k_{OR}^- vs. pK_a^{lg}) for the lyoxide-promoted solvolyses of **4.1** and **4.2** in methanol and water, which we compare with the computationally-derived ones. There are downward breaks observed in the two Brønsted plots, but the evidence indicates these do not occur at the quasi-symmetrical point where the nucleophile and leaving group have the same pK_a. The downward break in these plots is not due to a change in the rate-limiting step but rather to fundamental differences in the charge and solvation characteristics of aryloxy and alkoxy leaving groups. Finally, we have looked at the computed identity reactions with three phosphorothioate substrates having the same nucleophile and leaving group (methoxide, *p*-nitrophenoxide, and 2,4-dinitrophenoxide). The following reveals our findings on these three areas.

4.3. Experimental

4.3.1. Computational Details

Geometry optimizations and energy calculations of starting materials, intermediates, and transition states were conducted at the PBE1PBE[23] level of theory using the 6-311++G(2d,2p) basis set. This combination of method and basis set has been shown to be effective in the determination of activation and reaction energies for phosphodiester hydrolyses[24] and is presumably well-suited to the similar phosphate chemistry considered in this work. Frequency calculations were performed to obtain free energy corrections to the potential energies at 298 K, and to characterize all stationary points as minima or saddle points. Intrinsic reaction coordinate calculations were conducted to verify some transition states and to find shallow intermediates on the potential energy surface. The IEFPCM[25] solvation model was applied during the optimization and frequency calculations for solvated structures. Electrostatic-potential derived atomic charges were derived using the Chelp-G[26] method. Gaussian 09[27] was used to conduct all calculations.

Difficulties in calculating entropy with the application of continuum solvation models are well-known[28] and arise primarily from the inability to capture the effects of explicit solvent-solute interactions on the solute's translational and rotational degrees of freedom when the solvent is represented as a continuum. Although steps can be taken to address these errors, corrections to the calculated entropy were not employed here because the goal of this study is to compare *relative* rate constants rather than determine of *absolute* rate constants. Specifically, the similarity of reactions within each set of

substrates results in entropic errors that are approximately equivalent and cancel throughout. Additionally, accurate free energy determinations for bimolecular reactions in the condensed phase require a conversion from standard temperature/pressure in the gas phase to standard state in solution (1 M).[29] This conversion will be identical for all solution phase reactions studied in this work and has no effect on the gradients of the Brønsted correlations or relative stabilities of unimolecular intermediates. Thus all free energies presented are not corrected for concentration. Given in the Postscript (Section 4.7, Table 4-7, Table 4-8, Table 4-9) are tables of relative computed free energies (relative to the free energies of the starting materials) for transition states and intermediates for the cases where there is a concerted reaction or stepwise nucleophilic attack and leaving group departure.

Free energies of activation were used to calculate second-order rate constants using classical transition state theory.[30] Rate constants are plotted against leaving group pK_a to construct computationally-derived Brønsted plots.

4.3.2. Base-promoted methanolysis of esters 4.1 and 4.2

Phosphorothioates **4.1l-n** and phosphates **4.2l-n,p** were prepared following a published procedure[31] using either dimethyl chlorothiophosphate or dimethyl chlorophosphate and the corresponding alcohols as the starting materials. The ^{1}H, ^{31}P, ^{13}C, and ^{19}F NMR spectra given in the Supporting Information are consistent with the structure. Methoxide-promoted cleavages of phosphorothioate (**4.1l-n**) and phosphate (**4.2l-o**) triesters were followed by ^{31}P NMR spectroscopy at 162.04 MHz. Typically, 10

mM of a given triester was combined with tetrabutylammonium hydroxide (from a 1.0 M stock solution in methanol as supplied by Aldrich (Sigma-Aldrich Canada, Oakville, ON, Canada) and found to be 1.05 M when titrated against N/2 Fisher certified standard aqueous HCl solution (Fisher Scientific, Pittsburgh, PA, USA) in 800 μL of methanol in an NMR tube. A sealed glass tube containing CD_3OD was inserted into each NMR tube to provide a deuterium lock. The NMR samples were capped and sealed with Parafilm®. For each substrate, at least three concentrations of tetrabutylammonium hydroxide ranging from 100 – 300 mM were used, and the samples were prepared in triplicate at each [base]. At different times, the samples were removed from a 23 ^{o}C water bath and the proton-decoupled ^{31}P NMR spectra were acquired with at least 180 scans. ^{31}P NMR spectra of the starting triesters as well as that of the authentic trimethyl phosphate and trimethyl phosphorothioate in methanol were used as references (the chemical shifts of the known compounds in CD_3OD were referenced using an inserted sealed glass tube containing ~ 0.1 M phosphoric acid in CD_3OD). A competitive demethylation process,[32] resulting from nucleophilic attack on one of the CH_3 groups to form $X=P(OR)(OCH_3)(O^-)$, was observed for substrates **4.1n,o** and **4.2m,n**,**p** under basic conditions in methanol. The reaction progress was monitored by determining both the % conversion of the starting triester and the ratios of the P-Olg cleavage product (trimethyl phosphate/phosphorothioate triester) to the demethylation product (a diester). The % conversion of the starting substrate was plotted against time, and the data were fitted to a standard first order kinetic expression to yield the first order rate constants (k_{obs}^{SM}) for the disappearance of starting material at different [base]. The individual rate constants for P-Olg cleavage ($k_{obs}^{P\text{-}O}$) and demethylation ($k_{obs}^{C\text{-}O}$) were obtained from the product ratios

and the overall rate constants (k_{obs}^{SM}). The rate constants for the product formations were then plotted against the initial [tetrabutylammonium hydroxide], and fitting of the data to a linear regression forcing the fit through the origin generates the second-order rate constants (k_2^{P-O} and k_2^{C-O}). This forcing is justified since the lyoxide reactions for phosphate and phosphorothioate triesters dominate the solvolytic reactions under all conditions we have investigated.

4.4. Results

4.4.1. General Mechanistic Considerations

Transition states for the nucleophilic attack of methoxide on **4.1e**, **j**, and **n** were considered with the nucleophile attacking along each of the directions described in Scheme 4-1. The associated free energy barriers are given in Table 4-1 where the data show that the pathway involving nucleophilic approach opposite to the leaving group (direction A) has the lowest activation energy in all cases. Attack opposite the *O*-methyl groups (direction B) leads to slightly higher free energy barriers, while nucleophilic attack opposite to the sulfur (direction C) results in much higher free energies of activation. This is expected as more electronegative substituents are likely to occupy axial positions on phosphorus. Berry pseudorotations were also modeled and their free energies are considerably lower than those of the nucleophilic attacks and would not be kinetically relevant (Postscript, Section 4.7, Scheme 4-4). Thus, for this work, reactions were modeled as occurring via a nucleophilic attack in-line with the leaving group.

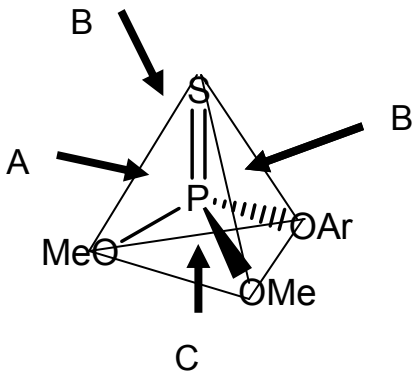

Scheme 4-1. Possible angles of nucleophilic attack.

Table 4-1. Free energy differences (kcal/mol) of SM and transition states associated with different approaches of nucleophiles shown in Scheme 4-1.

Substrate	A	B	C
4.1e	16.5	18.3	30.1
4.1j	18.4	20.8	28.5
4.1n	19.0	20.7	28.9

The free energies for the methanolysis of a series of dimethyl phosphorothioates with aryloxy (**4.1a,c,e,g-j)** or alkoxy (**4.1l-n,p)** leaving groups were determined as an associative nucleophilic attack on phosphorus occurring from a position opposite the leaving group (***TS**$_{nuc}$*). This transition state leads to an anionic thiophosphorane structure with the nucleophile and leaving group occupying the apical positions. The calculations showed that substrates with good leaving groups (with low $^{s}_{s}pK_a^{HOAr}$ values of ≤ 12.3 in methanol for the corresponding phenols) proceed directly to products after passing

through this transition state, indicating a concerted mechanism with highly asynchronous nuc—P and P-Olg bond lengths (*vide infra*). Meanwhile, substrates with poorer leaving groups generate a stable 5-coordinate thiophosphorane intermediate (***INT***) after passing through $\boldsymbol{TS_{nuc}}$, following a stepwise mechanism. In these cases, the system reaches the product by passing through a transition state for the departure of the leaving group ($\boldsymbol{TS_{lg}}$), which involves the lengthening of the P-Olg bond in the apical position.

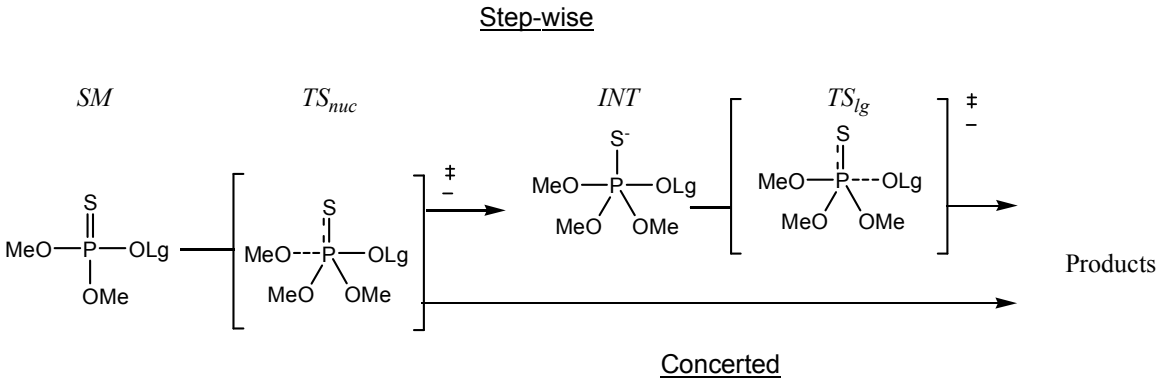

Scheme 4-2. Reaction map showing species considered in the calculations of methoxide attack on phosphorothioates.

4.4.2. Computed Brønsted plot for the methanolysis of phosphorothioates 4.1 in methanol

The free energy of activation for the nucleophilic attack is defined as the difference between the sum of the free energies of the infinitely separated nucleophile and SM, and that of the transition state (eq. (1)).

$$\Delta G_{nuc} = G_{\mathbf{TS,nuc}} - (G_{\mathbf{SM}} + G_{MeO^-}) \qquad (1)$$

The calculated values of ΔG_{nuc} were used to determine second-order rate

constants,[30] which were then used along with the experimental ${}^{w}_{w}pK_a$ (in water) or ${}^{s}_{s}pK_a$ (in methanol)[33] of the leaving group phenols or alcohols to construct the Brønsted plots. The absolute values of ΔG_{nuc} used to obtain the rate constants are likely inaccurate compared to experimental values because of the aforementioned difficulties in properly determining the contributions of translational and rotational degrees of freedom to the entropy. Such errors will affect the y-intercept of a Brønsted plot; however, the present study focuses on exploring the slope of the plot, which is expected to be insensitive to such inaccuracies due to a systematic cancellation of errors.

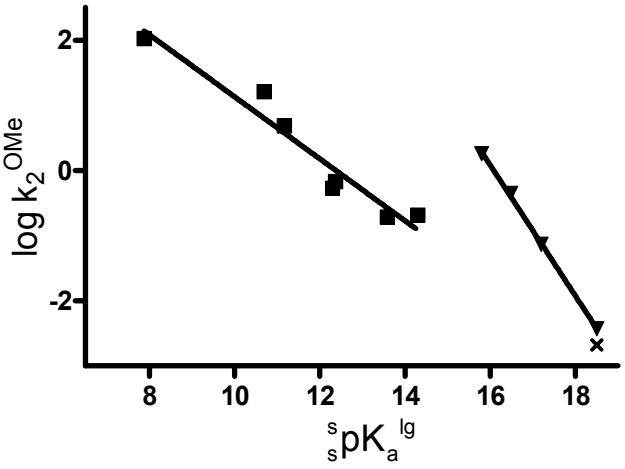

Figure 4-1. Plot of computationally-derived log k_2^{OMe} vs. the ${}^{s}_{s}pK_a^{lg}$ of the leaving groups for the methoxide-promoted cleavage of phosphorothioates **4.1** with the methanol continuum solvation model. The data were fitted to standard linear regression model to give the slopes of -0.48 ± 0.05 (■: **4.1a,c,e,g-j**; $r^2 = 0.9394$) and -1.02 ± 0.05 (▼: **4.1l-n,p**; $r^2 = 0.9993$). The x at the lower terminus of the alkoxy leaving group plot represents the predicted log k_2^{OMe} for the rate-determining leaving group expulsion transition state for poorest substrate **4.1p**.

Brønsted plots for the methoxide-promoted cleavage of phosphorothioate substrates **4.1** are shown in Figure 4-1. Note that the absolute values of the rate constants are not consistent with experimental values; however, their relative positions match well with experimental data (*vide supra,* Section 4.4.8). The data for the aryloxy and alkoxy substrates are clearly not collinear and were fitted separately. The exception is **4.1p** (indicated by the x on the alkoxy leaving group plot), where the rate-limiting step was defined by $\boldsymbol{TS_{lg}}$ and is not included in the regression analysis. Linear Brønsted relationships are evident for each set of substrates having either aryloxy or alkoxy leaving groups. This occurs because the $\boldsymbol{TS_{nuc}}$ involving nucleophilic attack is rate-limiting in all cases, except for **4.1p**, and hence the Brønsted plots are dictated by the relative free energy differences of ***SM*** and $\boldsymbol{TS_{nuc}}$ within each series of substrates. However, the linear Brønsted plots hide the fact that only substrates (**4.1a,c,e,g**) with stabilized leaving groups having ${}^{s}_{s}pK_a^{HOAr}$ values of $\leq$ 12.3 follow enforced concerted pathways but substrates **4.1h**, **i**, **j**, **k, l, m, n, p** follow stepwise pathways with a stable 5-coordinate intermediate in which $\mathbf{TS_{nuc}}$ is rate-limiting, as indicated by the free energy profiles in Figure 4-2 and Table 4-2. Note that the potential energy surface for **4.1h** contained a local minimum and maximum corresponding to **Int** and $\mathbf{TS_{lg}}$, respectively; however, the free energy of the intermediate was found to be greater than that of the subsequent transition state. The natures of these reaction pathways were confirmed with intrinsic reaction coordinate calculations. Table 4-3 lists relevant interatomic distances for atoms involved in bond forming/breaking transition states and phosphorane intermediates.

Table 4-2. Free energies (kcal mol^{-1}) of optimized intermediates and transition states for the methanolysis of **4.1a,c,e,g-j,l,m,n,p** using methanol continuum solvation. Free energy values (298 K) are relative to the energy of the infinitely separated phosphorothioate and nucleophile.

	TS_{nuc}	Int	TS_{LG}
4.1a	14.7		
4.1c	15.8		
4.1e	16.5		
4.1g	17.8		
4.1h	17.7	-2.7	-2.9
4.1i	18.4	-0.1	0.6
4.1j	18.4	1.8	4.8
4.1l	17.1	0.1	6.7
4.1m	17.9	3.3	10.2
4.1n	19.0	3.6	16.9
4.1p	20.8	7.5	21.1

Table 4-3. Interatomic distances (Å) of phosphorus-methoxide oxygen and phosphorous-alkoxyl/aryloxyl oxygen of the leaving group in optimized transition states and penta-coordinate phosphorane intermediates.

	TS_{nuc}		Int		TS_{lg}	
Substrate	P-nuc (Å)	P-Olg (Å)	P-nuc (Å)	P-Olg (Å)	P-nuc (Å)	P-Olg (Å)
4.1a	2.875	1.677				
4.1c	2.817	1.666				
4.1e	2.790	1.664				
4.1g	2.744	1.660				
4.1h	2.747	1.659	1.689	1.851	1.652	2.215
4.1i	2.708	1.654	1.696	1.821	1.647	2.289
4.1j	2.663	1.653	1.699	1.806	1.646	2.311
4.1l	2.682	1.646	1.709	1.761	1.638	2.450
4.1m	2.671	1.641	1.713	1.749	1.636	2.504
4.1n	2.634	1.637	1.718	1.737	1.634	2.626
4.1p	2.643	1.626	1.726	1.721	1.632	2.621

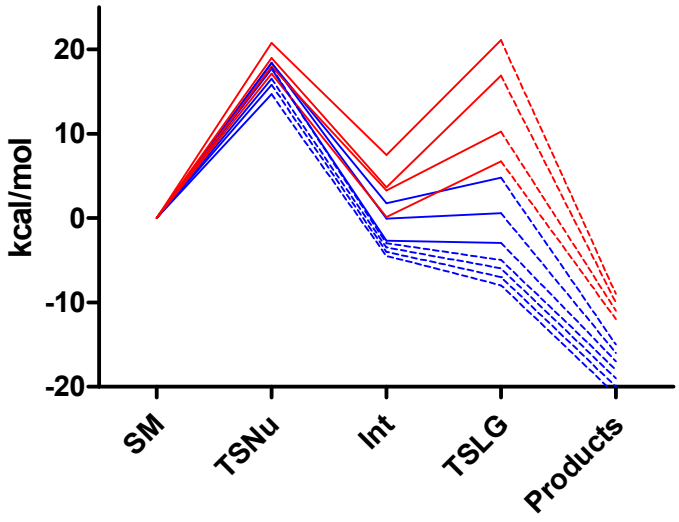

Figure 4-2. Computed reaction coordinate diagrams for the methanolysis of phosphorothioates **4.1a,c,e,g-j,l-m,p**. In blue are substrates with aryloxy leaving groups while in red are substrates with alkoxy leaving groups. Dotted lines correspond to structures along the reaction pathway that were not calculated due to absence of an intermediate minimum on the PES or because they led to products whose energies are not relevant to this study; they are included only to represent estimates of the PES following calculated transition states. The free energies of product phenoxide and trimethyl phosphorothioate were not calculated, as they are not relevant to the current study.

4.4.3. ChelpG population analysis

To follow the charge development over the course of each reaction, ChelpG population analyses were conducted for each **SM** and $\mathbf{TS_{nuc}}$ formed during the methanolysis of **4.1a,c,e,g-j, l-p**. Linear regression was conducted to fit each data set to Q (sum of group atomic charges) = m $^{s}_{s}pK_a$ + c. As expected, the leaving group of the **SM** structures bears more negative charge with more electronegative substituents (Figure

4-3), however there is a clear break between alkoxy and aryloxy groups. This break is less defined, but still present, in the $\mathbf{TS_{nuc}}$ structures. With increasing leaving group electronegativity, it is expected that increasing positive charge on the thiophosphate moiety would mirror the increasing negative charge of the leaving group. However, the bulk of change in positive charge development is found only on the sulfur atom (Figure 4-4), while the charge of the $P(OMe)_2$ moiety is largely unchanged (Figure 4-5). Interestingly, the addition of the negatively charged nucleophile results in an increase in positive charge about the $P(OMe)_2$ moiety.

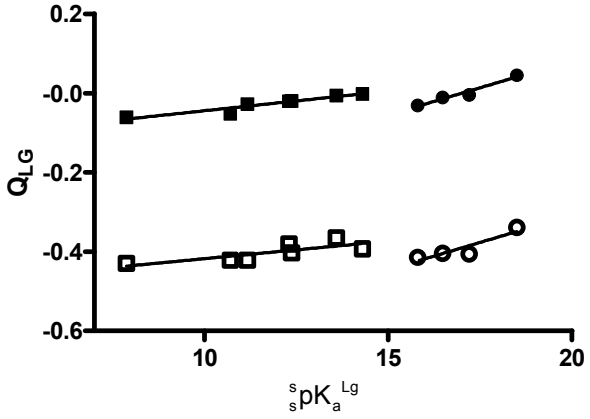

Figure 4-3. Total ChelpG charges for all leaving group atoms in **SM** (■, aryl, m = 0.010 ± 0.001 charge units · $_{s}^{s}pK_a^{-1}$; ●, alkyl, m = 0.027 ± 0.004 charge units · $_{s}^{s}pK_a^{-1}$) and $\mathbf{TS_{nuc}}$ (□, aryl, m = 0.009 ± 0.003 charge units · $_{s}^{s}pK_a^{-1}$; ○, alkyl, m = 0.027 ± 0.009 charge units · $_{s}^{s}pK_a^{-1}$), for the methanolysis reactions of **4.1a,c,e,g-j, l-n,p** with the methanol solvent model.

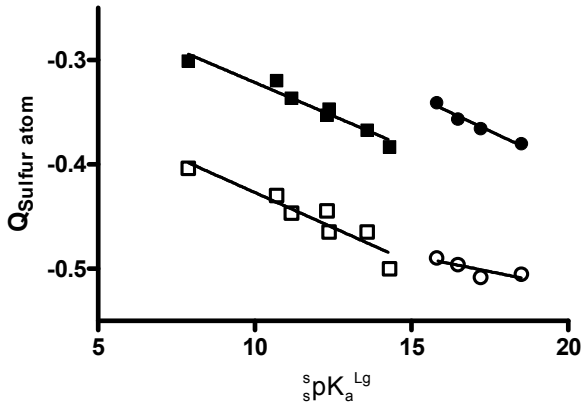

Figure 4-4. ChelpG charges of the sulfur atom in **SM** (■, aryl, m = -0.013 ± 0.001 charge units · $_s^spK_a^{-1}$; ●, alkyl, m = -0.013 ± 0.002 charge units · $_s^spK_a^{-1}$) and **TS$_{nuc}$** (□, aryl, m = -0.014 ± 0.002 charge units · $_s^spK_a^{-1}$; ○, alkyl, m = -0.006 ± 0.003 charge units · $_s^spK_a^{-1}$), for for the methanolysis reactions of **4.1a,c,e,g-j, l-n,p** with the methanol solvation.

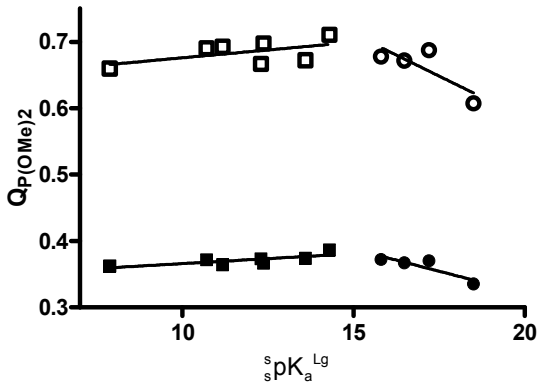

Figure 4-5. Total ChelpG charges of the P(OMe)$_2$ moiety in **SM** (■, aryl, m = 0.003 ± 0.001 charge units · $_s^spK_a^{-1}$; ●, alkyl, m = -0.013 ± 0.005 charge units · $_s^spK_a^{-1}$) and **TS$_{nuc}$** (□, aryl, m = 0.004 ± 0.003 charge units · $_s^spK_a^{-1}$; ○, alkyl, m = -0.025 ± 0.013 charge units · $_s^spK_a^{-1}$), for for the methanolysis reactions of **4.1a,c,e,g-j, l-n,p** in the methanol solvent model.

4.4.4. Computed Brønsted plot for the methanolysis of phosphates 2 in methanol

The methods described above were employed to construct a computed Brønsted plot for the methanolysis of phosphate triesters **4.2** (Figure 4-6) to complement and expand upon work conducted earlier in this laboratory.[31] This plot has a similar shape to the plot in Figure 4-1 determined for P=S ester methanolysis in that the alkoxy and aryloxy substrates form separate distinct linear regions. The reactions of P=O and P=S esters are similar also in the fact that substrates bearing good leaving groups (**4.2a, c, e, g**) react by concerted mechanisms while the methanolysis of substrates having poorer leaving groups (**4.2h-j, l-n,p**) are stepwise with rate-limiting nucleophilic attack.

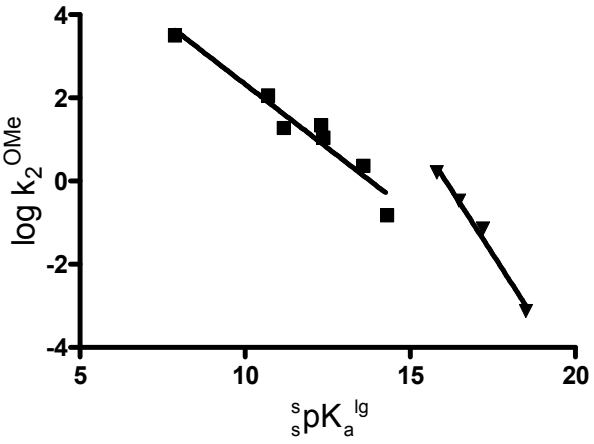

Figure 4-6. Plot of computationally derived log k_2^{OMe} vs. the $^{s}_{s}pK_a^{lg}$ of the leaving groups for the methoxide-promoted cleavage of phosphates **4.2** with the methanol continuum solvation model. The data were fitted to standard linear regression model to give the slopes of -0.61 ± 0.07 (■: **4.2a,c,e,g-j**; r^2 = 0.9367) and -1.24 ± 0.11 (▼: **4.2l-n,p**; r^2 = 0.9848).

4.4.5. Computed Brønsted plot for the methanolysis of phosphorothioates 1 in the gas phase

The Brønsted plot in Figure 4-7 was constructed using calculated gas phase free energies as well as experimental gas phase pK_a values[34] to ascertain the role of solvent in both the β^{lg} values and the difference in alkoxy/aryloxy reactivity. The free energies of the intermediate and the transition states are less than the combined G_{SM} and G_{MeO^-} due to the lack of stabilization of the small, negatively charged methoxide by solvent, so rate constants are presented relative to that with the phenyl leaving group (k^{OLG}/k^{OPh}). The lack of stabilization through solvation results in larger calculated rate constants than those reported above where the calculations were performed with the continuum solvation model. The resulting Brønsted plots are linear, with the plots for the alkoxy and aryloxy substrates having similar slopes, but are non-collinear. Detailed examination of the free energy profiles shows that the methanolysis of **4.1a** is concerted in the gas phase, while all other substrates follow a stepwise pathway. Gas phase calculations were also conducted with the P=O triesters **4.2** (Postscript Section 4.7, Figure 4-17), the overall shape of the Brønsted plots being similar to those of the P=S esters (aryloxy substrates, calculated $\beta^{lg} = -0.32 \pm 0.03$; alkoxy substrates, calculated $\beta^{lg} = -0.44 \pm 0.10$). The plots for alkoxy and aryloxy substrates are again not collinear.

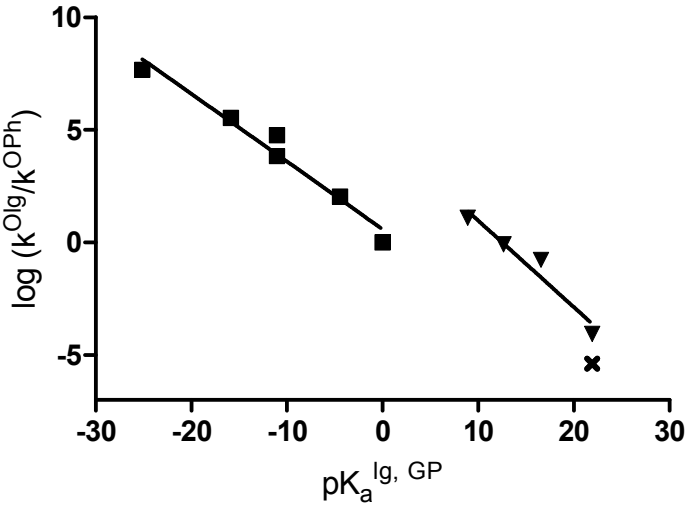

Figure 4-7. Plot of computationally derived log (k^{Olg}/k^{OPh}) vs. the $pK_a^{lg,GP}$ of the leaving groups for the methoxide-promoted cleavage of phosphorothioates **4.1** in the gas phase without any solvent model. The data were fitted to a standard linear regression model to give slopes of -0.30 ± 0.03 (■: **4.1a,c,e,g-j**; $r^2 = 0.9623$) and -0.38 ± 0.07 (▼: **4.1l-n,p**; $r^2 = 0.9377$). The x at the lower terminus of the alkoxy leaving group plot represents the predicted log k for the rate-determining leaving group expulsion transition state for poorest substrate **4.1p**.

4.4.6. Computed reaction coordinate diagrams for the substituted phenolysis/ethanolysis of phosphorothioates 4.1a,d,e,j

Reaction coordinate diagrams were calculated for the reaction of **4.1a,e,f,p** with each of 2,4-dinitrophenoxide, 4-nitrophenoxide, phenoxide and ethoxide using the methanol continuum solvation model (Figure 4-8 - Figure 4-11, Table 4-5. Interatomic distances for relevant atoms in bond forming and breaking events are listed in Table 4-4. The descriptors in Table 4-5 reflect the changes in the nature of the reaction mechanism

as the nucleophilic strengths of the nucleophile and leaving group are adjusted. In Figure 4-9 - Figure 4-11, when concerted and step-wise processes are plotted together, the single transition states of the concerted processes are labeled with TS_{nuc} or TS_{lg} although they involve both nucleophilic attack and leaving group departure. The designation of these transition states on the diagrams is arbitrary, and made for illustrative clarity only. All reactions involving the 2,4-dinitrophenoxide nucleophile result in concerted processes, but with poorer leaving groups and stronger nucleophiles, the systems gradually follow step-wise mechanisms. Reactions of moderate nucleophiles with substrates with moderate leaving groups show shallow intermediates in the free energy surface. It is noted that these free energy surfaces are independent of whether a participating alkyl/aryloxide is acting as a nucleophile or a leaving group, that is, they obey microscopic reversibility. For instance, the nucleophilic attack of ethoxide on **4.1a** will result in the same free energy surface as the nucleophilic attack of 2,4-dinitrophenoxide on **4.1p**.

Table 4-4. Interatomic distances (Å) of phosphorus-nucleophile oxygen and phosphorous-alkoxyl/aryloxyl oxygen of the leaving group in optimized transition states and penta-coordinate phosphorane intermediates formed during attack on **4.1a,e,f,p** by 2,4-dinitrophenoxide, 4-nitrophenoxide, phenoxide and ethoxide. With concerted processes (with only one transition state), the geometric data are listed in the TS_{nuc} column. For symmetrical reactions where $TS_{nuc} = TS_{lg}$, the bond distances are listed only once as their roles are mirror representations of each other.

		TS_{nuc}		Int		TS_{lg}	
Substrate	nucleophile	P-nuc	P-Olg	P-nuc	P-Olg	P-nuc	P-Olg
4.1a	2,4-diNO_2	1.799	1.783				
4.1e	2,4-diNO_2	2.225	1.730				
4.1j	2,4-diNO_2	2.509	1.696				
4.1p	2,4-diNO_2	2.880	1.683				
4.1e	4-NO_2	2.144	1.711	1.787	1.801		
4.1j	4-NO_2	2.437	1.680	1.756	1.847	1.694	2.145
4.1p	4-NO_2	2.810	1.631				
4.1j	PhO^-	2.344	1.667	1.762	1.769		
4.1p	PhO^-	2.670	1.653	1.708	1.793	1.650	2.351
4.1p	EtO^-	2.639	1.628	1.724	1.722		

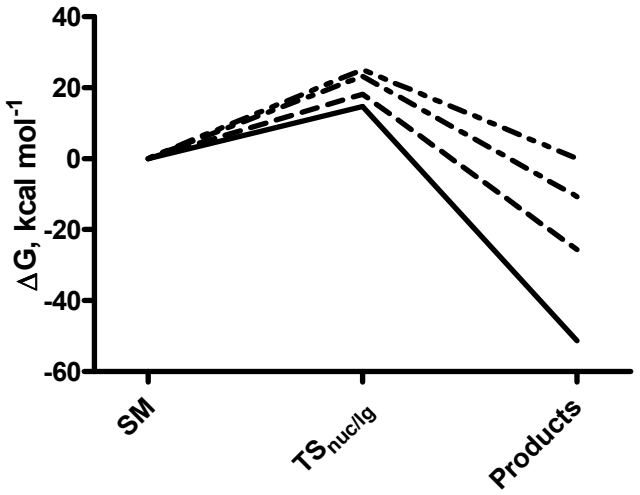

Figure 4-8. Computed free-energy reaction coordinate diagrams for the reaction of **4.1a** with substituted phenoxyl (2,4-dinitrophenoxide (— – – — – –) ; 4-nitrophenoxide (— – — –); phenoxide (– – – –)) or ethoxide (——) nucleophiles. $\mathbf{TS_{nuc/lg}}$ is the transition state involving both nucleophilic attack and leaving group departure.

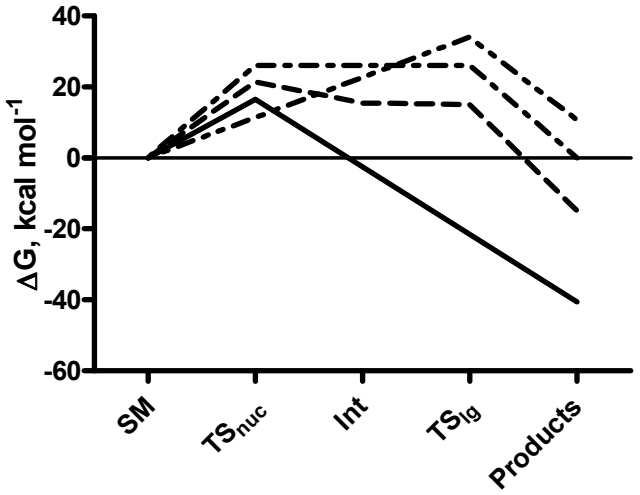

Figure 4-9. Computed free-energy reaction coordinate diagrams for the reaction of **4.1e** with substituted phenoxyl (2,4-dinitrophenoxide (— – – — – –) ; 4-nitrophenoxide (— – — –); phenoxide (– – – –)) or ethoxide (——) nucleophiles.

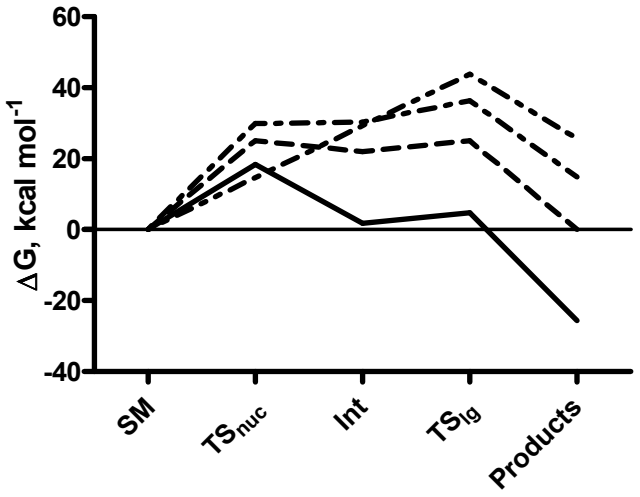

Figure 4-10. Computed free-energy reaction coordinate diagrams for the reaction of **4.1j** with substituted phenoxyl (2,4-dinitrophenoxide (— – – — – –) ; 4-nitrophenoxide (— – — –); phenoxide (– – – –)) or ethoxide (——) nucleophiles.

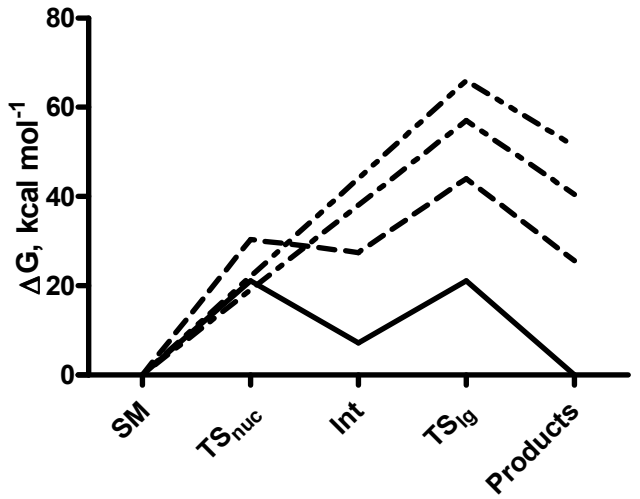

Figure 4-11. Computed free-energy reaction coordinate diagrams for the reaction of **4.1p** with substituted phenoxyl (2,4-dinitrophenoxide (— – – — – –) ; 4-nitrophenoxide (— – — –); phenoxide (– – – –)) or ethoxide (——) nucleophiles.

Table 4-5. Description of free energy surfaces for the reactions of **4.1a,e,j,p** with aryl nucleophiles and ethoxide using methanol continuum solvation.

Nucleophile	**4.1a**	**4.1e**	**4.1j**	**4.1p**
2,4-dinitrophenoxide	Concerted	Concerted	Concerted	Concerted
4-nitrophenoxide		Step-Wise	Concerted	Step-Wise
phenoxide			Step-Wise	Step-Wise
ethoxide				Step-Wise

4.4.7. Computed Brønsted plot for the hydrolysis of phosphorothioates 4.1 and phosphates 4.2 in water

Computed Brønsted plots were also constructed for the corresponding hydrolysis reactions. The necessary rate constants were calculated using $\Delta G_{\mathbf{nuc}} = G_{\mathbf{TS,\ nuc}} - G_{\mathbf{SM}} - G_{\mathbf{HO^-}}$ with the free energies computed in the presence of water treated as a continuum solvent. The Brønsted plots for this reaction are shown in the Postscript section (4.7), Figure 4-15 and Figure 4-16. As with the methanolysis and gas phase reactions, the alkoxy and aryloxy substrates lie on different lines, and intermediates exist only for substrates **4.1c, e, g-j, l-n,p** and **4.2g-j, l-n,p** (Table 4-8 in Postscript, Section 4.7).

4.4.8. Experimental Brønsted plots for the alkaline methanolyses of substrates 4.1 and 4.2

The Brønsted relationships for the methoxide-promoted cleavages of *O,O*-

dimethyl *O*-aryl phosphates[35] (β^{lg} = (-0.59 ± 0.07) and (-0.51 ± 0.04 for substrates with an *o*-carbomethoxy group) and *O,O*-dimethyl *O*-aryl phosphorothioates (β^{lg} = (-0.50 ± 0.04) from this work, within error of (-0.47±0.03) as reported by us previously[9a]). The plot of the log of the second order rate constants determined for the P-Olg fission ($k_2^{P\text{-}O}$) reactions vs. the ${}^{s}_{s}pK_a^{HOlg}$ of the departing alcohols/phenols is presented in Figure 4-12. The trends observed there are similar to the computationally derived Brønsted plots (Figure 4-1 and Figure 4-6) in which substrates containing alkoxy leaving groups sit on steeper Brønsted lines than those with aryloxy leaving groups. The alkaline methanolysis of P=O containing triesters (**4.2**) is approximately 10-100 times more rapid than their P=S counterparts (**4.1**) depending on the ${}^{s}_{s}pK_a^{HOlg}$ of the leaving group. It should be noted that, as the reactivity of the substrates decreases, a competing pathway (demethylation ($k_2^{C\text{-}O}$), Scheme 4-3) becomes important. For phosphate triesters **4.2** containing aryloxy leaving groups, no demethylation product was observed under basic conditions. For phosphorothioates **4.1**, demethylation was observed for **4.2i-k**. The demethylation process is more significant for the phosphorothioate substrates, which are intrinsically more resistant toward base-promoted solvolytic cleavage reactions than phosphates. In fact, for substrates **4.1**, the corresponding demethylation product (S=P(OAr)(OMe)(O^-)) was detected for reactions involving **4.1h-k**, **m-o** (the degree of demethylation for substrate **4.1f** and those with better leaving groups was not determined but by following the trend set by the less reactive substrates, approximately 7% of **4.1f** is expected to be converted to S=P(*O*-(3-methyl-4-nitrophenyl))(OMe)(O^-)).

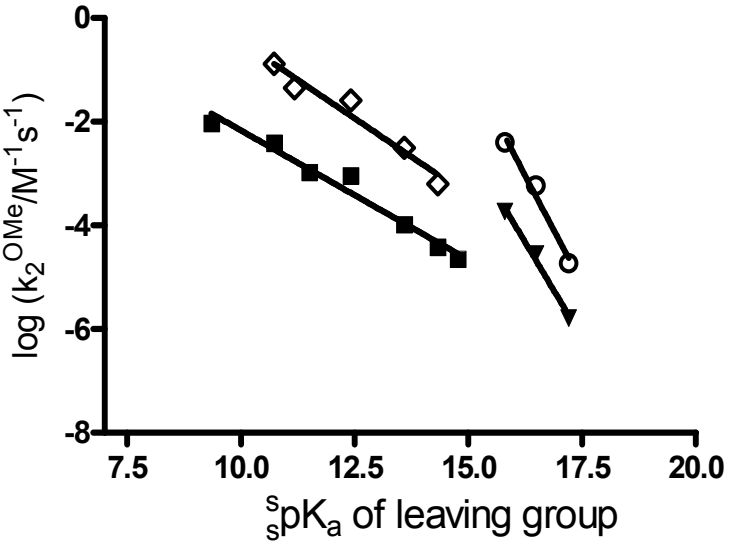

Figure 4-12. Plots of experimentally determined log (k_2^{OMe}) vs. the $^{s}_{s}pK_a^{lg}$ of the leaving group phenols for the methoxide-promoted cleavages of phosphorothioates **4.1** and phosphates **4.2** in anhydrous methanol. The data were fit to a standard linear regression model to give the slopes of -0.50 ± 0.04 (■: **4.1b,d,f**,**h-k**, r^2 = 0.9701), -1.48 ± 0.15 (▼: **4.1l-n**, r^2 = 0.9903), -0.59 ± 0.07 (◊: **4.2c,d,f-h**, r^2 = 0.9533), and -1.67 ± 0.25 (○: **4.2l-n**, r^2 = 0.9783).

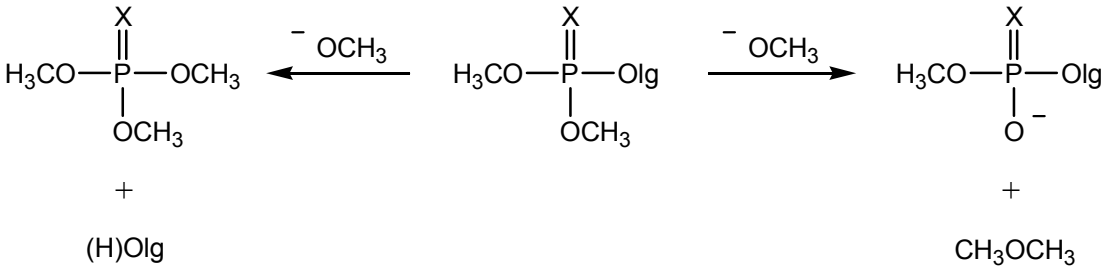

Scheme 4-3. Methoxide-promoted pathways for phosphate (X=O) and phosphorothioate (X=S) triesters in methanol.

4.5. Discussion

4.5.1. Approach of nucleophile

The axial positions of a phosphorus atom in a trigonal-bipyramidal coordination environment are preferentially occupied by more electronegative substituents.[36] It follows that nucleophilic reactions will occur with an electron-rich attacking nucleophile and leaving group occupying the apical positions in a 5-coordinate phosphorane-like transition state or intermediate. This was verified for phosphorothioate esters **4.1c**, **g**, and **j**, with the calculations showing that approach of the nucleophile from the direction opposite to the leaving group led to the lowest free energy of activation. However, approach of the nucleophile opposite to the spectator methyl groups had only slightly higher (~2 kcal mol^{-1}) free energy barriers. This led to an intermediate with both methoxy groups axial which undergoes pseudorotation to the most stable intermediate where one methoxy and the aryloxy group are axial from which product formation ensues (see Scheme 4-4). For the modes of attack where the nucleophile approaches opposite to the S or OMe, Berry pseudorotations required prior to leaving group expulsion are associated with low free energy barriers and are not expected to be kinetically relevant (Postscript Section 4.7, Scheme 4-4).

4.5.2. Computed β^{lg} values of aryloxy substrates

In Table 4-6 is a compendium of the experimentally determined and computed β^{lg} values for the methanolysis and hydrolysis of **4.1** and **4.2**. Construction of Brønsted plots

experimentally requires many independent kinetic runs to determine the second order rate constants for nucleophilic attack of several nucleophiles on a common substrate, or one nucleophile on several substrates. Comparison of all the data indicate that reasonably accurate β^{lg} values (given as the gradient of the Brønsted plot of log k_2^{nuc} vs. pK_a^{lg}) can be computed for the methanolysis of phosphorothioates and phosphates. The computational method employed does not require the absolute free energy of activation; rather it relies on the relative energy differences within a series of structurally related substrates. This is advantageous, as the determination of absolute free energy often involves entropic corrections due to systematic overestimation of vibrational entropy[28] and entropy due to solvation.[37] Our method assumes the entropic error is systematic throughout the series of substrates, and does not result in an altered gradient of the log k vs. pK_a^{lg} relationship.

Table 4-6. A compendium of experimentally determined and computational β^{lg} values for the lyoxide-promoted cleavage of **4.1** and **4.2** in methanol and water at 298 K.

4.1 Olg = OAr		**4.1** Olg = OR		**4.2** Olg = OAr		**4.2** Olg = OR	
Methanol							
Exp. β^{lg}	Comp. β^{lg}	Exp. β^{lg}	Comp. β^{lg}	Exp. β^{lg}	Comp. β^{lg}	Exp. β^{lg}	Comp. β^{lg}
-0.47 ±0.03[a]	-0.48 ±0.05	-1.48 ±0.15	-1.00 ±0.02	-0.51 ±0.04[c]	-0.61 ±0.07	-1.67 ±0.25	-1.2 ±0.1
-0.50 ±0.04[b]				-0.59 ±0.07[d]			
Water							
Exp. β^{lg}	Comp. β^{lg}	Exp. β^{lg}	Comp. β^{lg}	Exp. β^{lg}	Comp. β^{lg}	Exp. β^{lg}	Comp. β^{lg}
-0.32 ±0.04[e]	-0.54 ±0.07		-0.7±0.1	-0.43[f]	-0.57 ±0.06		-0.88 ±0.05
-0.35[f]							

a) ref. 9a.

b) this work

c) ref. 35; substrates with *ortho*-CO_2Me group

d) ref. 35; substrates with *ortho*-H.

e) ref. 10.

f) ref. 38; experimental β^{lg} data for hydrolysis of *O,O*-diethyl *O*-aryl phosphorothioates and phosphates.

Although the absolute free energy of each reaction is not accurately computed in this work, the relative free energies of activation for the methanolysis of chemically related substrates is predicted with good accuracy. The β^{lg} calculated for the methanolyses of **4.1** and **4.2** are similar to the experimentally determined values (P=S:

computed β^{lg} = -0.48 ± 0.05, exp. -0.47 ± 0.03[9a]; P=O: computed β^{lg} = -0.61 ± 0.07; exp. (β^{lg} = (-0.59 ± 0.07) and (-0.51 ± 0.04))[35]. The calculated results, and those in Figure 4-12, are in agreement with the phosphorothioate triesters being more resistant to P-Olg cleavage reactions than the phosphate triesters.[5,8]

The calculated β^{lg} values for the hydrolyses of *O,O*-dimethyl *O*-aryl phosphorothioate and phosphate substrates (**4.1a,c,e,g-j**, -0.54 ± 0.07; **4.2a,c,e,g-j**, -0.57 ± 0.06) are more negative than those determined experimentally for P=S esters (-0.32, $(MeO)_2P(=S)OAr$)[10]; (-0.35, $(EtO)_2P(=S)OAr$)[38]). These differences, while not great and possibly subject to greater uncertainty due to the lack of experimental data with similarly substituted substrates, are not captured in the calculations reported here, which do not incorporate any explicit solvent-solute interactions in the ground and transition states. Incorporation of explicit solvation in these calculations is problematic because subjective decisions regarding the number of solvent molecules to be included must be made and the number of such interactions can change within a series of substrates of differing basicity.[39] Problems associated with explicit solvation are compounded by inconsistencies that arise in assigning solvent molecule conformations.[40]

Solvent effects, both implicit and explicit, can be excluded by examination of the gas-phase data. In these calculations, decreased stabilization due to the continuum solvent model results in greatly increased sensitivity of the rate on the nature of the leaving group. This is paired with an expanded pK_a^{GP} range, resulting in β^{lg} values that are comparable to those determined with solvent for both sets of substrates where there is an aryloxy leaving group, (**4.1a,c,e, g-j** , -0.33 ± 0.03; **4.2 a,c,e, g-j**, -0.32 ± 0.03).

Previously[10], we reported a method of computationally determining β^{eq}, a coefficient defining the total effective charge change[41] felt by the leaving group in transition from reactant to product during the transfer of a *O,O*-dimethyl phosphorothioyl group between oxyanion nucleophiles. The Leffler parameter (α), defined as $\alpha = \beta^{lg}/\beta^{eq}$, is a measure of (effective) charge development on the leaving group in the transition state for its nucleophilic displacement. The computational β^{lg} values determined in this work (see Table 4-1) can be used in combination with previously published computational β^{eq} values of -1.75 and -1.69 for phosphorothioates **1** in water and methanol[10] and -1.54 for phosphates **4.2** in water[42] to determine an entirely computational Leffler parameter for the methanolysis of P=S esters (α = -0.48/-1.69 = 0.28) and P=O esters (α = -0.61/-1.54 = 0.40). Where there is an existing experimental β^{eq} value for the *O,O*-dimethylphosphorothioates, it can be used with the computationally derived β^{lg} to construct a semi-computational α that is gratifyingly close to the experimental one of 0.33.

It should be noted that Leffler's α is not related to absolute charge, but rather to a change in charge on the leaving group during oxyanionic nucleophilic attack relative to a change in charge in the equilibrium transfer of the *O,O*-dimethyl phosphorothioyl or phosphoryl group between oxyanion nucleophiles. With this in mind, the sum of the ChelpG-determined atomic charges (Q, defined in Section 4.4.3 above) of the leaving group within each structure (**SM**($Q_{LG,SM}$) or $\mathbf{TS_{NU}}$($Q_{LG,TS}$)) were examined as a metric for charge development during the course of the reaction. Treating calculated charges as effective charges, we may work backwards to study how an experimental Leffler's parameter correlates to computational atomic charge assignment. In this treatment, the

charge of the free anionic leaving group is assumed to be -1.

$$\alpha = \frac{Q_{LG,TS} - Q_{LG,SM}}{-1 - Q_{LG,SM}} \qquad (2)$$

Examination of the resulting α values for the methanolysis of phosphorothioates (Figure 4-13) reveals two things: 1) the Chelp-G determined α value (0.38 ± 0.02) is consistent throughout the range of leaving groups included, and is similar to the experimentally determined value of 0.33; and 2) there is no difference between the alkoxy and aryloxy substrates. Thus, these results are consistent with the experimentally-derived Leffler's parameter as a basis of charge progression of the leaving group, however they are less consistent with Leffler's parameters derived using computational Brønsted β values.

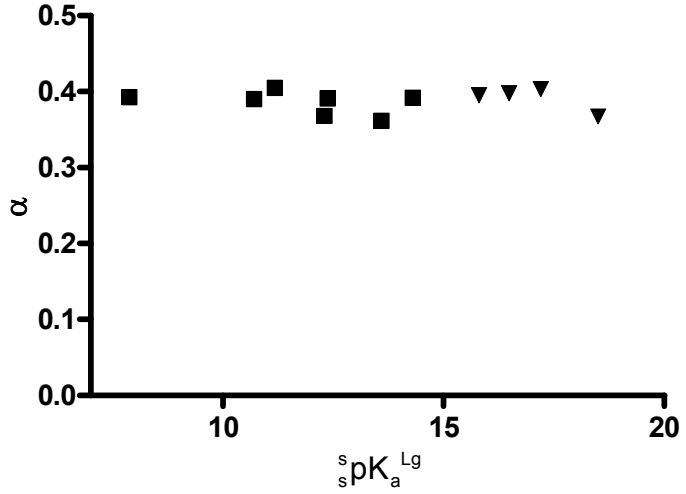

Figure 4-13. Leffler's α based on the ChelpG determined charges of the leaving group calculated using eq. 2 (■, aryl groups; ▼, alkyl groups)

4.5.3. Computed β^{lg} values of for substrates with substrates having alkoxy leaving groups

Although this method gives consistently larger β^{lg} values for alkoxy leaving groups relative to aryloxy ones, it underestimates the β^{lg} for the methanolysis of alkoxy P=S esters **4.1l-n,p** (computed β^{lg} = -1.00 ± 0.01, exp. -1.48 ± 0.15), or P=O esters **4.2l-n,p** (computed β^{lg} = -1.26 ± 0.11, exp. -1.67 ± 0.25). Discrepancies could be explained by the narrow range of ${}^{s}_{s}pK_a$ values available and the small number of substrates tested. However, the computational model does consistently predict alkoxy/aryloxy non-collinearity, an effect that was verified experimentally.

It is an interesting experimental and computational finding that there is a non-collinear pair of Brønsted relationships for aryloxy and alkoxy leaving groups departing from both phosphorothioates and phosphates. The appearance of the plots in Figure 4-1, Figure 4-6 and Figure 4-12 is atypical from Brønsted plots that show typical upward or downward breaks as a function of pK_a of leaving group or nucleophile due to changes in the mechanism or rate-limiting step of a reaction. A downward break in the Brønsted plot for the methanolysis of **4.1** or **4.2** might be predicted at the symmetrical point for the substitution reaction where there is a transition in rate-liming step from nucleophile attack to leaving group departure because there is an identical ${}^{s}_{s}pK_a$ for the nucleophile and leaving group. The range of alkoxy leaving groups available is limited, generally to ones having leaving group ${}^{s}_{s}pK_a{}^{lg}$ values lower than that of the attacking nucleophile, so it is difficult to define the relationship precisely, particularly to ascertain whether there is a

further break in the latter plot above the pK_a^{HOMe} for a symmetrical reaction displacing methoxide by lyate. Nevertheless, in the case of Figure 4-1, Figure 4-6 and Figure 4-12, the alkoxy leaving groups clearly form an independent relationship with a steeper dependence on pK_a^{lg} than do the aryloxy leaving groups.

It is possible that the difference in alkoxy/aryloxy leaving group reactivity is related to solvation in a manner similar to differences in alkoxy/aryloxy nucleophilicity,[39] and the data in Figure 4-7 show the effect is not present in the gas phase. Similar effects have been explained by steric[43] or electronic effects. To identify possible electronic effects, a ChelpG population analysis was conducted to determine any discontinuities in terms of charge distribution between the alkoxy and aryloxy series of P=S substrates. Here, it is shown that there are stark differences in aryloxy/alkoxy charge distribution in the starting material (Figure 4-3, Figure 4-4, Figure 4-5), indicating an inability of the alkoxy leaving groups to donate electron density to the phosphorothioate moiety (specifically, the sulfur atom), resulting in increased receptivity to the incoming nucleophile. Poor aryloxy leaving groups (associated with high ${}_s^s pK_a^{lg}$ values for the corresponding phenols) donate electron density to a greater extent than do alkoxy groups having the same leaving group pK_a^{lg}, resulting in decreased electrophilicity of the phosphorothioate group and a lower rate constant for attack of lyoxide on the aryloxy containing substrates.

The discrepancy in reactivity between P=O and P=S triesters containing aryloxy and alkoxy leaving groups is similar to the reported methoxide-promoted cleavages of carboxylate esters where substrates containing aryloxy leaving groups reside on a

different Brønsted line than those containing alkoxy leaving groups.[44] It is generally accepted that good linear Brønsted or other linear free energy relationships exist only for processes encompassing small changes in the nature of leaving group or nucleophile that do not greatly perturb the steric and electronic properties of the system. Despite this, due to the limitations on pK_a^{lg} scale imposed by phenol leaving groups, researchers often expand the scope of Brønsted relationships for acyl and phosphoryl transfer processes by using progressively poorer alkoxy leaving groups. However, the present study indicates that aryloxy and alkoxy groups are fundamentally different in their electron donating ability to P=X units and shows that mechanistic interpretations based on results obtained from structure-reactivity studies that encompass both should be made and accepted with caution. As a case in point, a non-linear Brønsted plot for the hydroxide-promoted cyclization of uridine 3'-phosphate esters in water has been interpreted as providing evidence for the existence of a 5-coordinate phosphorane intermediate formed along the transesterification reaction pathway.[45] The apparent break in the Brønsted plot occurred at the transition between substrates with aryloxy and alkoxy leaving groups, and may be a consequence of their difference in electron distribution, and may not provide evidence for a 2',3'-cyclic phosphorane intermediate. The absence of the isomerization product of uridine 3'-phosphate esters under alkaline conditions[46,45] is also not consistent with the presence of a stable phosphorane intermediate, unless it is too short-lived to allow for the required pseudo-rotation and resulting leaving group departure that would lead to isomerization.

In this work, the trends in charge development on the sulfur atom (Figure 4-4) show stark differences between the alkyl and aryl substrates. Within the **SM** structures

alkyl substrates display less negative charge than would be expected based on their ${}^{s}_{s}pK_a^{lg}$ and the trend of charge within the aryl substrates. This presents a possible explanation for the observed difference in alkyl/aryl reactivity, as the incoming anionic nucleophile is repelled by the greater negative charge.

4.5.4. Concertedness of phosphate/phosphorothioate methanolysis/hydrolysis

Experimentally, concerted reactions are distinguished from stepwise reactions by the absence of kinetically significant intermediates, the existence of which could be implied by breaks in free energy relationships, isomerization of, or positional isotope exchange in, recovered starting materials at incomplete conversion, or the lack of heavy atom kinetic isotope effects in the departing group which would signify little change in the force constant of the cleaving bond in the rate-limiting step of the reaction. However, the experimental observations cannot accurately depict the extent of bond loosening of the leaving group in terms of lengthening of the P—Olg bond in a transition state which is largely dominated by nuc—P bond formation. Calculations provide the ability to characterize concerted mechanisms as those having no intermediates along the reaction pathway[47], or those following stepwise pathways involving the presence of one or more intermediates along the reaction pathway, and furthermore can give an accurate depiction of the transition state structure in a one-step process with respect to nuc—P and P—Olg bond lengths. The present work identifies the geometries and symmetries of the various transition states and intermediate structures (Table 4-3 and Table 4-5) as well as the energies of 5-coordinate phosphorane intermediates that are produced during the

reactions of substrates. The linearity of experimentally determined Brønsted plots has been interpreted as evidence for the concertedness of the hydrolysis of phosphates[20] and phosphorothioates[19], although such data are also consistent with a two step process with rate-limiting nucleophilic attack followed by fast departure of the leaving group. Recent computational studies have shown that the attack of $^{-}$OH on P=O phosphate triesters in water is concerted (enforced concerted) for substrates having a $pK_a^{lg} < 8$, while intermediates are present on the free energy surface for substrates with greater leaving group pK_a values.[16] Our results with methanolysis mirror this gradual emergence of a second transition state for leaving group departure with increasingly poor leaving groups. This effect culminates with the prediction that the second transition state will become rate-limiting with the poorest leaving group considered in this work (ethoxide).

The effect of the leaving group is further complicated when paired with changes in the nucleophile, wherein the concertedness of the reaction is affected by both. This can be conceptualized by perusal of the More O'Ferrall – Jencks diagram in Figure 4-14 which depicts a concerted pathway (nearly symmetrical nucleophile and leaving group) and stepwise pathways through transition states 1 and 2. The computational data indicate that all reactions involving the 2,4-dinitrophenoxide nucleophile result in concerted processes, but with poorer leaving groups and stronger nucleophiles, the systems gradually follow step-wise mechanisms. One may predict, using pathway A with 2,4-dinitrophenoxide and substrate **4.1a**, that as the pK_a of the nucleophile increases (nucleophile is stronger), the bottom edge of the plot is raised in energy, shifting the reaction pathway to stepwise, with a rate limiting TS 1. Conversely, with the same starting point, making the leaving group worse (pK_a^{lg} increases) the right side of the

diagram is raised, also pushing the reaction to a stepwise one, with the rate limiting step being breakdown of the intermediate.

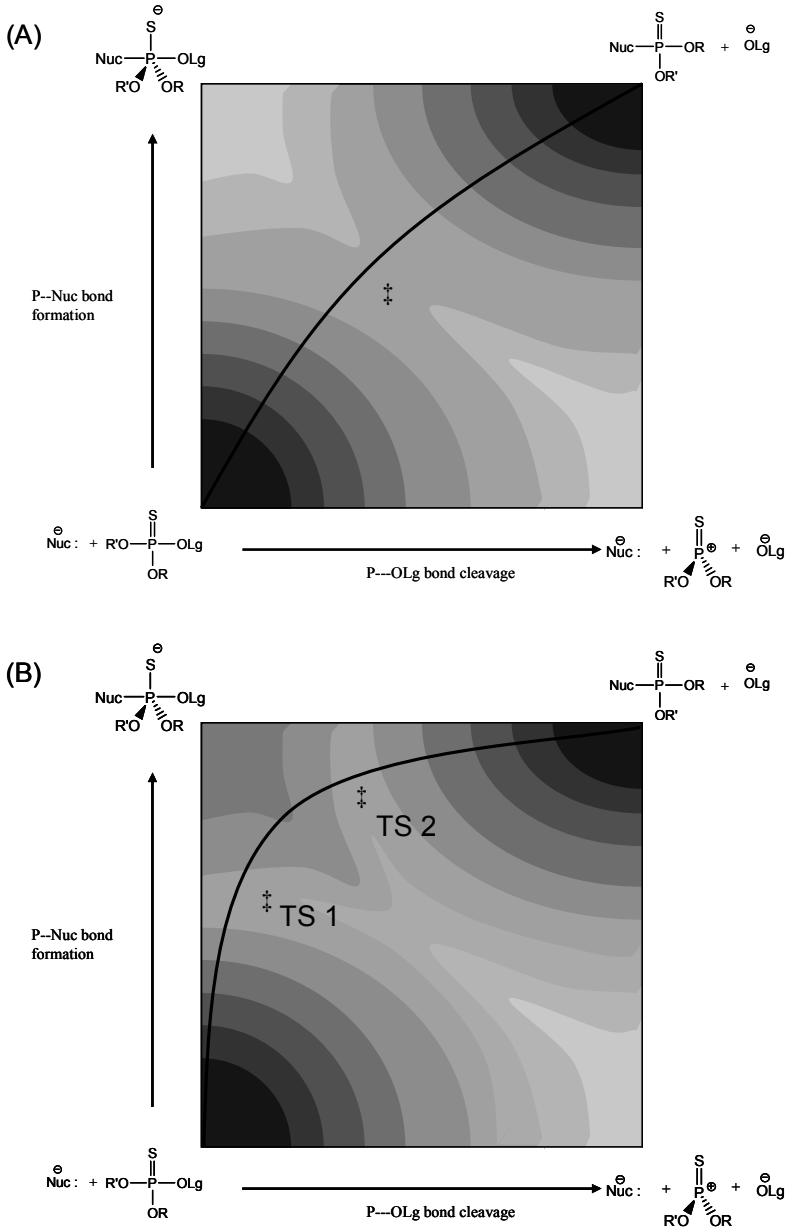

Figure 4-14. Conceptual 3D More O'Ferrall – Jencks diagrams for showing the transition in mechanism from the concerted process (A) such as the reaction of 2,4-dinitrophenoxide with substrate **4.1a** and a stepwise process (B) such as the symmetrical reaction of ethoxide with substrate **4.1p**.

4.6. Conclusion

We have examined computationally the methanolysis of a series of *O,O*-dimethyl *O*-aryl- and *O,O*-dimethyl *O*-alkyl- phosphorothioate and phosphate triesters, using experiment to substantiate and complement the theoretical results. This has revealed a diversity in reactivity from concerted to stepwise for substrates having leaving groups with increasing ${}^{s}_{s}pK_a^{lg}$ values.With a common methoxide nucleophile in methanol, these reactions proceed via a concerted mechanism through a single transition state that is highly asymmetric with respect to nuc---P bond formation and P—Olg bond cleavage only with very good leaving groups (${}^{s}_{s}pK_a^{lg}$ < ~12.3 in methanol). However, methoxide attack on substrates with more basic leaving groups (higher ${}^{s}_{s}pK_a^{lg}$ than 12.3) results in formation of 5-coordinate phosphorane intermediates with a well-defined, but not rate-limiting, transition state for leaving group departure. This finding also applies to hydrolysis reactions as well as reactions in the gas phase; however, the transitions between the asymmetric concerted and stepwise mechanisms seem to occur with better leaving groups in water. Notably, it is only with the best leaving group and worst nucleophile in the gas phase that the reaction is concerted, since without solvent present, all other reactions proceed through a substrate:nucleophile 5-coordinate thiophosphorane complex where the anionic charge is not stabilized in any way by solvation.

This work also demonstrates that the gradients (β^{lg}) of Brønsted relationships can be accurately predicted computationally without necessarily achieving pinpoint accuracy for the free energy of activation for individual reactions. Experimentally and computationally, one sees that Brønsted plots of log k_2^{-OMe} vs. the pK_a^{lg} the leaving group

have discontinuities appearing between aryoxy and alkoxy type leaving groups. The computations indicate that this does not arise from a change in the rate limiting step for the reaction, but rather from fundamental differences in electron distribution in the starting materials depending on the nature of the leaving group as well as differences in the solvation of aryl containing leaving groups relative to alkyl containing ones. Additionally, although it is well known that such Brønsted plots are really justified only for closely related leaving groups, this study has revealed that alkoxy groups must be treated separately from aryloxy groups when conducting this sort of study.

4.7. Postscript

Here are presented tables of free energies, figures and schemes that are referred to but not included in the main text.

Table 4-7. Free energies (kcal mol^{-1}) of intermediates and transition states for the methanolysis of **4.1a,c,e,g-j,l-n,p** and **4.2a,c,e,g-j,l-n,p**, relative to the energy of the starting material and nucleophile.

Substrate	**4.1**			**4.2**		
	TS_{nuc}	Int	TS_{LG}	TS_{nuc}	Int	TS_{LG}
a	14.7			12.7		
c	15.8			14.6		
e	16.5			15.7		
g	17.8			15.6		
h	17.7	-2.7	-2.9	16.0	-2.7	-2.4
i	18.4	-0.1	0.6	16.9	1.4	0.9
j	18.4	1.8	4.8	18.6	3.8	3.1
l	17.1	0.1	6.7	17.2	3.3	7.6
m	17.9	3.3	10.2	18.1	6.0	10.9
n	19.0	3.6	16.9	19.0	7.7	14.4
p	20.8	7.5	21.1	21.7	11.8	21.1

Table 4-8. Free energies (kcal mol^{-1}) of intermediates and transition states for the hydrolysis of **4.1a,c,e,g-j,l-n, p** and **4.2a,c,e,g-j,l-n,p**, relative to the energy of the starting material and nucleophile.

Substrate	**4.1**			**4.2**		
	TS_{nuc}	Int	TS_{LG}	TS_{nuc}	Int	TS_{LG}
a	14.2			12.5		
c	15.2	-14.0	-13.1	15.8		
e	16.8	-12.4	-12.1	15.5		
g	17.1	-9.5	-7.5	15.7	-6.2	-6.3
h	16.6	-9.2	-7.3	15.7	-5.6	-5.2
i	18.0	-5.8	-3.6	16.4	-3.1	-1.6
j	18.4	-5.6	-0.6	17.4	-0.6	0.8
l	16.0	-6.5	4.8	15.3	-0.7	6.9
m	17.8	-4.0	8.8	16.7	2.2	10.3
n	18.2	-2.5	13.9	17.9	3.8	13.3
p	19.5	0.7	19.4	19.7	7.5	21.3

Table 4-9. Free energies (kcal mol^{-1}) of intermediates and transition states for the methanolysis of **4.1a,c,e,g-j,l-n,p** and **4.2a,c,e,g-j,l-n,p** without continuum solvation (representing the gas phase), relative to the energy of the starting material and nucleophile.

Substrate		**4.1**			**4.2**	
	TS_{nuc}	Int	TS_{LG}	TS_{nuc}	Int	TS_{LG}
a	-17.8			-17.4		
c	-18.2	-42.7	-43.5	-18.3	-41.4	-41.3
e	-14.9	-54.0	-38.3	-14.2	-37.0	-36.6
g	-12.6	-33.2	-35.9	-12.2	-31.4	-30.2
h	-13.9	-32.7	-36.0	-12.8	-32.3	-30.3
i	-10.1	-27.8	-30.0	-9.0	-25.7	-28.5
j	-7.3	-23.4	-27.2	-6.4	-20.9	-19.4
l	-8.8	-23.0	-19.4	-8.2	-20.1	-17.3
m	-7.2	-20.8	-16.2	-7.5	-18.3	-14.1
n	-6.3	-18.4	-11.5	-5.6	-15.7	-9.5
p	-1.8	-12.1	-11.1	-0.4	-9.4	-1.0

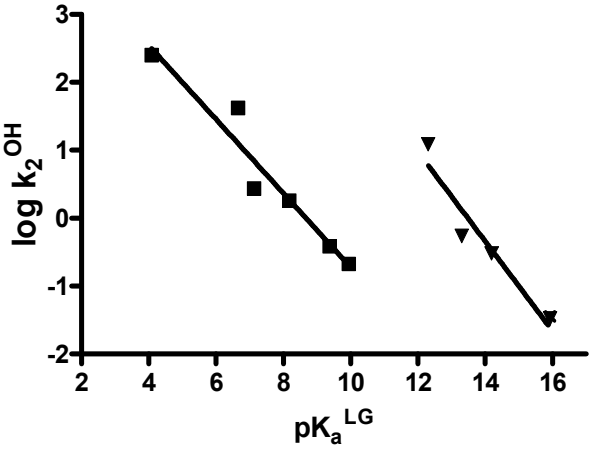

Figure 4-15. Plot of computationally derived log k_2^{OH} vs. pK_a^{lg} of the leaving groups for the hydroxide-promoted cleavage of phosphorothioates **4.1** with the water continuum solvation model. The data were fitted to standard linear regression model to give the slopes of -0.54 ± 0.07 (■: **4.1a,c,e,g-j**; r^2 = 0.9372) and -0.7 ± 0.1 (▼: **4.1l-n,p**; r^2 = 0.9229).

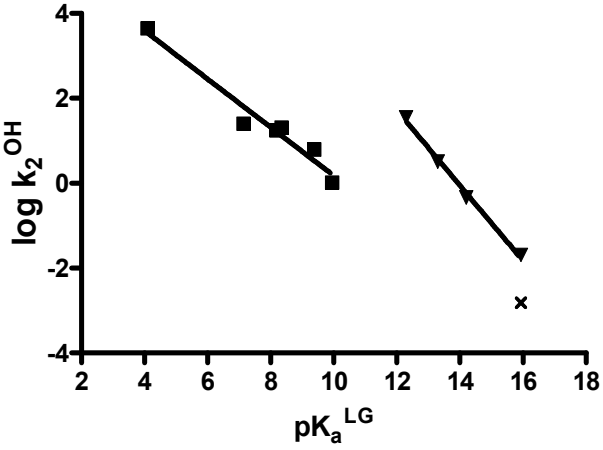

Figure 4-16. Plot of computationally derived log k_2^{OH} vs. pK_a^{lg} of the leaving groups for the hydroxide-promoted cleavage of phosphates **4.2** with the water continuum solvation model. The data were fitted to standard linear regression model to give the slopes of -0.57 ± 0.08 (■: **4.2a,c,e,g-j**; r^2 = 0.9570) and -0.88 ± 0.05 (▼: **4.2l-n,p**; r^2 = 0.9948).

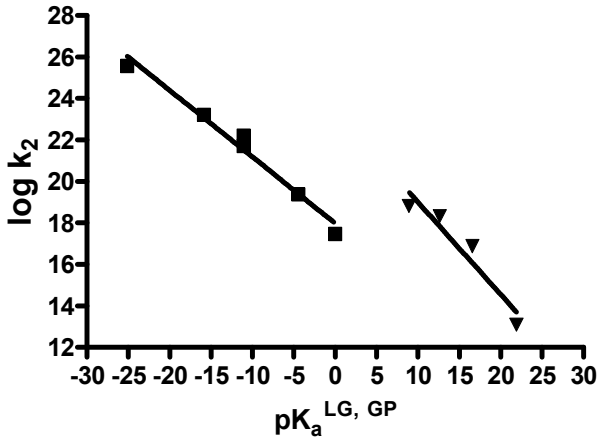

Figure 4-17. Plot of computationally derived log k_2^{OMe} vs. pK_a^{lg} of the leaving groups for the methoxide-promoted cleavage of phosphates **4.2** with no continuum solvation model (gas phase). The data were fitted to standard linear regression model to give the slopes of -0.32 ± 0.03 (■: **4.2a,c,e,g-j**; $r^2 = 0.9756$) and -0.44 ± 0.07 (▼: **4.2l-n,p**; $r^2 = 0.9146$).

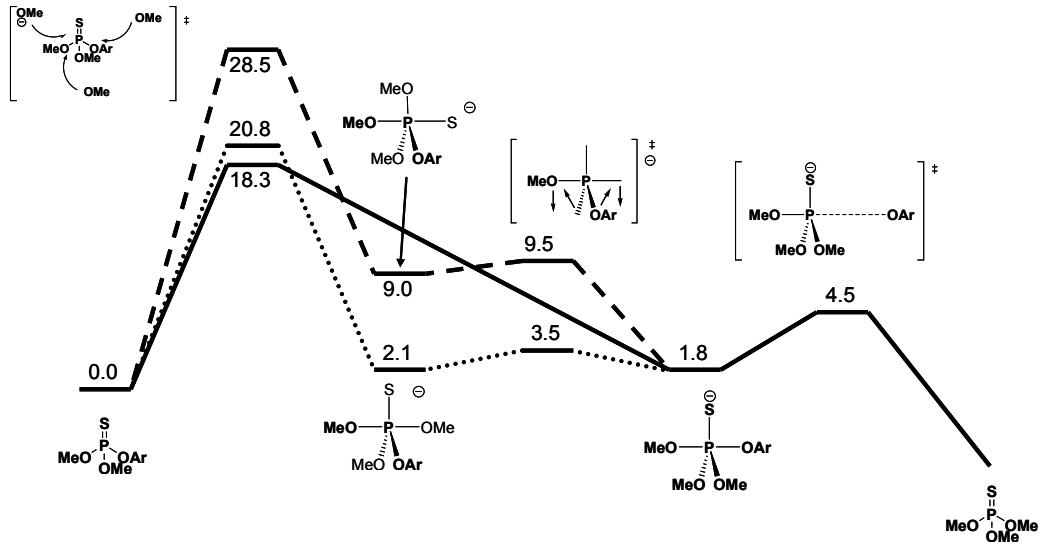

Scheme 4-4. Reaction pathways and the free energies (kcal/mol, 298K) for the nucleophilic attack of methoxide on **4.1j**. Only the productive pseudorotation transition states (that lead to OAr in the axial position) are considered. Free energy diagram not to scale.

4.8. References

1) a) Westheimer, F. H. *Chem. Rev.* **1981**, *81,* 313; b) Westheimer, F. H. *Science*, **1987**, *235*, 1173.

2) a) Cowan, J. A. *Chem. Rev.* **1998**, *98*, 1067; b) Weston, J. *Chem. Rev.* **2005**, *105*, 2151; c) Wilcox, D. E. *Chem. Rev.* **1996**, *96*, 2435; d) Sträter, N.; Lipscomb, W. N.; Klabunde, T.; Krebs, B. *Angew. Chem. Int. Ed.* **1996**, *35*, 2024; e) Lipscomb, W. N.; Sträter, N. *Chem. Rev*. **1996**, *96*, 2375.

3) Hengge, A. C. *Adv. Phys. Org. Chem.* **2005**, *40*, 49 and references therein.

4) a) Seckute, J.; Menke, J. L.; Emnett, R. J.; Patterson, E. V.; Cramer, C. J. *J. Org. Chem.* **2005**, *70*, 8649; b) Florian, J.; Warshel, A. *J. Phys. Chem. B.* **1998**, *102,* 719; c) Iche-Tarrat, N.; Ruiz-Lopez, M.; Barthelat, J-C.; Vigroux, A. *Chem. Eur. J.* **2007**, *13,* 3617; d) Iche-Tarrat, N.; Barthelat, J-C.; Rinaldi, D.; Vigroux, A. *J. Phys. Chem. B.* **2005**, 109, 22570.

5) Eckstein, F. Gish, G. *Trends Biochem. Sci.* **1989**; *14*, 97.

6) a) Roberts, T. L.; Dunn, J. A.; Sweet, M. J.; Hume, D. A.; Stacey, K. J. *Mol. Immunol.* **2011**, *48*, 1027; b) Sester, D. P.; Brion, K.; Trieu, A.; Goodridge, H. S.; Roberts, T. L.; Dunn, J.; Hume, D. A.; Stacey, K. J.; Sweet, M. J. *J. Immunol.* **2006**, *177*, 4473; c) Krotz, A. H.; Hang, A.; Gorman, D.; Scozzari, A. N. *Nucleosides, Nucleotides, and Nucleic Acids*, **2005**, *24*, 1293.

7) a) Toy, A. D. F.; Walsh, E. N. in *Phosphorus Chemistry in Everyday Living*; 2nd ed.; American Chemical Society: Washington, DC; 1987; pp. 18-20; b) Quin, L. D. in *A Guide to Organophosphorus Chemistry*; Wiley: New York; 2000; pp. 367-371.

8) Purcell, J. Hengge, A. C. *J. Org. Chem*. **2005**, *70*, 8437.

9) a) Liu, C. T.; Maxwell, C. I.; Edwards, D. R.; Neverov, A. A.; Mosey, N. J.; Brown, R. S. *J. Am. Chem. Soc.* **2010**, *132*, 16599; b) Liu, C. T.; Neverov, A. A.; Brown, R. S. *Inorg. Chem.* **2011**, 50, 7852; c) Mohamed, M. F.; Neverov, A. A.; Brown, R. S. *Inorg. Chem.* **2009**, *48*, 1183; d) Lu, Z.-L.; Neverov, A. A.; Brown, R. S. *Org. Biomol. Chem.* **2005**, *3*, 3379; e) Neverov, A. A.; Brown, R. S. *Org. Biomol. Chem.* **2004**, *2*, 2245.

10) Edwards, D. R.; Maxwell, C. I.; Harkness, R.; Neverov, A. A.; Mosey, N. J.; Brown, R. S. *J. Phys. Org. Chem.* Published online, July 31, 2011; DOI:10.1002/poc.1938.

11) a) Brown, R. S.; Lu, Z.-L. Liu, C. T.; Tsang, W. Y.; Edwards, D. R.; Neverov, A. A. *J. Phys. Org. Chem.* **2010**, *23*, 1; b) Brown, R. S.; Neverov, A. A. *Adv. Phys. Org. Chem.* **2008**, *42*, 271; c) Liu, T.; Neverov, A. A.; Tsang, J. S. W.; Brown, R. S. *Org. Biomol. Chem.* **2005**, *3*, 1525.

12) Khan, S. A.; Kirby, A. J. *J. Chem. Soc. B.* **1970**, 1172.

13) Rowell, R.; Gorenstein, D. G. *J. Am. Chem. Soc.* **1981**, *103*, 5894.

14) a) Bourne, N.; Williams, A. *J. Am. Chem. Soc.* **1984**, *106*, 7591; b) Bourne, N.; Chrystiuk, E.; Davis, A. M.; Williams, A. *J. Am. Chem. Soc.* **1988**, *110*, 1890; c) Ba-Saif, S. A.; Davis, A. M.; Williams, A. *J. Org. Chem.* **1989**, *54*, 5483.

15) Cassano, A. G.; Anderson, V. E.; Harris, M. E. *J. Am. Chem. Soc.* **2002**, *124*, 10964; b) Hengge, A. C.; Tobin, A. E.; Cleland, W. W. *J. Am. Chem. Soc.* **1996**, *117*, 5919.

16) Tarrat, N. *J. Mol. Struct: THEOCHEM,* **2010**, *941*, 56.

17) Jencks, W. P. *Acc. Chem. Res.* **1980**, *13*, 161.

18) Hong, S.-B.; Raushel, F. M. *Biochemistry.* **1996**, *35*, 10904.

19) Omakor, J. E.; Onyido, I.; vanLoon, G. W.; Buncel, E. *J. Chem. Soc., Perkin Trans*. *2*, **2001**, 324.

20) Ba-Saif, S. A.; Waring, M. A.; Williams, A. *J. Am. Chem. Soc.* **1990**, *112*, 8115

21) Jencks, W. P. *Acc. Chem. Res*. **1980**, *13*, 161.

22) More O'Ferrall, R. A. *J. Chem. Soc. B*, **1970**, 274.

23) Perdew, J. P.; Burke, K.; Ernzerhof, M. *Phys. Rev. Lett.* **1996**, *77,* 3865.

24) Ribeiro, A. J. M.; Ramos, M. J.; Fernandes, P. A. *J. Chem. Theory, Comput.* **2010**, *6*, 2281.

25) a) Tomasi, J.; Mennuccia, B.; Cancés, E. *THEOCHEM*, **1999**, *464*, 211. b) Tomasi, J.; Mennuccia, B.; Cammi, R. *Chem. Rev.* **2005**, *105*, 2999.

26) The acronym CHELP stands for charges derived from electrostatic potential using a grid-based method. Breneman, C. M.; Wiberg, K. B. *J. Comput. Chem.* **1990**, *11,* 361.

27) Gaussian 09, Revision **A.1**, Frisch, M. J.; Trucks, G. W.; Schlegel, H. B.; Scuseria, G. E.; Robb, M. A.; Cheeseman, J. R.; Scalmani, G.; Barone, V.; Mennucci, B.;

Petersson, G. A.; Nakatsuji, H.; Caricato, M.; Li, X.; Hratchian, H. P.; Izmaylov, A. F.; Bloino, J.; Zheng, G.; Sonnenberg, J. L.; Hada, M.; Ehara, M.; Toyota, K.; Fukuda, R.; Hasegawa, J.; Ishida, M.; Nakajima, T.; Honda, Y.; Kitao, O.; Nakai, H.; Vreven, T.; Montgomery, Jr., J. A.; Peralta, J. E.; Ogliaro, F.; Bearpark, M.; Heyd, J. J.; Brothers, E.; Kudin, K. N.; Staroverov, V. N.; Kobayashi, R.; Normand, J.; Raghavachari, K.; Rendell, A.; Burant, J. C.; Iyengar, S. S.; Tomasi, J.; Cossi, M.; Rega, N.; Millam, N. J.; Klene, M.; Knox, J. E.; Cross, J. B.; Bakken, V.; Adamo, C.; Jaramillo, J.; Gomperts, R.; Stratmann, R. E.; Yazyev, O.; Austin, A. J.; Cammi, R.; Pomelli, C.; Ochterski, J. W.; Martin, R. L.; Morokuma, K.; Zakrzewski, V. G.; Voth, G. A.; Salvador, P.; Dannenberg, J. J.; Dapprich, S.; Daniels, A. D.; Farkas, Ö.; Foresman, J. B.; Ortiz, J. V.; Cioslowski, J.; Fox, D. J. Gaussian, Inc., Wallingford CT, 2009.

28) Rosta, E.; Kamerlin, S. C. L.; Warshel, A. *Biochemistry*. **2008**, *47*, 3725.

29) Cramer, C. J. *Essentials of Computational Chemistry: Theories and Models*. John Wiley and Sons Ltd., West Sussex, England, 2004, 378.

30) The rate constant for a reaction is related to the free energy of activation by $k = \frac{k_B T}{h} e^{\frac{-\Delta G^{\pm}}{RT}}$ where kB is the Boltzmann constant, T is the absolute temperature, R is the gas constant and -ΔG‡ is the free energy of activation

31) Liu, T.; Neverov, A. A.; Tsang, J. S. W.; Brown, R. S. *Org. Biomol. Chem.* **2005**, *3*, 1525.

32) Churchill, D.; Dust, J. M.; Buncel, E. *Can. J. Chem*. **2007**, *85*, 421.

33) For the designation of pH in non-aqueous solvents we use the forms recommended by the IUPAC, *Compendium of Analytical Nomenclature. Definitive Rules 1997* 3rd ed., Blackwell, Oxford, U. K. 1998. Thus ${}^{s}_{s}\mathrm{pH}$ refers to the measured pH in a non-aqueous solvent references to that solvent. Since the autoprotolysis constant of MeOH is $10^{-16.77}$, neutral ${}^{s}_{s}\mathrm{pH}$ is 8.4.

34) Gas phase pKa values are relative to the phenyl substituent, and were determined using gas phase free energy of ionization values from using $\mathrm{pK_a^{GP}} = \frac{\Delta G^{ArOH} - \Delta G^{PhOH}}{2.303 \bullet RT}$; where ΔGArOH is the free energy for gas phase ionization, ΔGPhOH is the free energy for gas phase ionization of phenol, R is the gas constant and T is the temperature. Gas phase free energies of ionization from: a) Koppel, I. A.; Taft, R. W.; Anvia, F.; Zhu, S. Z.; Hu, L.Q.; Sung, K. S.; Desmarteau, D. D.; Yagupolskii, L. M. *J. Am. Chem. Soc.* **1996**, *116*, 3047; b) Fujito, M.; McIver (Jr.), R. T.; Taft, R. W. *J. Am. Chem. Soc.* **1981**, *103*, 4017; c) Bartmess, J. E.; Scott, J. A.; McIver, R. T. *J. Am. Chem. Soc.* **1979**, *101*, 6047. d) Graul, S. T.; Schnute, M. E.; Squires, R. R. *Int. J. Mass Spectrom. Ion Proc.* **1990**, *96*, 181.

35) Edwards, D. R.; Liu, C. T.; Garrett, G. E.; Neverov, A. A.; Brown, R. S. *J. Am. Chem. Soc.* **2009**, *131*, 13738.

36) Muetterties, E. L.; Mahler, W.; Schmutzler, R. *Inorg. Chem.* **1963**, *2,* 613.

37) Ayala, P. Y.; Schlegel, H. B. *J. Chem. Phys.* **1998**, *108*, 2314.

38) Hong, S.-B.; Raushel, F. M. *Biochemistry.* **1996**, *35,* 10904.

39) Jencks, W. P.; Brant, S. R.; Gandler, J. R.; Fendrich, G.; Nakamura, C. *J. Am. Chem. Soc.* **1982**, *104,* 7045.

40) Kamerlin, S. C. L.; Haranczyk, M.; Warshel, A. *ChemPhysChem*, **2009**, *10,* 1125.

41) Williams, A. *Acc. Chem. Res.* **1984**, *17,* 425.

42) Previously we have assumed that β^{eq} values determined in water can be applied to group transfer processes in methanol provided one gives due accounting of the changes in pK_a^{lg} that are brought about by solvent changes. On the basis of the recent work done with phosphorothioates where experimental β^{eq} values of -1.45±0.08 and -1.39±0.12 in water and methanol,[10] this appears to be the case. Note however, that the computed βeq values are somewhat higher, being -1.68 and -1.69 for P=S and P=O esters respectively.

43) Kirsch, J. F.; Jencks, W. P. *J. Am. Chem. Soc.* **1964**, *86*, 837.

44) Neverov, A. A.; Sunderland, N. E.; Brown, R. S. *Org. Biomol. Chem*. **2005**, *3*, 65.

45) Lönnberg, H.; Strömberg, R.; Williams, A. *Org. Biomol. Chem.* **2004**, *2*, 2165.

46) Kosonen, M.; Youseti-Salakdeh, E.; Strömberg, R.; Lönnberg, H. *J. Chem. Soc. Perkin Trans. 2*, **1997**, 2661.

47) Greig, I. R. *Chem. Soc. Rev.* **2010**, *39*, 2271.

Chapter 5. Palladacycle catalyzed methanolysis of neutral phosphorothioates

5.1. Introduction

As discussed in earlier chapters, phosphorothioates are effective acetyl cholinesterase inhibitors and are used agriculturally as insecticides and acaricides. The possible health effects of their accumulation in the environment merit research into methods for their bulk destruction and onsite decontamination. This research group has previously[1] shown that the palladacycle complex **5.1**(Py)($^-$OTf) is a potent turnover catalyst for the methanolysis of phosphorothioate triesters, however a complete mechanism was not reported. Here, a computational investigation using density functional theory (DFT) is used in conjunction with an experimental structure-reactivity study to discover the mechanism of the catalysis. In this section the experimental work, conducted by C. Tony Liu, will be briefly discussed followed by the in-depth report of the theoretical work, for which all calculations were conducted by C. Maxwell. The complete work was published in the Journal of the American Chemical Society (Liu, C. T.; Maxwell, C. I.; Edwards, D. R.; Neverov, A. A. Mosey, N. J.; Brown, R. S. *J. Am. Chem. Soc.* **2010,** *132,* 16599.).

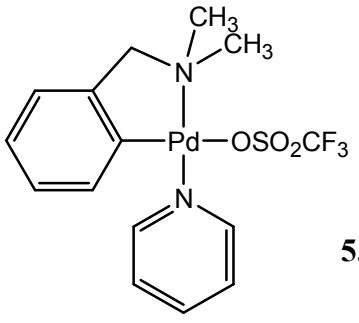

5.1(Py)($^-$OTf)

5.2. Experimental basis for the theoretical work

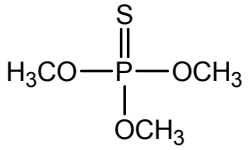

5.2

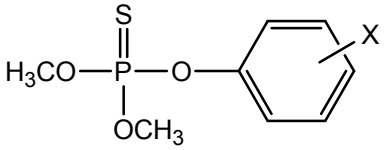

5.3

a) X = 2-Cl, 4-NO_2
b) X = 2,4,5-triCl
c) X = 3-Me, 4-NO_2
d) X = 3-NO_2
e) X = 4-Cl
f) X = H
g) X = 4-OMe

Recall from Section 1.4.4 that upon dissolution in methanol the triflate moiety in **5.1** exchanges with a solvent molecule and that methanol is deprotonated at $^{s}_{s}$pH > 10.8 (depending on what is bound to Pd). Experimental evidence suggests that the reaction progresses with a ligand exchange of substrate for pyridine, contrasting with the previously envisioned mechanism in which a 5-coordinate palladium complex acted as an intermediate. This is evident by a downward curvature in a plot of second order rate constants *vs*. catalyst concentration (Figure 5-1), consistent with the associative ligand exchange pathway.[2] This conclusion is supported by the observation that upon addition of pyridine the downward curvature in the plot is no longer present but the overall rate is depressed. Additionally, a binding experiment with the strong binding and slow reacting substrate **5.2** showed the release of pyridine as monitored by UV-Vis.

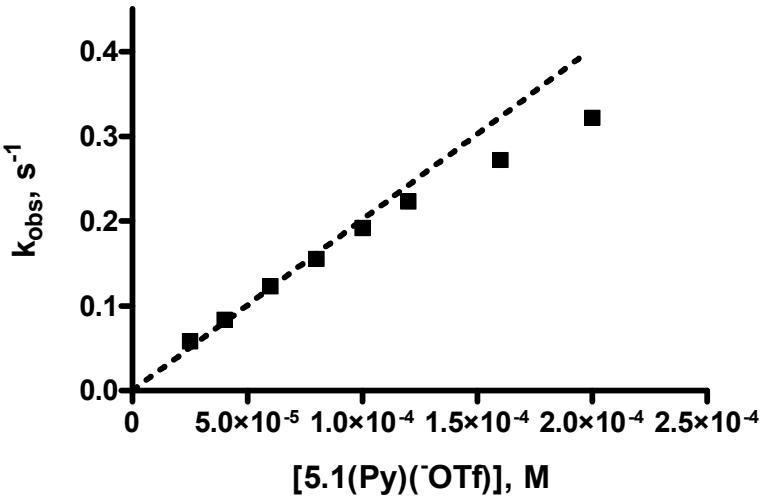

Figure 5-1. Plot of k_{obs} vs. [**5.1**(Py)(⁻OTf)] for the methanolysis of **5.3c** (5.0×10^{-5} M) buffered at ${}^{s}_{s}\mathrm{pH} = 11.7$ and at 25°C in anhydrous methanol.

The Brønsted plot of $\log(k_2^{cat})$ vs. phenol ${}^{s}_{s}\mathrm{pK_a}$ (Figure 5-2) shows a prominent break at ${}^{s}_{s}\mathrm{pK_a} = \sim 13$ with a flat β^{lg} of ~0 in the lower ${}^{s}_{s}\mathrm{pK_a}$ domain and a steep, negative β^{lg} of -1.93 at higher ${}^{s}_{s}\mathrm{pK_a}$s. This indicates a change in rate determining step from a process with no leaving group sensitivity at low ${}^{s}_{s}\mathrm{pK_a}$s to one in which the leaving group substitution plays a large role at high ${}^{s}_{s}\mathrm{pK_a}$s. Thus, a kinetically relevant intermediate must exist between these rate limiting processes.

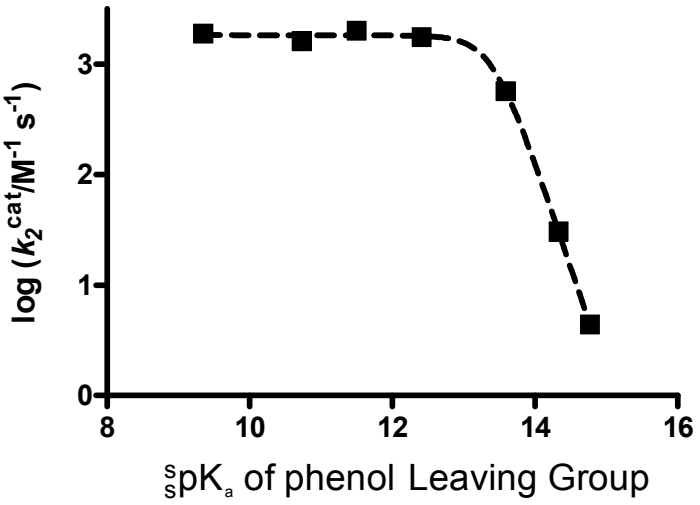

Figure 5-2. Plot of log(k_2^{cat}) vs. leaving group phenol $^{s}_{s}pK_a$ for the **5.1**(Py)($^{-}$OTf) catalyzed cleavage of **5.3a-g** (5.0×10^{-5} M) buffered at $^{s}_{s}pH = 11.7$ and at 25°C in anhydrous methanol. The line through the data comes from a NLLSQ fit to a previously derived equation,[3] to provide β^{lg} values of 0.00 ± 0.02 and -1.93 ± 0.06.

The experimental evidence is consistent, though not uniquely so, with the mechanism shown in Scheme 5-1. For substrates with leaving group $^{s}_{s}pK_a < 13$, **5.3a-d**, the rate determining step is postulated to be the ligand exchange process k_1 wherein the substrate replaces the pyridine. This is supported by the insensitivity of the rate constant to the leaving group, as a binding process will likely not be affected by the various substituents on the phosphorothioate. This might seem unusual considering that exchange processes on transition metal centers are typically very fast, however they have been shown to be much slower on Pd(II) center.[4] For worse leaving groups, with $^{s}_{s}pK_a > 13$, **5.3e-g**, the rate determining step is proposed to be the leaving group departure process, k_3. This is consistent with the large, negative β^{lg} determined for these substrates. In both

leaving group ${}^{s}_{s}pK_a$ domains, the nucleophilic attack step is fast, and two intermediates exist within the catalytic process, one of which is a 5-coordinate thiophosphorane intermediate that is stabilized by the metal ion.

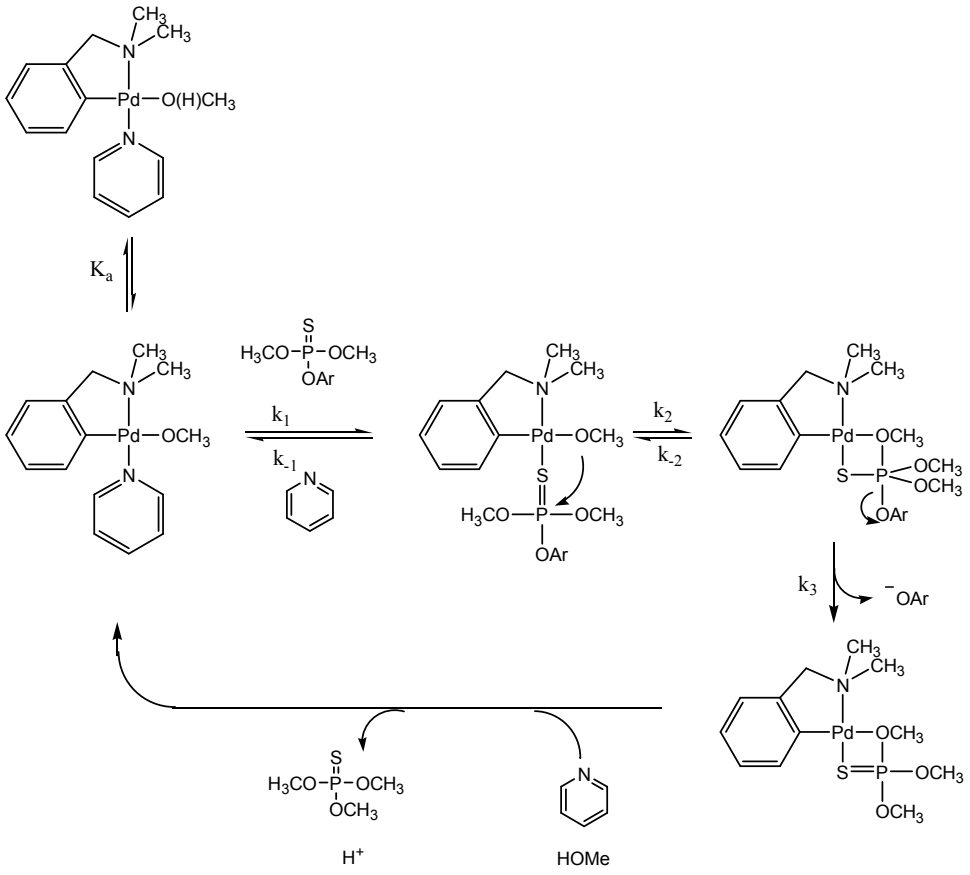

Scheme 5-1. Mechanism of **5.1** catalyzed methanolysis of **5.3** consistent with the experimental results.

5.3. Theoretical work

In order to provide further validation and details of this mechanism, an in-depth DFT study was undertaken. The reaction pathway was calculated for one sample substrate from within each ${}^{s}_{s}pK_a^{lg}$ domain of the Brønsted plot in order to probe each rate

determining step. Thus, in this work, fenitrothion **5.3c**, is representative of the good leaving groups and **5.3g** is chosen to represent substrates in the steeply sloped domain. For each substrate, the proposed mechanism will be modeled, as well as potential alternate mechanistic pathways.

5.3.1. Computational details

Geometry optimizations and energy calculations of ground and transition states were performed using DFT at the B3LYP[5] level of theory using Gaussian 09[6] with the application of the IEFPCM[7] solvent model for methanol. In all calculations the 6-31G(d,p) basis set was used for C and H atoms, while O, N, P and S atoms were assigned the 6-31++G(d,p) basis set. The effective core potential of Hay and Wadt with double-ζ valence basis set (LanL2DZ) was employed to describe Pd.[8] Frequency calculations were conducted to validate transition states as saddle points and intermediates as minima on the potential energy surface and to use as a basis for determining free energy values at 298 K.

To evaluate free energies of systems wherein ligands partition between complexes and free solution, care must be taken to approximate the free energy of solvation correctly. As ligands dissociate from complexes into a protic solution, they are stabilized by hydrogen bond donors of individual solvent molecules. These specific interactions are not included by the IEFPCM solvation model. To account for this stabilization, single explicit solvent molecules were included in some calculations where appropriate, in the form of hydrogen bonding interactions with dissociated ligands not bound to the complex

(Figure 5-3). Due to the perturbed atom balance in the cases in which the substrate is bidentate-bound to the metal ion, the energy contribution of extra methanol molecules must be included throughout the calculations. When not involved with either the complex or free ligands, these methanol molecules are part of the hydrogen bonding network of the bulk solvent, a situation that is difficult to model computationally. When free from H-bonding interactions with ligands, methanol is represented by a fractional value of the energy of a PCM solvated methanol hexamer cluster (Figure 5-4), mimicking as closely as possible the protic environment of a methanol molecule in solution. For instance, one methanol molecule released from H-bonding would be represented as 1/6 of the total free energy value of the hexamer. A hexamer was used, as there is an increase in dissociation energy per unit of methanol as the size of the cluster increases until it includes six molecules. For clusters of six molecules or more, the dissociation energy per methanol unit is constant.[9]

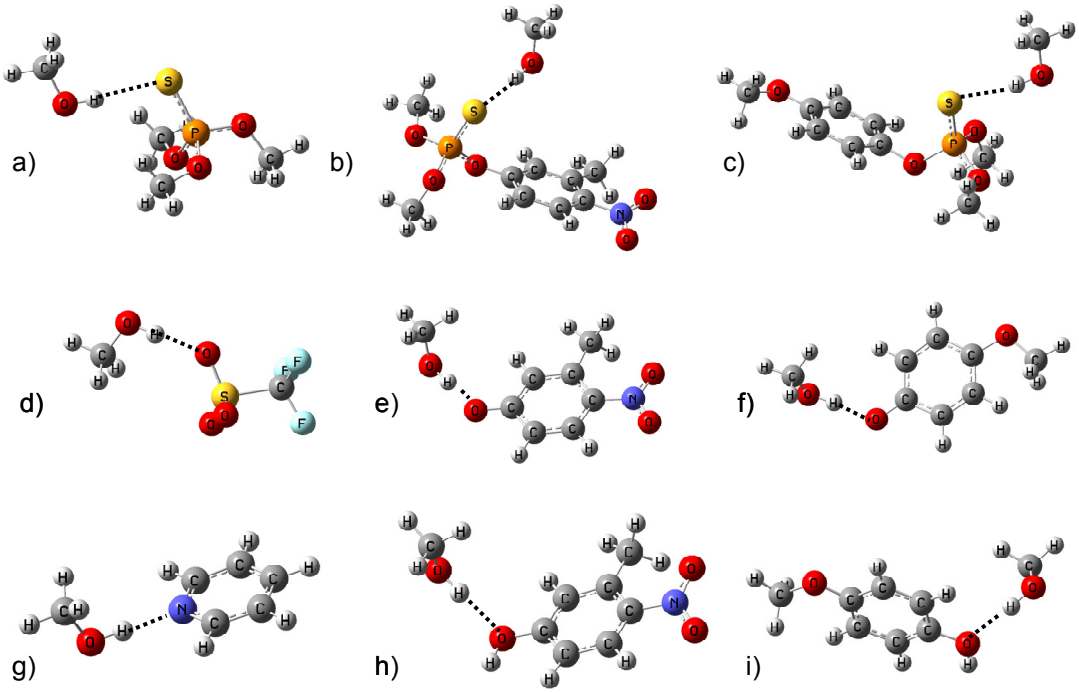

Figure 5-3. Placement of explicit solvent molecules on ligands not bound to Pd(II). (a) $P(S)(OMe)_3$, **5.2** (b) **5.3c** (c) **5.3g** (d) triflate (e) 4-nitro-3-methylphenoxide (f) 4-methoxyphenoxide (g) pyridine (h) 4-nitro-3-methylphenol (i) 4-methoxyphenol.

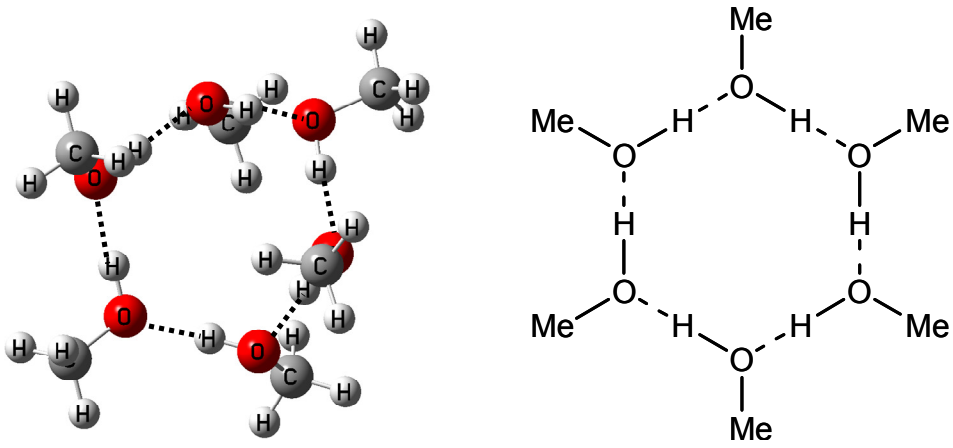

Figure 5-4. Cyclic hydrogen-bonded methanol hexamer.

The frequency calculations provide the free energies evaluated within the ideal

gas, rigid rotor and harmonic oscillator approximations. Such approximations can lead to relative free energies that differ significantly from values obtained in experiments where the systems are in solution. These deviations can be traced to an overestimation of the entropic contributions arising from translation and rotational motions, as the large suppression of these motions in solvent is not captured in the calculations. To correct for this behavior, we follow the method used by Sakaki *et al.*[10] and calculate the free energies without including any entropic contributions from translation and rotation. Equations (1) and (2) provide a comparison of the standard relative free energy (ΔG) and the definition employed in this work (ΔG_{corr}). The true free energy value would lie between these values, although there it has been argued that ΔG_{corr} is more accurate when describing bimolecular processes occurring in solvent.[11]

$$\Delta G = \Delta H - T(\Delta S_{elec} + \Delta S_{trans} + \Delta S_{rot} + \Delta S_{vib}) \quad (1)$$

$$\Delta G_{corr} = \Delta H - T(\Delta S_{elec} + \Delta S_{vib}) \quad (2)$$

For theoretical ^{31}P NMR predictions, molecular geometries were determined using B3LYP and the basis sets previously described. Due to reported inconsistencies[12] in differentiating four- and five-coordinate phosphorus using B3LYP, ^{31}P NMR chemical shifts were predicted at the HF/6-311++G(2d,2p) level of theory using the GIAO formalism.[13] The computed chemical shift of phosphoric acid was used to reference calculated shifts.

5.3.2. Modeling ligand exchange processes

Computational investigations into reaction mechanisms require detailed structural information for starting materials. The crystal structure for **5.1**(Py)(¯OTf) is reported,[1] and is used as a starting structure for this complex; that is, with the pyridine ligand *trans* to the ligand amino group and the triflate *trans* to the phenyl group (Figure 5-5-a). The thermodynamic equilibrium that exists between the precatalyst **5.1**(Py)(¯OTf), ***PC***, and **5.1**(Py)(¯OMe), ***GS***, wherein the latter is lower in free energy by 5.3 kcal mol^{-1}, consistent with the observation that the triflate dissociates upon dissolution in a basic solution. In this chapter, all free energies will be relative to this ground state structure.

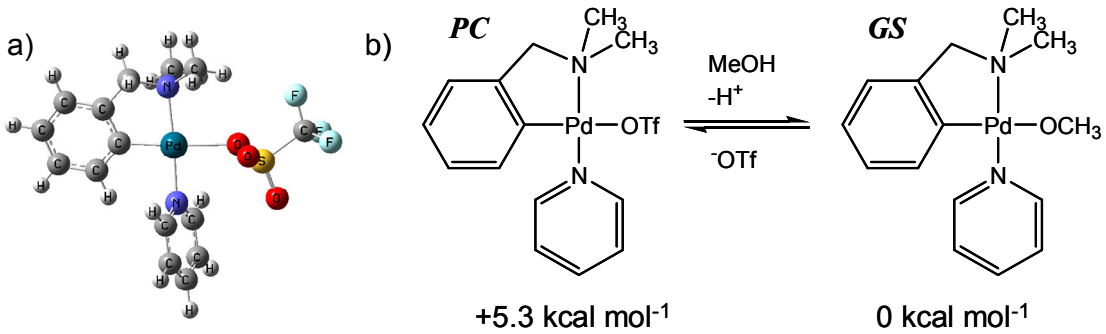

Figure 5-5. a) Calculated structure for **5.1**(Py)(¯OTf) b) thermodynamic equilibrium between **5.1**(Py)(¯OTf) and **5.1**(Py)(¯OMe). Relative free energy values (ΔG_{corr}) are given in kcal mol^{-1}.

The ligand exchange process leading from **GS** where pyridine is replaced by **5.3c** or **5.3g** was modeled as an associative axial attack of the sulfur atom on Pd concurrent with displacement of Pd-bound pyridine through a distorted trigonal-bipyramidal transition state (***TS$_{LE}$***, Figure 5-6, Scheme 5-2). No minima were found on the potential energy surface corresponding to the previously postulated 5-coordinate Pd(II) trigonal

bipyramidal or square pyramidal intermediate.[1] This is consistent with a previously observed concerted ligand exchange process.[14] Structurally, $\boldsymbol{TS_{LE}}$ is similar for both substrates in terms of bond lengths and bond angles (Table 5-1). The corrected free energy barrier for the ligand exchange is also similar for both substrates (**5.3c**, 10.6 kcal mol^{-1}; **5.3g** 8.4 kcal mol^{-1}). The indistinguishable free energy barriers for these substrates suggest little substituent effect on rate of reaction, consistent with a very small Brønsted slope, such as that observed for substrates **5.3a-d**. The resulting complex is **5.1**(OMe)(**5.3c** or **5.3g**), $\boldsymbol{INT_1}$.

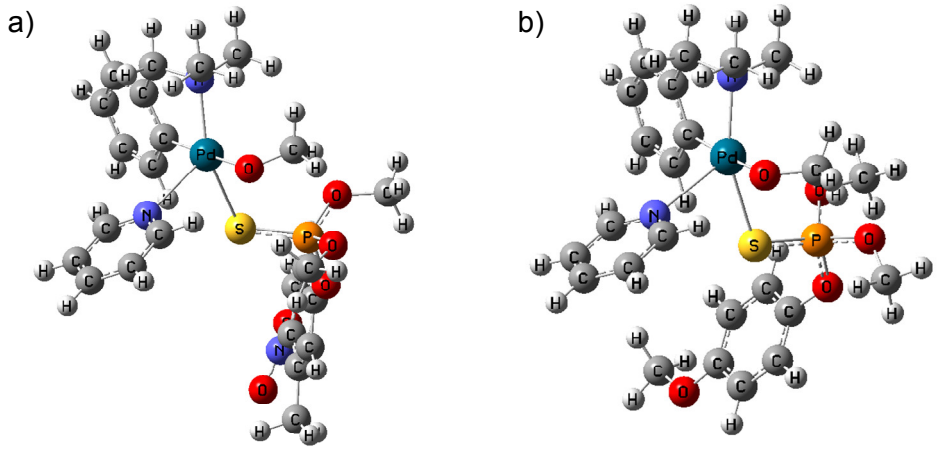

Figure 5-6. Trigonal bipyramidal transition state structures for the exchange of pyridine and substrate in the N-*trans* position. a) **5.3c** b) **5.3g**.

Table 5-1. Selected bond lengths and angles for computed structures ***TS$_{LE}$*-5.3c** and ***TS$_{LE}$*-5.3g**.

	***TS$_{LE}$*-5.3c**	***TS$_{LE}$*-5.3g**
Pyr(N) – Pd	2.62 Å	2.65 Å
Pyr(N) – Pd – N	121°	125°
S – Pd	2.69 Å	2.67 Å
S – Pd – N	156°	156°

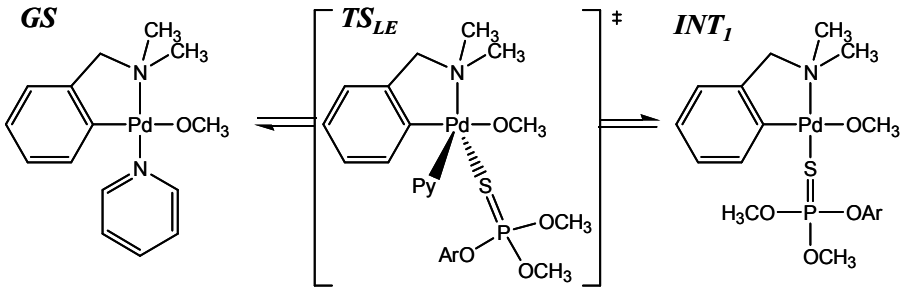

5.3c	0.0	10.6	7.5
5.3g	0.0	8.4	8.1

Scheme 5-2. Relative free energies (kcal mol^{-1}) for the GS → [TS$_{LE}$] → INT$_1$ process.

Previously reported studies[15] on similar Pd(II) complexes propose substrate binding in the position *trans* to the phenyl ring of the ligand. This might be anticipated, as the aryl portion of the palladacycle is kinetically *trans* directing and ligands opposite it will be expected to be more readily exchanged.[16] Conversely, the experiments show the

release of pyridine upon substrate binding. To clarify the likely regioselectivity of the substrate binding, the kinetic process involved in attaining each binding mode starting from ***GS*** was modeled. In order to place the substrate *trans* to the phenyl ring of the ligand, a mechanism involving ligand exchange *via* a solvent molecule was modeled with the **5.3c** substrate (Scheme 5-3). Each ligand exchange transition (***TS_{LE}'***, ***TS_{LE}''***; not shown) state has a trigonal bipyramidal structure, similar to ***TS_{LE}***. The proton transfer between ***INT_1'*** and ***INT_1''*** was not modeled, as it is unlikely to have a significant free energy barrier. The free energy barrier associated with this pathway is greater than the direct pyridine – substrate exchange and is unlikely to occur.

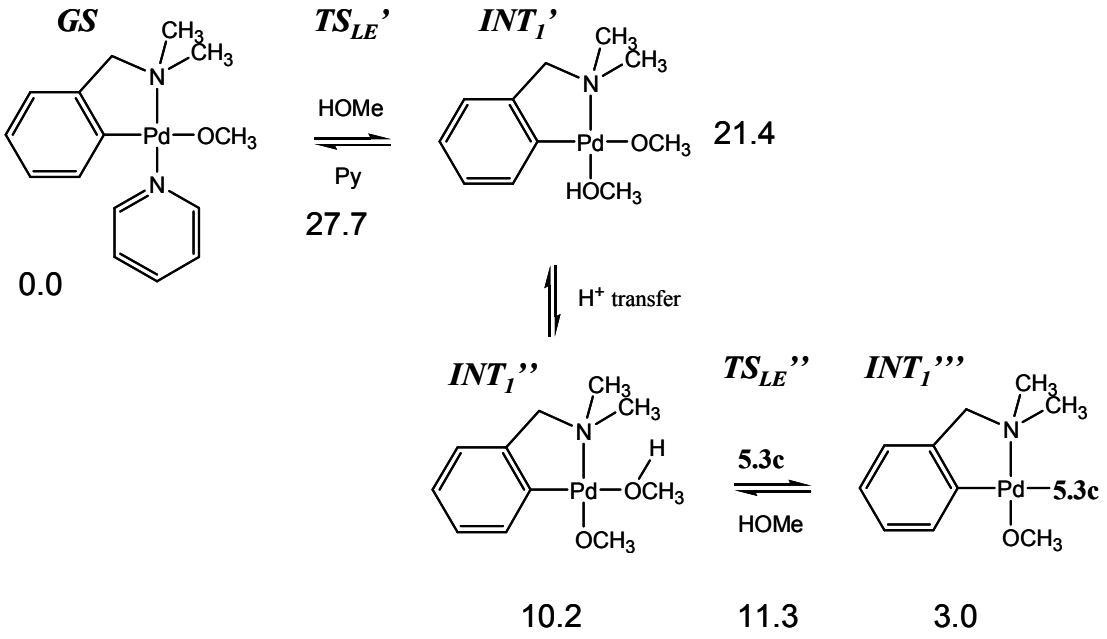

Scheme 5-3. Relative free energies (kcal mol^{-1}) for an alternate ligand exchange process placing **5.3c** in the C-*trans* position. The transition state for the proton transfer was not calculated.

5.3.3. Modeling nucleophilic attack

The generally accepted mechanism of the nucleophilic attack of a Pd(II) bound internal methoxide was modeled as a shortening of the P-OMe interatomic distance. The approach of the methoxide was directly opposite the leaving group, avoiding pseudorotation steps prior to leaving group expulsion. In the nucleophilic attack transition state structure (Figure 5-7), the length of the forming MeO – P bond is calculated to be longer for **5.3c** (2.88 Å) than that calculated for **5.3g** (2.63 Å), consistent with the 'tightening' of the transition state that is observed in the concerted and step-wise base-catalyzed solution reactions of P=O phosphate triesters.[17] Energetically, the nucleophilic attack (Scheme 5-4) is associated with a relatively small barrier of ~1 kcal mol^{-1}, a significant reduction in free energy of activation considering that this is typically the rate determining step for the base catalyzed reaction. The absolute ΔG_{corr} values are similar the free energy values for $\boldsymbol{TS_{LE}}$, indicating that potentially they could be rate limiting. If this were the case, however, a small negative β^{lg} would be expected.

The leaving group does not depart concurrently with the nucleophilic attack; instead a bidentate, 5-coordinate phosphorane intermediate $\boldsymbol{INT_2}$ was calculated to be a stable species thermodynamically downhill from the bound starting material $\boldsymbol{INT_1}$.

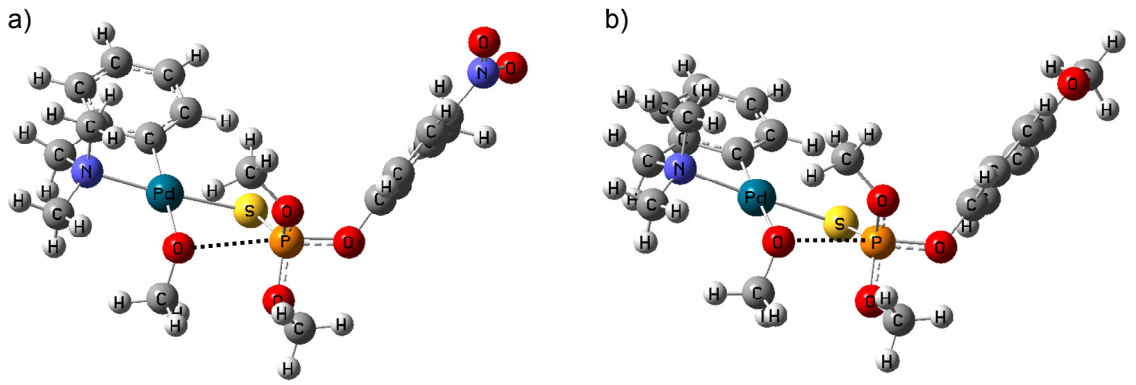

Figure 5-7. Transition state structures for the attack of the Pd(II) bound methoxide on a) **5.3c** and b) **5.3g**.

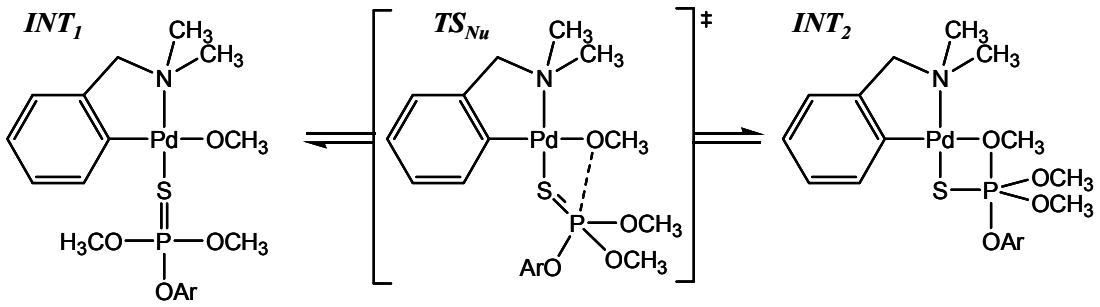

5.3c	8.1	9.1	-0.7
5.3g	7.5	8.1	-6.1

Scheme 5-4. Relative free energies (kcal mol^{-1}) for the $INT_1 \rightarrow [TS_{Nu}] \rightarrow INT_2$ process for **5.3c** and **5.3g** with free energies relative to the ***GS*** structure.

Metal bound hydroxides have been postulated to participate in catalyzed hydrolysis reactions through a general-base catalysis mechanism wherein the bound hydroxide deprotonates a neighboring solvent molecule which acts as the nucleophile.[18]

Solvent kinetic isotope effect studies can be used to detect the general-base mechanism, provided that it occurs in the rate determining step.[19] In this case, the nucleophilic attack is unlikely to be rate determining, as if it were to be the prominent pathway it would have to be of lower free energy than that of the internal nucleophilic attack, and thus it will have lower relative free energy to the ligand exchange step or subsequent leaving group departure steps. Thus, the general base mechanism will be inaccessible to solvent kinetic isotope effect experiments. Here, the general base mechanism was modeled computationally to determine its validity (Figure 5-8, Scheme 5-5). The resulting complex, ***INT$_2$'***, is a monodentate phosphorane structure with relatively high stability. However, the relative ΔG_{corr} associated with this mode of nucleophilic attack is greater than that of the direct attack of the internal nucleophile, and the latter is more likely to be the correct mechanism.

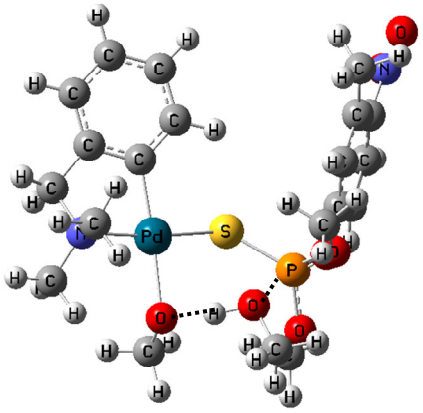

Figure 5-8. Transition state structure for the general base mechanism of nucleophilic attack on **5.3c** involving an external solvent molecule.

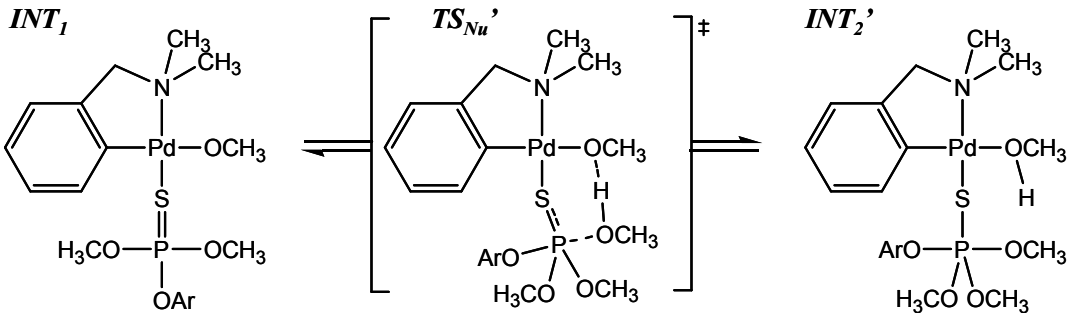

5.3c	7.5	14.5	-0.9
5.3g	8.1	14.7	4.6

Scheme 5-5. Relative free energies (kcal mol^{-1}) for the $INT_1 \rightarrow [TS_{Nu}] \rightarrow INT_2$ process for **5.3c** and **5.3g** with free energies relative to the ***GS*** structure.

5.3.4. Leaving group departure

The departure of the aryl leaving group is modeled as a lengthening of the P-OAr bond of ***INT₂***. The barrier associated with this transition state is low for **5.3c** (5.2 kcal mol^{-1}); however, a barrier of 15.2 kcal mol^{-1} is required to expel the poorer leaving group of **5.3g**. This represents the highest free energy value on the reaction pathway for **5.3g** methanolysis, and likely represents the rate determining step for this group of substrates. This is consistent with the large, negative β^{lg} observed as unassisted leaving group scission will be highly dependent on leaving group substitution. For **5.3c**, the free energy associated with leaving group departure is lower than that of the ligand exchange step and this process is therefore not rate liming. In the ***TS_{LG}*** structure, the P-OAr distance is larger with **5.3g** (2.87 Å) than it is for **5.3c** (2.46 Å). As the leaving group departs the phosphate adjusts from a trigonal bipyramidal structure to tetrahedral, increasing its ideal

MeO_{nuc}-P-OMe bond angle from ~90° to ~109° and creating greater strain on the Pd-OMe bond within the four-membered ring. This is evident by an increase in Pd-O bond length (for **5.3g** 2.49 Å *vs.* 2.26 Å in ***INT*$_2$**.) and a relatively high free energy for ***INT*$_3$**.

With these transition states, a complete picture of the reaction pathway that is consistent with the experimental data is formed, provided that no subsequent steps have higher associated barriers. However, to ensure that these are the highest points along the reaction free energy surface the ligand exchange steps required for catalyst turnover were calculated.

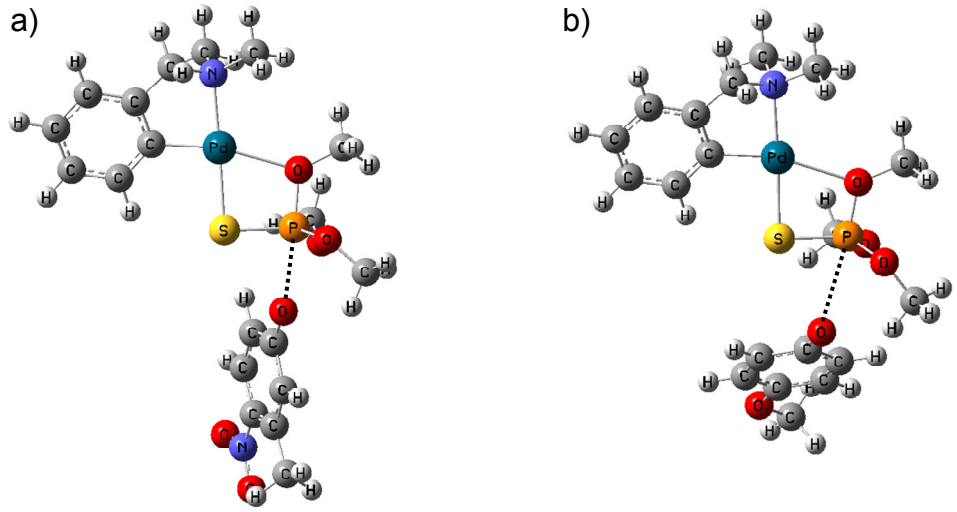

Figure 5-9. Calculated structures for ***TS*$_{LG}$**.

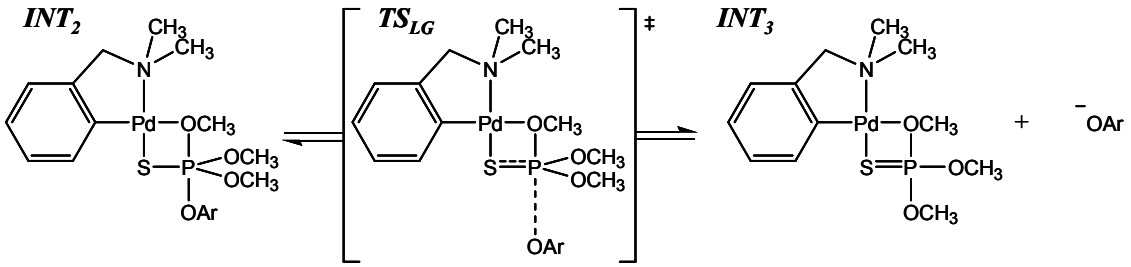

5.3c	-6.1	-0.9	-1.1
5.3g	-0.7	14.5	14.3

Scheme 5-6. Relative free energies (kcal mol^{-1}) for the $INT_2 \rightarrow [TS_{LG}] \rightarrow INT_3$ process for **5.3c** and **5.3g** with free energies relative to the ***GS*** structure.

5.3.5. Catalyst turnover mechanism

Catalyst turnover to re-form ***GS*** was modeled as a two step mechanism in which a methoxide molecule displaces the former nucleophile to form a complex in which the trimethyl phosphorothioate is monodentate bound (***INT4***). Pyridine then displaces the product (Scheme 5-7) in the N-*trans* position. It should be noted that in Scheme 5-7 the modeled complexes are the same for both substrates as the substrate has dissociated; the energy differences arise from the energetic difference between the expelled aryl leaving groups in solution. The bidentate bound product ***INT3*** being displaced by methoxide had only a very small barrier (***TSTO***, ~0.1 kcal mol^{-1}) associated with it, due to the instability of that intermediate. The formed monodentate bound product complex, ***INT4***, is 21.3 kcal mol^{-1} lower in free energy than the previous complex. The catalyst is regenerated when the trimethyl phosphorothioate product is exchanged for pyridine through the ***TSTO'*** structure. This completes the catalytic mechanism and shows that all rate determining

steps are in the TS_{LE} (for **5.3c**) and TS_{LG} (for **5.3g**) steps.

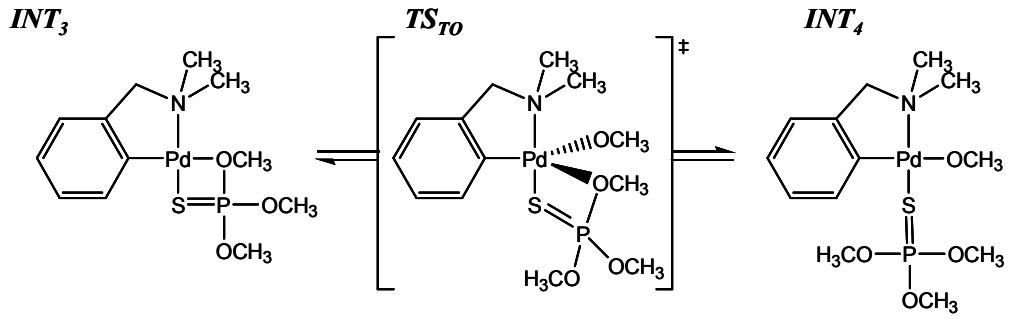

5.3c	-1.1	-1.0	-22.4
5.3g	14.3	14.4	-7.0

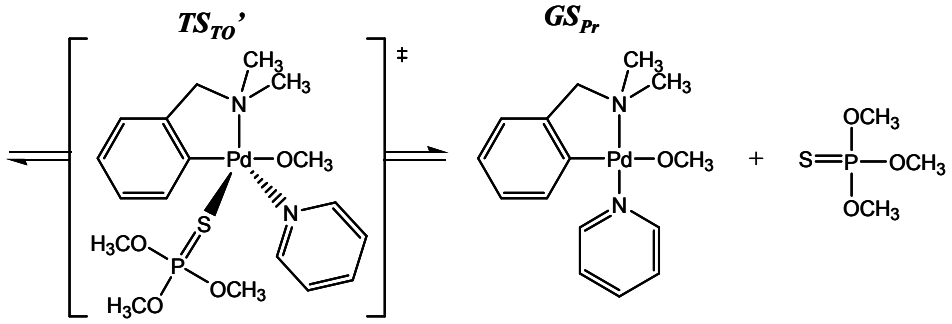

5.3c	-17.4	-28.3
5.3g	-2.0	-12.9

Scheme 5-7. Relative free energies (kcal mol^{-1}) for a proposed catalyst turnover process for **5.3c** and **5.3g** with free energies relative to the ***GS*** structure. Note that the complex structures are identical for **5.3c** and **5.3g** as the leaving group has departed. Energy differences arise from differences in free energy between the free aryloxide leaving groups.

5.3.6. Summary of the calculated mechanism

We now have a complete view of the mechanism and the rate limiting step for each of the substrate groups. The free energies of each structure (turnover steps excluded) are shown in Figure 5-10 and the calculated molecular structures are shown in Figure 5-11. The initial ligand exchange step, $\boldsymbol{TS_{LE}}$, is limiting for substrates with leaving groups with ${}^{s}_{s}pK_a < 13$ such as **5.3c**, consistent with the experimentally observed β^{lg} of 0. For these phosphorothioates, all subsequent chemical and ligand exchange steps are lower in free energy. The nucleophilic attack occurs as the internal nucleophile of $\boldsymbol{INT_1}$ directly attacks the phosphorus center of the bound phosphorothioate with a small ΔG_{corr} of activation through the transition state $\boldsymbol{TS_{Nu}}$ leading to a stable metal bound thiophosphorane intermediate $\boldsymbol{INT_2}$. Experimentally, the break in the Brønsted plot signifies the presence of at least one intermediate, however it would be exceedingly difficult to propose the existence of two intermediates ($\boldsymbol{INT_1}$ and $\boldsymbol{INT_2}$) without the computational study. The breakdown of this intermediate through the leaving group departure occurs through the transition structure $\boldsymbol{TS_{LG}}$ which is associated with a small ΔG_{corr} for **5.3c**. This transition state represents the highest point on the reaction free energy surface for **5.3g**, and is the rate determining step which is consistent with the large, negative β^{lg} observed for **5.3e,f,g**. A mode of catalyst turnover was also calculated, and shown to be energetically downhill for both substrates. The $\Delta G^{\ddagger}_{corr}$ for the highest barriers for each of the substrates (**5.3c**, 10.6 kcal mol^{-1}; **5.3g**, 14.6 kcal mol^{-1}) are in good accordance to the experimentally determined free energies of activation (**5.3c**, 12.9 kcal mol^{-1}; **5.3g**, 16.6 kcal mol^{-1}).

Table 5-2. Summary of B3LYP determined potential energies (ΔE), free energies (ΔG, 298 K) and corrected free energies (ΔG_{corr}, 298 K), in kcal mol^{-1}, for all intermediates and transition states for the **5.1** catalyzed methanolysis of **5.3c** and **5.3g**. All energies are relative to the ***GS*** structure.

	5.3c			**5.3g**		
	ΔE	ΔG	ΔG_{corr}	ΔE	ΔG	ΔG_{corr}
PC	9.9	7.1	5.3			
GS	**0.0**	**0.0**	**0.0**	**0.0**	**0.0**	**0.0**
TS_{LE}	**15.5**	**28.3**	**10.6**	**14.3**	**26.1**	**8.4**
INT_1	**6.5**	**8.7**	**7.5**	**7.6**	**9.3**	**8.1**
TS_{LE}'	30.7	33.8	27.7			
INT_1'	17.3	15.7	21.4			
INT_1''	9.9	8.1	10.2			
TS_{LE}''	13.0	17.7	11.3			
INT_1'''	3.6	4.2	3.0			
TS_{Nu}	**7.0**	**9.3**	**8.1**	**7.5**	**10.3**	**9.1**
INT_2	**-9.7**	**-4.9**	**-6.1**	**-5.1**	**0.5**	**-0.7**
TS_{Nu}'	12.1	19.3	14.5	17.9	19.5	14.7
INT_2'	-4.8	3.9	-0.9	7.0	9.4	4.6
TS_{Lg}	**-1.7**	**0.3**	**-0.9**	**14.1**	**15.6**	**14.5**
INT_3	-6.4	-17.0	-1.1	10.2	13.6	14.3
TS_{TO}	4.3	-6.0	-1.0	12.0	24.6	14.4
INT_4	-26.3	-23.2	-22.4	-9.7	7.4	-7.0
TS_{TO}'	-16.6	-19.1	-17.4	0.1	11.5	-2.0
GS_{Pr}	**-32.5**	**-29.8**	**-28.3**	**-15.7**	**0.8**	**-12.9**

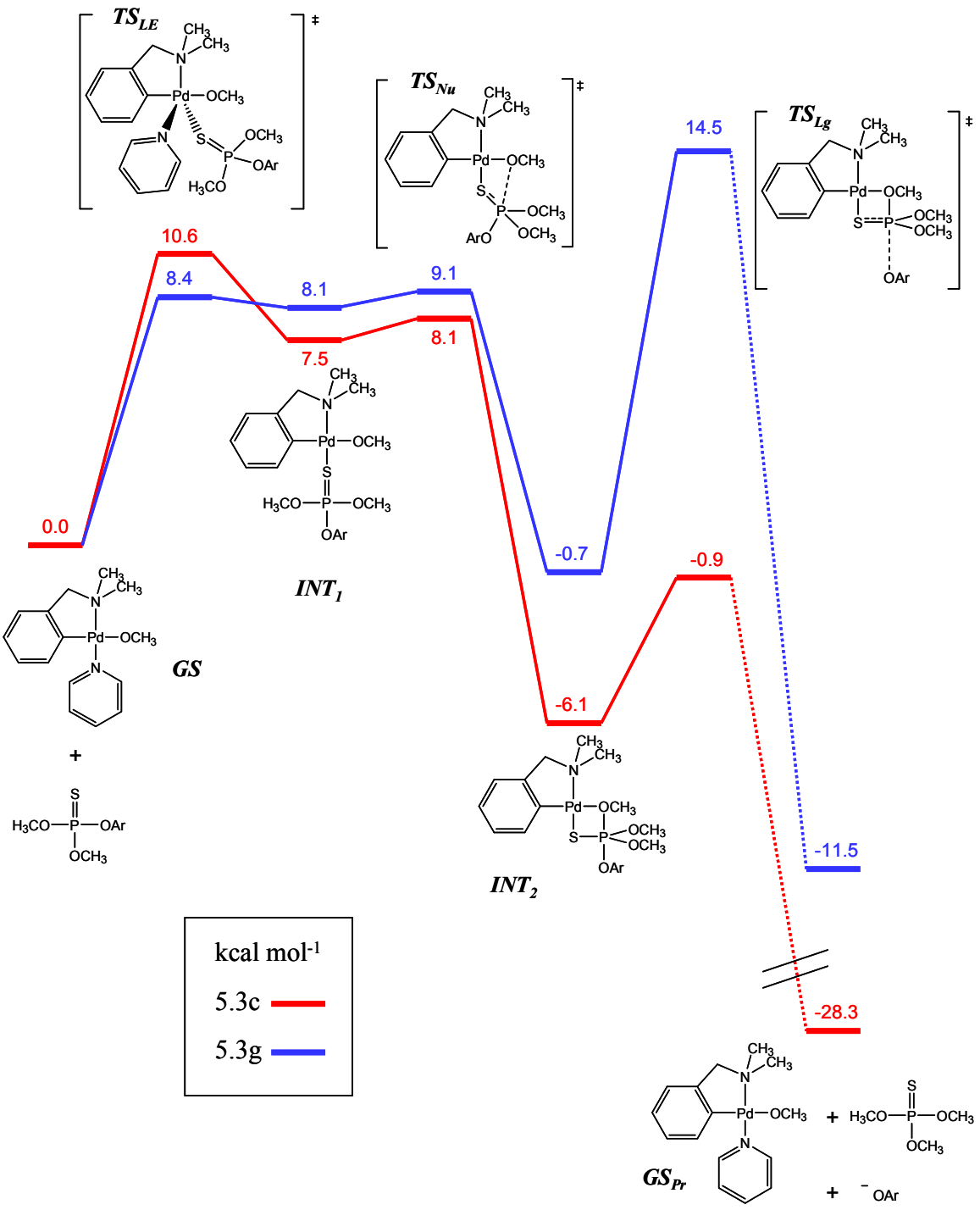

Figure 5-10. DFT computed reaction pathways (ΔG_{corr}) for the **5.1**(Py)($^{-}$OMe)-catalyzed methanolysis reactions of **5.3c** (Red) and **5.3g** (Blue). Dotted lines (•••) correspond to product dissociation steps that are not kinetically relevant and are not shown.

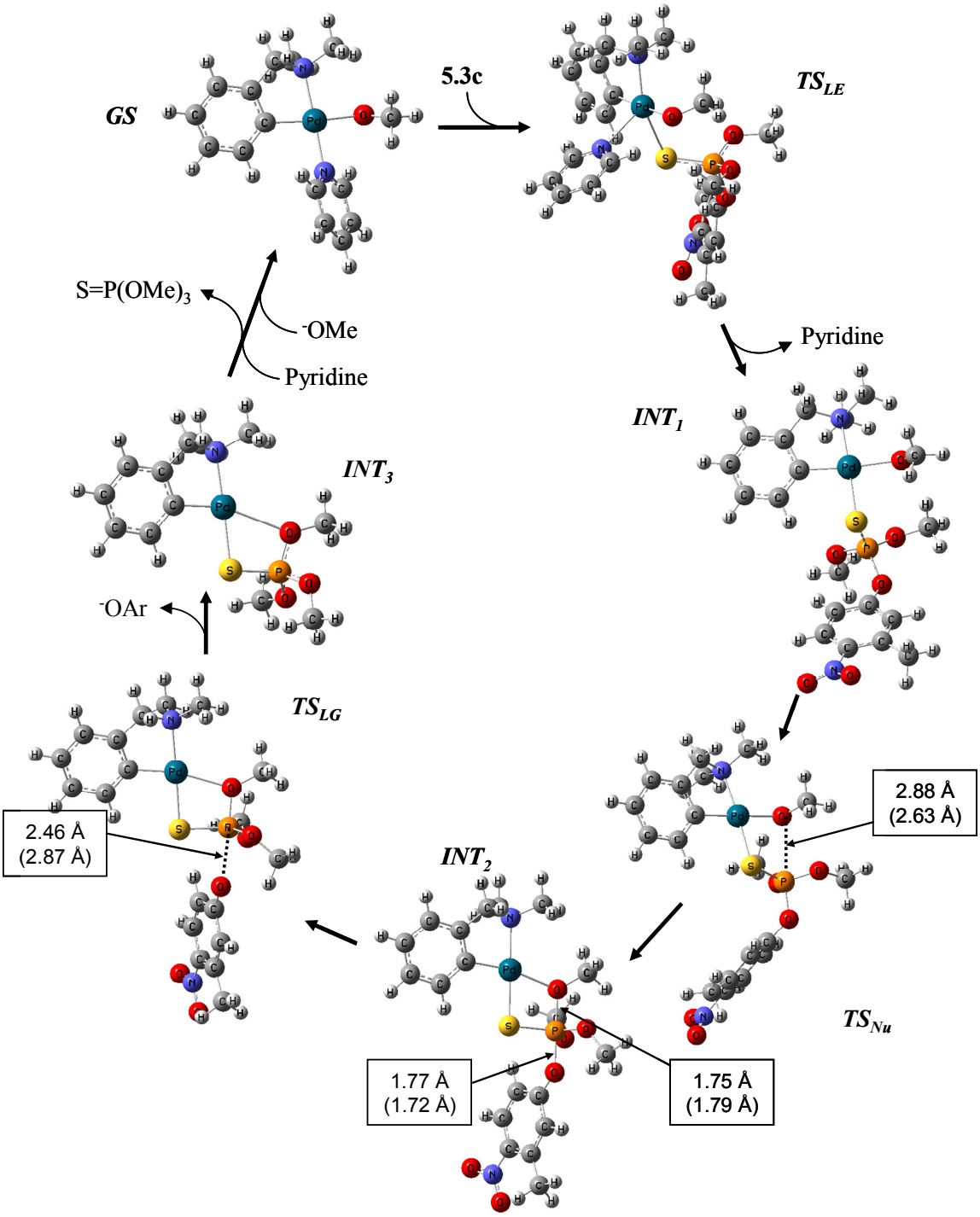

Figure 5-11. DFT computed structures for the methanolysis of **5.3c**. Selected internuclear distances are shown, with corresponding values for **5.3g** in parenthesis.

5.3.7. 5-coordinate thiophosphorane intermediate

The product of the internal nucleophilic attack is a bidentate thiophosphorane intermediate, ***INT*$_2$**, which for **5.3g** is 9.8 kcal mol^{-1} lower in free energy than its previous intermediate, ***INT*$_1$**, and requires 15.2 kcal mol^{-1} to expel the leaving group. While thiophosphoarane intermediates have been shown to be possible computationally with poor leaving groups,[20] with aryl groups they are unlikely to have any significant lifetime. When the intermediate is complexed with Pd(II) it is calculated to be thermodynamically and kinetically stable. It is postulated that this stability arises from the overall reduction in magnitude of charges on the S, P and methoxide group relative to the kinetically unstable free thiophosphorane. This occurs through transfer of electron density from the methoxy group and the sulfur to the metal center. Electrostatic potential determined (Chelp-G)[21] atomic and group charges support this view (Figure 5-12). While the thiophosphorane intermediate is stabilized by the metal center, the leaving group departure, which is associated with a low barrier with the solution reaction, is not stabilized by the Pd(II). The added depth to the energy well caused by the metal center in ***INT*$_2$** is not present for the leaving group departure, and thus, there is a larger barrier associated with the metal catalyzed reaction.

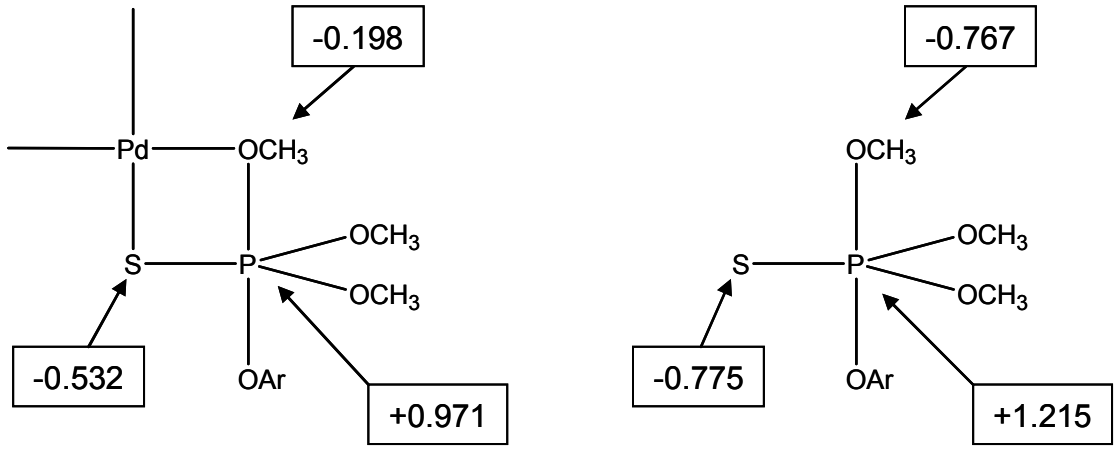

Figure 5-12. Electrostatic potential determined charges (Chelp-G) of a) the Pd(II) bound thiophosphorane intermediate of **5.3g** and b) free thiophosphorane intermediate of **5.3g**.

The computational prediction of a 5-coordinate thiophosphorane intermediate prompted an experimental ^{31}P NMR study to detect this structure using a non-reactive substrate (**5.2**, the cleavage product of **5.3a** – **5.3g**) where the leaving group departure from INT_2 will be exceedingly slow based on its predicted position in the Brønsted correlation. A computational prediction of the ^{31}P NMR shift of the Pd(II) bound thiophosphorane intermediate (with the method described in Section 5.3.1) predicted a shift of -22 ppm and experimental reports predict a range of -12 ppm to 18 ppm.[22] Upon measurement of the ^{31}P NMR spectrum, a signal was present at ~2 ppm which is consistent with the target complex; however it was found to come from trimethyl phosphate, the product of a so-far unexplained process. Thus, at the time of publication[23] of this work, the thiophosphorane complex had not been observed experimentally.

5.4. Conclusions and subsequent experimental work

This work has shown that the methanolysis of a series of O,O-dimethyl-O-aryl phosphorothioates **5.3a** – **5.3g** catalyzed by the palladacycle **5.1**(Py)(OMe) is a process involving several intermediates and transition states; for substrates with good leaving groups the substrate binding process is rate limiting, and for substrates with poor leaving groups the rate limiting step is leaving group departure. It has also shown that computational and experimental techniques can be used synergistically to solve reaction mechanisms.

The computational work predicts a stable 5-coordinate thiophosphorane intermediate stabilized by the metal center. The existence of this intermediate has since been confirmed.[24] It has been found that during the catalyzed reaction of **5.3e**, the substrate rapidly forms a transient intermediate (suggested to be the ***INT$_3$*** analogue) that exists long enough for its UV-Vis spectrum to be measured using stopped-flow spectrophotometry.

5.5. References

1) Lu, Z.-L.; Neverov, A. A.; Brown, R. S. *Org. Biomol. Chem.* **2005**, *3,* 3379.

2) Krüger, H.; van Eldik, R. *Chem. Commun.* **1990**, *4,* 330.

3) Equation (3) as published in Neverov, A. A.; Sunderland, N. E.; Brown, R. S. *Org. Biomol. Chem.* **2005**, *3,* 65.

4) a) Salas, G.; Casares, J. A.; Espinet, P. *Dalton Trans.* **2009**, 8413. b) Rau, T.; Shoukry, M.; Van Eldik, R. *Inorg. Chem.* **1997**, *36,* 1454.

5) a) Becke, A. D. *Phys. Rev. A.* **1988**, *38*, 3098; b) Lee, C.; Yang, W.; Parr, R. G. *Phys. Rev. B*. **1988**, *37*, 785.

6) Gaussian 09, Revision **A.1**, Frisch, M. J.; Trucks, G. W.; Schlegel, H. B.; Scuseria, G. E.; Robb, M. A.; Cheeseman, J. R.; Scalmani, G.; Barone, V.; Mennucci, B.; Petersson, G. A.; Nakatsuji, H.; Caricato, M.; Li, X.; Hratchian, H. P.; Izmaylov, A. F.; Bloino, J.; Zheng, G.; Sonnenberg, J. L.; Hada, M.; Ehara, M.; Toyota, K.; Fukuda, R.; Hasegawa, J.; Ishida, M.; Nakajima, T.; Honda, Y.; Kitao, O.; Nakai, H.; Vreven, T.; Montgomery, Jr., J. A.; Peralta, J. E.; Ogliaro, F.; Bearpark, M.; Heyd, J. J.; Brothers, E.; Kudin, K. N.; Staroverov, V. N.; Kobayashi, R.; Normand, J.; Raghavachari, K.; Rendell, A.; Burant, J. C.; Iyengar, S. S.; Tomasi, J.; Cossi, M.; Rega, N.; Millam, N. J.; Klene, M.; Knox, J. E.; Cross, J. B.; Bakken, V.; Adamo, C.; Jaramillo, J.; Gomperts, R.; Stratmann, R. E.; Yazyev, O.; Austin, A. J.; Cammi, R.; Pomelli, C.; Ochterski, J. W.; Martin, R. L.; Morokuma, K.; Zakrzewski, V. G.; Voth, G. A.; Salvador, P.; Dannenberg, J. J.; Dapprich, S.; Daniels, A. D.; Farkas, Ö.; Foresman, J. B.; Ortiz, J. V.; Cioslowski, J.; Fox, D. J. Gaussian, Inc., Wallingford CT, 2009.

7) a) Tomasi, J.; Mennuccia, B.; Cancés, E. *THEOCHEM*. **1999**, *464*, 211; b) Tomasi, J.; Mennuccia, B.; Cammi, R. *Chem. Rev.* **2005**, *105*, 2999.

8) a) Hay, P. J.; Wadt, W. R.; *J. Chem. Phys.* **1985**, *82*, 270; b) Wadt, W. R.; Hay, P. J. *J. Chem. Phys.* **1985**, *82*, 284.

9) Boyd, S. L.; Boyd, R.J. *J. Chem. Theory Comput.* **2007**, 3, 54.

10) Sakaki, S.; Takayama, T.; Sumimoto, M.; Sugimoto, M. *J. Am. Chem. Soc.* **2004**, 126, 3332.

11) a) Sumimoto, M.; Iwane, N.; Takahama, T.; Sakaki, S. *J. Am. Chem. Soc.* **2004**, *126*, 10457; b) Tamura, H.; Yamasaki, H.; Sato, H.; Sakaki, S. *J. Am. Chem. Soc.* **2003**, *125*, 16114.

12) Zhang, Y. and Oldfield, E. *J. Phys. Chem. B.* **2006**. 110, 579-586.

13) Ditchfield, R.; Hehre, W. J. and Pople, J.A. *J. Chem. Phys.* **1972**,54, 724-728.

14) Holmann, H.; Suvachittanont, S.; van Eldik, R. *Inorg. Chim. Acta* **1990**, *177*, 151.

15) a) Kazankov, G. M.; Sergeeva, V. S.; Efremenko, E. N.; Alexandrova, L.; Varfolomeev, S. D.; Ryabov, A. D. *Angew. Chem.* **2000**, *112,* 3247. b) Kazankov, G. M.; Sergeeva, V. S.; Borisenko, A. A.; Zatsman, A. I.; Ryabov, A. D. *Russ. Chem. Bull. Int. Ed.* **2001**, *50,* 1844. c) Kim, M.; Gabbaï, F. P. *Dalton Trans.* **2004**, 3403. b) Kim, M.; Picot, A.; Gabbaï, F. P. *Inorg. Chem.* **2006**, *45,* 5600. d) Kim, M.; Liu, Q.; Gabbaï, F. P. *Organometallics,* **2004**, *23,* 5560.

16) Coe, B. J.; Glenwright, S. J. *Coord. Chem. Rev.* **2000**, *203,* 5.

17) a) Rosta, E.; Kamerlin, S. C. L.; Warshel, A. *Biochemistry.* **2008**, *47,* 3725. b) Rowell, R. and Gorenstein, D. G.; *J. Am. Chem. Soc.* **1981**, *103,* 5894. c) Maxwell, C. I.; Liu, C. T.; Neverov, A. A.; Mosey, N. J.; Brown, R. S. *Submitted to J. Phys. Org. Chem.*.

18) a) Norman, P. R.; Tate, A.; Rich, P. *Inorg. Chim. Acta,* **1988**, *145,* 211. b) Kuusela, S.; Rantanen, M.; Lonnberg, H. *J. Chem. Soc. Perkin. Trans.* **1995**, *2269.*

19) Maxwell, C.; Neverov, A. A.; Brown, R. S. *Org. Biomol. Chem.* **2005**, *3,* 4329.

20) Maxwell, C. I.; Liu, C. T.; Neverov, A. A.; Mosey, N. J.; Brown, R. S. *J. Phys. Org. Chem.* Published online, October 21, 2011; DOI:10.1002/poc.1938.

21) a) Breneman, C. M.; Wiberg, K. B. *J. Comput. Chem.* **1990**, *11,* 361. b) Leach, A. R. *Molecular Modeling Principles and Applications*, 2nd ed.; Pearson Education Limited: Harlow, England, **2001**, 189. c) Bayly, C. I.; Cieplak, P.; Cornell, W. D.; Kollman, P. A. *J. Phys. Chem.* **1993**, *97,* 10269.

22) From the observed 73 ppm of free trimethyl phosphorothioate **5.2**. To this is added the downfield chemical shift range of -55 ppm to -85 ppm is reported for neutral and cyclic pentaoxy-phosphoranes and tetraoxy-monothiophosphoanes relative to their neutral 4-coordinate counterparts. a) Sherlock, D. J.; Chandrasekaran, A.; Day, R. O.; Holmes, R. R. *Inorg. Chem.* **1997**, *36,* 5082. b) Garrossian, M.; Bentrude, W. G.; Röschenthaler, G.-V. *J. Org. Chem.* **2001**, *66,* 6181.

23) Liu, C. T.; Maxwell, C. I.; Edwards, D. R.; Neverov, A. A. Mosey, N. J.; Brown, R. S. *J. Am. Chem. Soc.* **2010**, *132,* 16599.

24) Liu, C. T.; Neverov, A. A.; Brown, R. S. *Inorg. Chem.* **2011**, *50*, 7852.

Chapter 6. Palladacycle catalyzed N-methyl N-aryl thiobenzamide methanolysis

6.1. Introduction

Thioamides are more resistant to cleavage than their amide counterparts due to the increased double bond character between the C and N.[1] This makes them more resistant to hydrolysis[2] and adds to the challenge in developing catalysts for their cleavage. Work in this laboratory has recently shown that the palladacycle complex **6.1**$(MeOH)_2$ catalyzes the efficient C-N cleavage of N-methyl N-aryl thiobenzamides (**6.2a-e**) through a methanolysis process.[3] Here, a computational investigation using density functional theory (DFT) is used in conjunction with an experimental structure-reactivity study to develop a plausible mechanism for the catalysis. In this section the experimental work, conducted by C. Tony Liu and Stephanie Pipe, will be briefly discussed followed by the in-depth report of the theoretical work, of which all calculations were conducted by C. Maxwell.

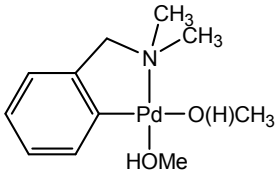

6.1$(HOMe)_2$

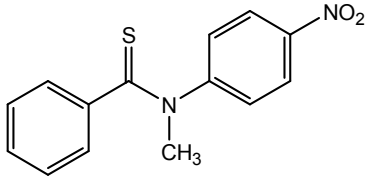

6.2a

6.2. Experimental basis for theoretical work

A plot of experimentally determined k_{obs} for the methanolytic cleavage of **6.2a** *vs.* [**6.1**] concentration shows saturation behavior and a maximum catalytic rate constant (k_{cat}) of 10.7 s^{-1} for the production of N-methyl-4-nitroaniline. From the ${}^{s}_{s}pH$ / k_{obs} profile, one obtains a catalytic ${}^{s}_{s}pK_a$ of 13.1, higher than that observed for the phosphorothioate methanolysis (10.8) catalyzed by this complex. Presumably the bound methanol ${}^{s}_{s}pK_a$ is raised by the anionic nature of the sulfur atom of the bound substrate. Kinetic measurements at high ${}^{s}_{s}pH$ s were measured using a 'pH-jump' method, wherein the substrate-catalyst complex is preformed at lower pH and the reaction is initiated by fast mixing with base.

Possible mechanisms for the chemical step of this catalysis are shown in Scheme 6-1. Two modes of leaving group departure are suggested, one involving direct departure with assistance from a hydrogen bond donating solvent molecule,[4] and one wherein the metal assists the leaving group departure, similar to what one might suggest occurs in metallopeptidase-catalyzed hydrolytic reactions of peptides.

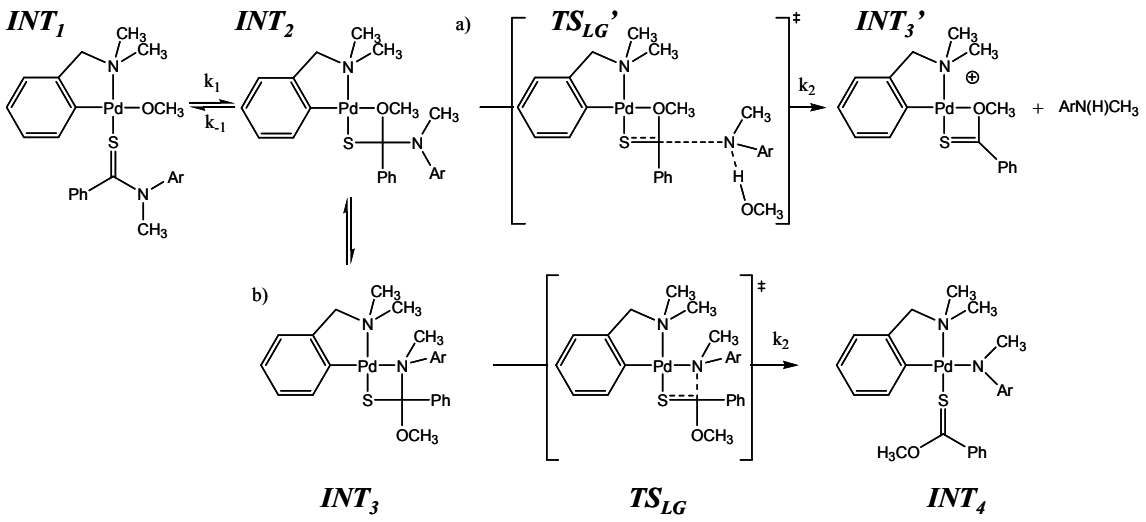

Scheme 6-1. Proposed mechanism for the chemical steps of the **6.1**$(MeOH)_2$ catalyzed methanolysis of thioamide **6.2a** with a) direct leaving group departure with solvent assistance and b) metal assisted leaving group departure.

6.3. Theoretical work

Herein is presented a computational study of the chemical steps for the **6.1**(HOMe)($^-$OMe) catalyzed methanolysis of the N-methyl N-aryl thiobenzoates **6.2** in order to differentiate between proposed mechanisms. The mechanism was intially mapped out using the 4-nitro substrate **6.2a**, then that mechanism was applied to model the catalyzed methanolysis of the other thioamide substrates. No binding steps or catalyst turnover steps are modeled in this work, only those involved in activating and cleaving the C-N bond. The theoretical work is focused on the different modes of nucleophilic attack and leaving group departure.

6.3.1. Computational details

Optimizations and free energy determinations of ground and transition states were calculated at the B3LYP[5] level with the IEFPCM[6] methanol solvent model applied. The 6-31G(d,p) basis set was used for C and H, while 6-31++G(d,p) was used for heteroatoms. The effective core potential of Hay and Wadt[7] with the double-ζ valence basis set (LanL2DZ) was used to describe Pd. Frequency calculations were used to characterize minima (intermediates) and maxima (transition states) on the PES and as a basis for free energy determinations at 298 K. All calculations were conducted using Gaussian 09.[8]

For the steps prior to those involving external methoxide nucleophiles, the methoxide is stabilized by a hydrogen bonding interaction with a methanol molecule (Figure 6-1-b). To maintain atom balance after nucleophilic attack the energetic contribution from this solvent molecule is represented as a fractional value of a PCM-solvated methanol hexamer as described previously (Section 5.3.1).[9] For the bimolecular steps of these reactions the entropic correction previously employed (also described in Section 5.3.1)[9] was used, wherein only vibrational contributions to entropy are considered in determining free energy (ΔG_{corr}). For unimolecular steps, free energies with this correction applied are very similar to uncorrected energies (typically within ~0.2 kcal mol^{-1}, Table 6-2). Uncorrected free energies (ΔG) are used for steps that do not involve the addition or removal of nucleophiles or solvent molecules. All free energies in this chapter (ΔG and ΔG_{corr}) are presented relative to the initial substrate bound starting structure ***INT$_1$***.

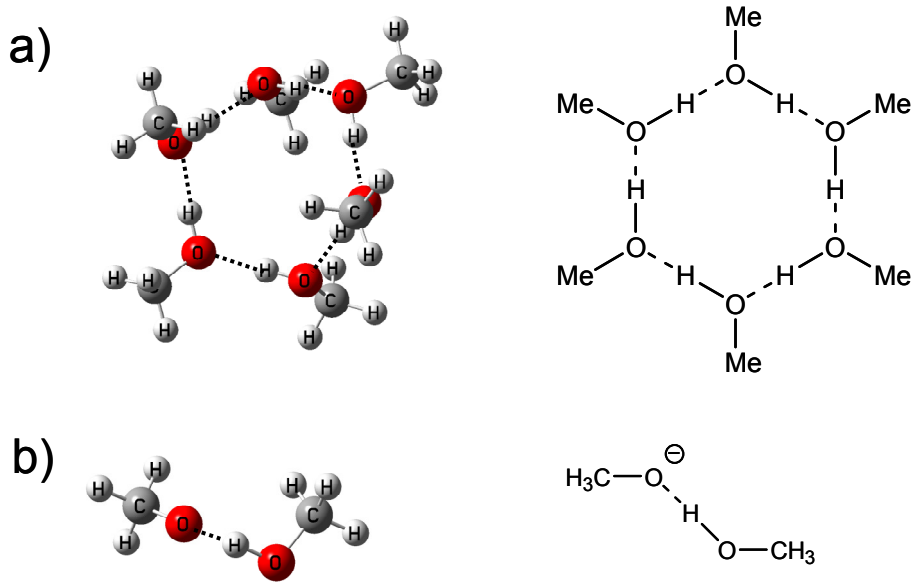

Figure 6-1. a) cyclic hydrogen-bonded methanol hexamer. b) Methoxide hydrogen bonded to a single solvent molecule.

6.3.2. Modeling nucleophilic attack

Starting with the likely structure of **6.1**($^{-}$OMe)(**6.2a**) with the substrate bound in the N-*trans* position (***INT*$_1$**) in Scheme 6-2, nucleophilic attack was modeled to proceed through a shortening of the relevant MeO – C interatomic distance and the transition state (***TS*$_{Nu}$**) is associated with a free energy (ΔG) of 10.0 kcal mol^{-1}. This leads to a bidentate metal bound tetrahedral intermediate (***INT*$_2$**) that has a free energy of -4.1 kcal mol^{-1}.

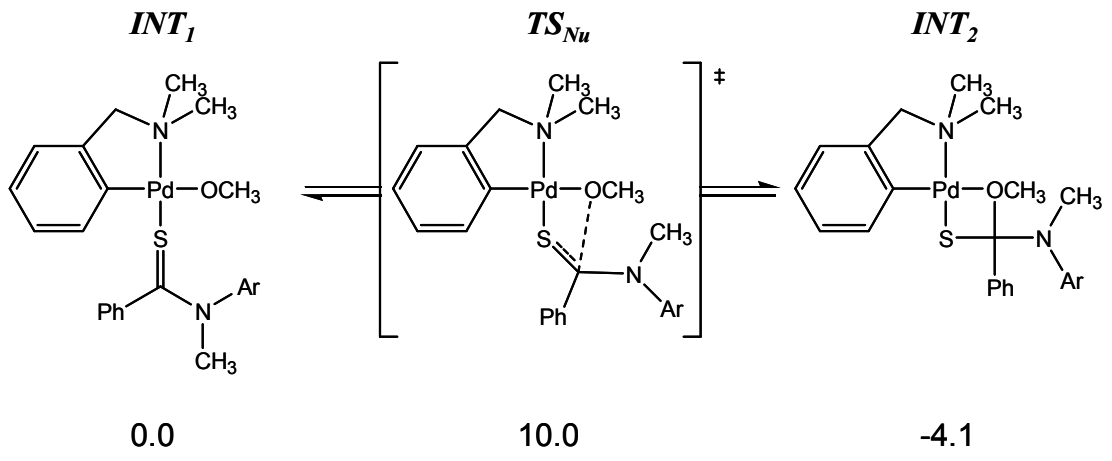

Scheme 6-2. Nucleophilic attack of metal-bound methoxide on **6.2a** complexed with **6.1**(OMe). Free energies (kcal mol^{-1}) are reported relative to ***INT1***.

Considering the potential importance of leaving group assistance, a hypothetical nucleophilic attack of free methoxide was envisioned on the substrate which is bidentate bound to the metal through both sulfur and nitrogen (Scheme 6-3). It was thought that this mode of attack might be favoured as it partially relieves the highly strained geometry of the four-member ring of ***INT1'*** as the carbon is converted form trigonal planar geometry to tetrahedral. It also results in a structure with the leaving group nitrogen being pre-positioned for metal assisted leaving group departure. Between ***INT1'*** and ***TSNu'*** atom balance was maintained using a hydrogen bonded methoxide and 1/6 of the free energy value of the aforementioned methanol hexamer (Figure 6-1). The instability of ***INT1'*** is evident by its high free energy (20.3 kcal mol^{-1}) relative to ***INT1***. The transition state associated with the nucleophilic attack of the free methoxide (***TSNu'***) has a barrier of 21.2 kcal mol^{-1} relative to ***INT1'*** (41.5 kcal mol^{-1} relative to ***INT1***). Thus, while this nucleophilic attack mechanism places the leaving group in position for ready metal

assisted departure (***INT$_3$***), its free energy is much higher then that of the internal nucleophilic attack mechanism (Scheme 6-2).

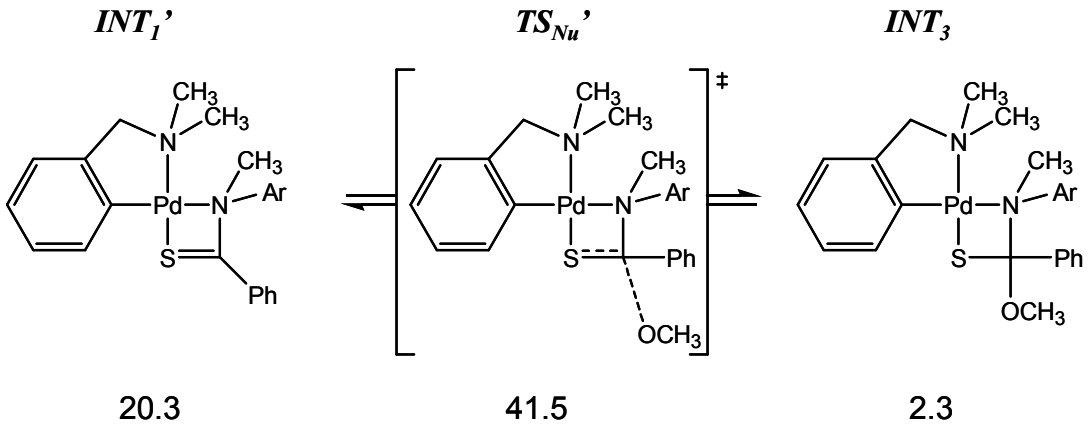

Scheme 6-3. Alternate mode of nucleophilic attack on metal bound **6.2a** with leaving group positioned for metal assisted departure. Free energies (ΔG_{corr}, kcal mol^{-1}) are reported relative to ***INT$_1$***.

6.3.3. Modeling leaving group departure

As described in Section 6.2, leaving group departure was considered to occur through one of two mechanisms a) free departure with solvent assistance and b) metal assisted leaving group departure. Free leaving group departure has the advantage that it does not require prior intramolecular OMe/NMeAr exchange on Pd. Initially it was modeled without explicit solvent interactions (Scheme 6-4-a) as a simple lengthening of the C-N bond of ***INT$_2$***, and the transition state, ***TS$_{LG}$'***, was found to have a free energy (ΔG) of 22.0 kcal mol^{-1} relative to the free energy of ***INT$_2$*** or 17.9 kcal mol^{-1} relative to ***INT$_1$***. When a solvent methanol molecule is placed on ***INT$_2$*** such that it can donate a hydrogen bond to the aniline nitrogen of the tetrahedral intermediate (***INT$_{2\text{-}(HB)}$***), the free

energy of the system increases by 3.8 kcal mol^{-1}. In order to maintain atom balance, the free energy of this methanol is represented by the addition of 1/6 of the solvent hexamer's free energy to that of ***INT$_2$***. Thus, the strong hydrogen bonding within the hexamer is replaced by a weaker hydrogen bonding to the aniline and causes the increased relative free energy. A free energy of 20.0 kcal mol^{-1} of is required to dissociate the hydrogen bonded aniline from the carbon center (***INT$_2$-(HB) → TS$_{LG-(HB)}$'***), less than that without the hydrogen bond, however the energetic cost of forming that hydrogen bond makes this process less energetically favourable overall (19.7 kcal mol^{-1} relative to ***INT$_1$***). While optimizing the bidentate bound thiobenzoate ester product ***Pr'*** structure, the (OMe) moiety dissociated from the metal centre due to increased Pd-OMe tension as carbon rehybridizes from sp^3 to sp^2, and its free energy was not determined.

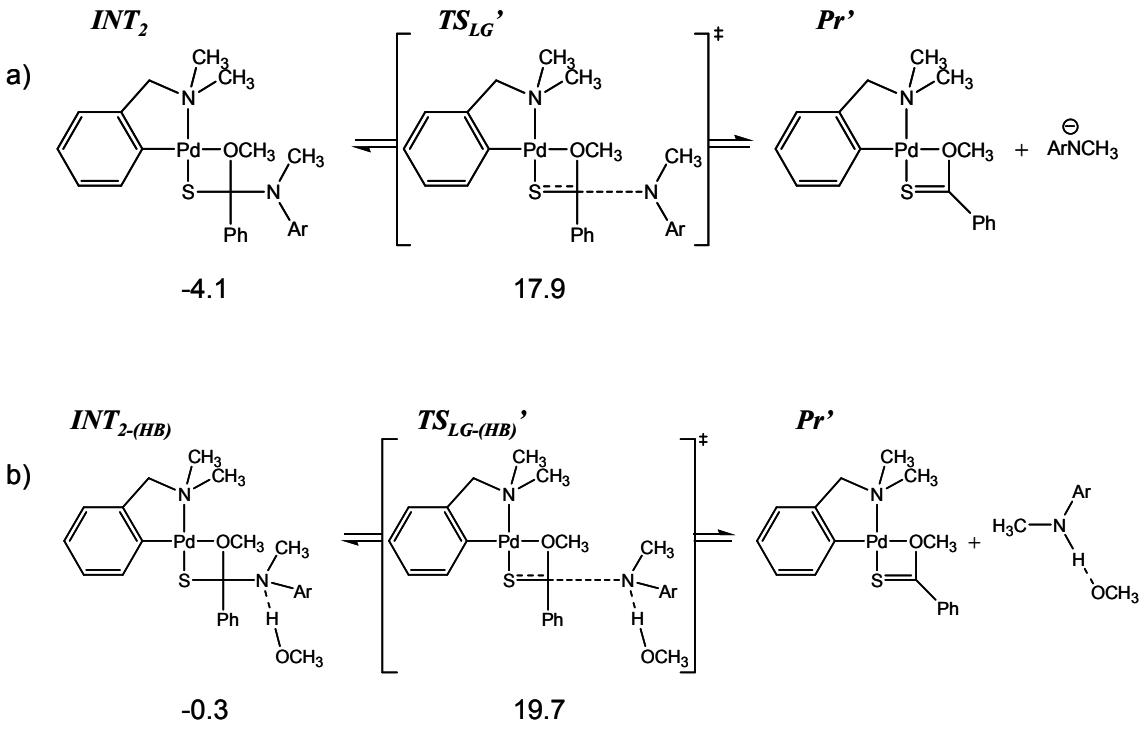

Scheme 6-4. Free leaving group departure a) with no explicit solvent interactions (ΔG) and b) with explicit solvent interactions (ΔG_{corr}). Free energies (kcal mol^{-1}) are reported relative to ***INT*$_1$**. The free energies of the ***Pr'*** structures were not calculated.

In order to permit metal assisted leaving group departure, a rearrangement step is necessary wherein the leaving group nitrogen replaces the methoxide moiety on the Pd(II). This occurs through a rotation about the Pd-S-C-OMe dihedral and is associated with a relatively low free energy barrier of 5.9 kcal mol^{-1} (***TS*$_{LE}$**). The resulting Pd-bound leaving group intermediate, ***INT*$_3$**, is energetically indistinguishable from ***TS*$_{LE}$** and is likely short-lived and exists transiently prior to leaving group expulsion.

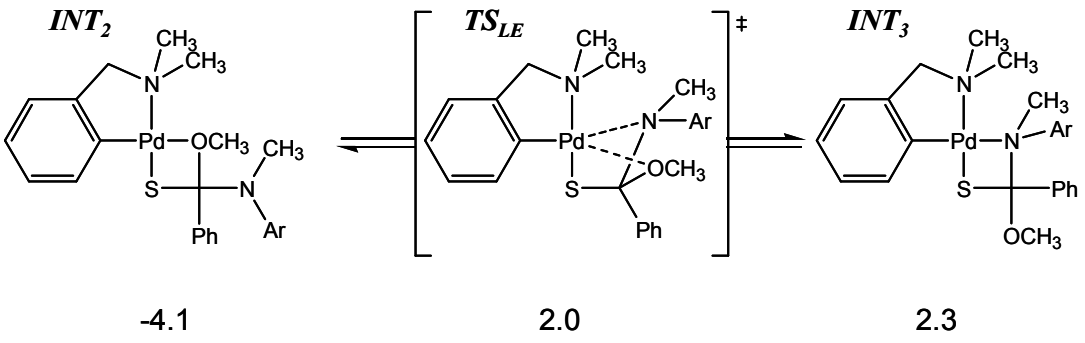

Scheme 6-5. Ligand exchange process where the leaving group nitrogen binds Pd(II). Free energies (ΔG, kcal mol^{-1}) are reported relative to ***INT*$_1$**.

Leaving group scission then proceeds through a lengthening of C-N bond (***TS*$_{LG}$**) with barrier of 11.4 kcal mol^{-1}, the highest point on the reaction pathway for this mechanism. Thus, the computational results indicate that the **6.1** promoted methanolysis of **6.2a** proceeds via the nucleophilic attack of an internal methoxide, followed by a rearrangement step to a precarious complex wherein the leaving group nitrogen is bound to the metal center. While it may be argued that ***INT*$_3$** is unlikely to exist as a discrete intermediate, it is likely that the reaction passes through it as a part of the leaving group expulsion mechanism. The complex, ***INT*$_4$**, is the final structure modeled here. The structures of each transition state and intermediate is shown in Figure 6-2.

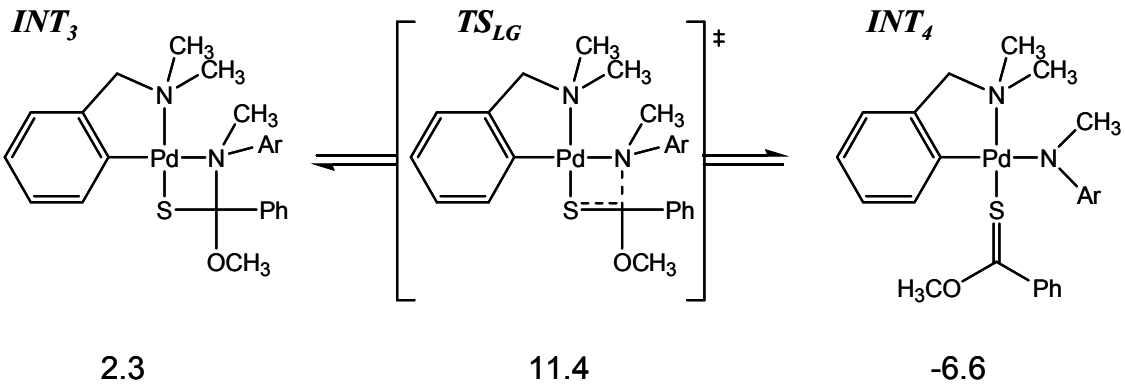

Scheme 6-6. Metal assisted leaving group departure. Free energies (ΔG, kcal mol^{-1}) are reported relative to ***INT₁***.

The calculated $\Delta G^{‡}$ of 15.5 kcal mol^{-1} for ***INT₂*** to ***TS$_{LG}$*** is in good agreement with the experimentally measured $\Delta G^{‡}$ of 16.2 kcal mol^{-1}. This may suggest that the experimentally observable process is the breakdown of the Pd-bound tetrahedral intermediate (***INT₂***). The calculated entropy for this process (-3 cal K^{-1} mol^{-1}) is also consistent with the experimentally determined entropy of activation (0.7 cal K^{-1} mol^{-1}). The fact that ***INT₂*** is lower in free energy than ***INT₁*** suggests that this intermediate could be experimentally observable under certain conditions.

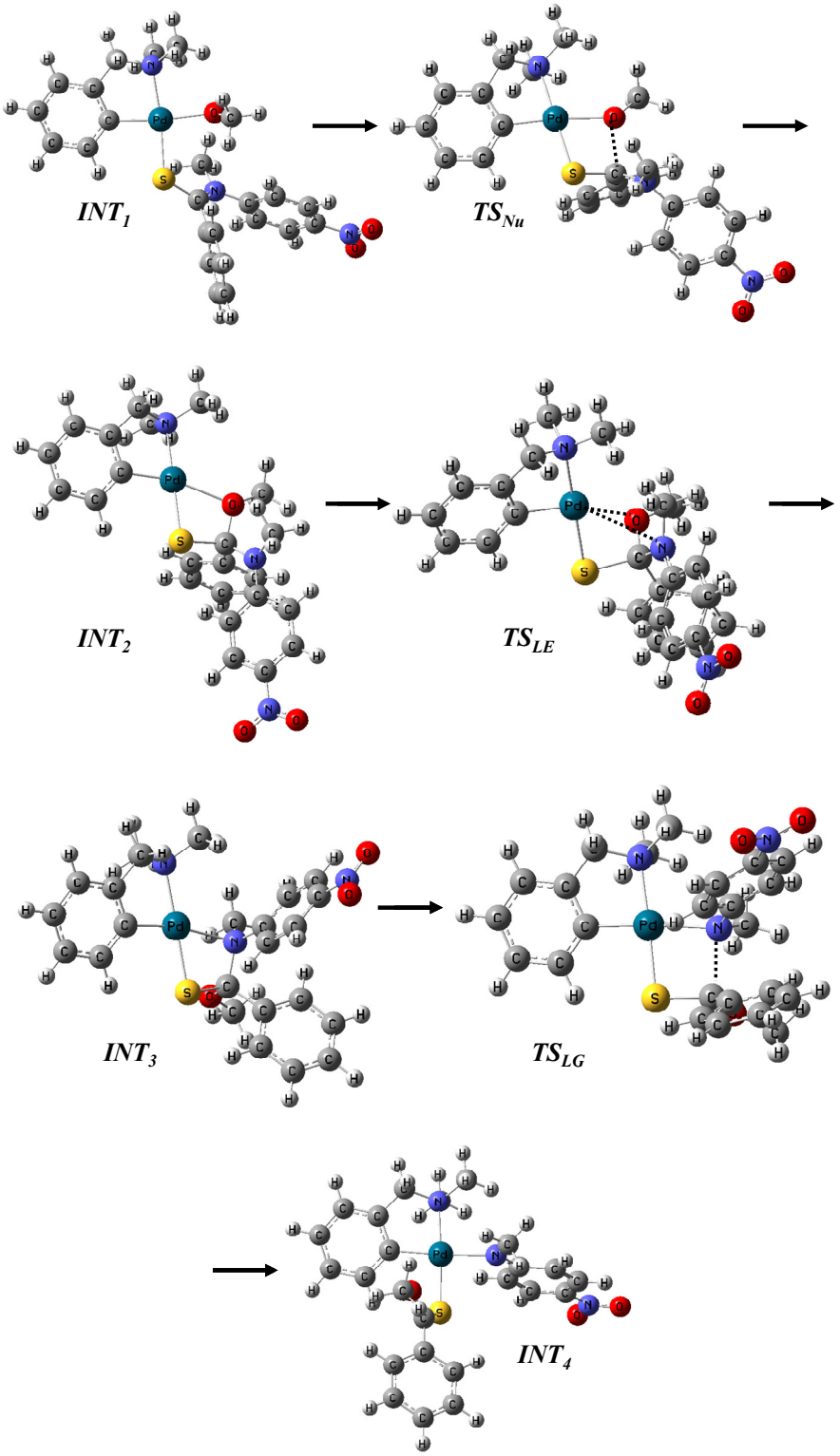

Figure 6-2. DFT optimized structures for the **6.1** promoted methanolysis of **6.2a**.

6.3.4. Palladacycle catalyzed methanolyses of a series of N-methyl-N-aryl thiobenzamides

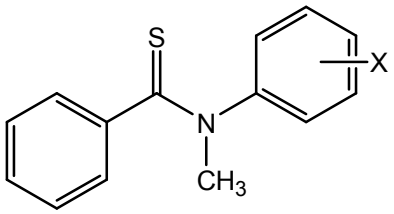

b) X = 3,5-dinitro
c) X = 3-nitro
d) X = 4-chloro
e) X = H

6.2

With a plausible mechanism established, the computational work was expanded to substrates with varying leaving group ability mirroring subsequent experimental work. Free energies (ΔG) for the reactions of **6.2a-e** following the above described mechanism are shown in Figure 6-3. For all substrates, free energies for the nucleophilic attack (***TS$_{Nu}$***) are similar (7.9 -10.6 kcal mol^{-1}), as are the nucleophile – carbon interatomic distances (Table 6-1). The stability of the first tetrahedral intermediate ***INT$_2$*** varies from -6.1 to 1.4 kcal mol^{-1}, with the greatest stability occurring when the N-aryl group has with the more electron withdrawing substituents. The apparent stability of ***INT$_3$*** increases with poorer leaving groups, that is, the depth of the local minimum on the free energy surface increases as the leaving groups become more electron donating. The increased stability is reflected in the shorter N-Pd bond lengths in this intermediate, indicating a greater association between the leaving group and the metal center. The free energy barrier for leaving group departure ***TS$_{LG}$*** ranges from 10.2 – 20.9 kcal mol^{-1}, with the greater values associated with the poorer leaving groups. For all substrates, this step represents the highest free energy value on the reaction pathway, and is therefore rate limiting. Relative to ***INT$_2$*** the free energies of activation range from 16.3 – 22.3 kcal mol^{-1}. A summary of

all computationally derived potential energies, free energies and corrected free energies for all structures calculated is shown in Table 6-2.

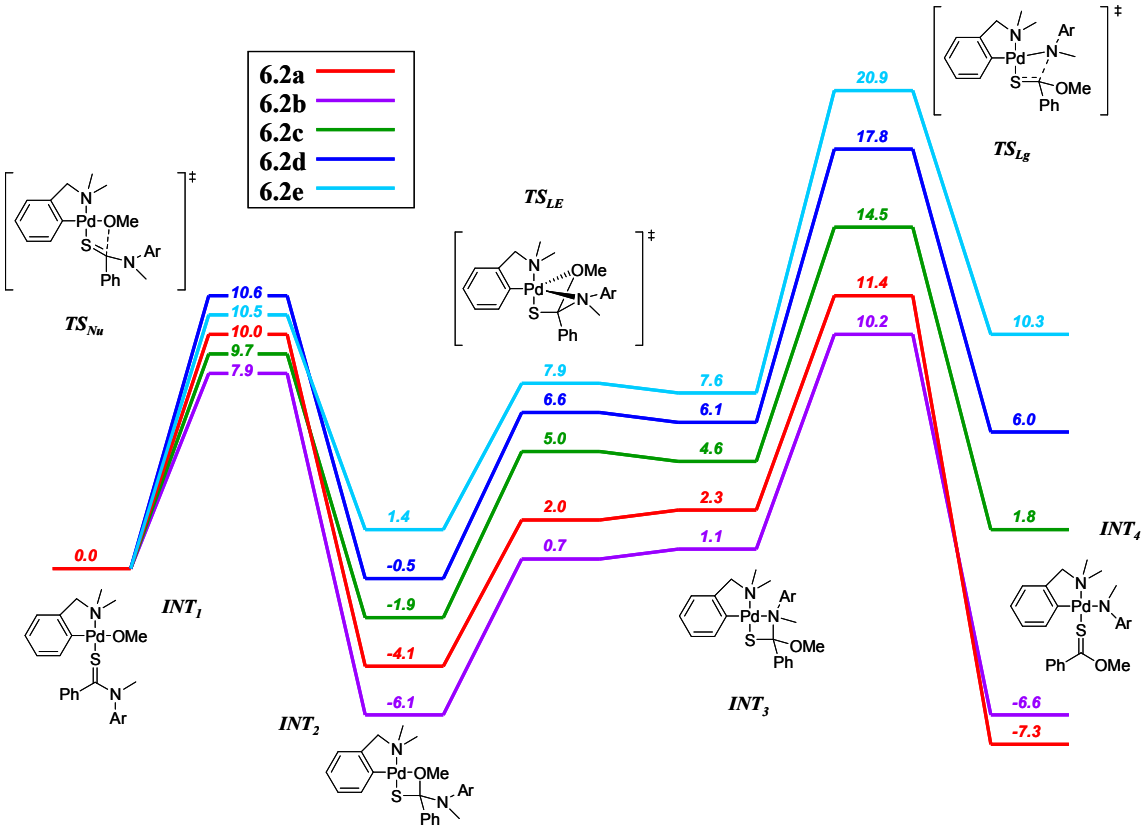

Figure 6-3. DFT computed reaction pathways (ΔG) for the **6.1** methanolysis reactions of **6.2a** (red), **6.2b** (purple), **6.2c** (green), **6.2d** (dark blue), **6.2e** (light blue). Free energies are in kcal mol^{-1} and relative to the free energy of ***INT*$_1$**.

Table 6-1. Selected bond lengths (Angstroms) for relevant intermediates and transition states.

Substrate	TS_{Nu}	INT_3		TS_{Lg}	
	C-OCH_3 (Å)	C-N_{Lg} (Å)	Pd-N_{Lg} (Å)	C-N_{Lg} (Å)	Pd-N_{Lg} (Å)
6.2a	2.10	1.57	2.67	2.17	2.25
6.2b	2.13	1.53	2.69	2.19	2.24
6.2c	2.07	1.56	2.43	2.34	2.21
6.2d	2.03	1.56	2.40	2.51	2.20
6.2e	2.01	1.56	2.37	2.87	2.18

Table 6-2. Summary of B3LYP determined potential energies (ΔE), free energies (ΔG, 298 K) and corrected free energies (ΔG_{corr}, 298 K), in kcal mol^{-1}, for all intermediates and transition states for the **6.1** catalyzed methanolysis of **6.2a-e**. All energies are relative to the ***INT*$_1$** structure.

Structure		ΔE	ΔG	ΔG_{corr}	Structure		ΔE	ΔG	ΔG_{corr}
6.2a	**INT_1**	0.0	0.0	0.0		**INT_1'**	19.9	15.1	20.3
	TS_{Nu}	8.0	10.0	9.9		**TS_{Nu}'**	40.7	33.0	41.5
	INT_2	-7.6	-4.1	-4.2		**TS_{Lg}'**	17.0	17.9	17.9
	TS_{LE}	-2.4	2.0	2.0		**$INT_{2\text{-}(HB)}$'**	-3.1	-0.3	-3.9
	INT_3	-1.0	2.3	2.2		**$TS_{Lg\text{-}(HB)}$'**	17.2	19.7	16.1
	TS_{Lg}	8.5	11.4	11.3					
	INT_4	-7.8	-7.3	-7.3					
6.2b	**INT_1**	0.0	0.0	0.0	**6.2d**	**INT_1**	0.0	0.0	0.0
	TS_{Nu}	7.6	7.9	7.8		**TS_{Nu}**	8.9	10.6	10.5
	INT_2	-7.8	-6.1	-6.1		**INT_2**	-2.3	-0.5	-0.5
	TS_{LE}	-3.0	-0.7	-0.7		**TS_{LE}**	3.9	6.6	6.5
	INT_3	-1.9	1.1	0.9		**INT_3**	2.7	6.1	6.0
	TS_{Lg}	7.4	10.2	10.4		**TS_{Lg}**	15.6	17.8	17.7
	INT_4	-4.5	-6.6	-6.6		**INT_4**	8.2	6.0	6.0
6.2c	**INT_1**	0.0	0.0	0.0	**6.2e**	**INT_1**	0.0	0.0	0.0
	TS_{Nu}	8.6	9.7	9.7		**TS_{Nu}**	9.3	10.5	10.4
	INT_2	-4.6	-1.9	-1.9		**INT_2**	-1.1	1.4	1.3
	TS_{LE}	2.3	5.0	5.0		**TS_{LE}**	5.2	7.9	7.8
	INT_3	1.0	4.6	4.6		**INT_3**	3.7	7.6	7.4
	TS_{Lg}	12.4	14.5	14.6		**TS_{Lg}**	18.5	20.9	20.7
	INT_4	3.1	1.8	1.7		**INT_4**	11.5	10.3	10.3

6.4. Conclusions

This work shows a plausible mechanism for the chemical steps of the **6.1** promoted methanolysis of **6.2a-e** that is consistent with experimental results determined so far with substrate **6.2a**. This process involves an internal nucleophilic attack of a bound methoxide attacking the bound substrate, followed by a rearrangement step wherein the nucleophile is replaced by the leaving group, which departs with the assistance of the metal ion. The leaving group departure step is limiting for all substrates calculated.

6.5. References

1) a) Neuman, R. C. (Jr.); Roark, D. N.; Jonas, V. *J. Am. Chem. Soc.* **1967**, *89,* 3412. b) Campbell, P.; Nashed, N. T. *J. Am. Chem. Soc.* **1982**, *104,* 5221.

2) a) Barlett, P. A.; Spear, K. L.; Jacobsen, N. E. *Biochemistry.* **1982**, *21,* 1608; b) Bond, M. D.; Holmquist, B.; Vallee, B. L. *J. Inorg. Biochem.* **1986**, *28,* 97.

3) Liu, C. T.; Maxwell, C. I.; Pipe, S. G.; Neverov, A. A.; Mosey, N. J.; Brown, R. S. *Submitted to J. Am. Chem. Soc.*

4) a) Schowen, R. L.; Hopper, C. R.; Bazikian, C. M. *J. Am. Chem. Soc.* **1972**, *94,* 3095; b) Broxton, T. J.; Deady, L. W. *J. Org. Chem.* **1975**, *40,* 2906.

5) (a) Becke, A. D. *Phys. Rev. A.* **1988**, *38,* 3098. (b) Lee, C; Yang, W.; Parr, R. G. *Phys. Rev. B*. **1988**, *37,* 785.

6) (a) Tomasi, J.; Mennuccia, B.; Cances, E. *THEOCHEM.* **1999**, *464,* 211. (b) Tomasi, J.; Mennuccia, B. Cammi, R. *Chem. Rev.* **2005**, *105,* 2999.

7) (a) Hay, P. J.; Wadt, W. R. *J. Chem. Phys.* **1985**, *82,* 270. (b) Wadt, W. R.; Hay, P. J. *J. Chem. Phys.* **1985**, *82,* 284.

8) Gaussian 09, Revision **A.1**, Frisch, M. J.; Trucks, G. W.; Schlegel, H. B.; Scuseria, G. E.; Robb, M. A.; Cheeseman, J. R.; Scalmani, G.; Barone, V.; Mennucci, B.; Petersson, G. A.; Nakatsuji, H.; Caricato, M.; Li, X.; Hratchian, H. P.; Izmaylov, A. F.; Bloino, J.; Zheng, G.; Sonnenberg, J. L.; Hada, M.; Ehara, M.; Toyota, K.; Fukuda, R.; Hasegawa, J.; Ishida, M.; Nakajima, T.; Honda, Y.; Kitao, O.; Nakai, H.; Vreven, T.; Montgomery, Jr., J. A.; Peralta, J. E.; Ogliaro, F.; Bearpark, M.; Heyd, J. J.; Brothers, E.; Kudin, K. N.; Staroverov, V. N.; Kobayashi, R.; Normand, J.; Raghavachari, K.; Rendell, A.; Burant, J. C.; Iyengar, S. S.; Tomasi, J.; Cossi, M.; Rega, N.; Millam, N. J.; Klene, M.; Knox, J. E.; Cross, J. B.; Bakken, V.; Adamo, C.; Jaramillo, J.; Gomperts, R.; Stratmann, R. E.; Yazyev, O.; Austin, A. J.; Cammi, R.; Pomelli, C.; Ochterski, J. W.; Martin, R. L.; Morokuma, K.; Zakrzewski, V. G.; Voth, G. A.; Salvador, P.; Dannenberg, J. J.; Dapprich, S.; Daniels, A. D.; Farkas, Ö.; Foresman, J. B.; Ortiz, J. V.; Cioslowski, J.; Fox, D. J. Gaussian, Inc., Wallingford CT, 2009.

9) Liu, C. T.; Maxwell, C. I.; Edwards, D. R.; Neverov, A. A. Mosey, N. J.; Brown, R. S. *J. Am. Chem. Soc.* **2010**, *132,* 16599.

Chapter 7. Summary and Conclusions

This thesis has two major foci. The first part is presented in Chapter 2, outlining our attempt to develop chiral catalytic lanthanide complexes for the asymmetric methanolysis of N-protected amino acid esters for kinetic resolution applications. The greatest selectivities were shown with the Yb^{3+}:**2.3** complex's reactivities with the enantiomers of racemic glutamine derivative **2.1**; however, this complex showed little selectivity with the racemic phenylalanine derivative **2.2**. The La^{3+} complex of the macrocyclic ligand **2.5** showed lower selectivity with the glutamine substrate, but gave fair selectivity with the phenylalanine substrate. The repetition of side-by-side kinetic runs with L and D substrates led to the development of a simplified kinetic method for determining rate constants for both substrates in a single experiment. This simple method involves placing respectively in the reference cell and sample cell of a duel beam spectrophotometer equal amounts of racemic and enantiomerically pure substrates, along with identical amounts of catalyst. Initially, the absorbance from each cell is equal and the net measured absorbance is zero; however, as the reaction progresses with different rates due to differences in enantioselectivity, the absorbance *vs.* time plot shows a characteristic "up-down" trace that can be analyzed to determine rate constants. The maximum or minimum value of the trace indicates the point of optimal catalytic conversion, a point at which the reaction should be stopped to maximize yield and e.e.

While the catalysts gave only modest results in terms of the substrate selectivity at room temperature, the detailed kinetic analysis allowed us to explore the kinetic resolution process and find ways to optimize it. The comparison of activation parameters

for the reactions predicted a greater difference in enantiomeric substrate methanolysis rate constants at lower temperatures, which was then confirmed experimentally. Lowering the reaction temperature slows the reaction rate, so a balance must be struck between enantiomeric selectivity and reasonable times for effecting the kinetic resolution.

A larger portion of this thesis was devoted to a detailed computational mechanistic examination of the cleavage reactions of phosphate and phosphorothioate triesters. These chemical species are used as agricultural pesticides and are related to chemical warfare agents, so understanding their reaction mechanism should be important for inventing methods for their decomposition. When their uncatalyzed cleavage reactions are understood, we can introduce catalysts to accelerate their reactions.

In Chapter 3, we establish a straightforward computational method for determining the Brønsted β^{eq} value for a reaction. This parameter is difficult to establish experimentally, and usually involves many time consuming kinetic determinations. This method serves to provide an initial estimate for this value. To calculate β^{eq} for a given reaction, the calculated differences in $\Delta G/2.303RT$ between starting materials and products within a series of substrates are plotted against leaving group pK_a. For instance, for the methanolysis reactions of a series O,O′-dimethyl O-aryl phosphorothioates in methanol, the free energy difference considered is that between the starting materials and the phenoxide leaving group. When $\Delta G/2.303RT$ is plotted against the ${}^{s}_{s}pK_a$ of the conjugate acid of the aryloxide leaving group the slope is the β^{eq} value. Starting material or product species that are common throughout the series of substrates ($^{-}$OMe, $S{=}P(OMe)_3$) need not be included as they will have no effect on the gradient of the free

energy *vs.* pK_a line, decreasing the total amount of calculations required. With the methanolysis reactions of O,O-dimethyl-O-aryl phosphorothioates **3.1** and their aryloxide products this method resulted in β^{eq} values that did not reproduce the experimental values. However, when the neutral phenol product is used the results are closer (within statistical uncertainty) to that determined experimentally. This depends on the assumption that the equilibrium of phenol and phenoxide is associated with a β^{eq} value of -1.0 which is added to the gradient of the plot, resulting in the total reaction Brønsted β^{eq} parameter. The method was tested with different phosphoryl and carbonyl transfer reactions, resulting in calculated values that are satisfactorily close to the experimental values. The addition of explicit hydrogen bonding to the calculated structures did not improve the reproduction of experimental β^{eq} values.

A further investigation into phosphate and phosphorothioate reactivity is presented in Chapter 4 where the kinetics of their solvolysis reactions in water and methanol are studied using DFT and experiments were conducted to validate the computational predictions. This involved mapping reaction starting material, transition state and intermediate structures computationally for the hydrolysis and methanolysis of O-alkyl or O-aryl dimethyl phosphates **4.2** and phosphorothioates **4.1**. We show that the reactions of these substrates cannot be simply classified as 'concerted' or 'step-wise'. Rather they represent in a continuum of reactivities depending on the nature of the leaving group or nucleophile. Leaving groups that are considered 'good' (low pK_a of their conjugate acid) generally have reactions that involve one transition state and no intermediate, while intermediates exist for substrates with 'poor' leaving groups. In comparing relative energies of transition states and starting materials, rates of reaction

can be predicted using classical transition state theory, allowing the determination of computational β^{lg} values which are found to be similar to experimentally determined β^{lg} values. Interestingly, the Brønsted relationship is non-collinear between substrates with alkyl and aryl leaving groups, an observation that was confirmed experimentally. This is not likely to be a solvation effect, as it is present with calculations conducted without a continuum solvent model applied; it is, however, likely due to a difference in electron distribution in the starting materials between the alkyl and the aryl leaving groups.

This laboratory specializes in the development of metal-ion based catalysts designed to promote the methanolysis reactions of phosphorus ester substrates. A palladacycle **5.1** has been shown to exhibit great reactivity toward the methanolysis of phosphorothioate esters. Chapter 5 describes a DFT study of the mechanism of its catalysis that has been conducted concurrent with an experimental study. For a contiguous series of phosphorothioate substrates, a downward break is found in the experimentally determined Brønsted plot of the **5.1** catalyzed methanolysis of a series of O,O′-dimethyl O-aryl phosphorothioates, indicating a change in rate determining step. With this in mind, the catalytic mechanism was calculated for a substrate from each kinetic domain. Specifically, the mechanism involved an initial substrate binding step followed by the nucleophilic attack of a bound methoxide to form a metal bound, 5-coordinate phosphorane intermediate. Leaving group departure was modeled as a direct departure of phenoxide. For substrates with lower leaving group pK_a values, the substrate binding step was associated with the highest point on free energy profile. The reaction of substrates with higher leaving group pK_a values, however, involved rate determining leaving group scission. Interestingly, the DFT studies predict the existence of the

kinetically a relatively stable 5-coordinate phosphorane intermediate. This investigation shows the degree to which theory and experiment can complement each other in solving a chemical puzzle.

The aforementioned palladacycle **5.1** has been recently shown to accelerate the methanolysis of N-methyl N-aryl thiobenzamides. In Chapter 6 of this thesis a preliminary DFT investigation into this mechanism is presented. In this case, only the chemical steps of the catalysis are modeled, the mechanism of which involves the direct nucleophilic attack of a bound methoxide on the amide carbon to form a Pd-bound tetrahedral intermediate. Rather than departing directly, the calculations indicate that the intermediate rearranges to a structure wherein the leaving group nitrogen is bound to the metal ion which facilitates its departure. Thus, this complex is able to catalyze the reaction with nucleophilic activation, activation of the carbonyl group and leaving group assistance.